RoMANS

Rocky Mountain Atmospheric Nitrogen and Sulfur Study







Volume 1

October 2009

ISSN 0737-5352-84

ISSN 0737-5352-84

RoMANS

Rocky Mountain Atmospheric Nitrogen and Sulfur Study Report

October 2009

Principal Investigators:
William C. Malm[1]
Jeffrey L. Collett, Jr.[2]
Authors:
Michael G. Barna[1]
Katie Beem[2]
Christian M. Carrico[2]
Kristi A. Gebhart[1]
Jenny L. Hand[3]
Ezra Levin[2]
Marco A. Rodriguez[3]
Bret A. Schichtel[1]
Florian Schwandner[2]
Contributors:
Derek E. Day[3]
Sonia M. Kreidenweis[2]
Taehyoung Lee[2]
Charles McDade[4]
Gavin R. McMeeking[2]
John V. Molenar[5]
Suresh Raja[2]
Amy P. Sullivan[2]
Courtney Taylor[2]

[1]National Park Service
CSU/CIRA
Fort Collins, Colorado 80523-1375

[2]Department of Atmospheric Science
Colorado State University
Fort Collins, Colorado 80523-1371

[3]Cooperative Institute for Research in the Atmosphere (CIRA)
Colorado State University
Fort Collins, Colorado 80523-1375

[4]Crocker Nuclear Laboratory
University of California
Davis, California 95616-8569

[5]Air Resource Specialists
Fort Collins, Colorado 80525

Disclaimer
The assumptions, findings, conclusions, judgments, and views presented herein are those of the authors and should not be interpreted as necessarily representing National Park Service policies.

TABLE OF CONTENTS

Appendices available on cd:

LIST OF FIGURES

LIST OF TABLES

RoMANS
Rocky Mountain Atmospheric Nitrogen and Sulfur Study

OVERVIEW AND SUMMARY

Introduction

Sulfur (S) and nitrogen (N) compounds are essential nutrients for life. In excess, however, S and N can be toxic, even life threatening, and in national parks excess N and S can upset the delicate balances in natural ecosystems. N and S species can cause rain and snowfall to be acidic, and particulate sulfate (SO_4^{-2}) and nitrate (NO_3^-) can cause significant visibility impairment and adversely affect human health.

Human activity, including combustion of fossil fuels, application of N fertilizers, animal husbandry, and cultivation of nitrogen-fixing legumes, has substantially altered the global N cycle. Wet and dry deposition of ammonia (NH_3) and atmospheric oxidation products of nitrogen oxides (NO_x) are significant N inputs in many environments. Within Rocky Mountain National Park (RMNP) wet deposition of inorganic N (nitrate and ammonium) currently contributes approximately 2–3 kg/ha/yr to total N input, depending on elevation (Figure S.1). Dry deposition of gaseous nitric acid (HNO_3) and particulate nitrate and ammonium (NH_4^+) increases total measured N deposition to approximately 3–4 kg/ha/yr. These are lower limits to the total N deposition, since important deposition inputs, including dry and wet deposition of organic N particles and gases and dry ammonia gas deposition are not currently measured in routine networks.

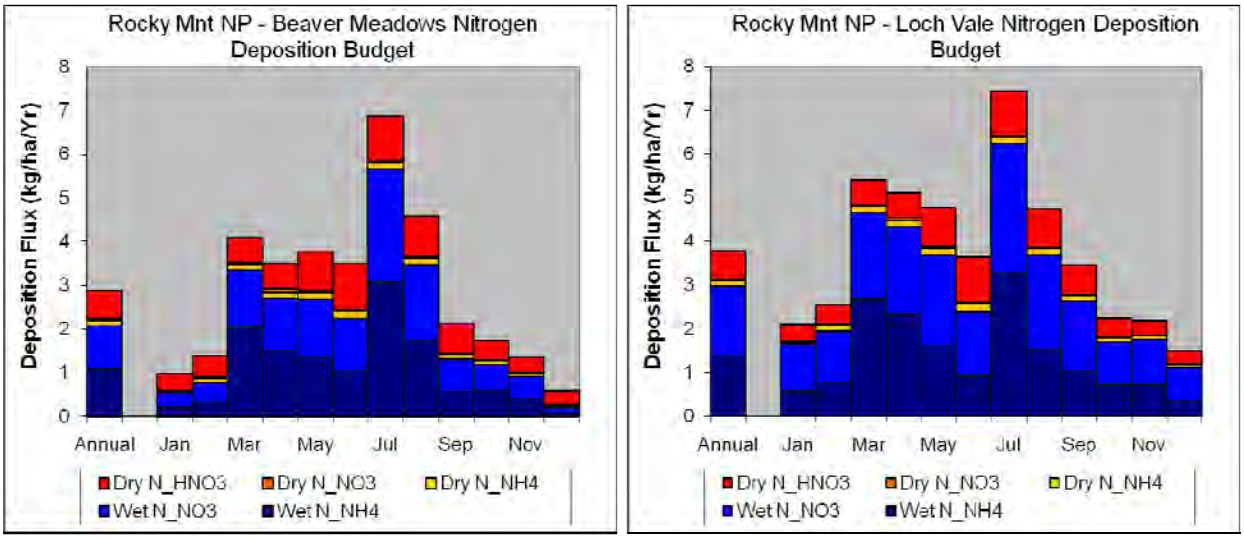

Figure S.1. The average monthly total N deposition budgets at Loch Vale and Beaver Meadows in RMNP. The National Atmospheric Deposition Program wet deposition data at Loch Vale and Beaver Meadows and RMNP Clean Air Status and Trends Network data from 2000 through 2005 were used.

The current inorganic N deposition fluxes appear to represent approximately a 20-fold increase above pre-industrial values for the western United States. In the last 20 years, as shown in Figure S.2, from 1985 through 2002, concentrations of inorganic nitrate in wet deposition

increased from 10% to 50% throughout the Rocky Mountains and surrounding areas. During this time period, the increase in ammonium wet deposition concentration was even greater, increasing from 50% to 90% in the Rocky Mountains. In contrast the wet deposition of S compounds decreased 20–60%. The differing trends in nitrate and ammonium wet deposition are shifting the relative contributions of reduced and oxidized N compounds, and as shown in Figure S.1, the measured reduced N and oxidized N currently have about equal contributions to the N wet deposition.

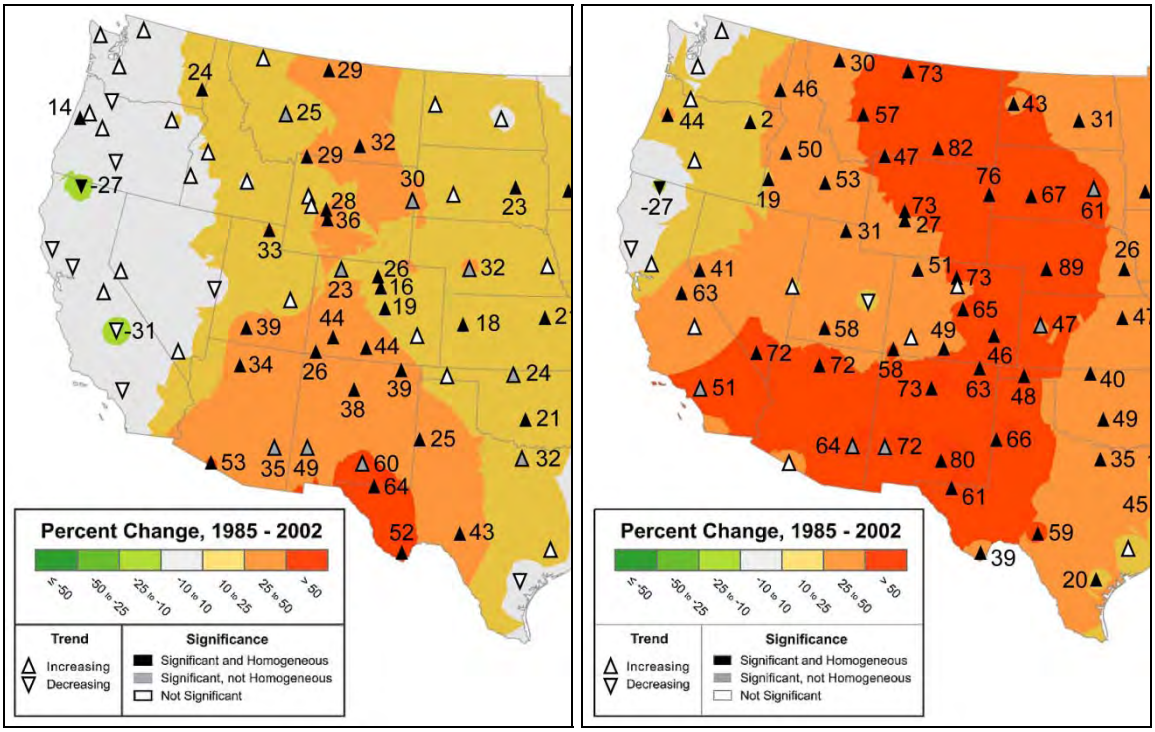

Figure S.2. Left panel: Percent change in the nitrate concentration in precipitation for the years 1985–2002. Right panel: Percent change in the ammonium concentration in precipitation for the years 1985–2002 (Lehmann et al., 2005, reproduced without permission).

The rate of deposition of N compounds in RMNP has crossed a crucial threshold called the "critical load." A critical load is the quantitative estimate of an exposure to one or more pollutants below which significant harmful effects on specified sensitive elements of the environment are not expected to occur, according to present knowledge. Consequently, changes are occurring to park ecosystems and these changes may soon reach a point where they are difficult or impossible to reverse. Observed ecosystem changes include changes in the chemistry of old-growth, Engelmann spruce forests and other alpine vegetation, shifts in population of lake diatoms, excess N leakage into lakes and streams, and alterations in biogeochemical cycling associated with increased microbial activity in high elevation soils and talus.

The park has set a resource-management goal for a critical input load of 1.5 kg/ha/yr of wet inorganic N deposition, a level considered protective of park ecosystems. Achieving this target will necessitate an approximately 50% reduction in wet N deposition from current levels. With growing evidence of increases in N deposition and its impacts, a cooperative effort between the National Park Service (NPS), the U.S. Environmental Protection Agency (EPA), and the state of Colorado recently resulted in the establishment of a RMNP nitrogen deposition reduction plan.

Atmospheric particles containing S and N also contribute to visibility-degrading haze that frequently impacts RMNP. Visibility is impaired to some degree in the park 90% of the time. Viewing distances in summer average 135 km but can drop to a few km episodically.

Programs are underway to reduce NO_x emissions throughout the United States, including in the West. This should help to reduce N deposition in RMNP; however, the current programs will not be sufficient to attain the goal of reducing inorganic N wet deposition to 1.5 kg/ha/yr. Other N compounds and their source emissions will need to be reduced. To better understand the rates of deposition of all N and S compounds in RMNP and their sources, the Rocky Mountain Atmospheric Nitrogen and Sulfur study (RoMANS) was conducted.
The RoMANS study included two 5-week sampling periods in 2006. One was a spring campaign from March 25 through April 30 and the second a summer campaign from July 7 through August 11. As shown in Figure S.1, these periods of the year typically have elevated wet deposition rates compared to other months. Climatologically, the deposition in these two periods is driven by different types of meteorological events. In the spring, large-scale upslope events occur that can bring contributions from the Front Range and beyond. During the summer, frequent precipitation, often in the afternoon, occurs due to convective activity. The field campaigns were followed by a 2-yr data and modeling analysis effort with the following objectives:

- Identify the overall mix of S and oxidized and reduced N in the air and precipitation on both the east and west sides of the Continental Divide.
- Identify the relative contributions to atmospheric oxidized S and oxidized and reduced N at Rocky Mountain National Park from emissions originating within the state of Colorado versus outside the state.
- Identify the relative contributions to atmospheric oxidized S and oxidized and reduced N at Rocky Mountain National Park from emissions originating along the Front Range versus other regions within the state.
- Identify the relative contributions of various source types within the state of Colorado to N and S species, including mobile, agricultural, other area sources, and large and small point sources.
- Map spatial and temporal variability of atmospheric deposition within the park and relate observed patterns to likely source types and locations.
- Characterize the meteorological conditions that lead to various atmospheric chemical conditions.

RoMANS Field Campaigns

Each field campaign consisted of monitoring at a core site, two secondary sites, and a series of satellite sites (Figure S.3). The core site was located on the east side of RMNP and had the most extensive set of instruments measuring fine and coarse particle species concentrations, trace gas concentrations (SO_2, NO_X, NH_3, HNO_3, CO, and O_3), ion size distributions, wet deposition, particle light scattering, and meteorology. Concentrations of key particle species and wet deposition were also measured at the secondary sites located just to the east and west of RMNP. Satellite sites were set up throughout Colorado and neighboring Utah and Nebraska. The measurements at the satellite sites varied between sites and depended on the type of sampling equipment available.

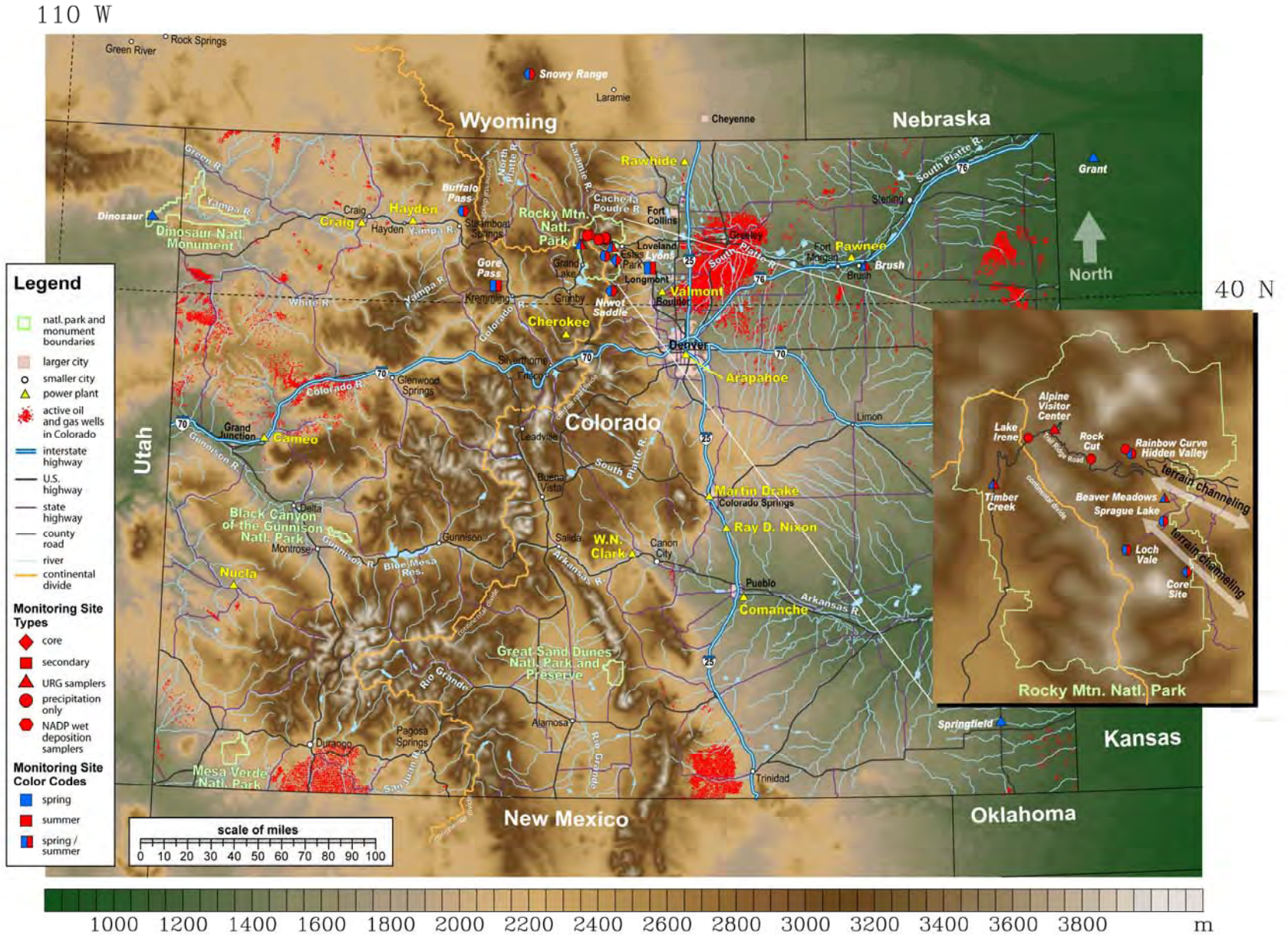

Figure S.3. Map of Colorado and adjacent areas illustrating the location of the monitoring sites used in the RoMANS study and the field campaign(s) each monitoring site was operational.

The field study included a number of quality assurance and control measures to ensure high-quality data. Procedures were established at the planning stage, with multiple instruments, collocated at some sites, measuring the same or related particulate and gaseous species and wet deposition rates. These redundant and related measurements were compared to identify biases, estimate errors, and assess the overall suitability of the data for the various analyses. This included comparing redundantly derived and directly measured species concentrations and their physical and optical properties at the same sites; performing closure studies for particulate mass, ionic balance, and light scattering; and comparing collocated wet-deposition-rate measurements and performing ionic balances on wet deposition data. For example, University Research Glass (URG) samplers were deployed to measure 24-hr-average concentrations of particulate ions, HNO_3, and NH_3. The URG samplers have been extensively used and validated in past studies, with well-defined uncertainties. At the core measurement site, semicontinuous instruments were also deployed to measure particulate ions, NH_3, and other species. These are more experimental instruments with varying quality. As shown in Figure S.4, the raw semicontinuous data match the day-to-day fluctuations; however, close statistical comparisons show that there were systematic differences in some of the continuous measurements. Based on these comparisons and the confidence in the URG measurements, the continuous data were adjusted to remove the systematic differences prior to use in source apportionment analyses.

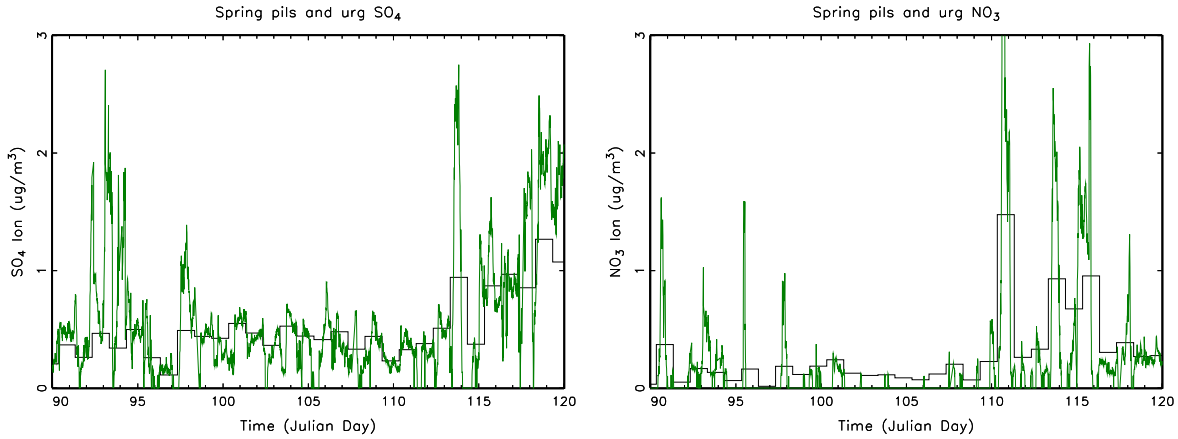

Figure S.4. Spring time series at the RoMANS core site showing (left) sulfate and (right) nitrate ion mass concentrations for the semicontinuous PILS (green) and 24-hr-average URG measurement systems (black). Graphs are for March 31 to April 30 (Julian Days 90–120), 2006.

Figure S.5 presents the comparison between the wet deposition data at the core site from an automated event precipitation collector and a manually operated subevent sampling system. As shown, deposited amounts of nitrate, sulfate, and ammonium generally show reasonable agreement between the two sampling approaches, with the subevent sampler sometimes underestimating deposition fluxes, due to these manually deployed samplers relying on site operators watching for the onset of precipitation to deploy them. Figure S.5 also clearly identifies an outlier in the comparison. The difference was found to be a problem with the solute deposition recorded by the automated collector for the July 7–8 event. In this case, the outlying data from the automated sampler were replaced with data from the subevent sampling.

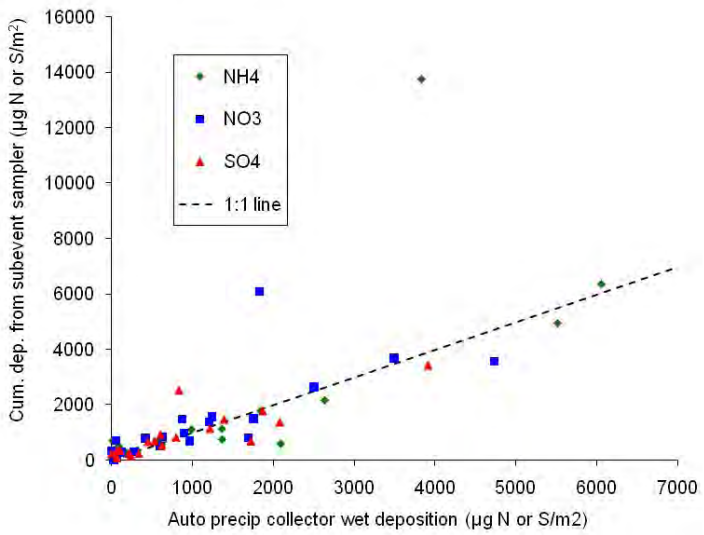

Figure S.5. Comparison of deposited amounts (µg/m^2) of ammonium, nitrate, and sulfate measured using the subevent (y-axis) and automated event precipitation collectors (x-axis) at the RoMANS core site. A 1:1 line is shown for comparison. The three high outlier points correspond to a July 7 precipitation episode.

In addition to the measured air quality and meteorological data, gridded meteorological data were extensively used in the analysis phase of the study as inputs to both back trajectory and chemical transport modeling. The fifth version of the meteorological mesoscale model (MM5) was used to generate hourly meteorological fields on three nested domains with horizontal grid sizes of 36, 12, and 4 km. The MM5 model was run with observational nudging on the 4-km domain that covered most of Colorado and analysis nudging over the 36-km domain that covered most of North America. The observational nudging used surface and upper-air observations obtained from the National Center for Atmospheric Research as well as meteorological data collected as part of RoMANS. The MM5 output was evaluated by an independent third party by comparing it to surface observations in Colorado. They found that the model's performance was within generally accepted ranges. Wind vectors were most accurate when the winds were from the west or south and less accurate with the more infrequent easterly (upslope) winds, especially in areas of complex terrain. The model accurately predicted where precipitation occurred, but generally overpredicted quantities. There was better agreement during the cooler months than in the summer when precipitation due to local convection was prominent.

Eleven years, 1997–2007, of meteorological data from the readily available Eta Data Assimilation System (EDAS) were also used to generate 5-day back trajectories, using the Hybrid Single Particle Lagrangian Integrated Trajectory Model (HYSPLIT) version 4.8. Comparison of trajectories generated with EDAS to those generated with the 2006 MM5 inputs showed that the MM5 trajectories were somewhat longer, implying higher wind speeds. The MM5 had greater horizontal and vertical resolution than the EDAS data and is expected to be better able than EDAS to capture shallow upslope flow along the Front Range and on the eastern side of RMNP. The MM5 trajectories did have more transport from the northeast during the afternoons and less in the morning than did EDAS-generated trajectories.

Characterization of Haze in RMNP

Haze is caused by scattering and absorption of light by suspended fine liquid or solid particles in ambient air, known collectively as atmospheric aerosol. The sum of the light scattering and absorption is known as the light extinction and can be thought of as the fraction of light lost per unit of distance. The units of light extinction are inverse distance, e.g., 1/(million meters) or Mm^{-1}. Higher light extinction levels correspond to hazier conditions.

Detailed particle size and chemical composition measurements made at RMNP during the RoMANS study were used to develop estimates for the hourly contributions to light scattering by the major aerosol components. These compared well to direct optical measurements of light scattering. Figure S.6 shows the hourly particulate light scattering contributions by the major aerosol components for the spring campaign and the nephelometer-measured atmospheric scattering coefficient. The most striking feature is the short-time-scale variability of the light scattering and associated mass concentrations. Unlike ecosystem effects, visibility impairment is a near-instantaneous phenomenon, and the highly variable aerosol concentrations and their light scattering result in visibility that can change from a low to a high level of impairment within time scales of an hour or less.

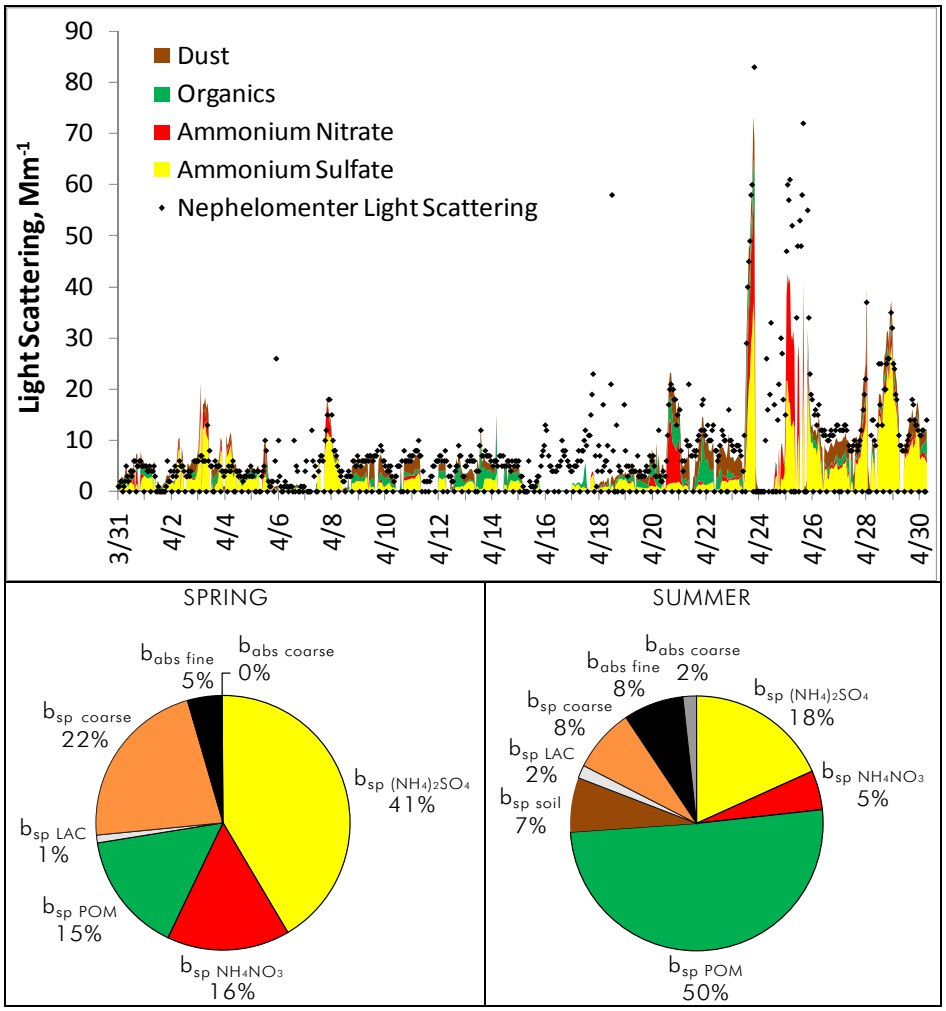

Figure S.6. Temporal plot of measured and estimated particulate atmospheric scattering (Mm^{-1}) of major aerosol species at the core monitoring site during the spring RoMANS time period and the approximate extinction budgets for the spring and summer RoMANS time periods. Note, gaps in the extinction budgets, e.g., April 16–17, are due to missing aerosol data.

The highest spring haze event occurred on the evening of April 23, with a nephelometer-measured aerosol scattering coefficient of 83 Mm^{-1} at sunset, a time when the sun often provides stunning illumination of the mountain vistas. This event was dominated by the ammonium sulfate and ammonium nitrate scattering accounting for 37 Mm^{-1} and 20 Mm^{-1}, respectively, or 48% and 26% of the reconstructed light scattering. If Rayleigh scattering, (light scattering due to atmospheric gases) and particle absorption are added to the measured scattering, the corresponding visual range is approximately 40 km. Visibility impairment in national parks is routinely accessed using 24-hr measurements. This long averaging time period can significantly underestimate shorter-time-scale visual impairment. For example, the 24-hr light scattering on April 23 was 23 Mm^{-1}, which corresponds to a visual range of approximately 100 km, more than double the visual range during the haziest hours. The summer sampling period also had similar short-time-period variability.

The estimated average particle extinction budgets for the RoMANS spring and summer sampling periods are also summarized in Figure S.6. During the spring, ammonium sulfate was the largest contributor to extinction at about 40%, with ammonium nitrate and particulate organic matter (POM) each contributing about 15% to the overall extinction. Coarse particle scattering contributed another 22%, and particle absorption (sum of fine and coarse particle absorption) contributed another 5%. During the summer the average extinction budget was quite different. POM contributed 50% to aerosol extinction while ammonium sulfate contributed another 18%. Coarse particle scattering contributed only 8% and total absorption contributed 10% to total extinction.

Characterization of RMNP Nitrogen Deposition Budget

The deposition of ambient N species occurs through dry and wet processes. In dry deposition, gases and particles are directly transported to the Earth's surface where they become incorporated into aquatic and terrestrial ecosystems. Deposition rate is expressed as mass per area per time, e.g., $\mu g/m^2$/day or kg/ha/year. The rate of dry deposition is assumed to be proportional to the species concentrations where the proportionality constant is the deposition velocity, i.e., deposition rate per unit concentration. The deposition velocity of a given species is dependent on a number of factors, including, size for particles; solubility or reactivity of the species at the surface; surface characteristics; and meteorology. Highly soluble and reactive gases such as nitric acid and ammonia have higher deposition velocities than relatively insoluble species such as NO and NO_2. Fine particles including ammonium nitrate and ammonium sulfate have aerodynamic properties that inhibit their contact with the surface, resulting in generally lower deposition velocities compared to soluble gases.

Wet deposition is the result of particles and gases being incorporated into atmospheric hydrometeors, i.e., atmospheric water droplets or ice crystals, through in-cloud and below-cloud scavenging processes. The hydrometeors are deposited to the Earth's surface through precipitation or direct deposition of fog droplets to surfaces, known as occult deposition, and incorporated into aquatic and terrestrial ecosystems. Occult deposition can be an important deposition mechanism in high altitude environments, but was not examined in this study. The

wet deposition rate is dependent on the ambient concentrations, properties of the gases and particles, and properties of the precipitation. These varying properties are important for light and moderate precipitation events. However, wet deposition is an efficient process for removing soluble gases and particles from the atmosphere, and during heavy precipitation events nearly all of the particles and soluble gases can be removed. Total wet deposition amounts are dependent on precipitation frequency and rates, which are highly variable in space and time.

Wet and Dry Deposition Fluxes

Figure S.7 shows N deposition inputs at the RoMANS core site by the various pathways, arranged from the largest contributors on the left to the smallest contributors on the right. The total amount of dry deposition flux was significantly smaller than wet deposition flux for all species measured during both the spring and summer. Nitrate and ammonium wet deposition and ammonia dry deposition were all more than twice as high during summer than during spring. Wet deposition of organic N and nitric acid dry deposition were also greater in summer, though by a smaller proportion. By contrast, dry deposition fluxes of particulate nitrate and ammonium were lower in the summer, though their deposition rates were small compared to the other species. Overall, in the spring a total of 45,000 µg/m^2 (0.45 kg/ha)of N was deposited by measured dry and wet deposition pathways at the RoMANS core site, while in the summer campaign the N deposition was more than twice as high, 95,000 µg/m^2 (0.95 kg/ha). These deposition rates are lower than those for species typically measured in past years.

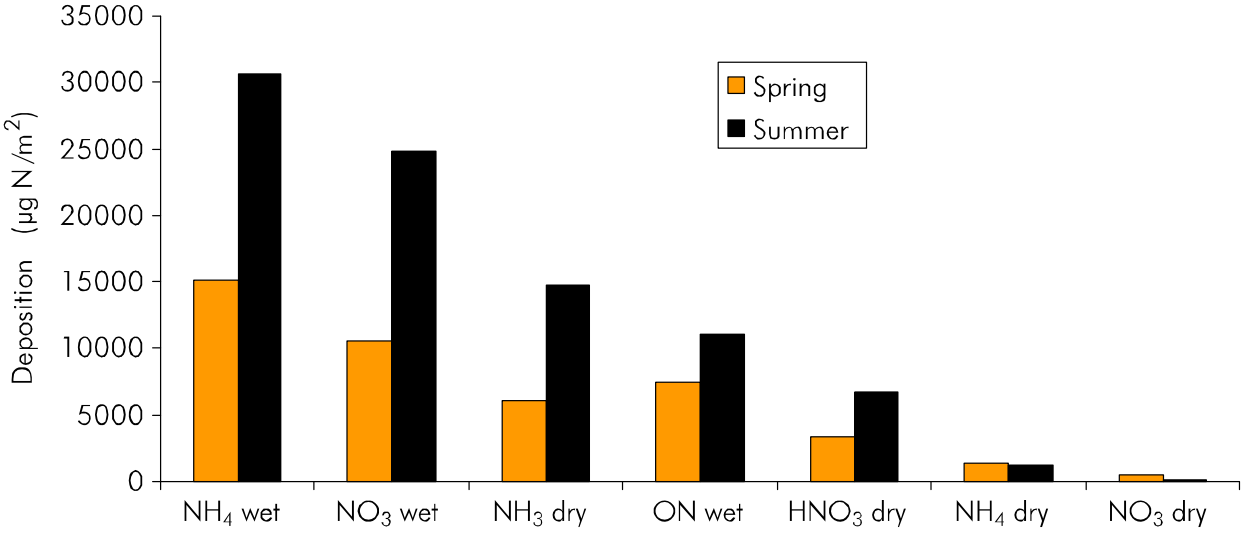

Figure S.7. N deposition totals (µg/m^2) by various species and pathways in order of contribution to total N deposition at the RoMANS core site.

As shown in Figure S.8, wet deposition is the major process by which N is deposited in RMNP during both spring and summer. The fractional contributions of the wet-deposited N species are similar in both seasons, with about 34% of the measured deposited N due to wet ammonium, 24–28% due to wet nitrate, and 12–17% due to wet organic N. Only 26% of measured N deposition occurred by dry processes, with NH_3 accounting for ~15%. Dry deposition of organic N was not measured. Although the spring and summer relative wet deposition rates for the different species were similar, they were due to very different meteorological processes. In the spring virtually all of the wet deposition was due to a single synoptic-scale event associated with sustained upslope transport. In the summer, precipitation occurred almost daily, due to convective activity.

Despite the higher N deposition in summer than in spring and the different meteorological processes causing the wet deposition, the relative proportions of various N deposition pathways and species were similar (Figure S.8). Overall, reduced N deposition accounted for about half of the total measured N deposition: oxidized N accounted for about one-third, and wet-deposited organic N for the remaining 12–17% of the deposited N. Similar results were found at Lyons east of RMNP. However, west of RMNP at Gore Pass, the relative contributions were quite different, with a lower contribution of reduced N in both spring and summer, increased contribution of wet-deposited organic N in summer, and increased contribution of inorganic oxidized N in the spring.

Together, wet deposition of organic N and dry deposition of gaseous ammonia composed ~30% of the total RoMANS N deposition budget. Neither of these two inputs is measured by the routine monitoring networks and they are missing from the climatological deposition rates presented in Figure S.1. In order to better quantify total N inputs into RMNP and determine which source types and regions are the biggest contributors to the problem, these two deposition pathways need to be measured more routinely. That will require routine measurements of gaseous ammonia concentrations and of organic N in precipitation. There is also a need to examine dry deposition inputs of organic N, a pathway not examined in the RoMANS study.

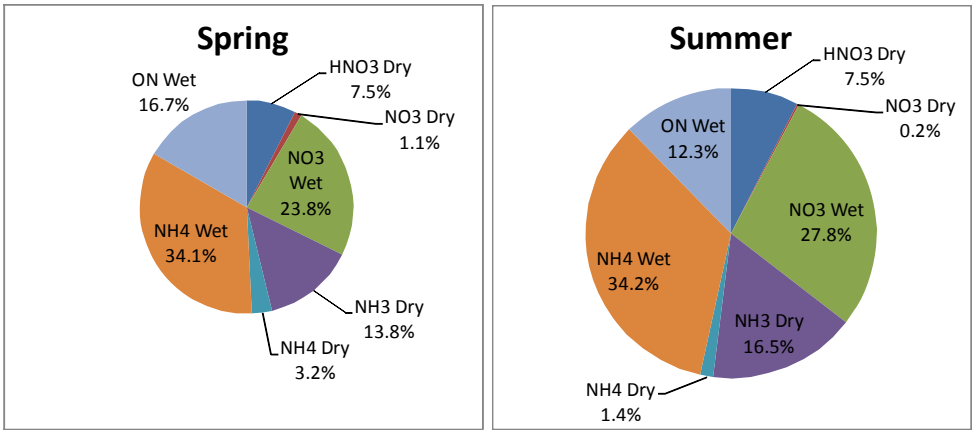

Figure S.8. Relative contributions of individual N deposition pathways to total measured N deposition at the RoMANS core site during the spring (left) summer (right) campaigns. The area of the pie is proportional to the total N deposition during each field campaign.

Sources and Emission Spatial and Temporal Patterns

The major contributors to N deposition can be classified as inorganic reduced N, primarily ammonia and ammonium, inorganic oxidized N, primarily nitric acid and particulate nitrate, and oxidized and reduced organic N. Emissions of organic N compounds such as amines are not well understood. Organic N emissions can come from biological sources, oxidation products of combustion emissions, and reduced forms of N primarily from agricultural sources. Due to the poor understanding of organic N emissions, they were not included in the emission inventories. However, due to their importance to the N deposition budget in RMNP and other places, there is a need for further research to better understand their emissions, their speciation, their main modes of deposition, and ecosystem availability.

Most ambient inorganic oxidized N is a secondary product of nitrogen oxides (NO_x: the sum of NO and NO_2). In the United States and Colorado it is estimated that about a third of NO_x is from

point sources such as coal-fired power plants, a third is from on-road mobile sources, and the remaining third consists of various source categories such as nonroad mobile, biogenic, and fertilizer applications. In Colorado, NO_x emissions from oil and gas development are estimated to be 7% of the state's total, but this is likely to be an underestimation, given that the inventory does not reflect the rapid expansion of leases in the West during the last several years. The uncertainty in the NO_x emissions varies by categories. The highest quality NO_x emissions are for large point sources that are directly measured. Emissions from other categories are based upon activity and emission factors and are of lesser quality, compared to point sources. Figure S.9 presents the average annual spatial pattern of NO_x emissions. The highest emissions in the West occur in urban areas associated with mobile emissions and large point sources located in urban and rural areas such as the Four Corners region. In Colorado the largest emissions are along the Front Range urban corridor. NO_x emissions from power plants in Colorado such as the Craig and Hayden facilities in northwestern Colorado are also evident.

Most ambient inorganic reduced N is due to NH_3 emissions. It is estimated that two-thirds of NH_3 emissions in the United States is due to agricultural activities, including animal husbandry. This increases to about 75% in Colorado. In Colorado mobile sources are estimated to account for 11% while area sources account for another 3%. The large contribution of agriculture to NH_3 emission is evident in the spatial emission plots in Figure S.9 where the highest emissions occur over agricultural lands. In Colorado the highest emissions are in the agriculture-intensive northeastern region, particularly along the Platte River valley. Both anthropogenic and natural emissions of NH_3 are highly uncertain. This was evident in chemical transport modeling (CTM) of NH_3, using the emissions shown in Figure S.9. The CTM modeling resulted in large spatial biases compared to measured NH_3 concentrations, which are likely due at least in part to errors in the emission inventory. In particular, ammonia emissions from fertilizer application and animal husbandry are highly variable and dependent upon the management practices being employed, time of year, and meteorological variables such as temperature. For example, ammonia emissions in April were significantly larger than during July, reflecting increased fertilizer application in the spring. Ammonia emissions from soil microbial respiration and mobile sources are also extremely uncertain.

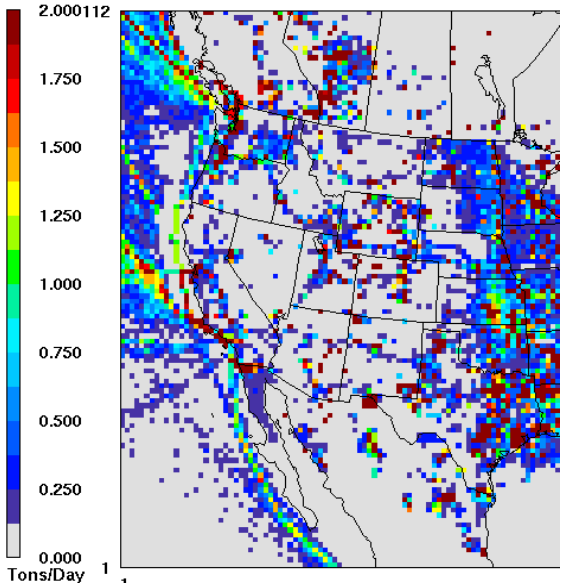

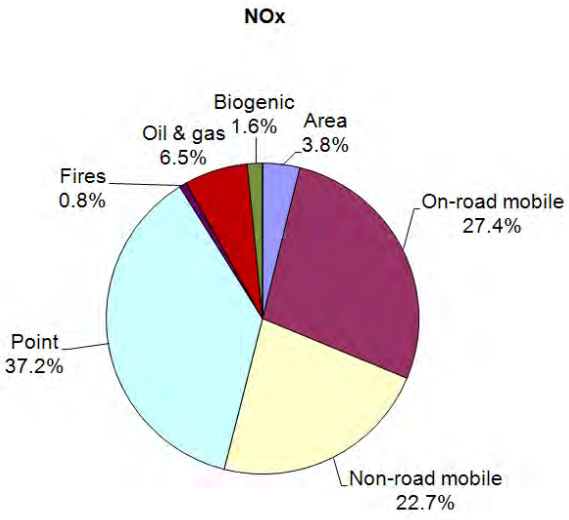

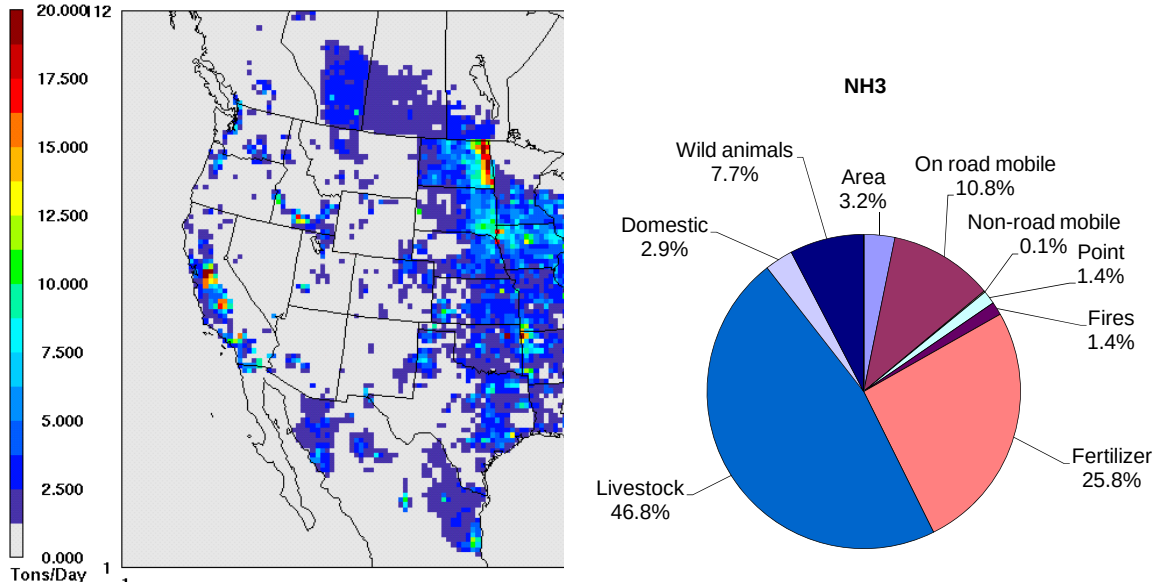

Figure S.9. Spatial distribution of annual average emissions of (top) NO_x and (bottom) NH_3. The pie charts are the contribution of different emission types within Colorado to NO_x and NH_3.

Source Apportionment of Ambient and Deposited N and S Species

A weight-of evidence approach, comparing and contrasting results from multiple analyses, was used to apportion the ambient and deposited N and S species to source regions within and outside of Colorado. This was done through a multistep process, starting from simple qualitative spatial data analysis to a final quantitative hybrid-receptor modeling technique. Each successive analysis built on the previous method, incorporating new data and/or more sophisticated statistical methods to refine the results.

Concentration Gradients of Aerosol and Trace Gas Species

Spatial concentration gradients are often the result of spatial variations in emissions, with increasing gradients pointing toward high emission regions that potentially contribute to the receptor ambient concentrations and deposition fluxes. Gradients in short-lived primary species, such as NH_3, tend to be sharp compared to those for secondary, longer-lived species, such as particulate sulfate.

In both the spring and summer campaigns, average concentrations for most species were highest in northeastern Colorado, with a sharply decreasing, east-to-west gradient, and the lowest measured concentrations occurring at Gore pass and Timber Creek, which are west of the Continental Divide (Figure S.10). This gradient was most dramatic for ammonia when in the spring, from east to west, ammonia concentrations increased from Nebraska to Brush, Colorado, then decreased with a minimum at Gore Pass, increasing again at Dinosaur, Colorado. The ammonia concentrations in Brush were 10–100 times greater than in RMNP. The peak concentrations in northeastern Colorado indicate significant local sources of ammonia contributing to the air quality. This is a region of known ammonia emissions (Figure S.9) from agricultural activities.

While S and oxidized N species concentrations also varied across the network, the differences were not as dramatic as seen for reduced N. Average concentrations of $PM_{2.5}$ sulfate showed a

modest increase, moving across the network from west to east. Sulfur dioxide concentrations were on average highest at the Lyons and Brush sites. Average $PM_{2.5}$ nitrate concentrations were highest in the northeastern part of the RoMANS network. Gas-phase nitric acid concentrations were highest at Lyons, consistent with its proximity to Front Range NO_x emissions sources. The gradients in the spatial patterns in the S and oxidized N species were more pronounced during the spring than summer.

Similar spatial patterns were also found in the average wet deposition concentration data. During the spring there was a large decreasing gradient in ammonium and nitrate concentrations, moving from east to west, and a smaller decreasing east-to-west gradient for sulfate concentrations. During the summer, wet deposition data were collected only from Lyons to Gore Pass. In these summer data, ammonium concentrations were highest at Lyons and lowest at the westernmost sites. The nitrate concentrations also peaked at Lyons but were relatively uniform across RMNP. The sulfate concentrations were also relatively uniform from Lyons to Gore Pass. During both seasons, the relative contribution of ammonium to wet deposition of N also increased when moving from western Colorado, east across the Continental Divide, reflecting the higher concentrations of reduced N in the eastern part of the state.

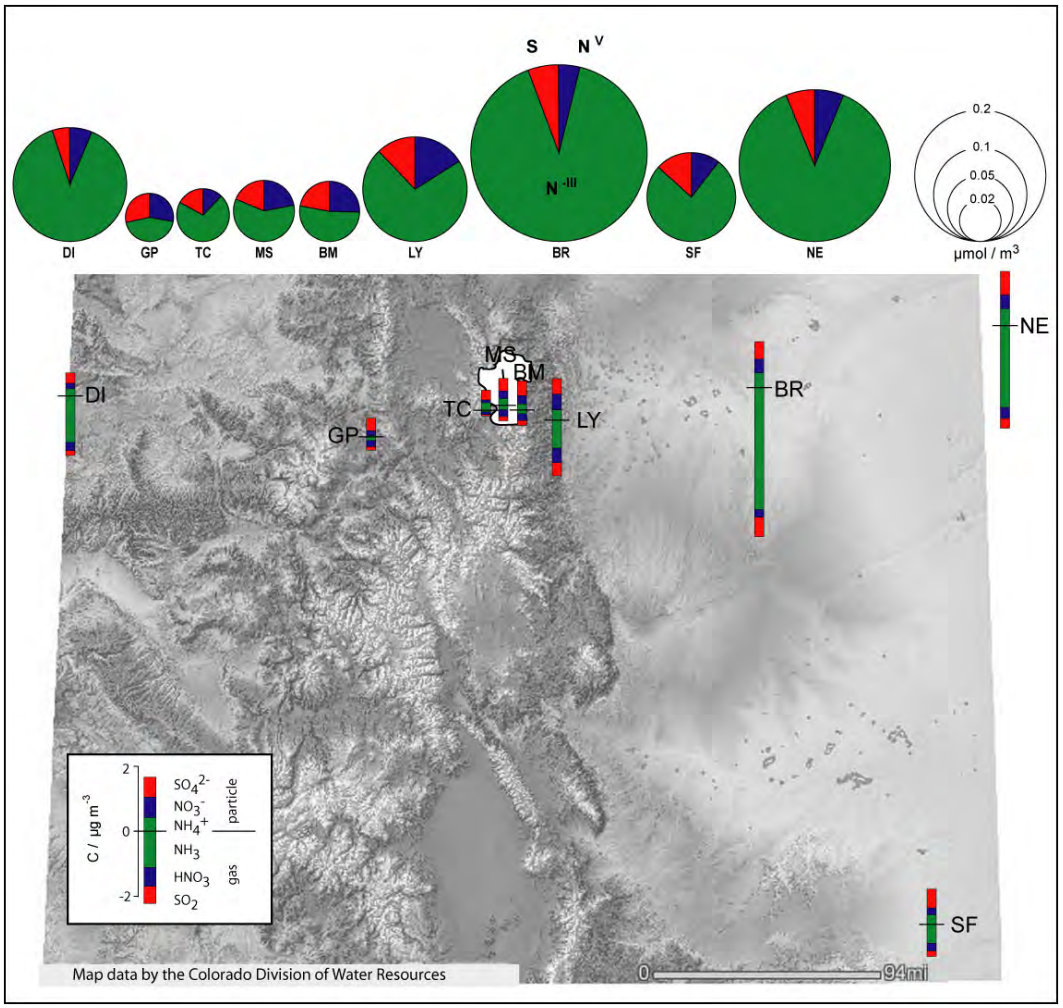

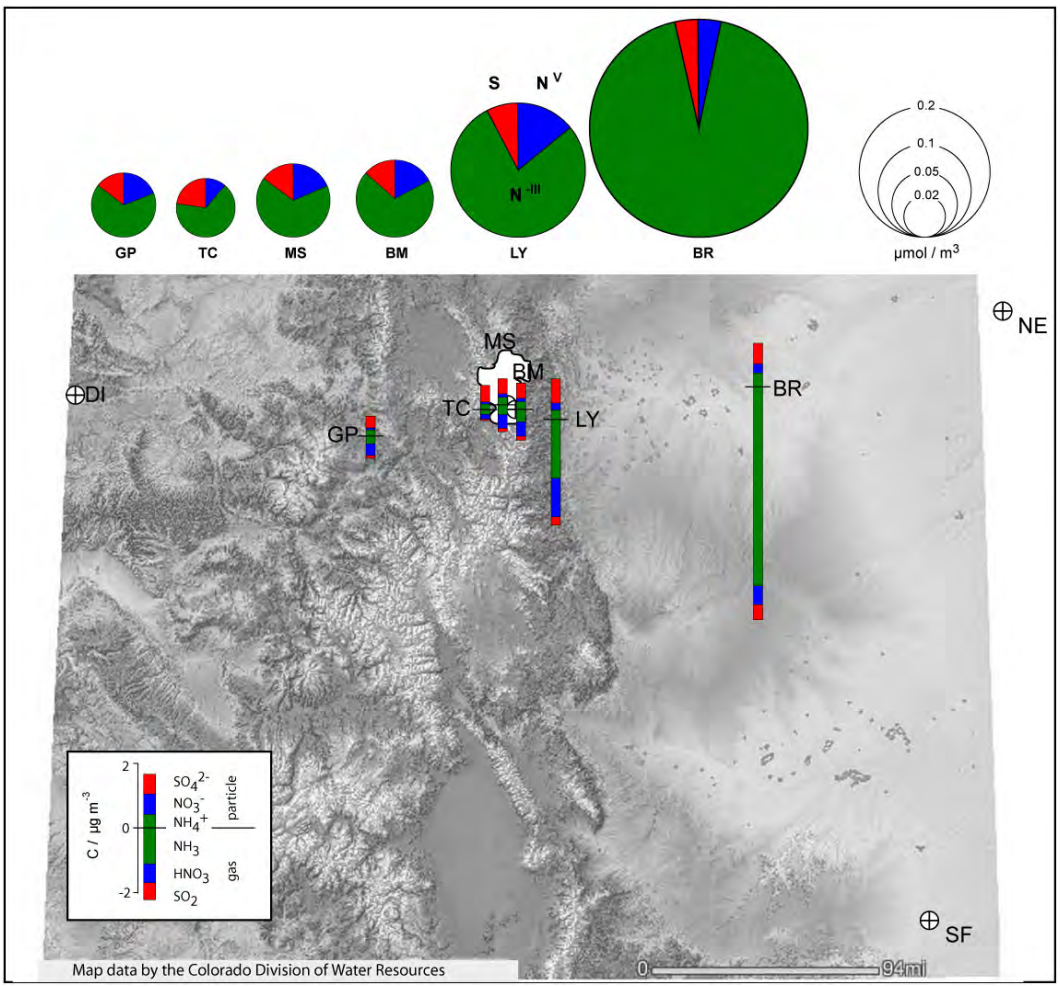

Figure S.10. Average concentrations of key particle- and gas-phase species measured across the RoMANS network during the spring (top) and summer (bottom) field campaigns shown as bar diagrams positioned at the location of each RoMANS network site. Pie diagrams show the average concentrations of S, reduced nitrogen (N^{-III}), and oxidized nitrogen (N^{V}) species measured at each site. The size of the pies is proportional to the sum of these average concentrations at each location.

The concentration gradients varied from day to day. On many days, concentrations of reduced N (ammonia + ammonium) and oxidized N (nitrate + nitric acid) at monitoring sites on the eastern side of the park were similar to concentrations on the western slope. However, on pollution episode days observed at the core site, there were strong spatial gradients in N species concentrations, with much higher concentrations of both oxidized and reduced N east of the Continental Divide. Furthermore, there were gradients in N concentrations moving from sites in RMNP toward eastern Colorado. Oxidized N concentrations often peaked at the Lyons site, while reduced N concentrations typically peaked farther east.

Association of N and S Species Concentration with Transport

The spatial gradients in N species concentrations show high concentrations of N species to the east of RMNP and low concentrations to the west. It was found that N species concentrations generally increased in RMNP when the transport was from the east, and the concentrations

remained relatively low when the transport was from the west during both the spring and summer. For example, time lines of $PM_{2.5}$ nitrate, sulfate, and ammonium from April 20 through April 23 measured at the core RMNP site are shown in Figure S.11. During this time period, there were three episodes of elevated particulate concentrations, and between the episodes the concentrations were very low. Also plotted in Figure S.11 is the surface (10 m) wind direction. Surface winds at this site from the west or northwest reflect downslope transport; winds from the east or southeast represent upslope transport as channeled by the local topography. The onsets of the increased fine particle concentrations during April 20 and April 23 were both preceded by a change in wind direction to upslope flow with air coming from the southeast. During the April 23 episode, the concentration rapidly decreased at midnight, with the onset of heavy precipitation, although the winds remained from the east. A day later the precipitation ended and the concentrations again rapidly increased, remaining elevated until the winds shifted to the northwest, reflecting downslope transport.

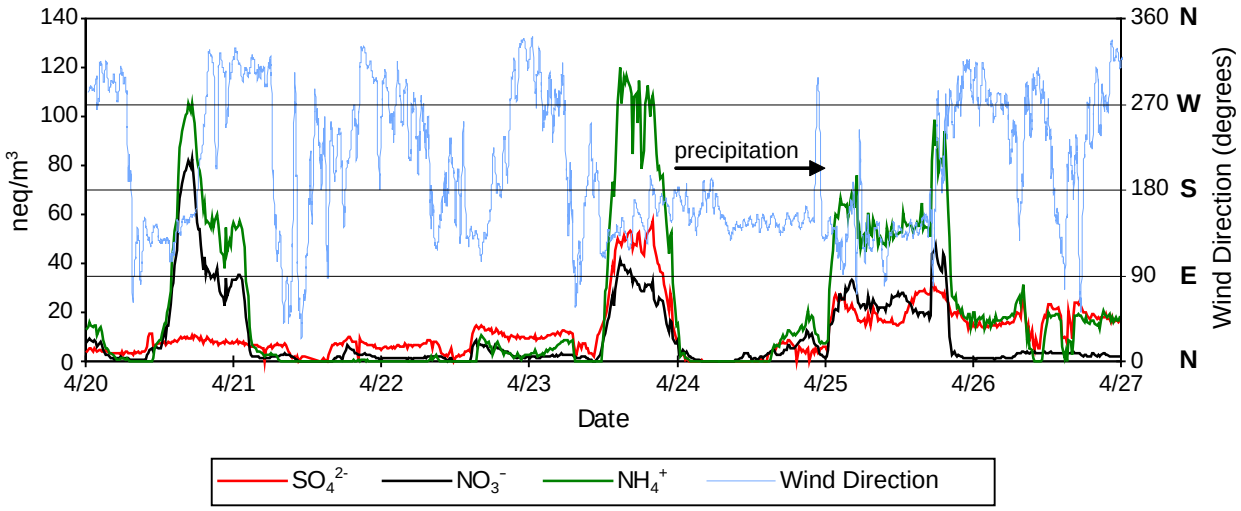

Figure S.11. Semicontinuous $PM_{2.5}$ major ion concentration (neq/m^3) and local 10-m wind direction (degree) time lines measured at the core site during late April 2006.

The period from April 23 to April 25 illustrates many of the key features observed during RoMANS to be important contributors to the deposition of large amounts of N and S to park ecosystems. First, transport from the east brings polluted air up into the park. Second, this transport from the east is also responsible for heavy precipitation, due to topographically forced lifting of the westward moving air, which effectively deposits ambient N and S species. The result, in this case, is the single most important deposition event observed during the entire RoMANS campaign. The association of upslope transport and precipitation was also seen for many of the precipitation events during the summer period. However, precipitation was also associated with more westerly transport than seen in the spring.

Surface winds can be influenced by channeling of winds by the terrain and may not necessarily be fully representative of the airmass transport direction. Back trajectories trace the transport pathways to the receptor sites over many hours and days at different elevations and provide a better picture of from where airmasses arrive. The examination of back trajectories shows that elevated N and S concentrations and wet deposition events were generally associated with near-surface upslope transport, with the trajectories traversing the Front Range and/or northeastern Colorado prior to reaching RMNP. This is illustrated in Figure S.12 where the trajectories

during high spring and summer NH_3, NO_2, and particulate NO_3^- concentration periods were aggregated together, using residence time differential probability (DP) analysis. The differential probability is the difference between the residence time for high concentration days, defined as concentrations above the 90th percentile, and all days. It addresses the question, when an air parcel traverses a given region, how much more or less likely than average is it that the air parcel will arrive at the receptor with high concentrations? Areas of high differential probability are often interpreted as potential source regions. Hourly HNO_3 data were not available for this analysis. NO_2, which has a negligible contribution to RMNP N deposition, is an important precursor to HNO_3 formation. Therefore NO_2 and HNO_3 likely have similar residence time analysis transport patterns.

As shown in Figure S.12, all three N species have high DP over the Front Range, indicating that prior transport over this region is associated with high concentrations at RMNP. However, the distance scales of transport for the three N species differ. NO_2 has low DP beyond the Front Range and high DP to the west of RMNP. The Front Range is a region of high NO_x emissions, with lower emissions to the east. In addition, NO_2 is a short-lived species in the atmosphere, minimizing contributions from distant sources. The particulate NO_3, a secondary species formed from NO_x, shows high DP east of Colorado, particularly in the spring, suggesting potential source contribution from more distant sources than NO_2. The NH_3 shows high DP east of the Front Range in the active agricultural area with high NH_3 emissions.

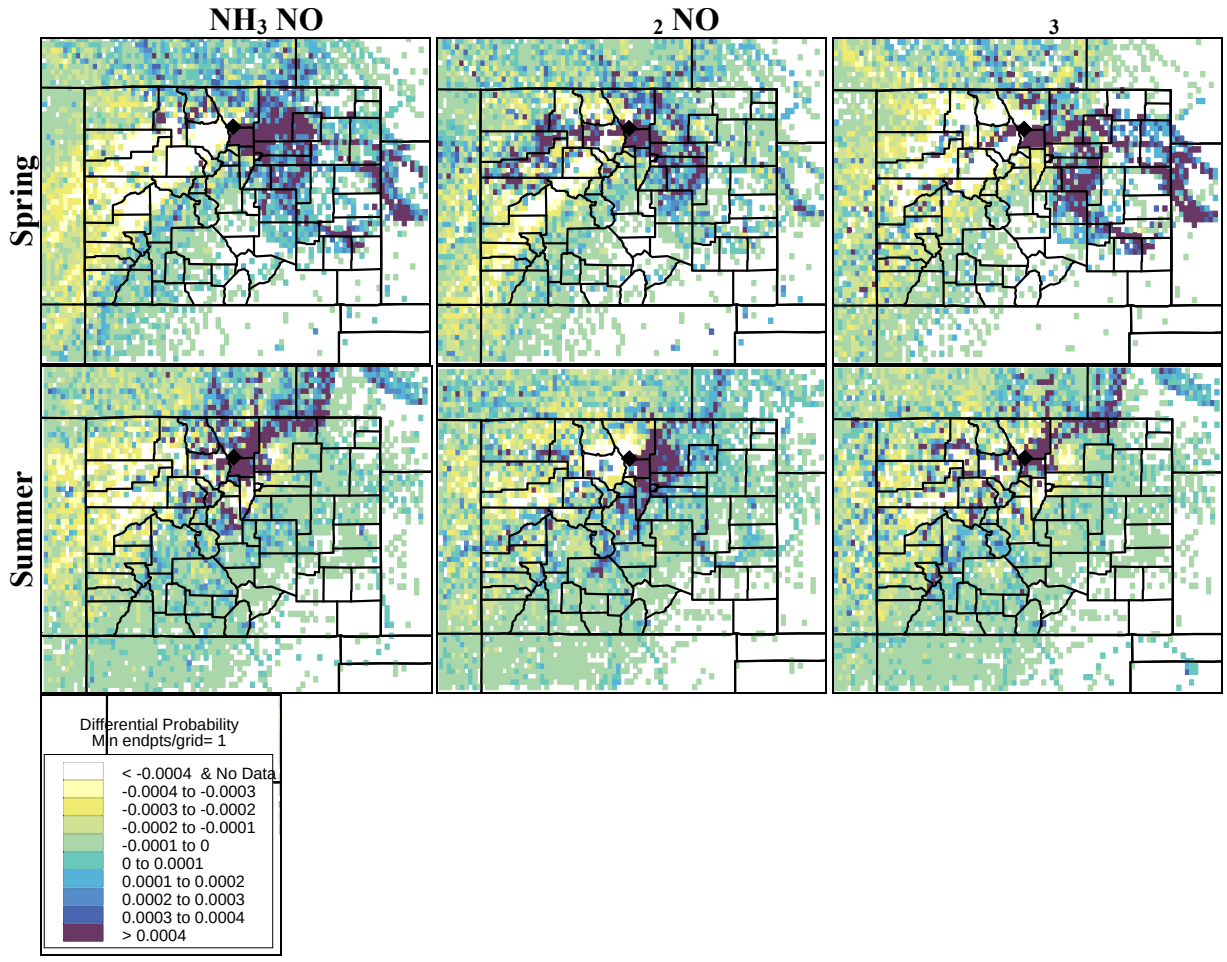

Figure S.12. High concentration differential probability for hourly NH_3, NO_2, and particulate NO_3 measured at the core site during the spring and summer field campaigns. The differential probability is the difference between the residence time probability for days with concentrations above the 90th percentile and the residence time probability for all days in the sampling period.

Transport Regression Receptor Models

Transport regression receptor models are based on the association of source signatures with measured concentrations. Two different methods were employed in the RoMANS study. One method, trajectory mass balance (TrMB), used the residence time over defined source regions, estimated from RMNP back trajectories to estimate the source signatures, while a hybrid approach developed source signatures from modeled concentrations of conservative tracers released from various source regions.

In TrMB the model establishes a "scaling" factor between the residence time over a source region and the measured concentrations at the receptor site. Average emission, dispersion, chemical transformation, and deposition processes are incorporated into this one scaling factor. However, all of these processes vary with time, and the source apportionments derived from this technique are more accurate on the average than on an hourly or episodic basis. A statistical apportionment approach will inherently tend to overestimate those source regions where

endpoints over the region are better correlated with measured concentrations while underestimating those source regions where endpoints over that source region show weak-to-little correlation with measured concentrations. Furthermore, emissions from two or more source regions often mix into the same air mass, causing the source signatures to be correlated, which increases the uncertainties in the analysis.

In the hybrid modeling approach, the apportionment analysis is more robust in that emissions and dispersion are explicitly modeled and only chemistry and deposition are incorporated into the "scaling" factor. In both approaches the scaling factors account for possible errors in the models used to develop the source signatures, such as any systematic biases in the emissions used in the hybrid approach. Like TrMB, the apportionment estimates are more accurate on the average than for an incrementally small time period.

The measurement uncertainties and standard errors of the regression coefficients are known, and through the propagation of uncertainties, it is possible to report errors for the apportionment estimates associated with these two variables. However, the underlying model uncertainties associated with the various assumptions are not known and are probably larger than measurement and statistical uncertainty. Therefore fractional apportionment estimates are not reported with an attached uncertainty. On the other hand, it is emphasized that the inherent limitations of statistical apportionment models should be kept in mind when referring to reported apportionment estimates.

Contributions of Colorado and non-Colorado Sources to Ambient Concentrations

In the TrMB analysis, residence time source signatures were calculated from 5-day back trajectories generated from the MM5 meteorological data. Source regions were defined based on high NH_3 and NO_x emissions. The sizes of the source regions generally increased with distance from RMNP, due to increased uncertainty in the transport with distance and to minimize transport collinearity.

In the hybrid approach, the tracer source signatures were calculated using the Comprehensive Air quality Model with extensions (CAMx) Eulerian chemical transport model. The 36-12-4 km nested MM5 meteorological data and the updated emission inventory (Figure S.9) were used as inputs. The CAMx model was modified to simulate an arbitrary number of conserved tracers, with no loss through chemical transformation or deposition. The model was used to simulate inert contributions from 94 to 100 different source regions throughout North America. The source regions were selected by centering them on high NH_3 or NO_x emission regions. The smallest source regions were selected near RMNP and they generally increased in size with distance from the park. Ten source regions were selected within Colorado, including one at RMNP, the neighboring population center at Estes Park, and Denver-Front Range, as well as the agricultural regions in northeastern Colorado. The Denver-Front Range region extended from north of Colorado Springs to south of Fort Collins and from Boulder to east of Greely Colorado.

The relative apportionment of Colorado and non-Colorado sources to ambient concentrations of S and N species measured at RMNP during RoMANS from the hybrid TrMB models is presented in Figure S.13. The TrMB model was used to estimate contributions from a subset of the available N and S species. For species modeled by both TrMB and the hybrid model, there is generally good agreement between the two methods, with the results within about 10 percentage

points. The one exception is for spring particulate nitrate where the hybrid model estimated the relative contribution from Colorado sources to be double the TrMB estimate at 50% verse 25%.

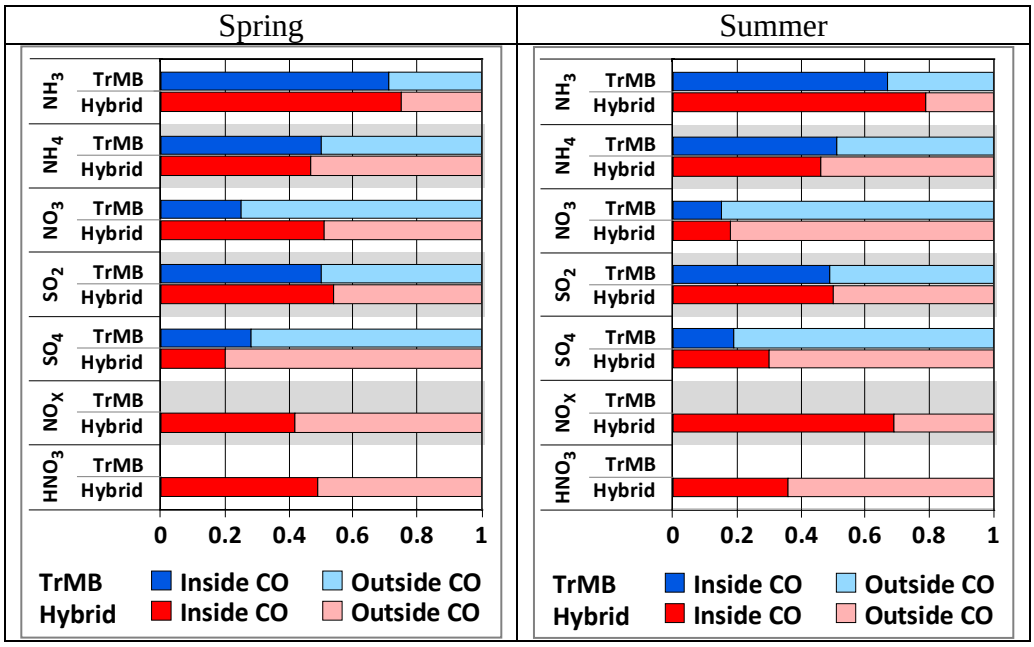

Figure S.13. Contribution of sources inside and outside of Colorado to ambient N and S species during the spring and summer RoMANS field campaigns, estimated from the TrMB and hybrid-receptor models. The TrMB model was not used to apportion NO_x and HNO_3 concentrations.

As shown in Figure S.13, during the spring the hybrid model estimates that Colorado sources contribute the majority, 50–75%, of the NH_3, NH_4, HNO_3, NO_3, and SO_2, while Colorado sources contributed 20% and 40% of the SO_4 and NO_x, respectively. During the summer, the relative Colorado source contributions were similar to those in the spring, except for NO_3, which had a summer Colorado contribution of ~20 % compared to ~50% during the spring, and for NO_x, which had a summer Colorado contribution of about ~70%, compared to ~40% during the spring.

Nitrogen Deposition Apportionment

The hybrid-receptor model explicitly incorporated atmospheric diffusion and emission processes and is more suited for estimating source contributions from smaller source regions and shorter time periods than the TrMB model. Therefore, this method was used to apportion the source contributions to ambient concentrations as well as dry and wet deposition, and these are considered the highest quality source attribution results from this study. The hybrid model was used to apportion ambient concentrations, which were converted to dry deposition rates by multiplying by the average estimated deposition velocity for each N species. The source contributions to wet deposition rates were estimated by multiplying the relative source apportionment results of the ambient N species by the wet deposition fluxes during precipitation events. The source contributions on precipitation days can be quite different from nonprecipitating days, leading to different source apportionment budgets for dry- and wet-deposited species.

The apportionment of the dry- and wet-deposited N species during the spring and summer RoMANS periods to Colorado and non-Colorado source regions are presented in Figures S.14

and S.15. The "Local" source region approximately encompasses RMNP, but excludes Estes Park, and is interpreted as coming from naturally occurring emissions within RMNP. Contributions from all modeled source regions in North America not explicitly defined were grouped into the "Other Non-CO" source region and are interpreted as a background value.

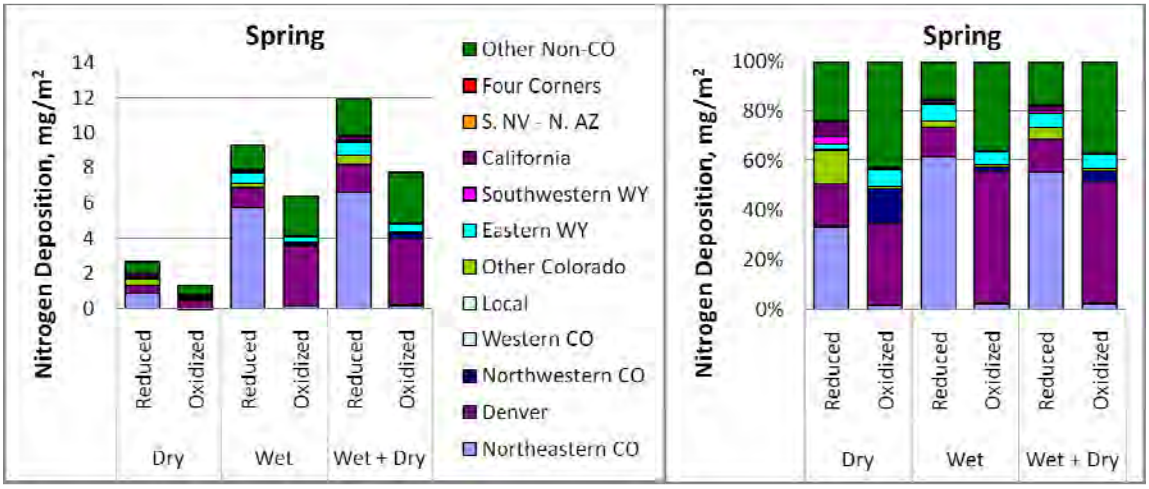

Figure S.14. RoMANS spring source apportionment of dry and wet N deposition. The contributions from NH_3 and NH_4 were combined into an inorganic, reduced N deposition category and contributions from particulate NO_3 and HNO_3 were combined into an inorganic, oxidized N deposition category. The left panel presents the absolute source contributions while the right panel presents the relative source contributions.

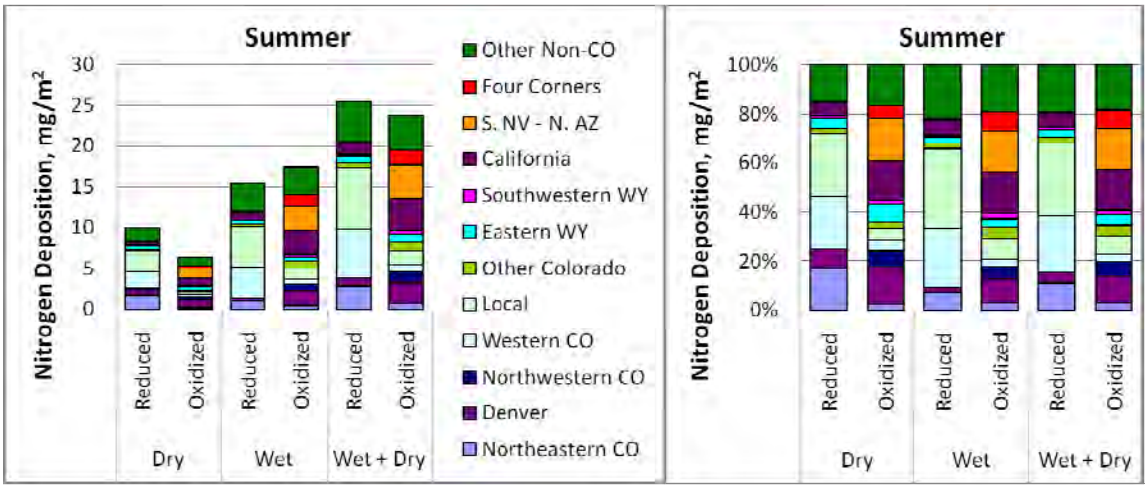

Figure S.15. RoMANS summer source apportionment of dry and wet N deposition. The contributions from NH_3 and NH_4 were combined into an inorganic, reduced N deposition category and contributions from particulate NO_3 and HNO_3 were combined into an inorganic, oxidized N deposition category.

NH_3 and NH_4 both originate primarily from NH_3 emissions and were combined into a reduced, inorganic N deposition (RIND) category. Similarly, particulate NO_3 and HNO_3 both originate from NO_x emissions and were combined into an oxidized, inorganic N deposition (OIND) category. NO_x has negligible contributions to total N deposition and was not included in the analysis. Organic N does have a significant contribution to N deposition, but the information to

apportion source contributions to organic N was not available and was also not included in the analysis.

Reduced, Inorganic Nitrogen (Ammonia/Ammonium) Deposition Source Attribution

As shown in Figure S.14, about 65% of the spring dry RIND is estimated to originate from sources within the state of Colorado. The single largest contributor to dry RIND was northeastern Colorado at about 35%, followed by the Denver-Front Range region at 15%. Northeastern Colorado is an area of high NH_3 emissions due to intense agricultural activities, while the Denver-Front Range region has high NH_3 emissions from mobile and other area sources. The periods of highest springtime dry RIND were associated with upslope flow. During these events, 80% of the dry RIND was estimated to come from northeastern Colorado and Denver.

The source contributions to the summer, dry RIND are more diverse than during spring. In total, about 75% of the summer, dry RIND is estimated to be due to Colorado sources, with the largest contribution from the local region at about 25%. Sources east of RMNP, including Denver and northeastern Colorado, and sources west of RMNP each contributed about 25% of the dry RIND. Outside of Colorado, eastern Wyoming and California were both estimated to contribute about 5% to the dry RIND. Consistent with the back trajectory analyses, the NH_4 had proportionately higher contributions from more distant sources than NH_3, including sources west of the Continental Divide from Colorado to California.

During the spring time period, wet deposition was dominated by one synoptic-scale precipitation event that occurred over several days. This precipitation event corresponded to upslope transport from east-northeastern Colorado. Consequently, the largest contributor to the wet RIND was northeastern Colorado at about 60%, followed by the Denver-Front Range region at about 10%. Overall, about 75% of the wet RIND is estimated to come from Colorado sources. Outside of Colorado, eastern Wyoming was the largest contributor at a little more than 5%.

Precipitation occurred nearly every day during the summer period and was associated with varied transport, leading to a more diverse set of source contributions. Colorado sources accounted for about 70% of the wet RIND, with the local source region being the largest contributor at about a third. Western Colorado was the second largest contributor at about 25%. Northeastern Colorado and California were smaller contributors at about 7%.

These wet deposition results possibly underestimate the relative contributions of sources east of RMNP. A few of the days prior to initial valid summer data collection and a few of the days after the study ended had two of the largest precipitation and wet deposition events. Both of these events were associated with upslope transport, with back trajectories showing prior transport over northeastern Colorado and the Front Range. In addition, comparison of the MM5 meteorological data used in the modeling to the measured upper air data near RMNP showed that MM5 underestimated the frequency of easterly transport near the surface. Transport of material from the east into RMNP in a surface layer could be an important source of dry- and wet-deposited N, based on the strong east-west gradients in both oxidized and reduced N species observed during RoMANS.

Overall, the total wet plus dry RIND apportionment is similar to the wet deposition attribution for both seasons, with 70–75% attributed to Colorado sources. During the spring, sources east of RMNP were the largest contributors, with northeastern Colorado and Denver contributing about

55% and 15%, respectively. During the summer, the local and western Colorado regions were the largest contributors at about 30% and 25%, respectively. Northeastern Colorado accounted for about 10%, and all other source regions were estimated to contribution less than 10%.

Oxidized, Inorganic Nitrogen (Nitric Acid/Particulate Nitrate) Deposition Source Attribution

Dry OIND, which was due primarily to HNO_3, was the smallest contributor to N deposition at 8–9% during the spring and summer (Figure S.8). As shown in Figure S.14, about 50% of the spring dry OIND was due to Colorado sources. The Denver-Front Range region is an area of high NO_x emissions due to mobile and point sources and was the largest contributor at about a third. Northwestern Colorado was the second largest contributor at about 15%. The NO_x emissions in the northwestern Colorado region are primarily due to the Craig and Hayden coal-fired power plants. Two types of spring, dry-deposited, oxidized N episodes occurred. One was associated with upslope transport where Denver was the largest contributor and the second was associated with transport from the southwest, with California, southern Nevada, and northern Arizona having the largest contributions. This southwestern region is an area of high NO_x emissions from large urban centers and a number of large, coal-fired power plants.

The summer apportionment of dry OIND had a somewhat different picture, with a number of sources having contributions of 5% to 15% and Colorado sources contributing only about a third. On average, sources west of the Continental Divide were responsible for most of the dry OIND, with the California and southern Nevada-northern Arizona regions each contributing about 15%, while western Colorado sources contributed about 10%. To the east of RMNP, Denver contributed about 15%, and NO_x sources in eastern Wyoming contributed about 7%.

Wet OIND contributed about a quarter of the total N deposition budget during both spring and summer. Over 50% of the spring, wet OIND was estimated to be due to Denver sources, with a negligible contribution from northeastern Colorado. Eastern Wyoming was the next largest defined source region contributing to about 5% of the spring, wet OIND, while ~35% was due to a diverse set of sources outside of Colorado. During the summer period, about 40% of the wet OIND was from southwestern sources, including California, southern Nevada-northern Arizona, and the Four Corners regions. The Four Corners region has high NO_x emissions from coal-fired power plants and extensive oil and gas developments. Denver was the largest Colorado source region in summer at about 10%, with 25% from other Colorado sources.

Overall, Colorado sources contributed approximately 55% and 35% of the total wet plus dry OIND during the spring and summer periods, respectively. The apportionment of the total wet plus dry OIND to individual source regions is similar to the wet deposition attribution for both seasons. This is due to the larger contributions from the wet OIND compared to the dry deposition.

How Applicable are RoMANS Results to Other Years and Other Times of the Year?

The source attribution and N deposition results from the RoMANS study are based on about 10 weeks during 2006, leaving a question as to how representative these results are for the average N deposition source attribution at RMNP. In other words, are the RoMANS study source attribution results similar to or dramatically different from those expected for other years and

other times of the year? In order to address this question, the measured ambient and wet deposition data, precipitation rates, and air parcel transport patterns during the RoMANS field campaigns were compared to historical values.

As shown in Figure S.1, the N deposition rates of typically measured species can vary by an order of magnitude, depending on the month of the year. The two RoMANS field campaigns were selected to occur during the high-N-deposition, spring and summer periods, and the measured inorganic N deposition during these 10 weeks accounts for about a third of the total measured N deposition in a typical year. At Loch Vale, Colorado, the average wet-deposited, inorganic N, during the same weeks of the year as the RoMANS study, from 2000 to 2005 is ~0.95 kg N/ha/yr, which is almost two-thirds of the recently established critical load for inorganic N wet deposition in RMNP of 1.5 kg N/ha/yr. Consequently, a significant portion of annual N deposition occurs during the same weeks of the year as the RoMANS study periods and this deposition represents a significant portion of the critical load.

The high N deposition rates that historically occur during the spring and summer also occurred during the RoMANS study period. During the summer field campaign, the ambient concentrations of N species were similar to average values for past years. However, precipitation had high spatial variability leading to spatially variable wet deposition rates. In RMNP at Beaver Meadows, the wet deposition concentrations were very low compared to historical averages, but the higher altitude site at Loch Vale had wet deposition concentrations similar to the historical averages. During the RoMANS spring campaign, the ambient concentrations of the N species and their peak values, as well as the precipitation rates and frequencies, were low compared to past years. The low precipitation rates led to low wet deposition rates; however, when precipitation did occur, the wet deposition concentrations were similar to past years.

Air parcel transport is one of the most influential meteorological processes affecting the N species concentrations and deposition because it determines which potential source regions are upwind of RMNP. The transport patterns were examined using the 5-day, EDAS back trajectories from 2000 through 2007 in a residence time analysis. All other things being the same, a source region's potential to contribute to N deposition at a receptor site, e.g., RMNP, increases for time periods when air parcels frequently pass over and spend more time, i.e., have higher residence time, over the source region prior to transport to RMNP. Therefore, if the trajectory residence times for the study period are similar to other years and other time periods, it can be expected that sources contributing to N deposition during the study are representative or typical of other years. This analysis differs from the differential probability (DP) residence time analysis used in Figure S.12. In Figure S.12 the DP analysis is used to help identify potential source regions contributing to the various N species, while the following analysis uses residence time to identify transport pathways.

The N-deposition-weighted residence time plots for the 2006 RoMANS study period and all days of the year from 2000 to 2007 are presented in Figure S.16. These residence time plots are strongly influenced by the transport during precipitation events, since hours with precipitation tend to have the highest deposition rates. On average, transport to RMNP is predominately from the west. However, as shown in Figure S.16, over the course of a typical year, N deposition at RMNP is associated with air parcel transport both from the west and the east. To the west of RMNP the N deposition is associated with air parcel transport from the southwest from southern Utah to northwestern Colorado to RMNP, and from the northwest from southern Idaho through

northern Utah and southwestern Wyoming to RMNP. To the east of RMNP, the N deposition is associated with transport from the northeast from the Dakotas through Nebraska and northeastern Colorado and from the southeast from Kansas.

The N-deposition-weighted residence time for only the 2006 RoMANS study period shows similar transport patterns to the historical average, with high residence time both east and west of RMNP. Also, the common transport pathway from the southwest is well represented and transport from the northeast occurred during RoMANS. Transport over southern Idaho and Kansas also occurred, though less frequently than on average. One important difference is that it appears that the 2006 RoMANS period had less transport from northeastern Colorado than seen on average, an indication that the contributions from this region may have been underestimated compared to other years.

Overall, during the RoMANS study period, a number of the important transport pathways, precipitation events, and N species ambient concentration and wet deposition events were captured within the field campaigns. As shown in Figure S.16, the RoMANS source attribution results imply that sources to the east of RMNP in the Denver-Front Range and northeastern Colorado regions are important contributors as are sources in western Colorado and from the southwest including California, southern Nevada, and the Four Corners region. Although the mix of sources impacting RMNP over a particular year may be different than those during the RoMANS study period, the analysis of air quality data and air parcel transport supports the notion that there will likely be broad similarities in the most important contributing source regions, and the general source attribution results from the RoMANS study are applicable to other years and other times of the years beyond the 10-week RoMANS study period.

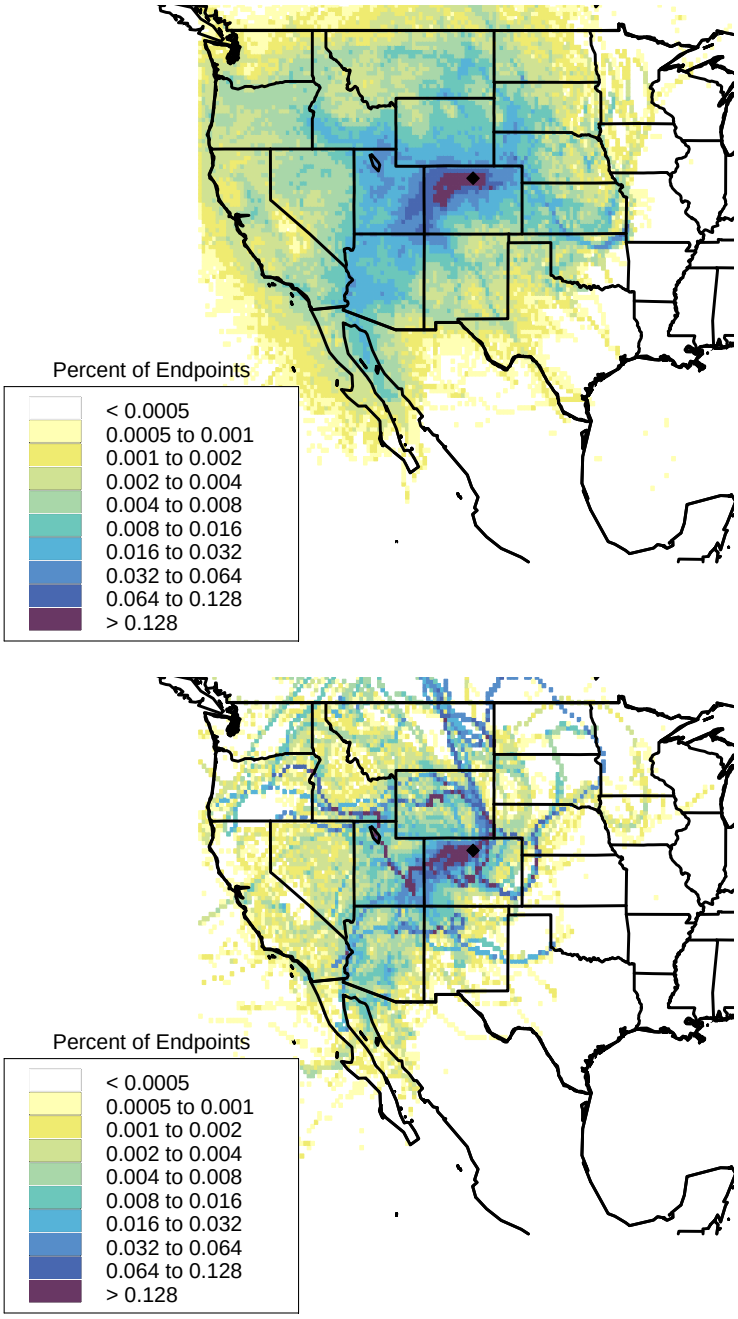

Figure S.16. Total measured N-deposition-rate-weighted residence time analysis for all days of the year in 2000 to 2007 (top) and during the 2006 RoMANS study period (bottom).

The Final Total Inorganic Nitrogen Deposition Apportionment Budget

During the spring time period, source areas responsible for most of the inorganic N deposition were northeastern Colorado and the Denver-Front Range area at about 40% and 25%, respectively. During the summer the source regions were more varied, with 25% of deposition associated with southwesterly transport and the associated source regions. Twenty per cent of

inorganic N deposition was linked to local source areas, with western Colorado contributing about 13%. The Denver area contributed another 8%.

The average source apportionment budget for total inorganic N deposition, wet plus dry and spring plus summer, between in-state versus out of state, was predicted to be about 55:45. The source area deposition budget for total deposition is shown in Figure S.17. The total inorganic N deposition is spread nearly evenly between transport from Denver, western and northeastern Colorado, local sources, and the southwest, which includes California plus southern Nevada and the Four Corners region. Although the RoMANS study period was only 10 weeks in 2006, analyses of airmass transport patterns and air quality data indicate that there should be broad similarities in the RoMANS N deposition source attribution results compared to those for a typical year.

The source attribution results indicate that roughly half of the N deposition in RMNP originates from sources east of RMNP and half from sources west of RMNP; however, the mechanism causing the deposition from east and west sources are quite different. In general, emissions of N compounds west of RMNP are low or distant from the park, but airmass transport to RMNP is persistently from the west. This leads to a diverse set of westerly sources that continually contribute low levels of N to RMNP's ecosystems. The high frequency of low rates of N deposition results in a high contributions of N over the study period.

To the east of RMNP are a number of high N emission regions including the nearby Front Range and the agriculturally intensive northeastern Colorado. The upslope easterly airmass transport is relatively infrequent; however, when it does occur, RMNP often experiences its highest ambient N concentrations. In addition, upslope transport is more frequently associated with precipitation at higher rates compared to westerly transport, causing high N deposition rates in RMNP. The less frequent but high rate of N deposition associated with sources east of RMNP leads to the high N contributions from these sources during the study period.

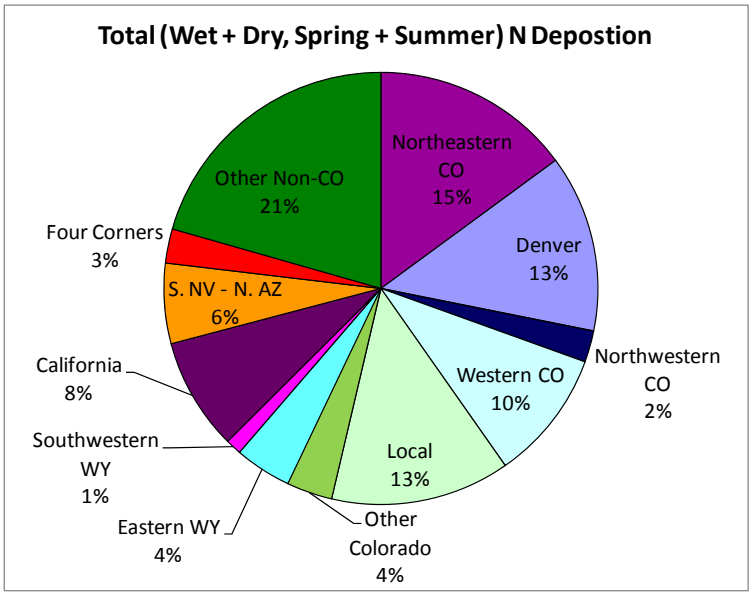

Figure S.17. The contributions of source regions to the total inorganic N deposition from both dry and wet processes, measured at RMNP during the spring and summer RoMANS campaigns.

Chapter 1. Introduction and Study Objectives

Both sulfur and nitrogen are chemicals that are essential nutrients for life. In some ecosystems, a limited supply of sulfur and nitrogen restricts biological activity. In fact, sulfur and nitrogen products are often applied as fertilizer to maintain high crop productivity. In excess, however, sulfur and nitrogen can be toxic, even life threatening, and in national parks excess nitrogen and sulfur can upset the delicate balances in natural ecosystems. Nitrogen and sulfur species can cause rain and snowfall to be acidic, and sulfate (SO_4^{-2}) and nitrate (NO_3^-) particles can cause significant visibility impairment.

Human activity has substantially enhanced rates of nitrogen fixation on land (Smil, 1990; Vitousek and Matson, 1993; Ayers et al., 1994; Galloway et al., 1995). Combustion of fossil fuels, production of nitrogen fertilizers, cultivation of nitrogen-fixing legumes, and other actions have been identified as major sources altering the global nitrogen cycle (Galloway et al., 1995). Wet and dry deposition of ammonia (NH_3) and atmospheric oxidation products of nitrogen oxides produced by combustion processes represent significant nitrogen inputs in many environments.

Wet and dry deposition of several inorganic nitrogen species are measured at numerous locations in the United States by the National Atmospheric Deposition Program (NADP, http://nadp.sws.uiuc.edu) and the Clean Air Status and Trends Network (CASTNet, http://www.epa.gov/castnet). One region receiving increasing attention, due to the sensitive nature of its high-elevation ecosystems, is the Rocky Mountain West. Atmospheric nitrogen deposition to the Rocky Mountain region of Colorado and southern Wyoming, measured during 1995–1999, ranged from 1 to 7 kg/ha/yr (Burns, 2003). Within Rocky Mountain National Park (RMNP), an area of particular interest, wet deposition of inorganic nitrogen (nitrate and ammonium) currently contributes approximately 3 kg/ha/yr to total nitrogen input. Dry deposition of nitric acid (HNO_3) and particulate nitrate and ammonium (NH_4^+) increases total measured nitrogen deposition to approximately 4 kg/ha/yr. These current nitrogen deposition flux values appear to represent approximately a 20-fold increase above pre-industrial values for the western United States (Galloway et al., 1982, 1995; Hedin et al., 1995).

Increased deposition of nitrogen in RMNP has been demonstrated to contribute to a number of important ecosystem changes (see Blett and Morris, 2004, for a review). Among these are changes in the chemistry of old-growth Engelmann spruce forests (Rueth and Baron, 2002), shifts in population of lake diatoms (Baron et al., 2000), excess nitrogen leakage into lakes and streams at certain times of the year (Campbell et al., 2000), and alterations in biogeochemical cycling associated with increased microbial activity in high elevation soils and talus (Campbell et al., 2000, 2002; Rueth and Baron, 2002). Several of these effects have been noted mainly on the east side of the Continental Divide that runs through RMNP. Nitrogen deposition levels have also been determined to be higher on the eastern slope of the park (Burns, 2003).

The rate of deposition of nitrogen compounds in RMNP has crossed a crucial threshold called the "critical load." This means that changes are occurring to park ecosystems and that these changes may soon reach a point where they are difficult or impossible to reverse. Soils, waters, and aquatic plants are showing evidence of change from wet deposition of nitrogen species in rain and snow and dry deposition of nitrogen-containing particles and gases. Excess deposition

of nitrogen, although a fertilizer, creates an imbalance in natural ecosystems. It also acts as an acidifying agent in water and soil, leaving these resources vulnerable to future acidification effects on fish and forests. The park has set a resource-management goal for a critical input load of 1.5 kg/ha/yr of wet nitrogen deposition, a level considered protective of park ecosystems. Achieving this target will necessitate approximately a 50% reduction in wet nitrogen deposition from current levels. With growing evidence of increases in nitrogen deposition and its impacts, a cooperative effort between the National Park Service (NPS), the U.S. Environmental Protection Agency (EPA), and the state of Colorado recently resulted in the establishment of a nitrogen deposition reduction plan for RMNP.

Atmospheric particles containing sulfur and nitrogen are also contributors to visibility-degrading haze that frequently forms in RMNP. Visibility is impaired to some degree in the park 90% of the time. Viewing distances in summer average 83 miles but can drop to 30 miles on high pollution days.

Although much has been learned about reactive nitrogen and sulfur concentrations and deposition in RMNP and their effects on ecosystems and visibility, several key issues need further attention if we are to develop an effective strategy for protecting park resources from adverse impacts of elevated nitrogen deposition. These include determining the importance of previously unquantified nitrogen inputs within the park and identification of important nitrogen sources and transport pathways.

Routine measurements of nitrogen deposition fluxes in RMNP include neither quantification of dry and wet inputs of organic nitrogen species nor dry deposition inputs of ammonia. Previous studies in western Colorado and in the Colorado Front Range suggest that approximately 20% of total nitrogen wet deposition was associated with organic nitrogen (Williams et al., 2001; Sickman et al., 2001). Although measurements of gas-phase ammonia in the region are rare, the substantial contribution of ammonium to wet nitrogen deposition (ammonium and nitrate contributions are currently similar) suggests that dry deposition of ammonia should not be ignored.

While prevailing winds in RMNP are usually from the west, transport patterns in the region can be complex. Transport of air masses from the east can occur, for example, in conjunction with radiatively driven upslope/downslope wind patterns, especially in summer. Larger-scale pressure gradients also periodically produce upslope transport from the east that can result in significant precipitation along the eastern slope of RMNP. Periods of transport from the east are of particular interest because of large NO_x ($NO+NO_2$) emissions from population centers and large NH_3 emissions from agricultural regions east of RMNP. Routine RMNP wet and dry deposition fluxes are both determined at weekly time resolutions, while changes in transport patterns often occur on much shorter time scales; therefore it is difficult to use these measurements to identify key regions and source types that may contribute the most to increasing levels of RMNP nitrogen deposition.

1.1. SOURCES AND PREVIOUS OBSERVATIONS OF ATMOSPHERIC SULFUR- AND NITROGEN-CONTAINING POLLUTANTS AND THEIR DRY DEPOSITION

Decreases in nitrogen-containing pollutants in RMNP are needed to protect sensitive park resources from excess nitrogen inputs, while decreases in both nitrogen and sulfur-containing pollutants would reduce the haze that impacts the park's scenic vistas. Effective strategies for controlling nitrogen and sulfur-containing pollutant levels in the park can best be formulated with an accurate understanding of the sources of these pollutants and knowledge about how they are transported into this pristine environment.

Figure 1.1 is a simplified schematic diagram of chemical processes involved in atmospheric processing of nitrogen and sulfur emissions into molecules affecting visibility, ecosystems, materials, and/or human health. Volatile hydrocarbon emissions, both natural and anthropogenic, react with NO_x emissions to form a variety of oxidizing gases such as ozone. These oxidants react with sulfur dioxide (SO_2) and ammonia gas, through wet or dry physico-chemical processes, to form ammoniated particles or droplets of ammonium, sulfate, and hydrogen ions (H^+). Particles affect visibility while deposition of sulfur in all its chemical forms can affect an ecosystem either through acidification or sulfur enrichment.

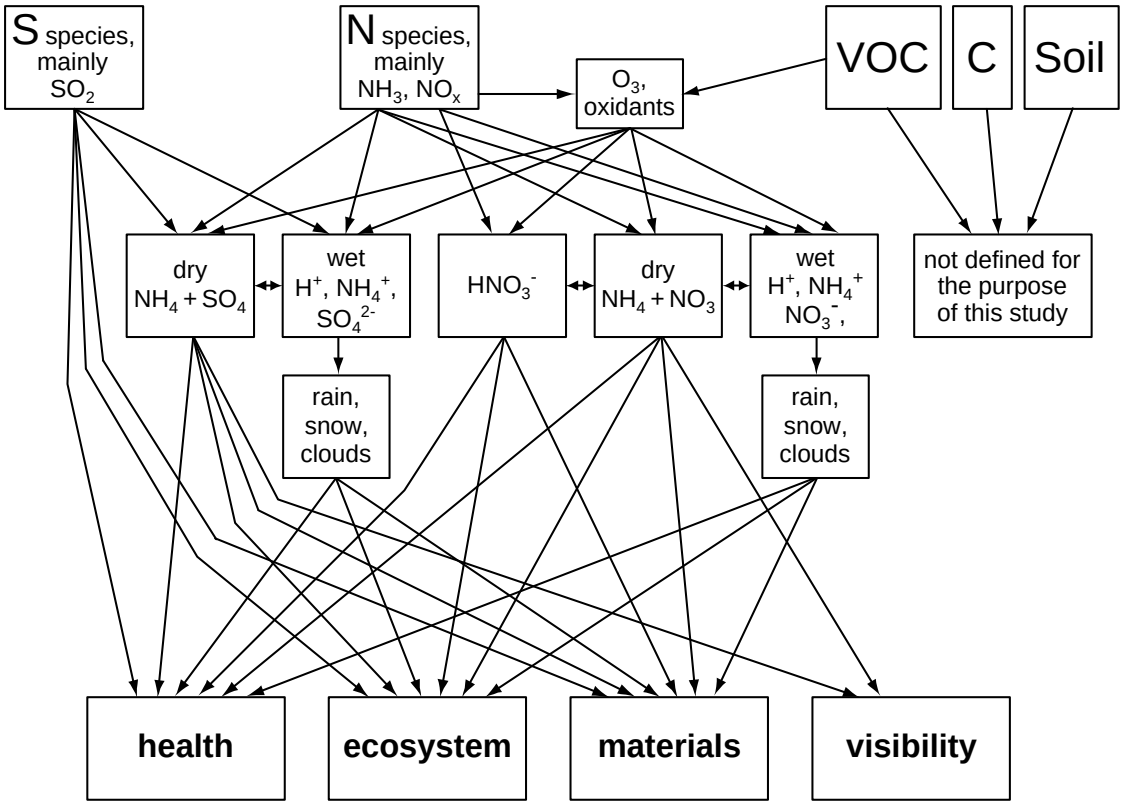

Figure 1.1. Schematic of chemical processes associated with nitrogen and sulfur species that lead to aerosol formation and deposition.

Similar mechanisms are involved with nitrogen emissions. Oxidants react with NO_x emissions to form nitric acid vapor, which can react to form other chemical species in the atmosphere or can

deposit and either contribute to acidification, expand the nitrogen nutrient load, or release elements toxic to the ecosystem. Through wet or dry processes, NO_x is formed into ammonium nitrate particles or droplets of ammonium and nitrate and hydrogen ions. These compounds are then available as nutrients to aquatic and terrestrial ecosystems. Because nitrogen is commonly a growth-limiting nutrient in streams and lakes, increased concentrations can lead to eutrophication, followed by depletion of oxygen in surface water as algae die off and decompose. It is these processes that are of primary concern in RMNP.

Ambient levels of particulate sulfate, nitrate, and ammonium cause visibility impairment. Particulate nitrate, ammonium, and sulfate also contribute to nitrogen and sulfur deposition, although as will be discussed below, their contributions in RMNP tend to be small compared to wet deposition of the same species or dry deposition of gas-phase counterparts, including gaseous nitric acid, ammonia, and sulfur dioxide. Historical data are most readily available, however, for concentrations of particulate nitrate and sulfate, making this a useful place to begin an assessment of historical observations of nitrogen and sulfur containing atmospheric pollutants.

Figure 1.2 shows an isopleth map of fine particulate sulfate concentrations interpreted as ammonium sulfate ($(NH_4)_2SO_4 = 1.375 * SO_4^{-2}$) from the Interagency Monitoring of PROtected Visual Environments (IMPROVE) program (Malm et al., 1994). Sulfates are primarily a product of SO_2 emissions and photochemical reactions in the atmosphere. The highest sulfate mass concentrations are found in the eastern United States where concentrations are spatially uniform at about 5.0 $\mu g/m^3$. Sulfate concentrations decrease to the northeast, southeast, and west. The central western United States, including RMNP, has annual average sulfate concentrations that are for the most part less than 1.0 $\mu g/m^3$, while in an area consisting of northern California, Nevada, Oregon, Idaho, and western Montana the sulfate concentrations are near 0.5 $\mu g/m^3$. Generally, southern Arizona and California and western Washington have sulfate concentrations between 1.0 and 2.0 $\mu g/m^3$.

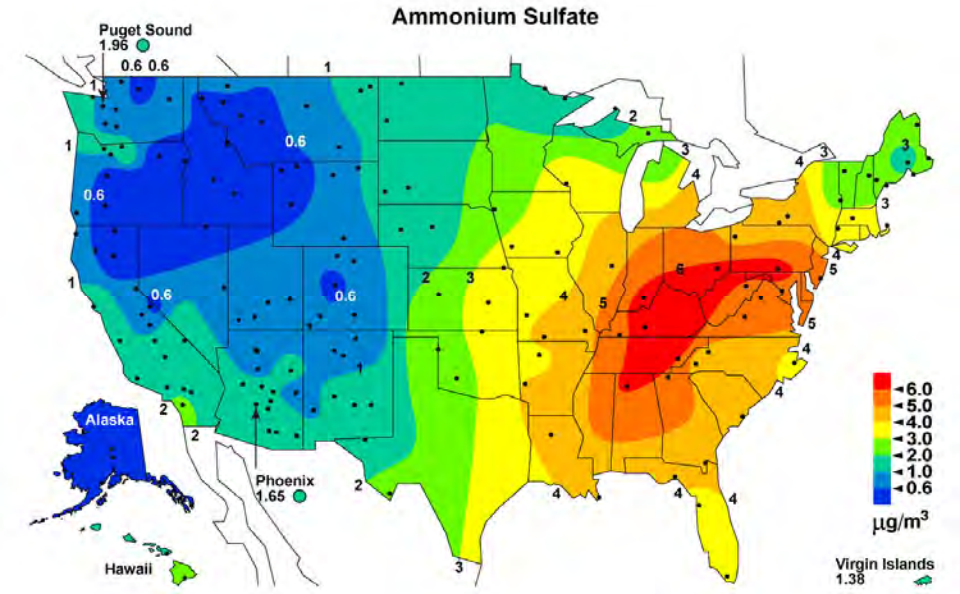

Figure 1.2. Isopleths of average fine particle sulfate (interpreted as ammonium sulfate, $\mu g/m^3$) concentrations from 2000 to 2004 in the United States.

Seasonally, sulfate concentrations tend to be higher during the summer months (June, July, and August) in almost all regions of the country. The ratio of the highest to lowest monthly sulfate concentrations varies from about 2 to3 in most of the United States, with regions along the western seaboard having ratios from 5 to10. On a fractional basis, contributions of sulfates to fine mass in most of the western United States are between 20% and 40%, with a few months near 50%. The sulfate mass fraction tends to peak during the winter months throughout the Rocky Mountains and the Great Basin.

The annual nitrate concentrations (interpreted as ammonium nitrate) from the IMPROVE program are presented in Figure 1.3. Not surprisingly, fine nitrate concentrations tend to be highest around central and southern California and the Midwest where ammonia and nitrogen oxide emissions are greatest. In the West, southern California has the highest nitrate concentration levels, exceeding 2.0 µg/m^3, while RMNP has annual average concentrations of about 0.5 µg/m^3. The highest average fractional contributions of nitrate to fine mass at 48% and 39% occur in southern California at San Gabriel and the San Gorgonio Wilderness Area, respectively. Much of southern California has fractional contributions that exceed 20%, while northern California has fractional contributions that are near 5%. Most of the remaining West has nitrate fractional contributions in the 5–10% range, except for a narrow region extending from southern Idaho through Utah where the values are between 10% and 20%. The average nitrate contribution to fine particle mass at RMNP is on the order of 15%.

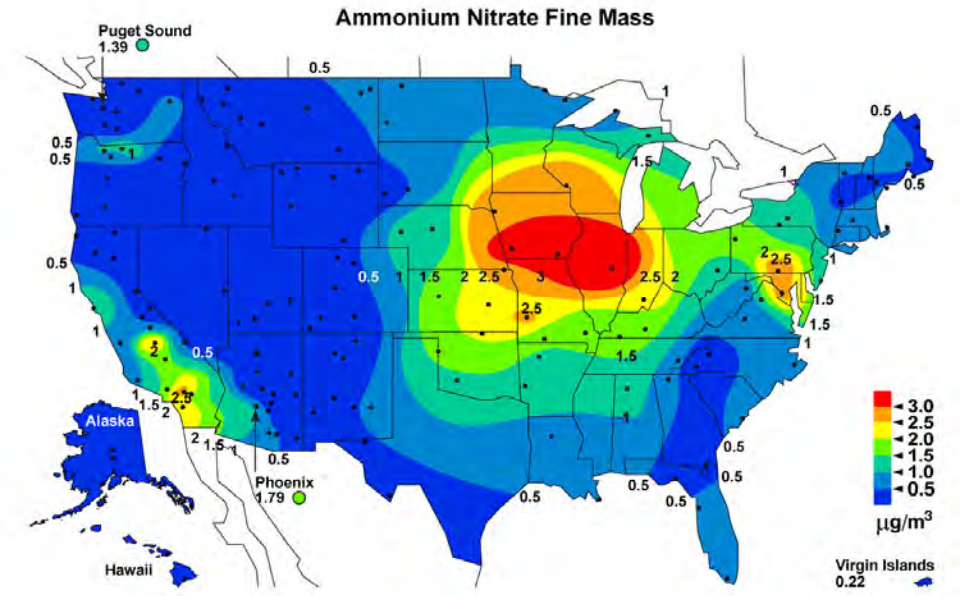

Figure 1.3. Isopleths of the average fine nitrate (interpreted as ammonium nitrate, µg/m^3) concentrations from 2000 to 2004 in the United States.

While sulfate concentrations tend to peak during the summer months, nitrate concentrations are highest during the winter season because the cooler winter season temperatures favor particulate nitrate formation. On a fractional basis, nitrates have their greatest contribution to fine mass during the winter months. The highest fractions of 40–50% nitrate contribution to fine mass occur in the Midwest and the southern California, California coastal, Sierra Nevada, Hells Canyon, and Columbia River Gorge regions. The lowest maximum fractional contributions of

about 10% or less occur in the Southeast, Great Basin, Alaskan, Hawaii, and Virgin Island regions.

Figure 1.4a shows the average winter 12-year fractional contribution of each fine particle species in RMNP. Nitrates and sulfates make up 19% and 35% of the fine mass, respectively. On many days, nitrates are about 50% of the fine mass as illustrated in Figure 1.4b, where on March 3, 2002, the fine particle nitrate mass concentration was 2.9 $\mu g/m^3$ and made up 44.5% of the fine mass.

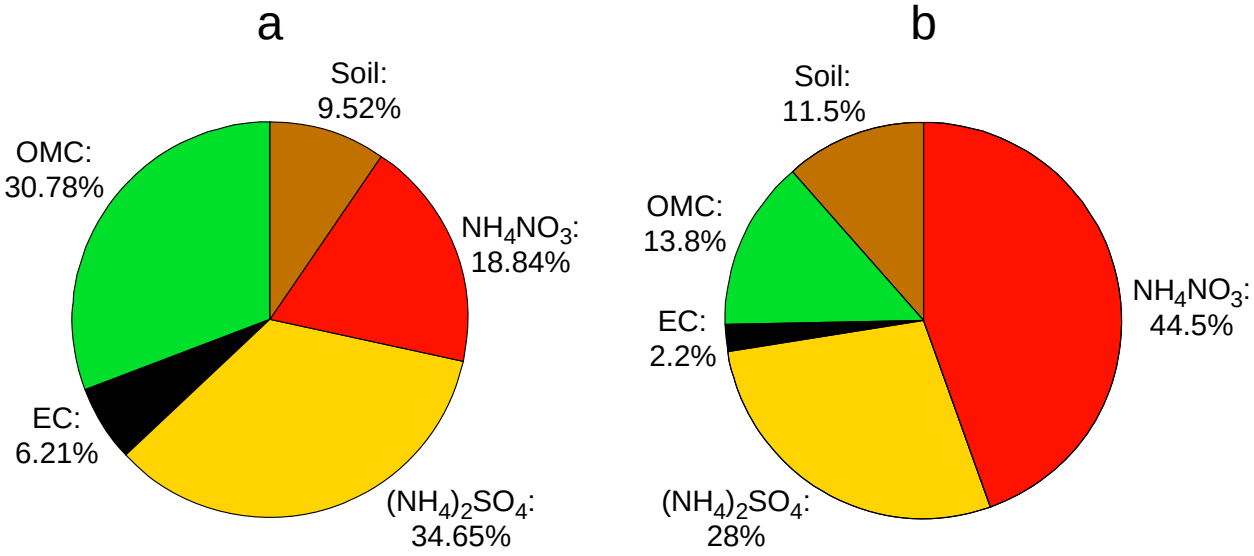

Figure 1.4. (a) Twelve-month-average winter fine particle mass composition in RMNP. (b) RMNP fine mass composition on March 3, 2002. Species included are ammonium nitrate, ammonium sulfate, elemental carbon (EC), organic matter (OMC), and fine particle soil.

Information on particulate nitrate from the IMPROVE program can be augmented with measurements of other species made by the Clean Air Status and Trends Network (CASTNet). The CASTNet program includes a site in RMNP that is collocated with the IMPROVE monitoring site. In addition to particulate nitrate and sulfate, the CASTNet program makes measurements of particulate ammonium, gas-phase nitric acid, and gas-phase sulfur dioxide. Measurements are made on a weekly average basis. The CASTNet program does not measure gas-phase ammonia.

The ambient nitrogen and sulfur budgets at RMNP are presented in Figure 1.5. As shown, the nitrogen (from fine particle NH_4^+ and NO_3^- and gas-phase HNO_3) and sulfur (from gaseous SO_2 and fine particle SO_4^{-2}) have similar monthly mean concentrations. Concentrations peak during the spring and summer months (May–August) at about 0.5 $\mu g/m^3$ and are the lowest during the fall and winter months (November–January), with concentrations between 0.2 and 0.3 $\mu g/m^3$. During the winter months, sulfate accounts for 35–50% of the total sulfur, but during the spring and summer months sulfate accounts for 55–62% of the total sulfur. NH_4^+ is the largest contributor to total measured nitrogen, accounting for about half during all months, while gaseous nitric acid accounts for 25–40% of the nitrogen, and particulate nitrate contributes only 10–25%. The contribution of particulate nitrate is likely underestimated due to volatilization of particulate nitrate from the Teflon filter used by CASTNet to collect particles. This volatilized

nitrate is captured on the nitric acid filter, resulting in overestimated nitric acid concentrations. In parallel with the nitric acid loss, one also expects some loss of ammonium (as ammonia) from volatilized ammonium nitrate.

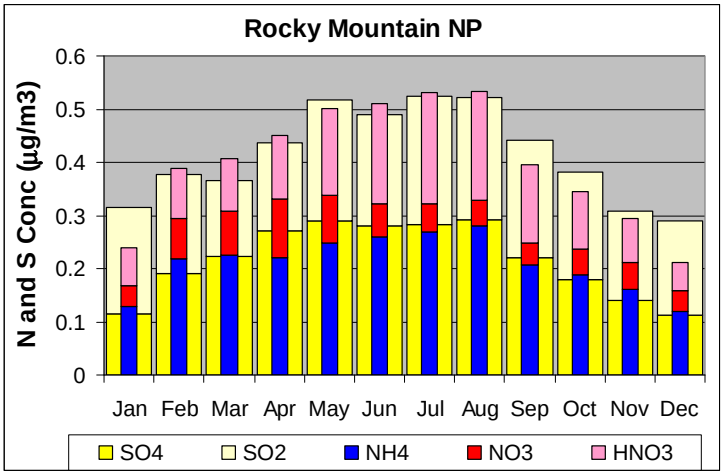

Figure 1.5. RMNP monthly average nitrogen and sulfur concentration budgets (µg/m^3), based on 2000–2004 CASTNet data.

Figure 1.6 presents sulfur and nitrogen dry deposition fluxes determined from the CASTNet measurements at RMNP. Dry deposition refers to the direct deposition of gas- and particle-phase species to the surface. As shown, nitrogen and sulfur dry deposition rates have similar seasonality as their ambient concentrations and peak in the spring and summer months. However, while the nitrogen and sulfur ambient concentrations are similar, the nitrogen dry deposition rates are 2–3 times larger than sulfur dry deposition rates. This is due to the high nitric acid deposition velocity relative to the other species, so that nitric acid accounts for 75–85% of the nitrogen deposition compared to 25–40% of the ambient nitrogen concentration. An analysis of the CASTNet historical data record for this period reveals that nitrogen and sulfur deposition episodes, defined as periods where deposition amounts exceed the 80th percentile of all observation periods, occur most frequently during the spring and summer months, with few episodes in the fall and winter months. In June and July, 60% of the samples had total nitrogen deposition fluxes above the annual 80th percentile.

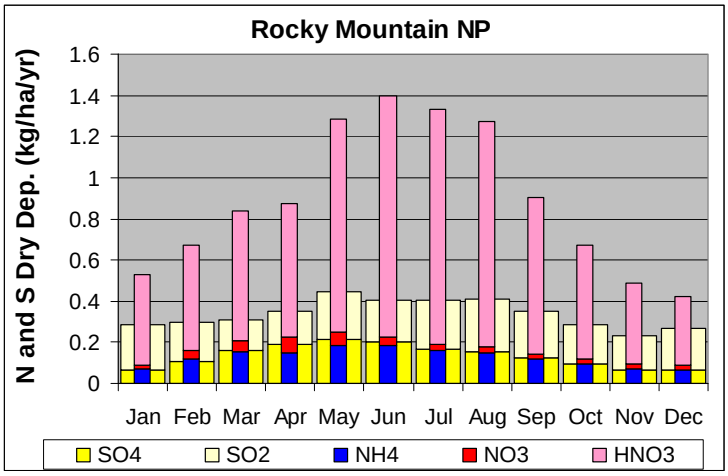

Figure 1.6. Monthly average nitrogen and sulfur dry deposition budgets (kg/ha/yr) based on CASTNet 2000–2004 observations.

1.2. WET DEPOSITION OF SULFUR AND NITROGEN IN RMNP AND THE WESTERN UNITED STATES

Wet deposition fluxes of nitrogen and sulfur species are determined by a variety of factors. These include the amount of precipitation, the availability of precursor particle and gas-phase species to be scavenged, and the efficiency of scavenging mechanisms. We provide here a brief overview of spatial variability of wet deposition in the western United States, including a look at historical data from RMNP.

Figure 1.7 shows sulfate wet deposition in the western United States for 2002 (left panel). Sulfate deposition throughout the western United States, including RMNP, is approximately 2 kg/ha, except around the urban areas in the northwestern United States. During the course of the 15-year time period from 1985 to 2000, sulfate ion concentrations in precipitation decreased dramatically in the eastern United States. In much of the western United States, sulfate concentrations have also decreased (see Figure 1.7, right panel) but at a rate that is approximately 5–10 times less than in the Northeast (Lehmann et al., 2005). Although sulfate deposition also decreased in RMNP over this time period, the rate is not statistically significant.

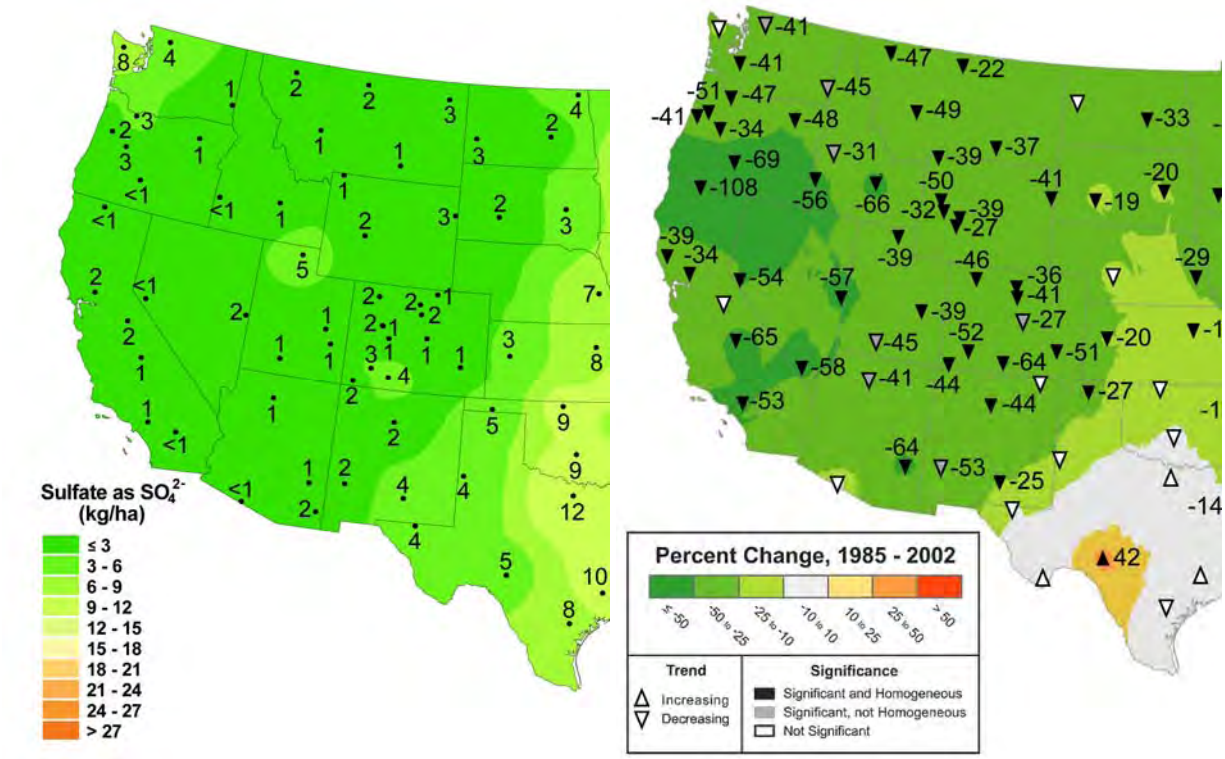

Figure 1.7. Left panel: Sulfate ion 2002 annual wet deposition rate in kg/ha (Source: National Acid Deposition Program/National Trends Network). Right panel: Percent change in the sulfate concentration in precipitation for the years 1985–2002 (Lehmann et al., 2005, reproduced without permission).

Figure 1.8 depicts maps of both 2002 annual average wet deposition of nitrate (left panel) and the percent change in nitrate concentration in precipitation for 1985–2002 (right panel, Lehmann et al., 2005). Nitrate deposition throughout the West is on the order of 2–4 kg/ha, while at RMNP it is 5 kg/ha. Furthermore, at many sites in the western United States, nitrate has a statistically significant rate of increasing nitrate ion concentration over the time period from 1985 to 2000.

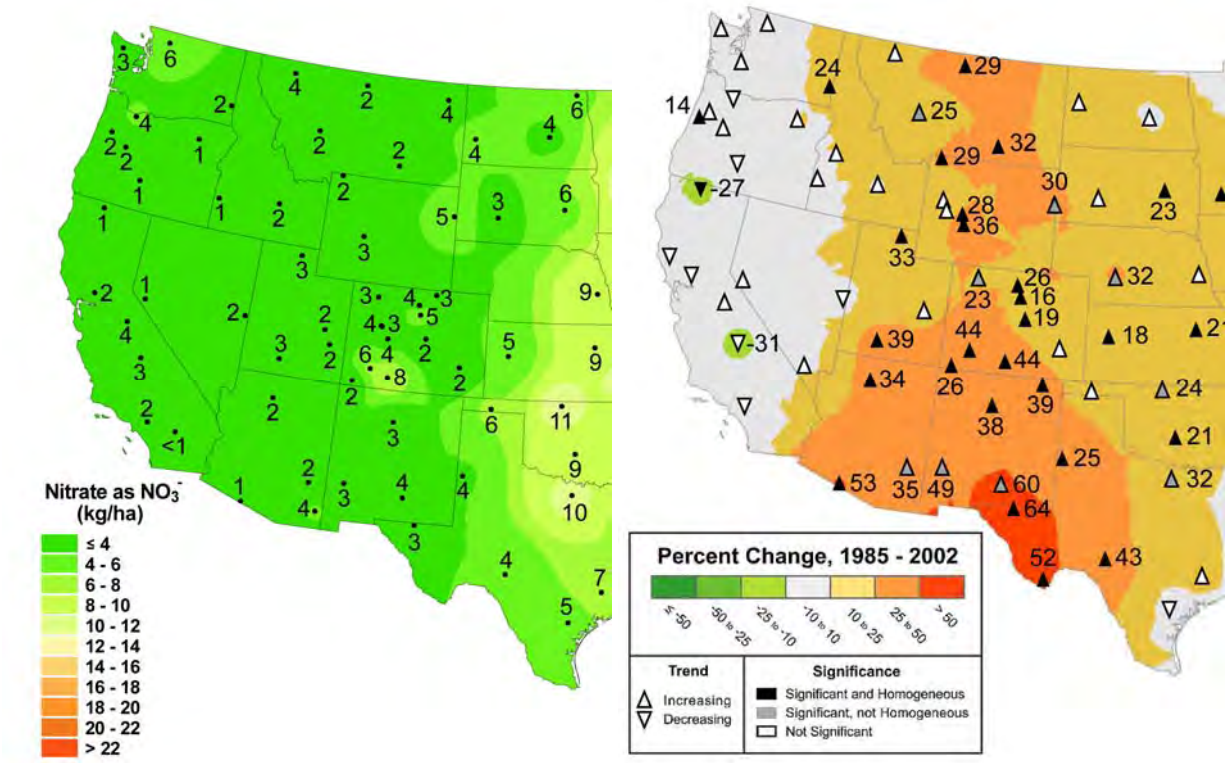

Figure 1.8. Left panel: Nitrate ion 2002 annual wet deposition in kg/ha (Source: National Acid Deposition Program/National Trends Network). Right panel: Percent change in the nitrate concentration in precipitation for the years 1985–2002 (Lehmann et al., 2005, reproduced without permission).

Figure 1.9 (left panel) shows annual wet deposition of ammonium for 2002. As might be expected, ammonium deposition is greatest in the Midwest where there is a high density of farming activities that include the raising of livestock and fertilizer application. The highest annual wet deposition fluxes of ammonium ion are on the order of 6–7 kg/ha, while in much of the Intermountain West the rate drops to less than 1.0 kg/ha. Generally speaking, the percent change in ammonium ion concentrations in precipitation, as shown in Figure 1.9 (right panel), are increasing throughout large areas of the United States (Lehmann et al., 2005).

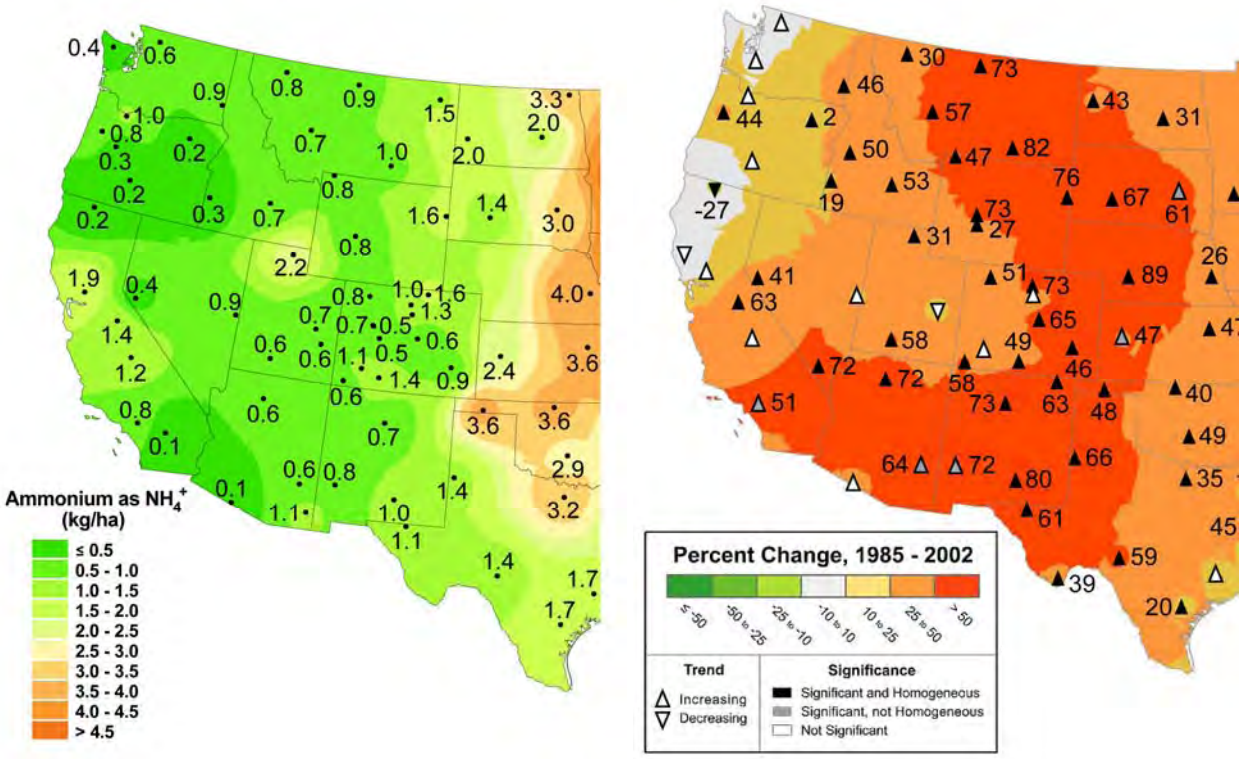

Figure 1.9. Left panel: Ammonium ion annual wet deposition for 2002 in kg/ha (Source: National Acid Deposition Program/National Trends Network). Right panel: Percent change in the ammonium concentration in precipitation for the years 1985–2002 (Lehmann et al., 2005, reproduced without permission).

Deposition of nitrogen and sulfur pollutant species in RMNP reflects the combined deposition of gas- and particle-phase species through dry and wet deposition processes. Atmospheric nitrogen deposition in the Rocky Mountain region of Colorado and southern Wyoming ranges from 1 to 7 kg/ha/yr (Burns, 2003) and may be even greater at high elevations (> 3500 m) in the Front Range. Atmospheric nitrogen deposition generally is greater east than west of the Continental Divide (Baron et al., 2000; Heuer et al., 2000), except in areas that are directly downwind of large power plants, such as the Buffalo Pass NADP site. Despite the prevailing west winds at this latitude, westward upslope movement of air masses with elevated concentrations of nitrogen from the Denver-Boulder-Fort Collins metropolitan area may be contributing to atmospheric deposition of nitrogen east of the divide. A tendency toward higher NH_4^+ concentrations in wet deposition at NADP sites east of the divide compared to west of the divide is evident.

Three NADP monitoring sites with increasing nitrogen trends (Baron et al., 2000; Burns, 2003), Loch Vale, Niwot Saddle, and Snowy Range, are at high elevations east of the divide in the Front Range. Because there is little to no trend of increasing wet deposition of nitrate at the Loch Vale site, the recent trend in nitrogen deposition is attributed mainly to increasing NH_4^+ concentrations in precipitation, whereas the trend at the Niwot Saddle site results equally from increasing precipitation and increasing concentrations of NO_3^- and NH_4^+ in precipitation.

While the effects of nitrogen and sulfur compounds on visibility and the park ecosystem have been documented, less is known about the origin of precursor sulfur and nitrogen species.

Nitrogen compounds (e.g., nitrogen oxides and ammonia) and sulfur compounds are emitted into the atmosphere by a variety of air pollution sources, including automobiles, power plants, industry, agriculture, and fires. Colorado's Front Range is an area of rapid population growth, escalating urbanization, oil and gas development, and agricultural production. Increases in these activities may be a factor contributing to increases in nitrogen deposition in RMNP, although pollutant emissions from the western slope, from agricultural activities on the eastern plains, and from outside Colorado probably contribute as well

1.3. PREVIOUS BACK-TRAJECTORY TRANSPORT MODELING AT RMNP

Bresch et al. (1986) first examined back trajectories associated with high sulfur concentrations at RMNP for 1979–1985. Using simple atmospheric transport and dispersion (ATAD) back trajectories generated by relatively coarse rawinsonde data, they found a predominantly westerly flow into the park, with southwesterly transport being more common than northwesterly. High sulfur concentrations occurred mostly during either spring or summer and were associated with air masses from southern California during the summer and from the Midwest during the spring. Air masses from the north, though more infrequent than westerlies, were also associated with high sulfur concentrations at the park. Nitrates were not examined and sulfur emissions in the western United States have changed substantially since that study.

A 1990 study (Malm et al., 1990) of the areas of influence of major sulfur sources in the western United States on several Class I areas during 1983–1985 again found that peak sulfur concentrations at RMNP were generally observed during the summer, with the lowest seasonal mean during the winter. They found varying influences on sulfur concentrations at RMNP from southern California, the Four Corners electric-generating stations, the Arizona copper smelters, the Texas Gulf coast, industry in the Salt Lake City region, and Mexico.

Gebhart and Malm (1991) again used ATAD back trajectories to examine sources of particulate sulfur and elemental and organic carbon at RMNP and other parks during 1984–1989. The upwind areas most frequently associated with high sulfur concentrations were again southern California and also areas in Mexico and Arizona, which at that time had high SO_2 emissions from metal smelting. High conditional probabilities (areas associated with high concentrations without regard to frequency) included a strip along the front range of the Canadian Rockies, with moderately high values also in Mexican smelter areas and the Colorado Front Range. High conditional probabilities for carbon were located in Alberta and Saskatchewan, with moderately high values in the Front Range of Colorado through Montana.

Results from all of these studies are dated and may not be applicable to recent years, especially for sulfur, because SO_2 emissions have changed substantially since the 1980s.

More recently, as part of the Causes of Haze Assessment (COHA) conducted by Desert Research Institute for the Western Regional Air Partnership (WRAP), the Central Regional Air Planning Association (CENRAP), and the EPA, both back-trajectory and deterministic air quality modeling were conducted to examine source attributions of sulfate and particulate light extinction in Class I areas, including RMNP for 2000–2002. COHA defined four source areas within each receptor’s state (northeast, northwest, southeast, and southwest of the site) and full neighboring states, then divided the rest of the United States into regions by directional

quadrants and considered Mexico, Canada, the Gulf of Mexico, Pacific coastal waters, and the Pacific Ocean. A quantitative back-trajectory regression technique, using HYSPLIT (HYbrid Single-Particle Lagrangian Integrated Trajectory) trajectories started at 500 m above ground, found that the largest five contributors to sulfate at RMNP were 1) the northwestern United States (Washington, Oregon, Montana, and Idaho), followed by 2) northwestern Colorado, 3) southeastern Colorado, 4) Arizona, and 5) the southwestern United States (California and Nevada). The exact relative contributions from each region depend on modeling details. The five largest contributors to aerosol light extinction obtained from the same technique are 1) the Pacific Ocean, 2) northwestern Colorado, 3) the northwestern United States, 4) the southwestern United States, and 5) southwestern Colorado.

1.4. DESCRIPTIVE METEOROLOGY OVERVIEW FOR RMNP

1.4.1. Overview of Important Transport Patterns and Climatology, Including Meteorology Associated with Different Precipitation Modes

Temperatures, wind patterns, and storm tracks in Colorado are heavily influenced by the state's complex topography as illustrated in Figure 1.10. The high plains of eastern Colorado, dissected by two major river valleys, the South Platte in the north and the Arkansas in the south, slope gently upward from the state's eastern border to the base of the foothills. At 5000–6000 ft (1500–1800 m) the plains abruptly turn to foothills with elevations of 7000–9000 ft (2100–2700 m). West of the foothills are mountain ranges above 9000 ft (2700 m) with the highest peaks over 14,000 ft (4300 m). West of these "front ranges" are additional ranges, generally extending north-south but with extensions in other directions. Farther west are high mesas, some more than 10,000 ft (3000 m) in elevation, extending to the western border. The mesas are often cut by rugged stream and river canyons. (Colorado State Climatologist; Doesken, et al., 2003).

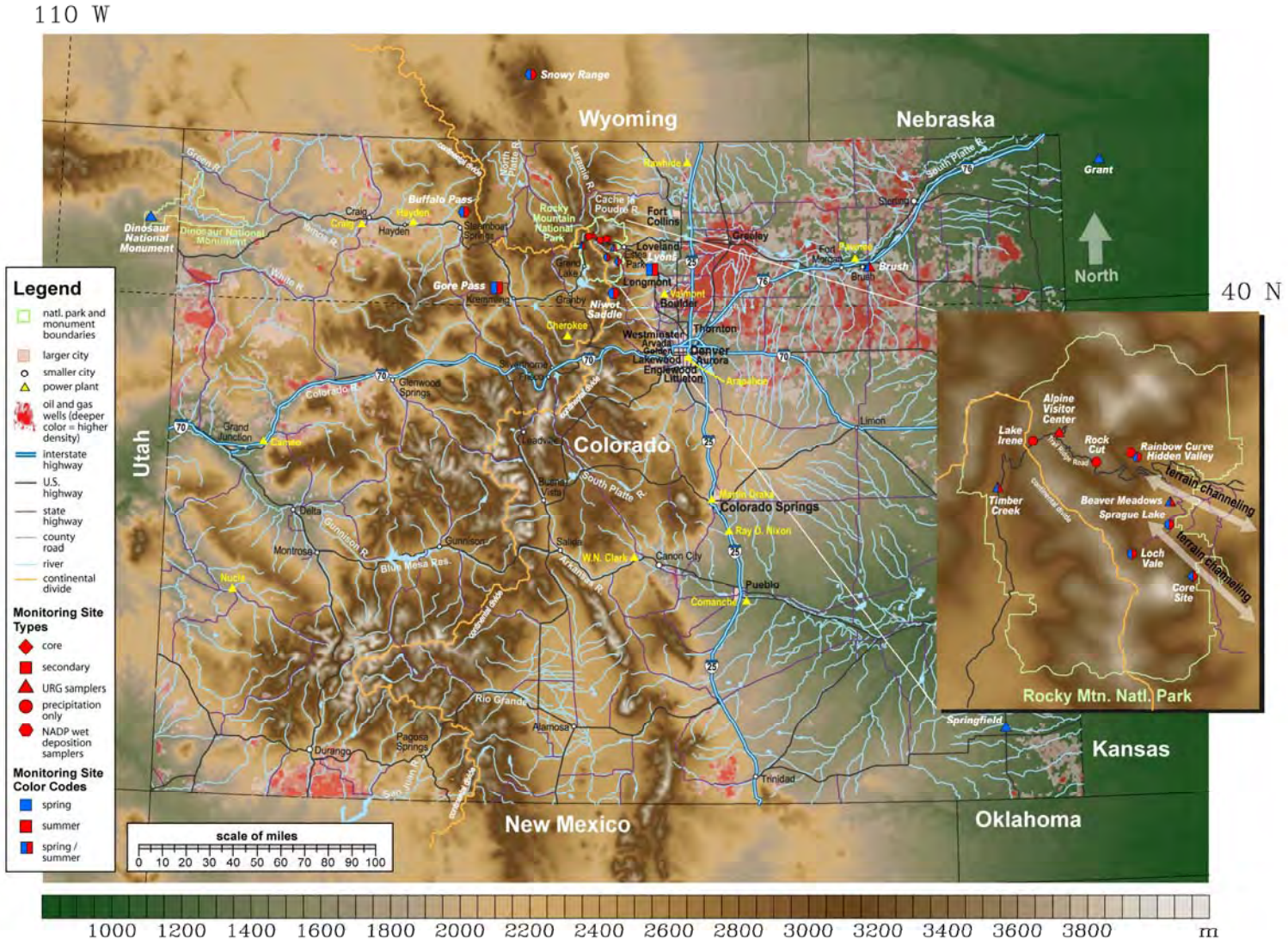

Figure 1.10. Map of Colorado showing major cities, rivers, topography, and location of RMNP.

In general, temperature decreases about 4–5 F per thousand ft of elevation (7–9 C/km) with July means of 70–80 F (20–25 C) in lower mountain valleys and 50–60 F (10–15 C) in the higher mountains. However, elevational temperature changes can be masked by inversions, especially at night and in the winter. Cold, dense air pools in some mountain valleys, especially on clear winter nights when the ground is snow covered and strong inversions form from surface radiative cooling. These cold temperatures are nearly always accompanied by light or calm winds.

1.4.1.1. Winds Statewide

Prevailing winds across the state are westerly. Areas east of and very near the mountains are subject to periodic, severe turbulent winds from the effects of high speed winds over the mountain barrier. Strong winds are common at elevations above tree line, approximately 11,500 ft (3500 m) throughout the winter months and can exceed 50–100 mph (20–45 m/s) in exposed locations. Mountain-valley circulations are common, with winds blowing up valley during the day and reversing at night. Due to the significant mountain barrier, winds west of the Continental Divide can be very light in most valleys, especially in the fall and winter, while winds along and east of the crests are much stronger and typically from the west during the cool half of the year.

1.4.1.2. Front Range Upslope/Downslope Winds

While westerly (downslope) flow is the predominant wind direction along the Front Range, upslope, easterly winds occur during every month (Losleben et al., 2000). The two major causes of upslope winds are 1) differential surface heating and 2) large-scale (synoptic) weather conditions conducive to easterly winds. In the first case, the east-facing slopes of the Front Range warm more rapidly than the more horizontal plains during the morning just after sunrise. The warm air near the sloped surfaces then rises, creating a circulation pattern that pulls air from the east at ground level. Synoptic weather patterns that can lead to generalized Front Range upslope conditions include low pressure (counter-clockwise circulation) to the south or west or high pressure (clockwise circulation) to the north. Synoptic forcing of easterlies is more common during the winter than during the summer.

The frequency of upslope winds varies diurnally, seasonally, and by elevation. There are also other confounding factors such as the shape of the terrain and surface vegetation and characteristics. In a 1988–1999 study of three elevations, 3000, 3500, and 3700 m, at Niwot Ridge near Boulder, Colorado, Losleben et al. (2000) found that the lowest of these sites had the highest frequency of upslope flow, with the highest frequency during May (31% of all hours) and the lowest frequency during December (18%), while the highest elevation site had the most upslope winds during July (22%), and the middle elevation site had the most during April (13%). All three sites had more hours of upslope during the day than at night, with the peak hours being about 1:00–5:00 pm (all times are local standard time) depending on location. Upslope winds tend to begin and end earlier in the day at lower elevations. The diurnal variation in upslope frequencies was greatest at the lowest elevation site and smallest at the highest elevation site. The highest site was subject to more synoptic as opposed to thermally driven upslope winds. There was less diurnal difference in upslope frequency during the winter than during the summer at all sites, and diurnal differences were greater than seasonal differences.

1.4.1.3. Long-term Wind Patterns in RMNP

Wind patterns at RMNP show these typical mountain upslope/downslope patterns, both at a local scale in the valleys and canyons within the park, as well as at a mesoscale, influenced by the Front Range. Front Range upslope winds have the potential to bring pollutants into the park area from the urbanized and agricultural areas, from Fort Collins in the north to Pueblo in the south. Front Range downslope winds can be enhanced by synoptic features such as a low pressure trough over the plains and by a lee wave effect when westerly winds cross the divide into the plains, sometimes resulting in high-speed winds in lee-side canyons such as Big Thompson. (Big Thompson Canyon runs approximately from Estes Park to Loveland. See Figure 1.10.) This may be effective at times in ventilating the atmosphere above eastern RMNP locations (Green et al., 2005).

The NPS gaseous pollutant monitoring site for RMNP is located near the RoMANS core monitoring site and has hourly meteorological data including winds, temperature, moisture, solar radiation, and precipitation, dating to 1995. Measurements there should be representative of similar elevations within RMNP east of the divide, though directional channeling within individual valleys and canyons also certainly occurs. The mean fraction of winds from the east for each month of the year and hour of the day are shown in Figure 1.11. Wind was considered to be from the east if it was from any direction in the 180 degree arc from north through east to south.

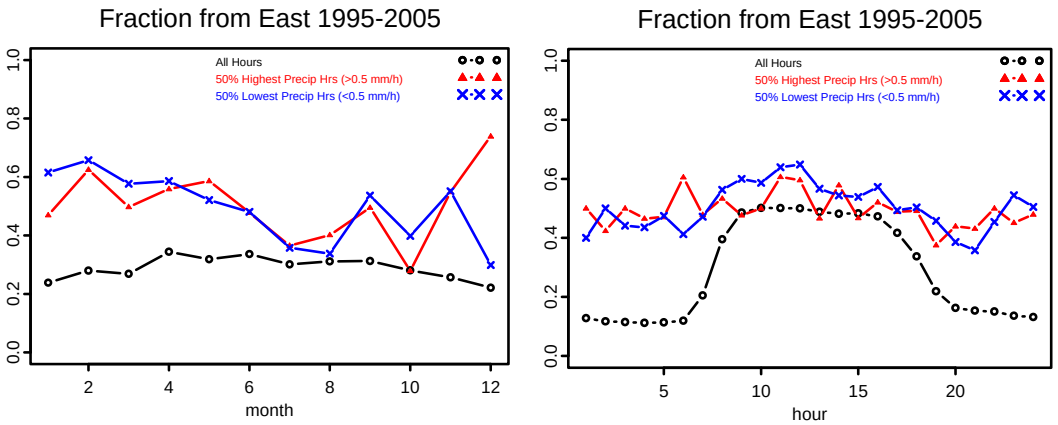

Figure 1.11. Fraction of winds from the east by month and by hour of day for 1995–2005. Fractions are shown for all hours and for hours with light precipitation and heavy precipitation. Data are from the NPS gaseous monitoring network 10-m tower at RMNP.

The 10-m wind directions at this site are predominantly westerly. Only about 20–25% of hours on average had winds from the east. There is some seasonal variation, with upslope winds being the most frequent during April and least frequent during December and January. The diurnal pattern is much more pronounced than the seasonal pattern, with upslope winds being much more frequent (about 40% of hours) during midday than at night (about 15% of hours). The peak upslope frequency at this site is from about 9:00 am to 4:00 pm. Easterly winds are much more frequent during precipitation events than when the weather is dry. Though only about 5% of all hours have precipitation, of these hours, approximately half have winds from the east. Contrary to dry hours, there is little diurnal variation in the frequency of easterly flow during precipitation.

Seasonally, easterly flow during precipitation is somewhat more likely during the winter months than during the summer. This is consistent with the summer storms being preferentially caused by convective lifting of air masses crossing the Rockies from the west, while winter and spring storms are more likely to be synoptic storms in which associated upslope flow brings air masses and Gulf of Mexico moisture from the east.

Figure 1.12 shows these same wind direction data for April and July as frequency plots of the winds from each of 16 directional bins, rather than from two bins, for all days and for days with precipitation. These graphs illustrate that the winds at this site are not really "easterly" and "westerly" but tend to be either northwesterly or southeasterly. This is partially due to the northwest to southeast orientation of the valley in which the measurement site sits and so may not be totally representative of all valley locations in RMNP. During hours of precipitation, the winds tend to be rotated a bit to more northerly and southerly and to have a higher frequency of the southerly to southeasterly wind directions than during nonprecipitating hours. This is true of both April and July.

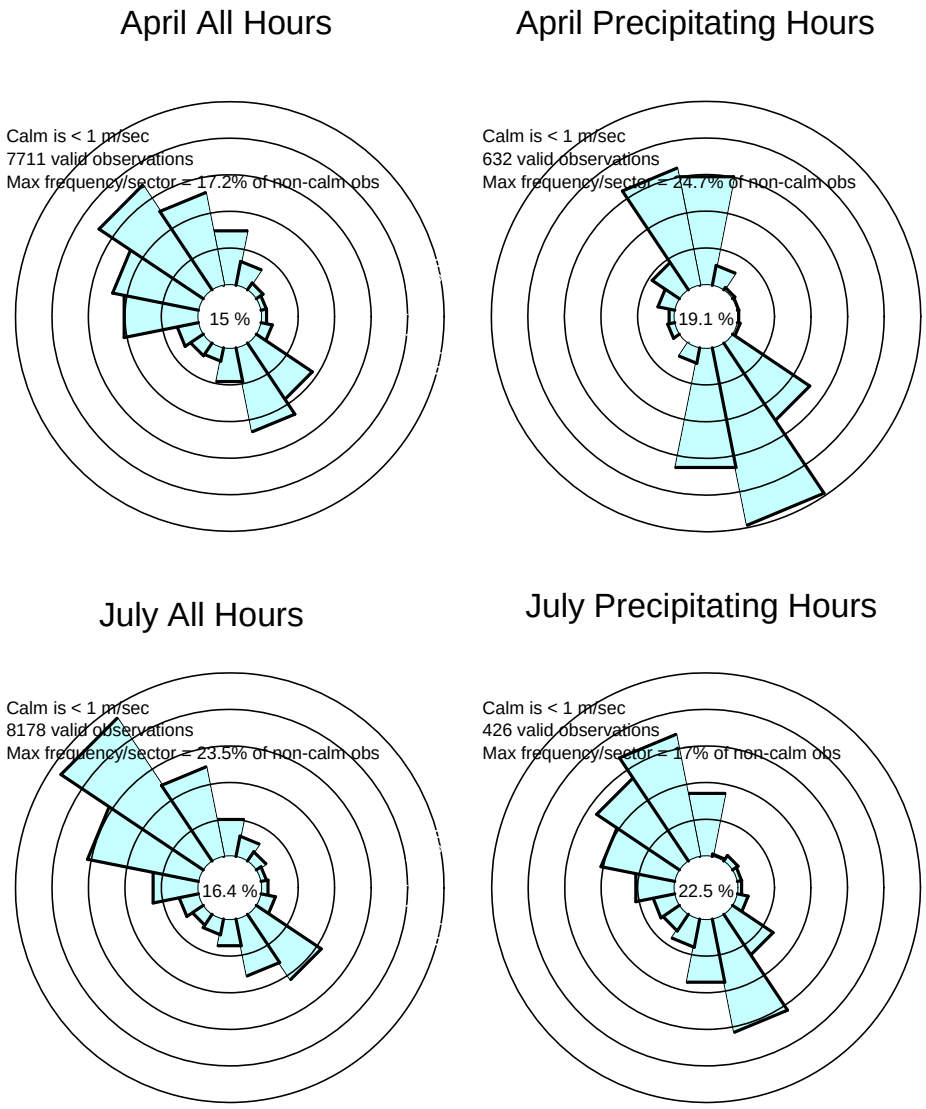

Figure 1.12. Directional frequency of winds from 16 directional bins at the RoMANS core site during 1995–2005 for April (top) and July (bottom) for all hours (left) and hours with precipitation (right). Data are from the NPS gaseous monitoring network.

Upslope winds occur both locally and as part of the Front Range upslope wind pattern. Nighttime winds are predominantly from the northwest, which is the direction for night drainage as well as for channeled, westerly synoptic winds. Transport from local sources such as wildland fires and emissions within the Estes Park area will be influenced by upslope/downslope flow within local valleys and basins (Green et al., 2005).

Local emissions and air pollutants are also highly subject to trapping inversions in the valleys and basins of RMNP. Higher elevations will typically be above trapped local haze and may also be above regional haze trapped below large-scale subsidence inversions. Long-term records show an average of about one air stagnation event every 2 months during May to October in

north-central Colorado. A stagnation event is defined as stagnation conditions that persist for 4 days or longer (Wang and Angell, 1999; Green et al., 2005).

1.4.1.4. Precipitation

Statewide, storms from the west generally lose much of their Pacific moisture on mountaintops and west-facing slopes, with east slopes receiving relatively little precipitation, especially in winter. Precipitation increases with elevation during both winter and summer, but the effect is greatest in midwinter. High peaks generally receive most of their precipitation during the winter, while during the summer, lifting of air masses over mountain peaks and ranges generates thunderstorms whenever regional air masses are sufficiently moist. This is nearly every afternoon in some years. The last half of July and much of August are particularly prone to these convective storms. Within RMNP, the western slope is directly impacted by prevailing westerly winds and receives more precipitation than the eastern slope, which is in the rain shadow of the Rockies. Annual average precipitation in Colorado varies from less than 7 in (18 cm) per year in the San Luis Valley in south-central Colorado to over 60 in (150 cm) per year in some mountain locations. The spatial distribution of annual mean precipitation across the state during 1961–1990 is shown in Figure 1.13. Figure 1.14 shows the month of maximum precipitation in each part of Colorado for the same time period. RMNP is in the area that generally receives maximum precipitation during either July or August.

Most of Colorado's heaviest precipitation events occur during either late May through early June or late July through early September (Peterson et al., 1999). There is a lull in convective activity during late June through mid-July. The late spring peak is associated with quasi-stationary late spring storms bringing Gulf of Mexico moisture westward to the Front Range of the Rockies. The second and greater peak in storm frequency has a pronounced maximum frequency from the last week of July into the first few days of August. These storms are often small in areal extent and have occurred in nearly all parts of Colorado, but the greatest storms have occurred east of the mountains and often near the eastern foothills of the Rockies. The Fort Collins flood of July 28, 1997, and the Big Thompson flood of July 31, 1976, were among these storms. (See Figure 1.10 for locations of Fort Collins and Big Thompson Canyon, which runs approximately from Estes Park to Loveland.)

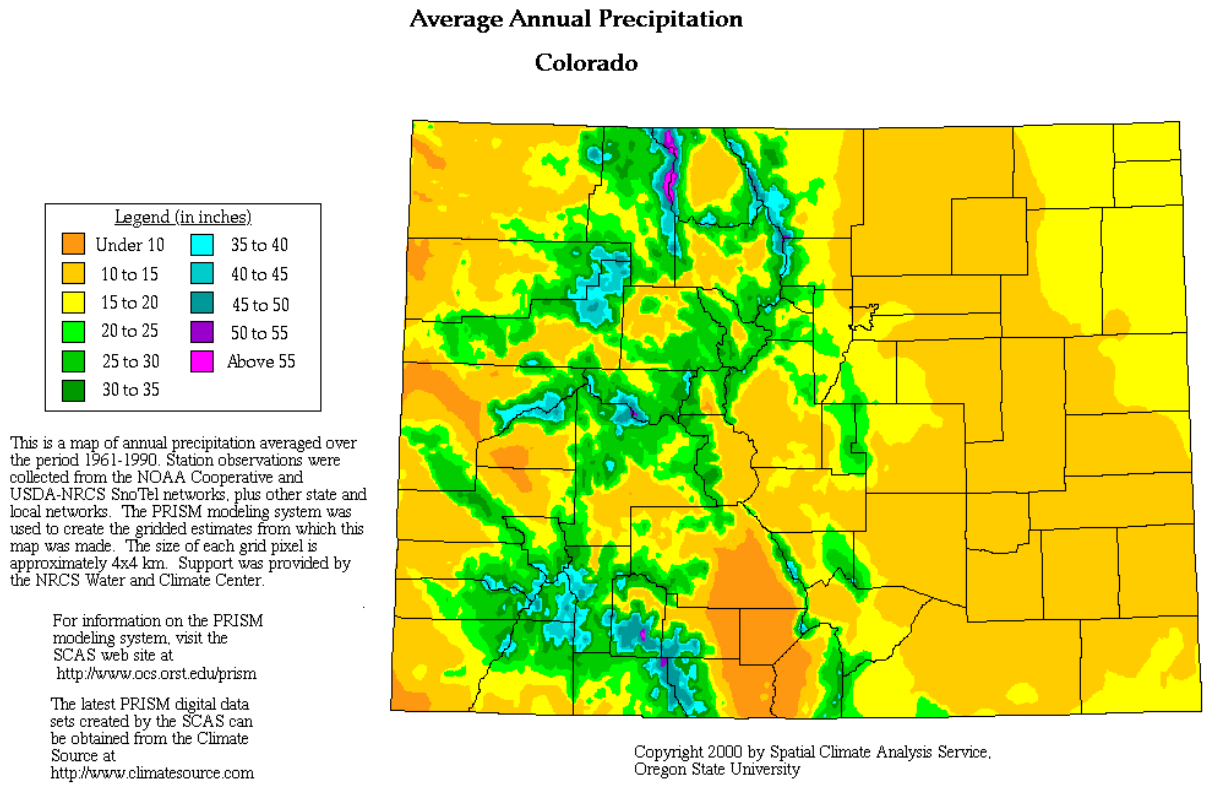

Figure 1.13. Annual average precipitation in Colorado during 1961–1990. From the Spatial Climate Analysis Service at Oregon State University.

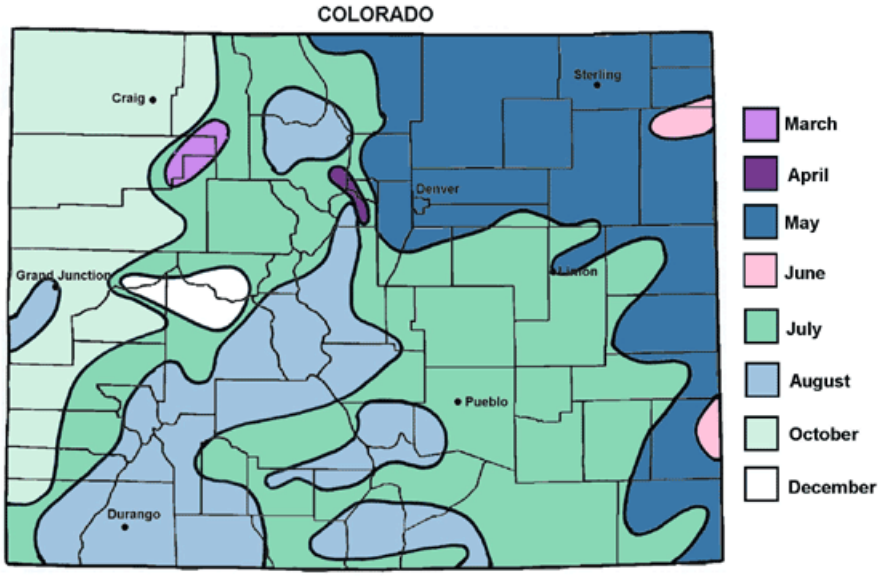

Figure 1.14. Month of maximum precipitation 1961–1990. Downloaded from http://ccc.atmos.colostate.edu/wettestmonth.php.

Hourly precipitation measurements on the east side of RMNP at the NPS gaseous monitoring site are available from 1995 to the present and can be analyzed for multiyear, seasonal, and diurnal patterns in precipitation. Figure 1.15 shows the total measured precipitation and the total number of hours of precipitation by year, by month of year, and by hour of day. These graphs show the previously discussed peak in precipitation amount during July and August but also show that measured precipitation amounts are almost as high during April and May as during July and August and that the number of hours of measurable precipitation peaks in April rather than during the summer. Both the number of hours of precipitation and the precipitation total amounts are much higher during the afternoon and evening than during the morning hours at this site. From 1995 to 2007, in terms of annual totals, the wettest year was 2004 and the driest was 2002. There may be no "typical" year at this site since there are factors of 2–3 in the precipitation amounts between the dry years and the wet years.

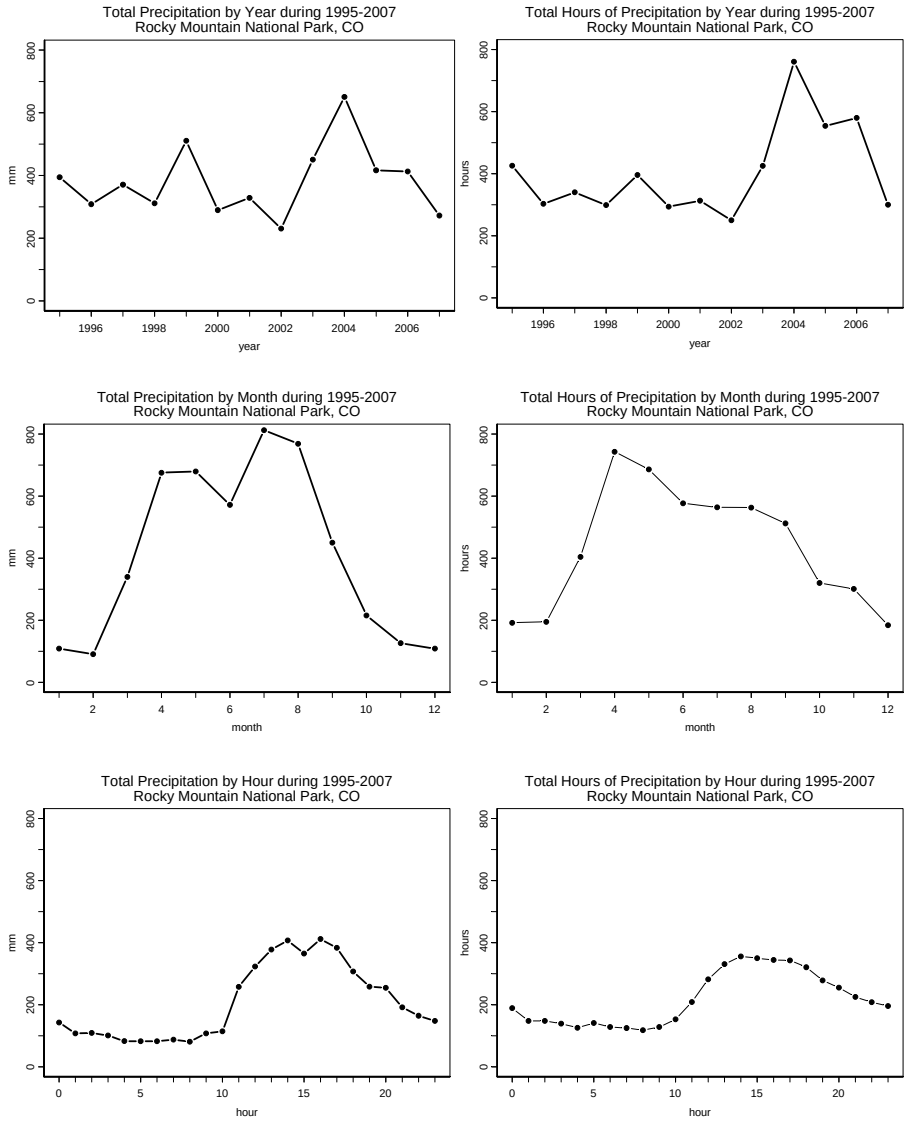

Figure 1.15. Total measured precipitation (mm) during 1995–2007 (left) and total number of hours of measurable precipitation during 1995–2007 (right) by year (top), month of the year (middle), and hour of day (bottom). Data are from the NPS gaseous monitoring network.

1.4.1.5. Temperatures

Temperature can affect the emission rates of biogenic compounds including ammonia from soil, and temperature influences chemical transformation rates. Though no formal trends analyses have been completed, Figure 1.16 shows the mean temperatures during April and July in the hourly NPS gaseous monitoring data. During April it appears that the years since about 2000 are somewhat warmer than the earlier years. For July, there was an apparent gradual warming trend from 1995 through 2003, a cold July in 2004, and then the years 2005–2007 were somewhat cooler than the early 2000s.

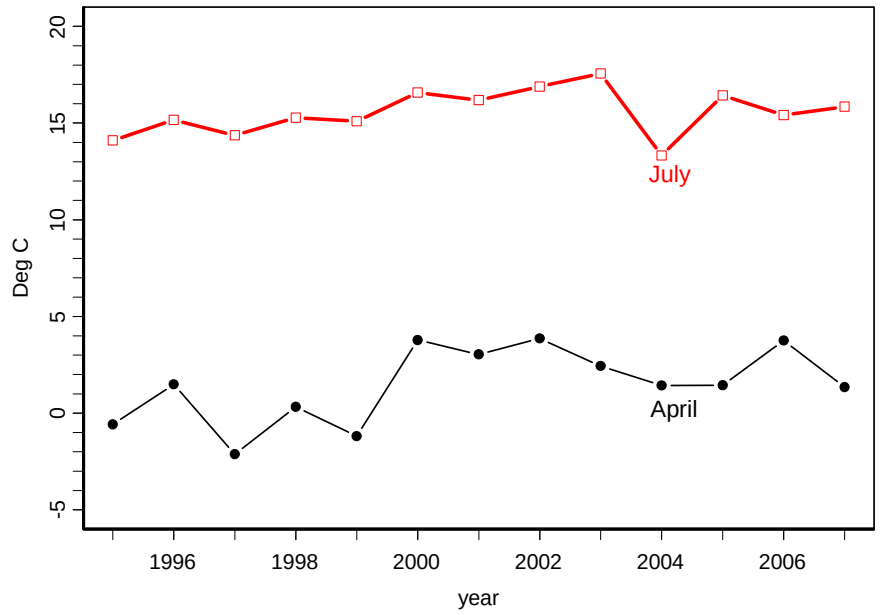

Figure 1.16. Monthly mean temperatures during April (black, closed circles) and July (red, open boxes) during 1995–2007. Data are from the NPS gaseous monitoring network.

1.5. STUDY OBJECTIVES

Rocky Mountain National Park is experiencing a number of deleterious effects due to atmospheric nitrogen and sulfur compounds. The nitrogen compounds include both oxidized and reduced nitrogen. The effects of organic nitrogen compounds are not known at this time. Emissions of both sulfur and nitrogen compounds need to be reduced to alleviate these deleterious effects. Various regulatory programs are underway to address emission reductions, many of which will be achieved from the most easily identified contributors to oxidized sulfur- and nitrogen-related effects at the park. The objectives of this study are to further our understanding of what will be needed in the longer term to address effects at the park and to reduce uncertainties for future planning efforts. Specific study objectives include the following:

- Identify the overall mix of sulfur and oxidized and reduced nitrogen in the air and precipitation on both the east and west sides of the Continental Divide.

- Identify the relative contributions to atmospheric oxidized sulfur and oxidized and reduced nitrogen at Rocky Mountain National Park from emissions originating within the state of Colorado versus outside the state.
- Identify the relative contribution to atmospheric oxidized sulfur and oxidized and reduced nitrogen at Rocky Mountain National Park from emissions originating along the Front Range versus other regions within the state.
- Identify the relative contribution of various source types within the state of Colorado to nitrogen and sulfur species, including mobile, agricultural, other area, and large and small point sources.
- Map spatial and temporal variability of atmospheric airborne concentrations and deposition within the park and relate observed patterns to likely source types and locations.
- Characterize the meteorological conditions that lead to various atmospheric chemical conditions.

Chapter 2. Study Design and Methods

Historically, peak periods of nitrogen deposition have been observed within RMNP in spring and summer. One of the goals of RoMANS was to better understand the meteorology, especially the wind flow patterns that bring nitrogen- and sulfur-containing species into RMNP and to also understand the clouds, moisture, temperature, and precipitation patterns associated with wet deposition. As discussed in Chapter 1, the precipitation climatology of this area shows that the two periods of the year when precipitation is most likely to occur are late July into early August for convective storms and April to May for upslope, synoptic storms. The two storm regime types are also likely to have different air pollutant transport patterns and different moisture sources associated with them. In order to better understand airborne pollutant concentrations, transport patterns, and key deposition mechanisms during these important seasons, a spring field campaign was conducted over 5 weeks in March and April 2006, and a summer field campaign was conducted over 5 weeks during July and August 2006.

2.1. ROMANS STUDY NETWORK

In order to examine airborne concentrations and deposition of sulfur- and nitrogen-containing air pollutants within the park and at locations potentially upwind, a large network of sites was operated as part of the RoMANS study. Due to RMNP's complex terrain, precipitation amounts and associated wet deposition fluxes can vary within the park. In order to assess this spatial variability, several sampling sites were located within the park boundaries. Additional measurement sites were located on the east and west sides of the park, with more sites situated in the plains of Colorado and near the eastern, western, and southeastern boundaries of Colorado, to assess the transport of sulfur and nitrogen species into Colorado.

2.1.1. Meteorological Measurements

Figure 2.1 is a map of the sites where meteorological measurements were conducted during the RoMANS study, and Table 2.1 summarizes the instrumentation for the three non-upper-air sites: the RMNP core site, Lyons Crest, and Gore Pass. The radar profiler and SODAR are discussed in later sections.

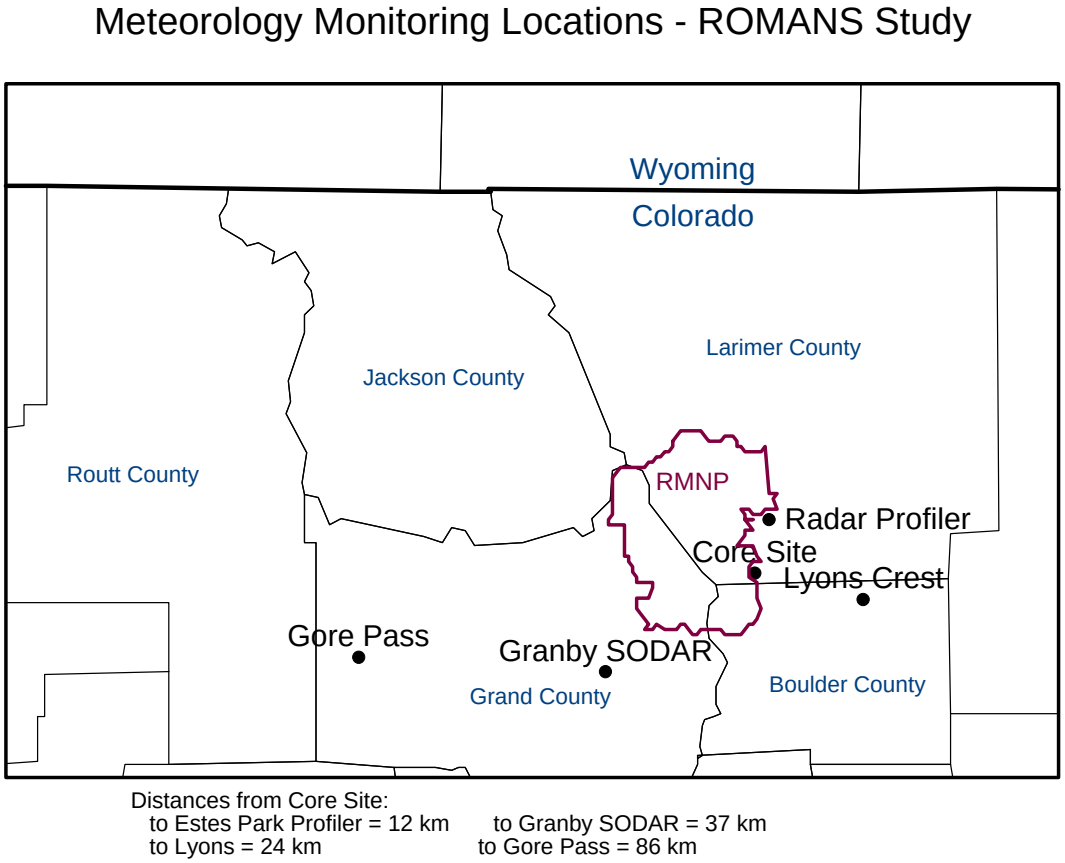

Figure 2.1. Map of north-central Colorado showing locations of meteorological monitoring sites operated during RoMANS. . Rocky Mountain National Park (RMNP) boundaries are shown in red.

Table 2.1. Summary of RoMANS instrumentation for visibility and meteorological measurements.

Site Site	Location			Instrument Quantitative	Measurement Reported
	Lat (ºN)	Lon (ºW)	Elev (m)		
Gore Pass	40º 07' 0.6"	106º 31' 55.9"	2,641	Nephelometer (Optec NGN2) Meteorological (Rotronics) Meteorological (RM Young)	Light scattering Temperature/RH Wind speed and direction, pressure, rainfall
Lyons Crest	40º 13' 38.6"	105º 16' 30.5"	1,684	Nephelometer (Optec NGN2) Meteorological (Rotronics) Meteorological (RM Young)	Light scattering Temperature/RH Wind speed and direction, pressure, rainfall
Core Site	40º 16' 40"	105º 32' 43"	2,743	Nephelometer (Optec NGN2) Meteorological (Rotronics) Meteorological (RM Young)	Light scattering Temperature/RH Wind speed and direction, pressure, rainfall

Note: Optec NGN2 Nephelometers are mounted at a height of 10–15 ft.
Temperature/RH Sensors (Rotronics) are at the same height as nephelometer.
RM Young Meteorological Sensors are mounted at a height of 10 meters

Each of the three non-upper-air meteorological sites was equipped with an Optec NGN2 nephelometer to measure light scattering, a Rotronics sensor for temperature and humidity, and RM Young sensors for wind, pressure, and precipitation.

2.1.2. Chemistry Measurements

The site locations where the chemical and physical properties of aerosols were measured are illustrated in Figure 2.2. Table 2.2 lists location coordinates and altitudes for the sites. Four types of sites were established in the RoMANS monitoring network. In descending order of measurement complexity, these categories are (1) core site, (2) secondary sites, (3) satellite sites, and (4) passive monitoring sites.

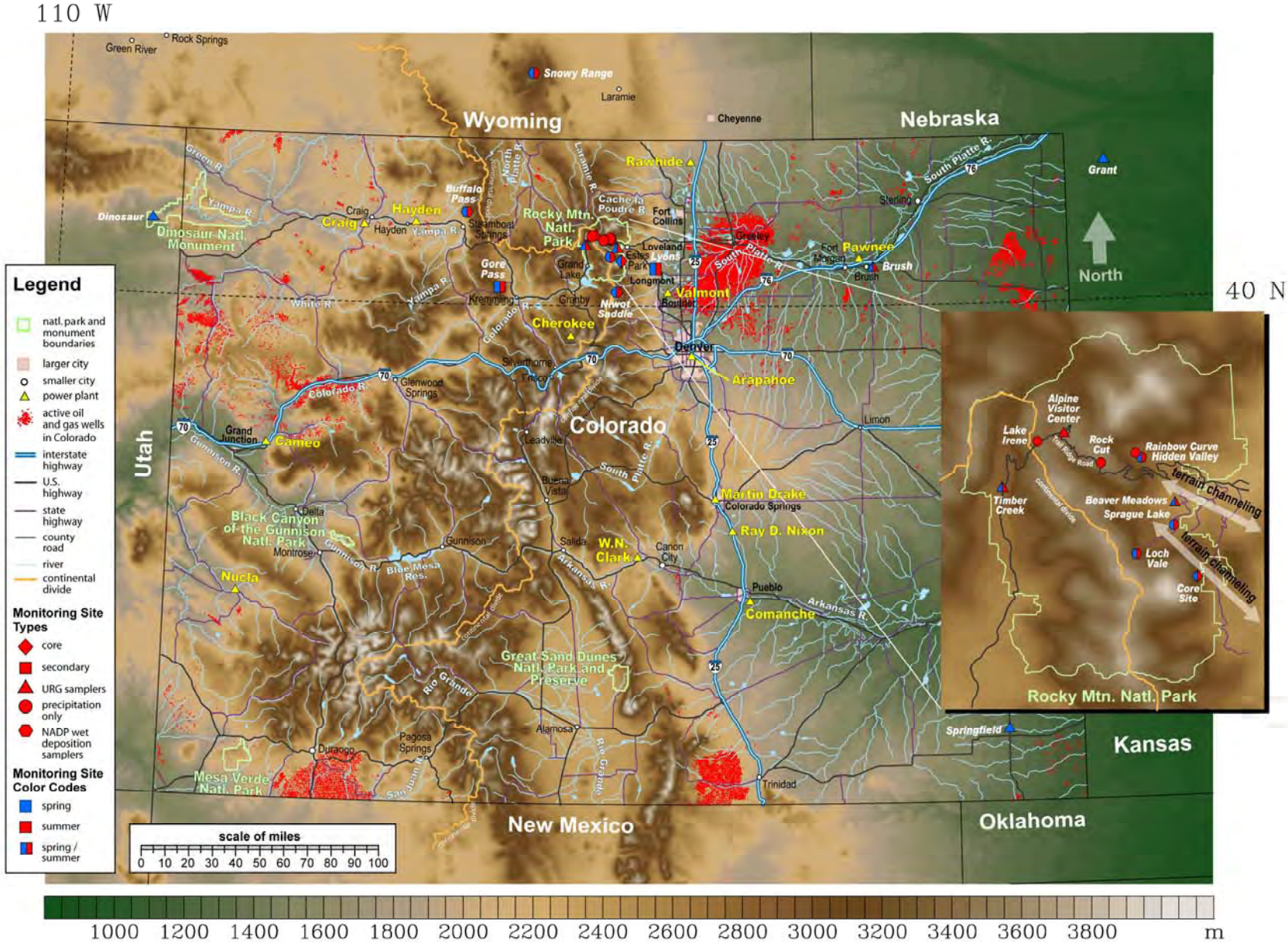

Figure 2.2. Map of Colorado and adjacent areas, illustrating the location of the monitoring sites used in the RoMANS study and the field campaign(s) during which each monitoring site was operational.

Table 2.2. Locations of RoMANS monitoring sites during the spring and summer campaigns.

Spring					
Site ID	**Site Name**	**Site Type**	**Lat**	**Lon**	**Elevation (m)**
BM	Beaver Meadows	RMNP satellite	40.364	-105.581	2509
BR	Brush	Satellite	40.314	-103.602	1270
DI	Dinosaur	Satellite	40.437	-109.305	1463
GP	Gore Pass	Secondary	40.117	-106.532	2641
HV	Hidden Valley	RMNP satellite (precip)	40.394	-105.656	2879
LV	Loch Vale	RMNP satellite (precip)	40.288	-105.663	3170
LY	Lyons Crest	Secondary	40.227	-105.275	1684
MS	Main Site (IMPROVE)	RMNP core site	40.278	-105.546	2760
NE	Grant, Nebraska	Satellite	40.87	-101.731	1100
SF	Springfield	Satellite	37.37	-102.743	1320
SL	Sprague Lake	RMNP satellite (precip)	40.321	-105.608	2656
TC	Timber Creek	RMNP satellite	40.38	-105.85	2767
Summer					
Site ID	**Site Name**	**Site Type**	**Lat**	**Lon**	**Elevation (m)**
AL	Alpine Visitor Center	RMNP satellite	40.442	-105.754	3599
BM	Beaver Meadows	RMNP satellite	40.364	-105.581	2509
BR	Brush	Satellite	40.314	-103.602	1270
GP	Gore Pass	Secondary	40.117	-106.532	2641
HV	Hidden Valley	RMNP satellite (precip)	40.394	-105.656	2879
LI	Lake Irene	RMNP satellite (precip)	40.413	-105.819	3260
LV	Loch Vale	RMNP satellite (precip)	40.288	-105.663	3170
LY	Lyons Crest	Secondary	40.227	-105.275	1684
MS	Main Site (IMPROVE)	RMNP core site	40.278	-105.546	2760
RB	Rainbow Curve	RMNP satellite (precip)	40.401	-105.665	3271
RC	Rock Cut	RMNP satellite (precip)	40.392	-105.72	3664
SL	Sprague Lake	RMNP satellite (precip)	40.321	-105.608	2656
TC	Timber Creek	RMNP satellite	40.38	-105.85	2767

The RoMANS core study site, featuring the most extensive suite of integrated and continuous measurements, was collocated with the IMPROVE and CASTNet monitoring sites in a small piece of park-owned property off Hwy. 7. Figure 2.3 is a photograph of the core measurement site. The core site was selected because of the advantages of collocating with both the IMPROVE and CASTNet sites and because it provided the best access to the study's substantial power needs. A wide variety of continuous and integrated measurements of particles, trace gases, and precipitation were made at the core site. Table 2.3 lists measurements made at the core, secondary, and satellite sites. Equipment at the core site was deployed in the CSU-UCD-NPS (Colorado State University; University of California, Davis; National Park Service) Mobile Air Sampling Lab, in existing shelters on site and outdoors, as appropriate. Measurements at the core site included 24-hr integrated measurements of $PM_{2.5}$ inorganic ion composition (including SO_4^{2-}, NO_3^-, and NH_4^+) and key trace gas (NH_3, HNO_3, and SO_2) concentrations, using a University Research Glassware (URG) denuder/filter-pack sampler; 15-min measurements of $PM_{2.5}$ inorganic composition, using a particle-into-liquid sampler (PILS) coupled to two Dionex

ion chromatographs; particle size distributions of inorganic ion species, using a micro-orifice uniform deposit impactor (MOUDI); a suite of 5-min gaseous measurements of O_3, NO, NO_2, NH_3, CO, and SO_2, particle light scattering, using an Optec nephelometer; and particle size distributions over the range of 40 nm to 15 µm diameter, using a particle sizing rack containing a TSI aerodynamic particle sizer (APS), a Particle Measurement Systems optical particle counter (OPC), and a TSI differential mobility particle sizing (DMPS) system. A variety of precipitation sampling approaches were also used at the core site. Event samples were collected using a Yankee Environmental Systems, wet-only precipitation collector and with open buckets placed outside at the onset of precipitation. Subevent samples (typically 1- to 2-hr duration) were also collected during many precipitation events, using a large polyethylene funnel. Precipitation samples were analyzed for major inorganic anions and cations. Many precipitation samples were also analyzed for total nitrogen. The difference between total nitrogen (TN) and measured inorganic nitrogen species (NO_3^-, NO_2^-, and NH_4^+) is a measure of organic nitrogen (ON). In addition to these CSU measurements, precipitation samples were also collected for U.S. Geological Survey (USGS) analysis of nitrogen isotopes, using sampling supplies and procedures provided by the USGS. Meteorological measurements were made on site on a 10-m tower at 1-min time resolution by Air Resource Specialists (ARS).

Figure 2.3. Photo taken at the RoMANS core site.

Table 2.3. Measurements made during the RoMANS spring and summer campaigns.

Instrument	**Measurement**	**Time Resolution**	**Notes Core**	**Site**	**Secondary Sites**	**Satellite Sites**
URG annular denuder/filter-pack sampler	$PM_{2.5}$ inorganic ions Gaseous NH_3, HNO_3, and SO_2	24 hr		X	X	Beaver Meadows, Brush, Dinosaur, Grant (NE), Springfield, Timber Creek

Instrument	Measurement	Time Resolution	Notes Core	Site	Secondary Sites	Satellite Sites
R&P Partisol denuder/filter-pack sampler	$PM_{2.5}$ inorganic ions Gaseous NH_3, HNO_3, and SO_2	24 hr	Operated only during last several days of summer campaign			Alpine Visitor Center
Particle-into-liquid sampler (PILS) – IC	$PM_{2.5}$ inorganic ions	15 min/2 hr	15-min on-line operation at core site; 2-hr off-line with sample archival at secondary sites; spring only at Lyons Crest	X	X	
Sunset OC/EC analyzer	$PM_{2.5}$ OC and EC	1–2 hr		X		
IMPROVE sampler	$PM_{2.5}$ and PM_{10} mass, ions, elements, H, and OC/EC	24 hr		X		
MOUDI impactor	Inorganic ion size distributions	48 hr	8 stages from ~0.02-18 µm aerodynamic diameter; samples archived	X	Lyons Crest (spring only)	
Continuous gas monitors	SO_2, NO_x, NH_3, CO, O_3	1 min		X		
Wet-only auto precip sampler	Precipitation	Event/ daily		X	Lyons Crest (spring) Gore Pass (summer)	
Subevent precipitation sampler	Precipitation	Subevent (e.g., hourly)		X	X	
Open bucket precipitation collector	Precipitation	Daily	Changed daily at most sites; 48-hr change typical at Brush and Grant (NE)	X	X	X
Met station	T, RH, WD, WS, Precip, SR,BP	1–5 min	1 min core; 5 min secondary; hourly data only 1st week of spring study at core site	X	X	
Particle sizing rack	Aerosol particle size distributions	15 min	Differential mobility particle sizing (DMPS) system, optical particle counter (OPC), aerodynamic particle sizer (APS); ~0.05–10 µm diameter	X		

Instrument	Measurement	Time Resolution	Notes Core	Site	Secondary Sites	Satellite Sites
Optec nephelometer	Particle light scattering	5 min	Open air; no RH control or size cut	X	X	

Two secondary measurement sites were established: one was located just west of the town of Lyons at the base of the Rocky Mountain foothills and one was located on the east side of Gore Pass on Colorado's western slope. These sites were chosen to characterize air masses potentially entering RMNP from the east (Lyons) or west (Gore Pass). As indicated in Table 2.3, measurements at the secondary sites included 24-hr URG denuder/filter-pack samples, off-line collection of PILS samples (archived for possible future analysis), event precipitation samples, and meteorological measurements from 10-m towers (by ARS). Subevent precipitation samples were also collected at the Gore Pass and Lyons sites as access and staffing permitted.

Third-level "satellite" sites were established at many locations to map out variations within RMNP and across Colorado in airborne nitrogen and sulfur species concentrations and wet deposition. Some difference in the satellite site network occurred between the spring and summer measurement campaigns due to access and budgetary limitations. The spring network included sites in RMNP at Loch Vale, Beaver Meadows, Sprague Lake, Hidden Valley, and Timber Creek. Both Loch Vale and Beaver Meadows are NADP measurement sites on the east side of the Continental Divide. As discussed in the introduction, the Loch Vale watershed has also been the site of many studies of nitrogen deposition impacts on ecosystem function. Sprague Lake and Hidden Valley are also located on the east side of the RMNP. Timber Creek is located at lower elevation on the west side of the Continental Divide and near the western boundary of RMNP. Outside of the park, spring campaign satellite sites were located in Dinosaur National Monument, near Brush, Colorado, near Grant, Nebraska, and near Springfield, Colorado. The Dinosaur site was selected to characterize air mass composition near the western border of Colorado. The Grant, Nebraska, site served a similar purpose for characterizing air mass composition near the eastern border of Colorado. The Brush site was situated in northeastern Colorado, a region of high ammonia emissions. The measurement site itself was situated in a wildlife refuge, away from any large ammonia emission sources. The Springfield measurement site was located in southeastern Colorado. The location was selected in order to characterize the composition of air masses that might enter Colorado from the southeast on their way to RMNP. Twenty-four-hr URG denuder/filter-pack measurements were made at all of the spring campaign satellite sites except Loch Vale, Sprague Lake, and Hidden Valley. These sites collected only precipitation. Event precipitation samples were collected at the spring satellite sites, using open buckets. Operators were stationed at the Dinosaur and Springfield sites. Operators had to travel to the other sites, producing some compromise in the ability to capture individual precipitation event samples at some locations. Due to the difficulty in accessing Loch Vale during spring, a group of local individuals with backcountry experience was hired to service the site. All other sites were staffed/serviced by CSU personnel.

The satellite site network was reconfigured during the summer campaign to eliminate the most outlying stations (Springfield, Grant, and Dinosaur), due to budget constraints. Additional measurement sites were added in RMNP at the Alpine Visitor Center (near the Continental Divide), at Lake Irene (on the western slope between the Continental Divide and Timber Creek), and at Rock Cut, a site on the eastern slope of the park close to the Continental Divide. Daily

open bucket precipitation samples were collected at Lake Irene, Sprague Lake, Hidden Valley, and Rock Cut. $PM_{2.5}$ and trace gas measurements were made at the Alpine Visitor Center, using a Rupprecht and Patashnick honeycomb denuder/filter-pack sampler. These measurements were made only during the final 2 weeks of the summer campaign, due to equipment delivery problems from the manufacturer.

A network of passive ammonia samplers was operated during the RoMANS spring and summer campaigns. Weekly samples of ammonia were collected using Ogawa passive samplers. The measurement network is depicted in Figure 2.2. Most sites were operated by volunteers recruited through the Colorado Collaborative Rain and Hail Study (CoCoRAHS). Samplers were shipped to and from volunteer operators who deployed the samplers on their property or at a nearby location. Sampling sites were chosen to avoid immediate proximity to substantial ammonia emissions sources. High and variable sample blanks and low concentrations at mountain sites rendered the weekly passive ammonia data of little value. Consequently, these measurements are not discussed further in this report.

2.2. MEASUREMENT METHODS

This section describes measurement methods utilized in the RoMANS field study.

2.2.1. Radar Wind Profiler

A 915 MHz radar wind profiler located near Lake Estes in Estes Park, Colorado, was installed and operated by National Oceanic and Aeronautics Administration Environmental Technology Laboratory (NOAA ETL) staff during RoMANS. Table 2.4 summarizes the specifics of the installation and Figure 2.4 shows the installation including the associated 10-m meteorological tower.

Table 2.4. Details of radar wind profiler installation in Estes Park, Colorado.

Parameter Detail	
Site Latitude (deg N)	40.38
Site Longitude (deg W)	105.51
Site Elevation (m MSL)	2286
Antenna Azimuth Directions (deg)	0 (vertical), 332 (north), 62 (east)
Antenna Elevation Directions (deg)	90 (vertical), 66.4 (north), 66.4 (east)
Mode 1: Pulse Length (m), Spacing (m)	62, 57
Mode 2: Pulse Length (m), Spacing (m)	106, 97

Figure 2.4. Radar wind profiler and 10-m meteorological tower in Estes Park, Colorado.

A radar wind profiler measures winds by transmitting electromagnetic energy into the atmosphere, then measuring the strength and Doppler frequency of backscattered energy. Wind speed is determined from the Doppler frequency of energy scattered from refractive index fluctuations caused primarily by moisture fluctuations but also by temperature fluctuations embedded within the atmosphere. Higher signal-to-noise ratios are obtained when there is greater moisture, precipitation, or vertical temperature discontinuities in the atmosphere. If none of these exist, it is sometimes not possible to estimate the winds aloft.

The profiler transmits in three different vertical planes and receives backscattered energy from refractive index fluctuations that are moving with the mean wind. By sampling in the vertical direction and in two tilted planes, the three components of motion can be determined. The system consists of a single, phased array antenna that transmits alternately along vertical, north-south, and east-west planes. The nonvertical beams are tilted at about 23 degrees from vertical.

The system can transmit pulses at about 1–10 kHz rate into the atmosphere. If the backscatter from each pulse is sampled at, for example, a 1-MHz rate, this results in one sample every 150 m in range. For RoMANS, the profiler was operated in two modes, resulting in wind estimates approximately every 57 m of height above ground in Mode 1 and every 97 m for Mode 2. The vertical ranges of these two modes were nominally about 3000 m and 6000 m, so Mode 1 had approximately double the vertical resolution and half the vertical extent of Mode 2.

2.2.2. SODAR

A phased-array Doppler SODAR (Remtech PA0 on loan from the U.S. Forest Service) was used to measure the vertical wind structure in 20-m intervals up to 400 m above ground level at the Granby, Colorado, airport (latitude 40.089 N, longitude 105.917 W, 2500 m elevation) during the spring study only. SODAR is similar to radar but utilizes sound rather than radio waves. SODAR systems typically have maximum ranges varying from a few hundred up to several

hundred meters, with better results obtained when there is low ambient noise and at least moderately high relative humidity.

2.2.3. Denuder/filter-pack Aerosol Composition Measurements

24-hr integrated samples of $PM_{2.5}$ and key trace gases were collected at the core, secondary, and most satellite sites. Occasionally, samples ran 48 hr, in cases when daily sample changes could not be completed due to personnel constraints. Annular denuder/filter pack systems (URG-3000C) were manufactured by University Research Glassware, Incorporated. Two sampling configurations were utilized, as described below, in the experiments reported here.

The first sampling configuration consisted of a $PM_{2.5}$ cyclone, a carbonate-coated annular denuder to remove gaseous HNO_3 and SO_2, a phosphorous-acid-coated annular denuder to remove gaseous NH_3, a filter pack containing one nylon (Nylasorb, pore size 1.0 µm, Pall Corporation) filter to collect fine particles, and another phosphorous-acid-coated annular denuder to capture any ammonia volatilized from collected particles. Previous work has shown that nitrate loss from nylon filters is negligible (Yu et al., 2005). This sampling configuration was used at the core site, Beaver Meadows, Lyons, Gore Pass, and Timber Creek. A second configuration, used at other satellite sampling sites, differed from the configuration above by replacement of the backup phosphorous acid denuder with a phosphorous-acid-impregnated cellulose filter. The purpose of the coated cellulose filter was also to collect any ammonia volatilized from particles collected on the nylon filter. Denuders used in both configurations were 242-mm long (URG-2000-30X242-3CSS). Blanks were regularly collected from all filter and denuder types to determine minimum detection limits for particle- and gas-phase species of interest.

Denuders were cleaned and coated for each use. The coating solution to collect nitric acid and other acidic gases contained 10 g Na_2CO_3, 10 g glycerol, 500 ml deionized water, and 500 ml methanol. To remove NH_3(g), the coating solution was made of 10 g phosphorous acid, 100 ml deionized water, and 900 ml methanol. The denuders were dried following coating, using pure nitrogen. Denuders were extracted using 10-ml deionized water following collection, either in the field or in the laboratory at CSU, depending on where the samples were collected, and the extracts were refrigerated before ion chromatography (IC) analysis. Filters were stored in clean sample tubes in a refrigerator/freezer until extraction. The nylon filter was extracted using deionized water in an ultrasonic bath. Cellulose filters were also extracted with deionized water and ultrasonication. Filter extracts were refrigerated until analysis by IC.

Due to a lack of electric power at the Alpine Visitor Center, denuder/filter-pack samplers were collected at this site using a battery-powered Rupprecht and Patashnick Mini-Partisol sampler. The sampler contains a $PM_{2.5}$ precut impactor followed in series by two honeycomb denuders and a filter pack. The denuders in this sampler were also coated, using the same coating solutions described above, to collect HNO_3, SO_2, and NH_3. A nylon filter was used for particle collection, followed by a back-up citric-acid-coated cellulose filter to measure the ammonia that could potentially volatilize off the nylon filter. Denuder extractions were performed at the RoMANS core site. Filters were extracted later in the lab at CSU, following procedures similar to those used for the URG system.

2.2.4. IMPROVE Sampler Measurements

As mentioned previously, the RoMANS core site was collocated with the existing IMPROVE site in RMNP. The standard IMPROVE sampler, described by Malm et al. (1994), consists of four modules, each with its own pump, size-selecting cyclone, and sample substrate. Three modules have a 2.5 μm aerodynamic size cut ($PM_{2.5}$) and collect aerosols onto Teflon, nylon, and quartz filter substrates, respectively. The fourth module uses a 10-μm aerodynamic size cut (PM_{10}) and collects particles onto a Teflon filter. During the RoMANS study, two additional PM_{10} modules were installed for collection on nylon and quartz filters. The IMPROVE modules collected 24-hr-integrated samples on the same 8:00 am to 8:00 am schedule used for the URG samplers. Samples were changed by on-site CSU personnel using materials provided by UCD.

Once returned to UCD, the filters collected during RoMANS were analyzed using the same procedures routinely employed for IMPROVE network samples, with the addition of inorganic cation analysis. The $PM_{2.5}$ and PM_{10} Teflon filters were weighed at UCD before and after sampling in a clean, climate-controlled room kept at an RH of 20–40% to determine total gravimetric mass loading. The Teflon filters were also analyzed at UCD by X-ray fluorescence for elemental composition. Concentrations of inorganic anions and cations were measured by IC at the Research Triangle Institute in aqueous extracts of the nylon filters. The quartz filters were analyzed at the Desert Research Institute (DRI) via thermal optical reflectance (TOR) for organic and elemental carbon.

2.2.5. MOUDI Impactor Ion Size Distributions

Aerosol particle ion (Cl^-, SO_4^{2-}, NO_3^-, Na^+, NH_4^+, K^+, Mg^{2+} and Ca^{2+}) mass size distributions were determined using a MOUDI operated at 30 L/min. Samples were typically collected over 48-hr periods to ensure adequate mass collection at these rural sites. To reduce particle bounce, silicone-spray-coated aluminum foil was used as the impaction substrate, with a 37-mm Teflon after-filter, following the last impaction stage. The MOUDI was operated with eight stages with aerodynamic diameter size ranges of $D_p > 18$ μm, 18–10 μm, 10–5.6 μm, 5.6–3.2 μm, 3.2–1.8 μm, 1.8–1.0 μm, 1.0–0.56 μm, and 0.32–0.18 μm, and an after-filter ($D_p < 0.18$ μm). Samples were collected at the core site and, during the spring campaign, at Lyons. Budgetary constraints prevented analysis of the MOUDI samples immediately after the study. These samples were archived for possible future analysis.

2.2.6. $PM_{2.5}$ Semicontinuous Composition Measurements using the PILS-IC

Semicontinuous measurements of $PM_{2.5}$ ion composition were made using a PILS system coupled to two ion chromatographs (PILS-IC). The design and operation of the PILS has been previously described by several authors (Weber et al., 2001; Orsini et al., 2003; Sorooshian et al., 2006) and will be only briefly summarized here. The PILS nucleates aerosol particles to form water droplets by mixing a denuded aerosol stream with supersaturated steam. The nucleated droplets are collected into a flowing liquid stream by inertial impaction. The liquid stream, containing an internal LiBr standard to determine dilution by condensed water vapor, is split into two streams that are injected every 15 min to two ion chromatographs (Dionex, ICS-1500) for measurement of major inorganic ion (Cl^-, SO_4^{2-}, NO_3^-, Na^+, NH_4^+, K^+, Mg^{2+}, and Ca^{2+}) concentrations. Each IC system consisted of a six-port valve injector fitted with a 200 μL

sample loop, a pump, a conductivity detector, an analytical separation column, and a suppressor. The cation eluent was 20 mM MSA (methanesulfonic acid). Cation separations were completed on a Dionex CG12A/CS12A column and CSRS-ULTRA II suppressor. The anion system used a Dionex AS14A column (8 mM Na_2CO_3 / 7 mM $NaHCO_3$ eluent), with an ASRS ULTRA II suppressor.

A $PM_{2.5}$ cyclone (16.7 LPM, URG-2000-30EH) and two URG annular denuders (URG-2000-30X242-3CSS) were used upstream of the PILS-IC. The first denuder was coated with Na_2CO_3 for removal of acidic gases, and the second denuder was coated with phosphorous acid to remove basic gases. Denuders were exchanged every 5–6 days during the spring campaign and once at the study midpoint during the summer campaign. PILS-IC calibration and blank checks were also performed approximately every 5–6 days. Approximately every 10 days during the spring campaign, the impaction surface inside the PILS was cleaned and the ion chromatographs recalibrated. The ion chromatographs were calibrated at the start and conclusion of the summer campaign. A sample flow rate of 16.7 L/min for the PILS-IC was controlled by a critical orifice with a vacuum regulator. An independent measurement of the flow rate was made periodically using a bubble flow meter (Sensidyne Gilibrator).

In addition to the PILS-IC measurements made as described above at the RoMANS core study site, off-line PILS samples were also collected at the Lyons and Gore Pass secondary measurement sites. Two-hr samples were collected at both sites during spring and at Gore Pass only during the summer campaign. Samples were collected into plastic storage vials, using a Gilson fraction collector, frozen, and archived for possible future analysis by IC.

2.2.7. Continuous Gas Measurements

Continuous trace gas measurements were made at the RoMANS core site during spring and summer for the following species: nitrogen oxides ($NO_x = NO_2 + NO$), ammonia (NH_3), ozone (O_3), carbon monoxide (CO), and sulfur dioxide (SO_2). The instruments collected data averaged (arithmetic means) and recorded over 1-min periods. Concentrations are reported as mixing ratios in parts per billion by volume (ppb).

NH_3 was converted to NO and measured by chemiluminescence using a Teledyne-Advanced Pollution Instruments (API) Model 201E analyzer. The instrument consists of a Model 501NH converter (molybdenum catalyzed converter heated to 825°C) upstream of a Model 200E NO/NO_x analyzer. The same analyzer measured total NO_x (conversion at 315°C) and NO (no conversion).

CO was measured using gas filter correlation (at wavelength = 4.3 μm) with a Teledyne-API Model 300EU analyzer. O_3 was measured using photometric UV-absorption (at wavelength = 254 nm) using a Teledyne-API Model 400E. Sulfur dioxide (SO_2) was measured using UV-fluorescence with a Thermo-Environmental Corporation Model 43C Trace Level instrument.

Sampling occurred in a temperature-controlled (20 ± 1°C) shelter (NPS-CSU-UCD mobile air quality laboratory). No additional sample conditioning was applied except for that internal to each instrument (e.g., Teflon particle filter, removal of water vapor).

Ambient air was sampled through a 1-m long, ¼-in outside diameter (OD), Teflon sampling line, sampling at a height of 2.5 m above ground level. Residence time in the sampling line was less than 1 sec. The inlet line was heated to approximately 35°C to minimize losses of ammonia to the tubing walls. To improve low level sensitivity, the ammonia/nitrogen oxides instrument was retrofitted with a gold-plated reaction cell and pumped with an external, high-vacuum pump.

Due to the typical low concentrations during the study, zero gas measurements were performed on an approximately daily basis, while span measurements were performed approximately weekly. NO_2 and NH_3 converter efficiencies were tested once during the middle of each study for several hours and verified to be 95%+ efficient.

2.2.8. Precipitation Collection

Three different methods were used to collect precipitation during the RoMANS study. The type of sampler at each location was dependent on equipment availability, the availability of a site operator, and particular measurement objectives for that site.

The simplest collection method used an open, polyethylene bucket. The bucket sampling system consisted of an open bucket, 23.02 cm in diameter, placed inside a second bucket with a weight to anchor it down. The open bucket typically collected samples for 24 hrs (approximately 8:00 am to 8:00 am). At the end of the sampling period it was exchanged for a clean bucket and any collected precipitation was processed.

Two automated sampling systems, Model TPC-3000 (Yankee Environmental Systems, Inc., Turners Falls, Massachusetts), were used in the study. One was located at the core site. The second was located at Lyons during the spring study and at Gore Pass during the summer study. This system is a wet-only collector and features a precipitation sensor that opens a lid to a polyethylene bucket (diameter = 25.26 cm) when precipitation is sensed; an internal data logger records when the lid to the bucket is opened and closed. This system is similar to that used by the NADP network. The sample was typically collected every morning at 8:00 am for a 24-hr sample, and a clean bucket was placed in the autosampler.

At the core site and at Gore Pass, subevent precipitation samples were collected during many snow/rain events. The subevent sampling system collected precipitation with a large polyethylene funnel (diameter = 52.71 cm) that drained into a polyethylene collection bottle or bucket that was changed periodically (typically hourly) throughout a precipitation event. The funnel was supported inside a large, heatable livestock water bucket. Heat was applied during spring snow periods to melt collected precipitation so it would flow into the collection bottle/bucket. The collection time for the subevent samples changed with site and event. A log book was kept for each site to record stop and start times of collection and blank collection.

At the core site and Gore Pass, all three types of samplers were used. At Lyons a bucket was used during both campaigns and the subevent sampler only in the spring. At the satellite sites only a bucket was used. Because the Brush and Grant, Nebraska, sites were visited only every 2 days, longer integrated precipitation samples were collected at those locations.

Precipitation collectors were rinsed thoroughly with deionized water prior to each sample collection period. Blanks were collected periodically by pouring or spraying approximately 500

mL of deionized water into the collector and processing that water as a blank sample. Because the water used for blank collection can absorb soluble atmospheric trace gases, measured blank solute concentrations can overstate the amount of contamination present on a precipitation collector. Further, any contamination present at the start of a precipitation event is likely to decrease over time. This is especially relevant for subevent sampling where blank values appropriate for an initial sample may be inappropriate for use in correcting solute concentrations measured in subsequent samples.

Empty bottles were weighed prior to sample collection and then after to determine the total volume of sample collected. pH measurements were completed after the weighing. Two aliquots of 650 µL were taken for IC analysis and one aliquot of approximately 10 mL was placed into an amber Nalgene bottle and immediately frozen for later organic nitrogen (ON) analysis. ON samples were taken only at the core and secondary sites and then only when enough sample was collected.

2.2.9. Aerosol Size Distribution and Scattering Measurements

A suite of instruments located at the RoMANS core study site measured aerosol physical and optical properties. Three instruments measured aerosol number size distributions with 15-min time resolution: a differential mobility particle sizer (DMPS; TSI 3085), an optical particle counter (OPC; PMS LASAIR 1003), and an aerodynamic particle sizer (APS; TSI 3021). These three instruments nominally measured over the diameter ranges 0.03–0.84 µm, 0.1–5 µm, and 0.53–22 µm, respectively. However, because of greater uncertainties near the measurement limits, we only use DMPS data over the range 0.04–0.63 µm, OPC data from 0.39 to 0.95 µm, and APS data from 1.0 to 20 µm. The DMPS measures a physical diameter (particles are, however, assumed to be spherical), the OPC measures an optical particle diameter (based on the light scattered by each measured particle but corrected to a physical diameter for a particle of specified refractive index), and the APS measures a particle's aerodynamic diameter. As explained below, these different diameter types can be aligned across instruments to gain information about particle properties (e.g., refractive index or density). The DMPS was operated with a sheath flow rate of 3.0 lpm and a sample flow of 0.3 lpm. The OPC had a sample flow rate of 0.056 lpm. Instrument calibrations were checked twice during the spring study period and three times during the summer period with polystyrene latex spheres of known sizes.

The sizing instruments were housed in a rack inside the temperature-controlled, mobile air sampling lab for both study periods. Sample flow at 0.6 lpm was pulled through an inlet in the roof of the lab and then passed through a Perma Pure dryer that dried the sample to RH < 10% by supplying dry air to the sheath of the Perma Pure. After passing through the dryer, the flow was split into two 0.3 lpm flows that were sent to the OPC and DMPS. Because the OPC operated at a flow rate of only 0.056 lpm, the excess 0.244 lpm was siphoned off before the OPC inlet, using a critical orifice to control the flow. To avoid losses of larger particles, the APS sampled through a separate inlet at 5.0 lpm. The APS sample was dried by heating using a heating tape wrapped around the inlet tube.

An Optec NGN-2 integrating nephelometer located at the RoMANS core study site measured ambient aerosol scattering with 5-min temporal resolution. This instrument has an open-air inlet that does not deliberately exclude any particles by size. The nephelometer uses a Lambertian

light source with an effective wavelength of 550 nm to illuminate a sampling chamber. Aerosols in this chamber scatter light out of the beam that is detected over the range of angles 5–175˚ (Optec NGN-2 Instrument Manual). An internal RH sensor measures the ambient RH of the incoming sample. Similar nephelometer measurements were also made at the secondary study sites at Lyons and Gore Pass. The nephelometers used in the study were installed, calibrated, and operated by ARS.

Particle losses in the sizing rack sampling lines and the Perma Pure dryer were calculated based on the procedures in Hand (2001) and McMeeking (2004), using the equations in Baron and Willeke (2001). Aerosol concentrations were adjusted to account for these losses. Data from both the sizing system and the Optec nephelometer were screened to remove spikes in the data when there was greater than a 100% increase between two adjacent data points. The Optec data were also filtered to remove times when the RH was greater than 90%.

Because the three aerosol sizing instruments all measure over different size ranges and exploit different aerosol characteristics to make their measurements, the output from the instruments has to be reconciled to produce one continuous size distribution. This was done following the alignment method developed by Hand and Kreidenweis (2002). The data from the DMPS, OPC, and APS were first fit to the same diameter grid using a Twomey fit (Twomey, 1975; Markowski, 1987; Winklmayr et al., 1990). The alignment method then reconciled DMPS, OPC, and APS data in two separate steps.

The first step fit the OPC data to the DMPS by adjusting real refractive index, since the OPC output is a function of aerosol refractive index. To characterize the OPC response to different refractive indices, aerosols of known refractive index were size selected by a DMA and then sent through the OPC. By performing this test with oleic acid, which has a real refractive index (m) of 1.46, ammonium sulfate, m = 1.53, and using the manufacture's PSL calibrations, m = 1.588, OPC response curves can be calculated for each of the seven bins (Hand and Kreidenweis, 2002). The alignment process scans through real refractive index, from 1.4 to 1.6 in increments of 0.005 and adjusts the OPC output, based on the previously calculated calibration curves. The DMPS data were also inverted in this step of the alignment. The DMA was run without an impactor, which would give a known upper size limit to sampled particles. Instead, OPC data were used in the DMA inversion to correct for multiply charged particles (Hand and Kreidenweis, 2002). The fit between the refractive-index-adjusted OPC and inverted DMPS data were tested using the χ^2 statistic.

The second step of the alignment fit the APS data to the aligned OPC data in much the same way, by scanning through densities from 1.2 to 3.0 g cm^{-3} in 0.05 g cm^{-3} increments. The APS measured aerodynamic diameter (d_a), which is related to equivalent spherical diameter (d_e) via the equation (Hinds, 1999)

Equation 2.1. $$d_e = d_a \left(\frac{\rho_0}{\rho_e} \right)^{\frac{1}{2}}$$

where ρ_0 is 1.0 g cm^{-3}. The APS output was therefore converted to the equivalent spherical diameter, using the assumed particle density (ρ_e), and compared to the aligned OPC data in the overlap region, using χ^2.

The final output from the alignment technique is a dry aerosol number distribution between 0.04 and 20 μm, expressed as $dN/d\log_{10}D_p$ evaluated at 96 diameters with a base 10 logarithmic bin width of 0.03. The alignment also records the real refractive index and the particle density, resulting in the "best fit" at each measurement point. This technique was successfully employed during the Big Bend Regional Aerosol and Visibility Observational (BRAVO) study in 1999 (Hand and Kreidenweis, 2002) and the Yosemite Characterization Study (YACS) in 2002 (McMeeking et al., 2005).

Volume distributions ($dV/d\log_{10}D_p$) were calculated from the aligned number distributions, and both number and volume distribution statistics were calculated following the procedure described by Seinfeld and Pandis (2006). Integrated total number and volume concentrations were also calculated using bin midpoint diameters for the integration.

2.2.10. Semicontinuous OC/EC

Semicontinuous (1 hr) measurements of $PM_{2.5}$ organic (OC) and elemental (EC) carbon concentrations were made at the RoMANS core site, using a Sunset continuous OC/EC analyzer. The analyzer was installed in the mobile air sampling lab. Aerosol was sampled through a $PM_{2.5}$ size cut and an activated carbon denuder was used to remove volatile organic compounds from the sampled air stream. OC and EC concentrations were measured using thermal evolution in a controlled atmosphere. Pyrolysis/charring artifacts were corrected through monitoring optical transmission through the quartz sample filter, in accordance with the National Institute for Occupational Safety and Health protocol for OC/EC measurement.

2.2.11. CSU Laboratory Analyses of URG, Partisol, and Precipitation Samples

Extracts of URG and Partisol sampler filters and denuders and precipitation samples were analyzed following the RoMANS campaigns in the laboratory at CSU. Analyses of both cations (Na^+, NH_4^+, K^+, Mg^{2+}, and Ca^{2+}) and anions (Cl^-, NO_3^-, NO_2^-, SO_4^{2-}) were made by IC. Cations were separated using a Dionex CS12A column followed by a CSRS ULTRA II suppressor and detected using a Dionex CD-20 conductivity detector. Anions were separated using a Dionex AS14A column followed by an ASRS ULTRA II suppressor and detected using a Dionex CD-20 conductivity detector. The instruments were calibrated daily, using a series of calibration standards prepared from analytical grade salts. Periodic standard and replicate sample analyses were used to monitor calibration stability and analytical precision.

Samples for ON analysis were kept frozen until analysis. Samples were thawed completely, immediately before ON analysis. Inorganic nitrogen species (nitrite, nitrate, and ammonium) were measured in these samples by IC before photooxidation. Prior to photooxidation, samples were acidified to a pH of approximately 3, using concentrated H_2SO_4 (5% (v/v)). A photolysis carousel chamber was used to expose samples in quartz tubes to UV radiation for 24 hrs. The photooxidized samples were then reanalyzed by IC. The difference between the sums of inorganic nitrogen before and after photooxidation represents the amount of ON in the sample.

Chapter 3. RoMANS Field Campaign Observations

The RoMANS spring and summer field campaigns were conducted for approximately 5 weeks each as outlined in the previous chapter. Here we present observations from those campaigns, beginning with wet deposition and moving on to measured gases and particles. More detailed discussion of these observations is presented in Chapter 4.

3.1. PRECIPITATION AMOUNT

Time lines of the hourly precipitation measured at the core site during April, July, and August are shown in Figure 3.1 and summary statistics by month are included in Tables 3.1–3.3. Precipitation data were obtained from the National Park Service Air Resources Division Gaseous Pollutant Monitoring Program (http://ard-request.air-resource.com/). Measurable precipitation occurred during 5%, 13%, and 7% of the hours of April, July, and the first half of August 2006, respectively. The maximum hourly precipitation amount during April was 4.2 mm on April 24 and the maximum hourly precipitation amount in July was 7.5 mm on July 25. Multiday precipitation events occurred during April 23–25 and July 7–10. The total measured amounts were 26 mm during April, 116.3 mm during July, and 24.6 mm during the first half of August 2006.

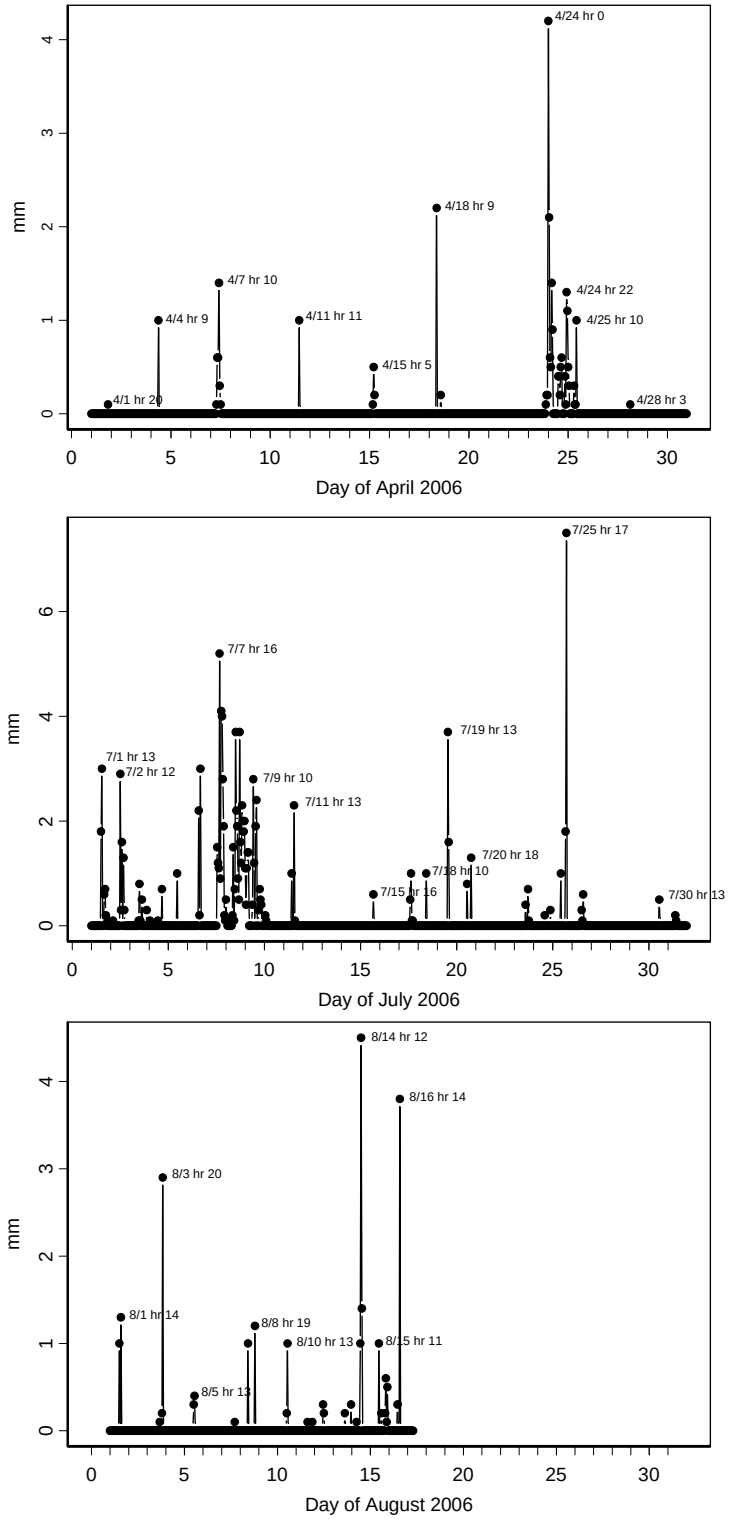

Figure 3.1. Hourly precipitation (mm) measured at the RoMANS core site during April (top), July (middle), and August (bottom) of 2006.

Table 3.1. Summary statistics for core site hourly meteorological data during April 2006.

720 Observations	Temperature (C)	Relative Humidity (%)	Precipitation (mm)	Wind Speed (m/sec)	Wind Direction (degrees)
Minimum	-9.68	6.12	0.00	0.04	1.91
Mean	3.75	42.69	0.04	2.56	235.98
Median	3.72	38.75	0.00	1.99	277.97
Maximum	15.89	96.00	4.20	13.68	358.58
Standard Deviation	5.88	23.09	0.23	1.99	98.52

Table 3.2. Summary statistics for core site hourly meteorological data during July 2006.

744 Observations	Temperature (C)	Relative Humidity (%)	Precipitation (mm)	Wind Speed (m/sec)	Wind Direction (degrees)
Minimum	6.25	10.35	0.00	0.09	0.52
Mean	15.41	54.38	0.16	1.53	241.33
Median	15.28	49.58	0.00	1.44	294.77
Maximum	25.80	97.00	7.50	3.81	359.98
Standard Deviation	4.53	23.34	0.61	0.72	104.56

Table 3.3. Summary statistics for core site hourly meteorological data during August 1–15, 2006.

392 Observations	Temperature (C)	Relative Humidity (%)	Precipitation (mm)	Wind Speed (m/sec)	Wind Direction (degrees)
Minimum	5.50	18.20	0.00	0.11	0.67
Mean	14.30	54.77	0.06	1.48	226.48
Median	14.42	53.82	0.00	1.32	275.11
Maximum	23.20	95.35	4.50	4.31	358.68
Standard Deviation	3.66	16.90	0.37	0.76	102.00

3.2. CORE SITE METEOROLOGY

Summary statistics for hourly averaged, measured meteorological values at the core site for April, July, and the first 15 days of August are shown in Tables 3.1–3.3, and time lines of hourly temperature, relative humidity, wind speed, and wind direction are shown in Figures 3.2–3.5, respectively. There are a few notable features for each measured parameter. For temperatures, there were unusually cold periods during April 6–7, April 18–19, April 25, July 8–9, and August 14–15, though the last of these was after the end of the RoMANS study period. These periods all included at least some hours of precipitation. Much higher wind speeds occurred during April than during the two summer months, and wind directions were predominantly northwesterly but with many hours of southeasterly winds, especially during the cold precipitating events. Relative humidity was variable and included days-long periods of both higher than average (April 7–8, April 23–25, April 28–30, July 7–10) and lower than average (April 8–11, July 12–17, Aug 8–12) relative humidity.

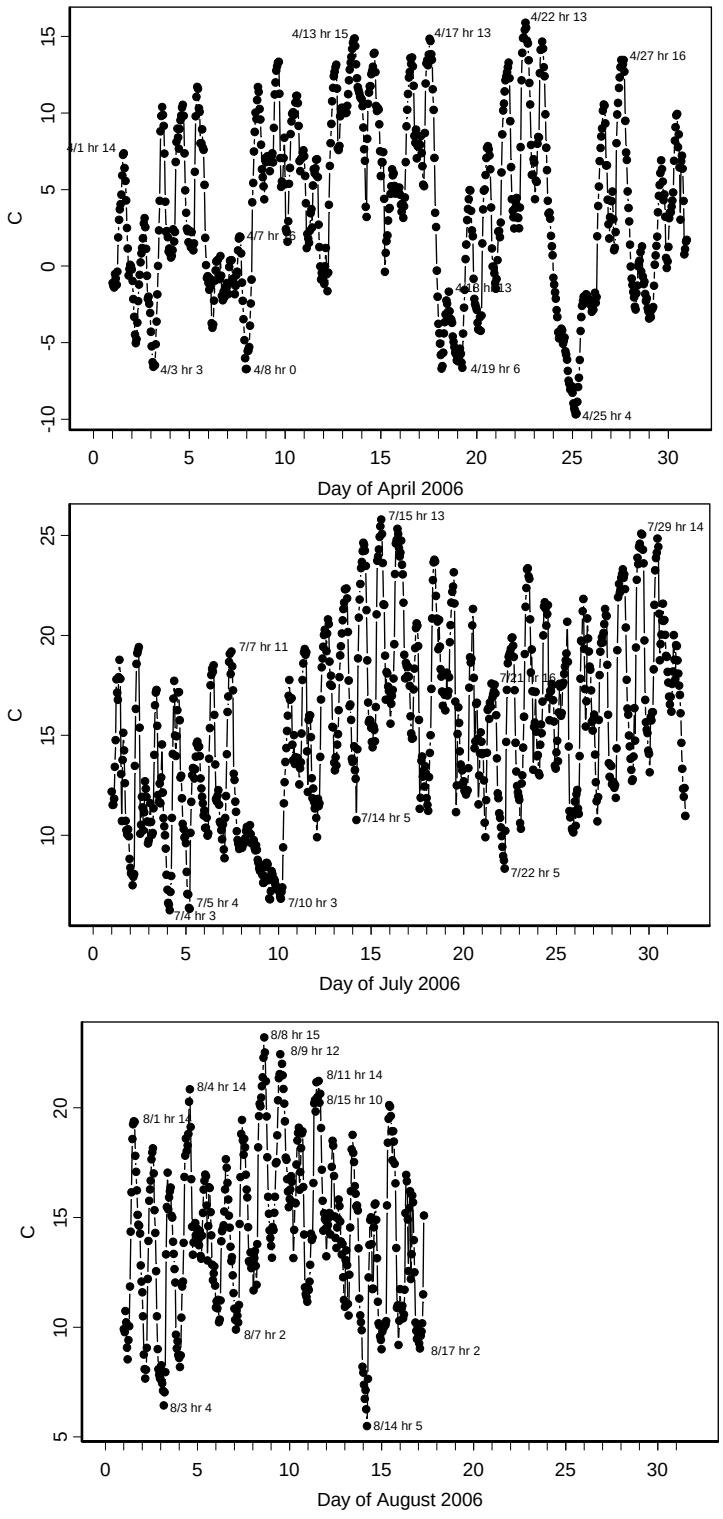

Figure 3.2. Hourly temperatures (deg C) measured at the RoMANS core site during April (top), July (middle), and August (bottom) of 2006.

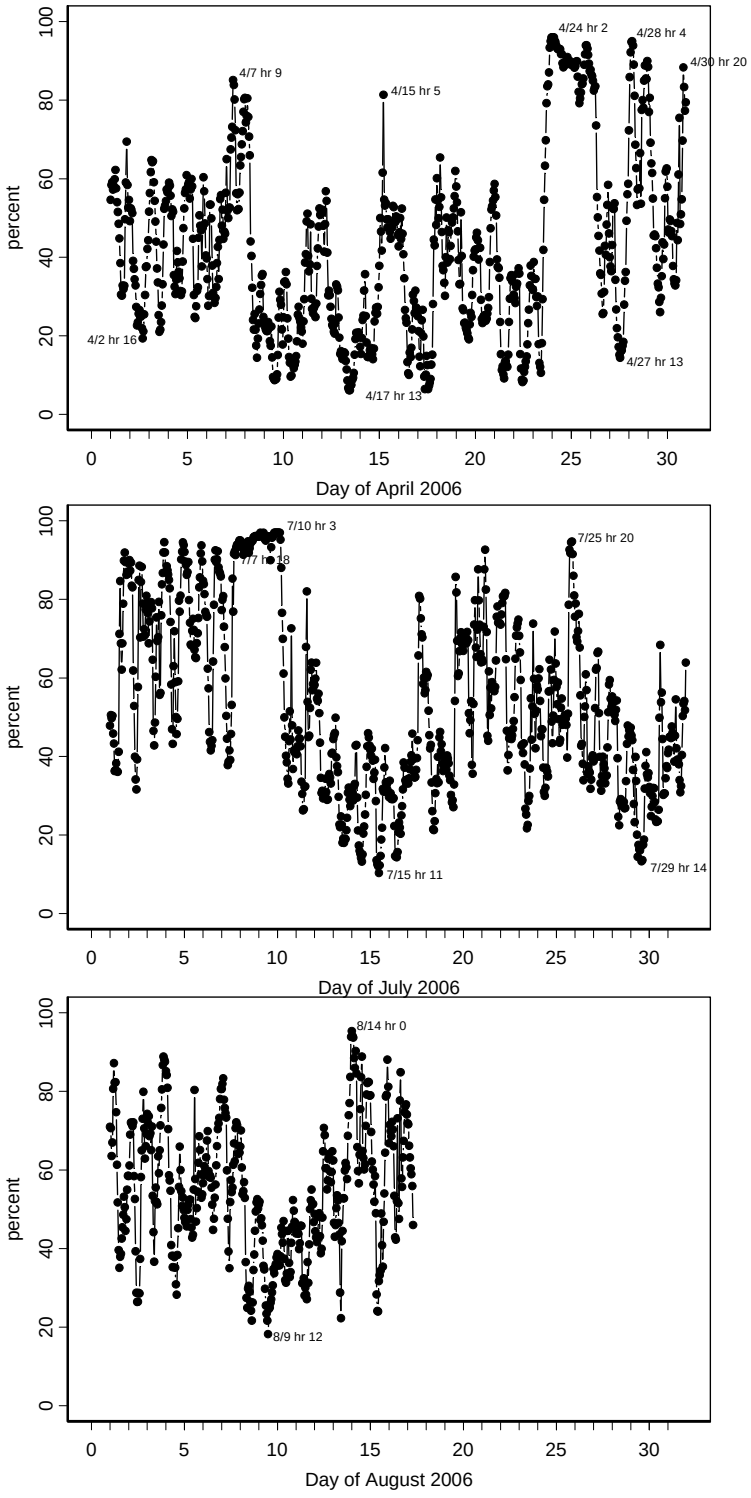

Figure 3.3. Hourly relative humidities (%) measured at the RoMANS core site during April (top), July (middle), and August (bottom) of 2006.

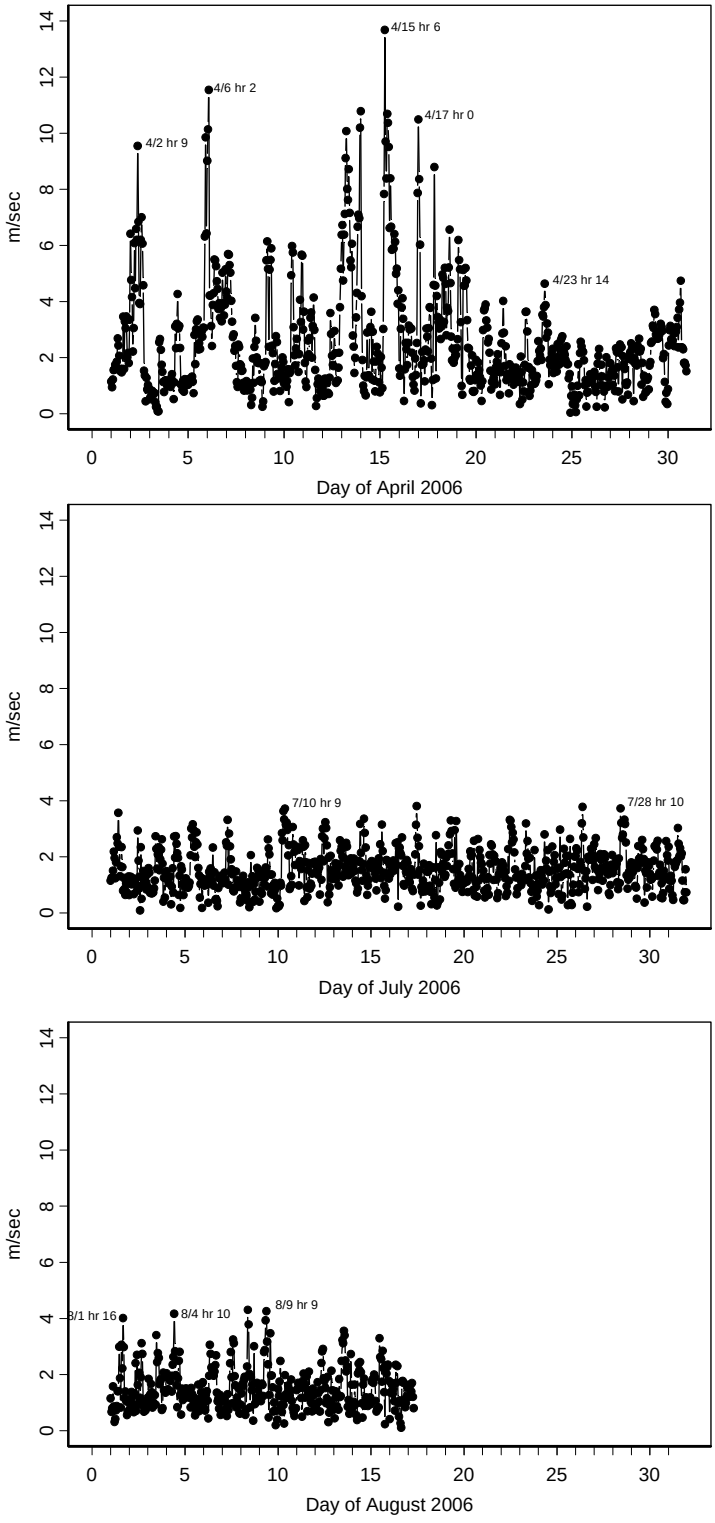

Figure 3.4. Hourly wind speeds (m/sec) measured at the RoMANS core site during April (top), July (middle), and August (bottom) of 2006.

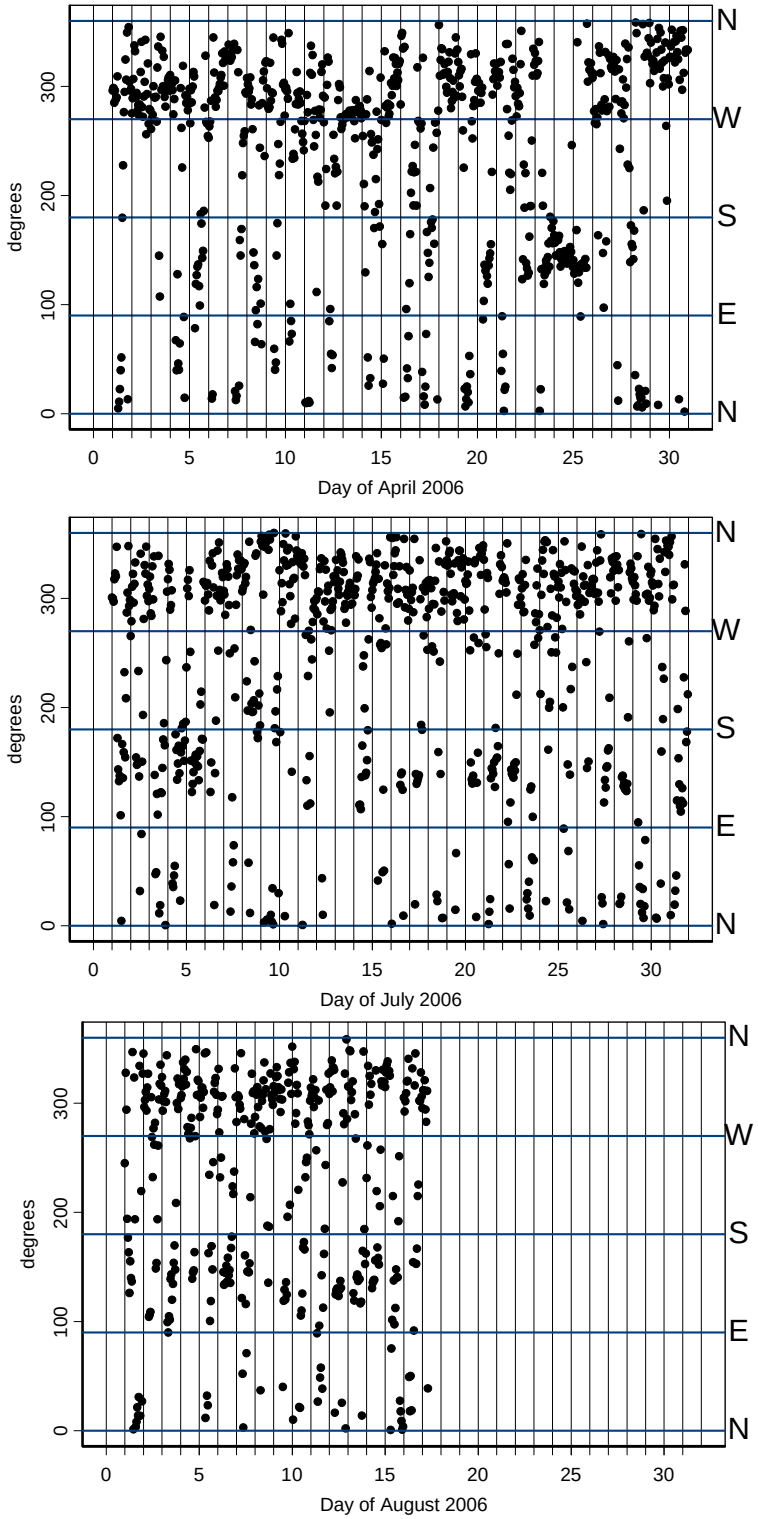

Figure 3.5. Hourly wind directions (degrees) measured at the RoMANS core site during April (top), July (middle), and August (bottom) of 2006.

3.3. RADAR WIND PROFILER

The primary use of the Estes Park wind profiler data during RoMANS was for input to and later evaluation of the mesoscale meteorological modeling; however, the data also provide some insights into the typical upper-air wind patterns in and near the east side of RMNP. For example, there was interest in how often upslope (easterly) winds occurred and the vertical depth of the layers of upslope winds. Figure 3.6 shows the percent of hours during April and July when the horizontal winds at each height arrived from each directional bin in the lowest 2500 m above ground. Winds from 0, 90, 180, 270, and 360 deg are from the north, east, south, west, and north, respectively. As expected, the highest percentage of winds during both spring and summer are from the southwest, near the surface, moving more toward west through northwest with height. Easterly winds occur during both seasons, but the depth of the easterly layer is considerably greater during the summer than during the spring, rising as high as 1500–2000 m above ground level (AGL) during the summer but usually below 1000 m in the spring.

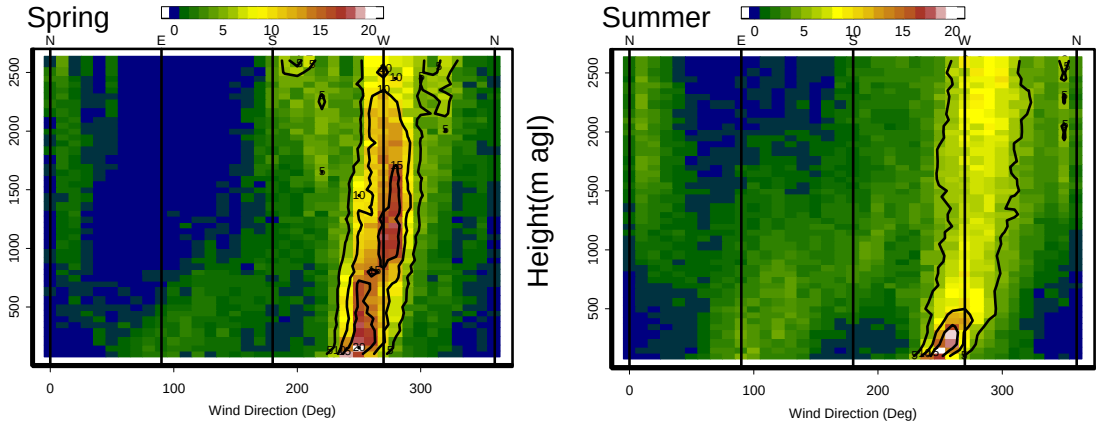

Figure 3.6. Percentages of winds arriving from each direction at each height during the spring (April) and summer (July) RoMANS periods. Data are from the radar wind profiler in Estes Park, Colorado.

Directional roses showing the fraction of Estes Park radar profiler winds from each of 16 directional bins, by four height bins, and by RoMANS season are shown in Figure 3.7. During both spring and summer the winds were predominantly westerly through southwesterly in the lowest 1500 m AGL, and the 1500–3000 m layer included more northwesterly winds than the lowest level during both seasons. In the 3000–4500 m layer, summer winds continued to be predominantly westerly through northwesterly, while in the spring they were mostly westerly through southwesterly at this height level. At the 4500–6000 m level, spring winds were predominantly southwesterly but with a notable fraction from the northeast. During the summer, winds at 4500–6000 m were predominantly westerly through northwesterly but with a large fraction from the southwest. The largest fraction of easterly winds was in the lowest 1500 m during the summer. The spring period also had easterly winds in this layer, but there were also northeasterly winds in both the 3000–4500 m and 4500–6000 m layers.

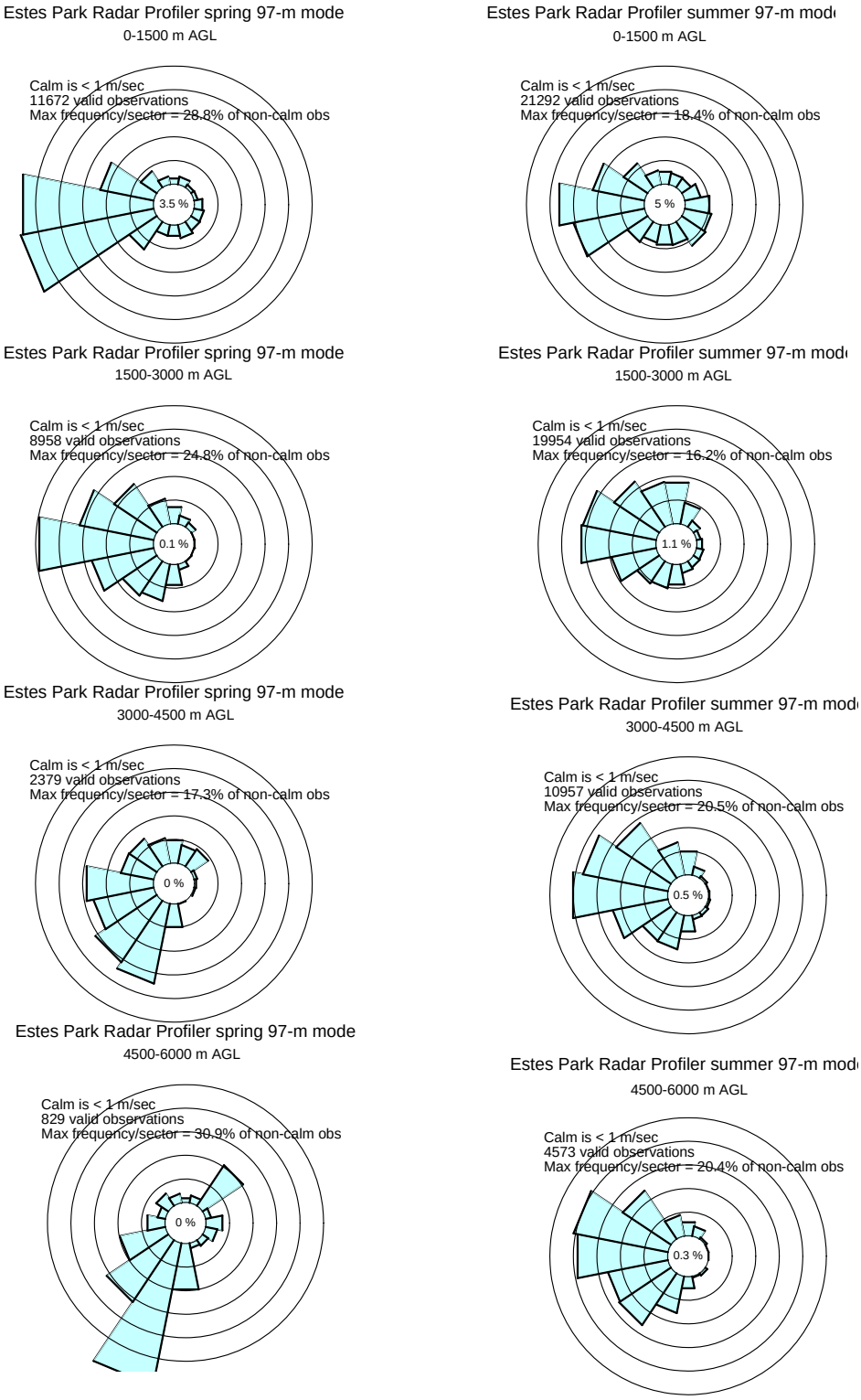

Figure 3.7. Roses showing the percent of radar profiler wind observations from each of 16 directional bins during the spring (left) and summer(right) RoMANS periods for heights of 0–1500 m (top), 1500–3000 m (second row), 3000–4500 m (third row), and 4500–6000 m (bottom) AGL. Rings are in increments of five percent.

Figures 3.8 and 3.9 show box plots of the profiler wind speeds by height for spring and summer, respectively. The centerline of each box is the median, tops and bottoms are the 75th and 25th percentiles, respectively, the whiskers extend to 1.5 times the interquartile range, and more extreme value are shown as horizontal lines. As expected, the wind speeds generally increase with height. As at the 10-m level, spring wind speeds aloft were also higher on average than summer wind speeds.

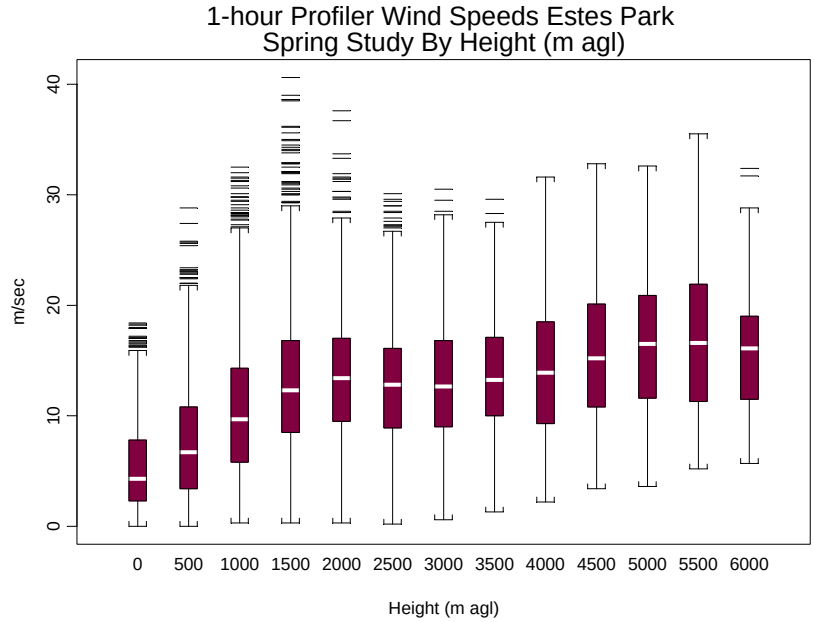

Figure 3.8. Box plots of radar wind profiler wind speeds (m/sec) by height during the spring RoMANS study.

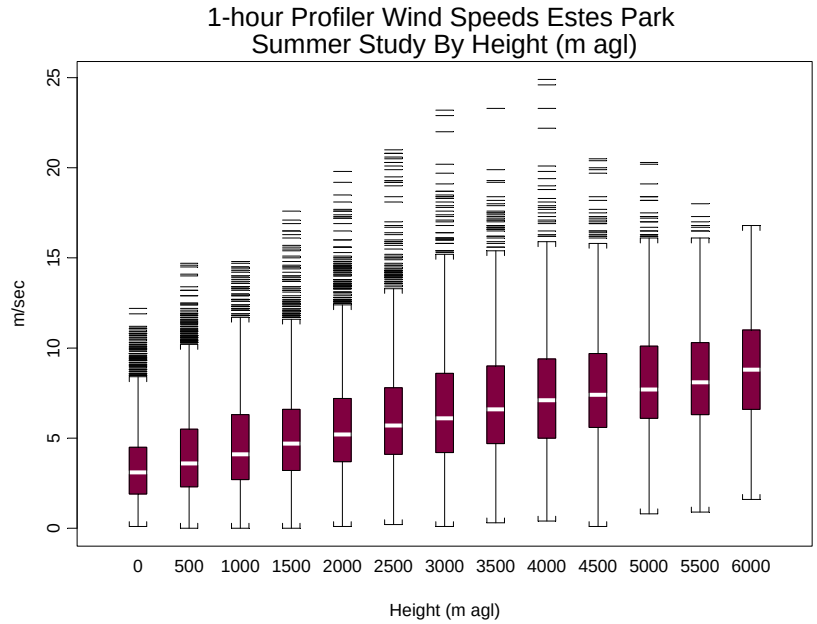

Figure 3.9. Box plots of radar wind profiler wind speeds (m/sec) by height during the summer RoMANS study.

3.4. ROMANS PRECIPITATION CHEMISTRY

As mentioned in Chapter 2, precipitation was sampled at a variety of locations across the RoMANS network. Table 3.4 lists the average concentrations of key species measured in precipitation collected at different RoMANS network sites during the spring campaign. Table 3.5 presents similar observations for the RoMANS summer campaign.

Table 3.4. Average precipitation composition measured during the spring RoMANS campaign.

RoMANS Spring	Average pH	NH_4^+ µg/L	Cl^- µg/L	NO_3^- µg/L	SO_4^{2-} µg/L
Core Site	5.43	317.5	116.4	1151.5	1051.5
Gore Pass	5.21	420.6	87.6	1289.3	1203.9
Lyons	5.71	1263.2	145.7	2959.9	1985.6
Beaver Meadows	5.35	1094.9	682.7	3141.1	3474.5
Brush	7.11	2469.0	293.8	5512.3	2908.5
Dinosaur	6.20	1546.2	1095.5	4235.4	3752.0
Hidden Valley	5.43	284.4	155.7	1658.5	1727.4
Loch Vale	5.42	234.1	153.0	1460.4	1688.6
Grant (NE)	6.43	2345.9	2004.9	1344.5	4122.9
Springfield	6.69	918.8	400.8	1976.1	1596.8
Sprague Lake	5.46	318.0	142.8	1992.6	1794.1
Timber Creek	5.42	469.8	112.9	1457.9	1367.0

Table 3.5. Average precipitation composition measured during the summer RoMANS campaign.

RoMANS Summer	Average pH	NH_4^+ µg/L	Cl^- µg/L	NO_3^- µg/L	SO_4^{2-} µg/L
Core Site	4.52	1031.5	951.9	3158.0	1757.8
Gore Pass	4.40	545.7	131.2	1933.9	811.9
Lyons	5.16	2424.5	195.6	5381.3	1206.4
Alpine	4.65	439.2	764.2	2421.2	1389.2
Beaver Meadows	4.24	2769.0	1492.8	2248.4	4125.7
Hidden Valley	5.07	313.8	1066.2	3305.1	1899.2
Lake Irene	4.52	435.2	425.0	2478.2	1108.5
Loch Vale	4.45	3185.8	1383.6	5187.2	5297.9
Rainbow Curve	4.56	1318.9	1289.1	3876.7	2478.8
Rock Cut	4.48	533.3	298.4	2320.1	1049.9
Sprague Lake	4.56	728.2	531.4	3316.6	1732.0
Timber Creek	4.50	325.1	291.3	1958.6	939.6

The average pH at the various sites ranged in spring from approximately 5.2 to 7.1. Precipitation pH is determined by a balance of acidic and basic inputs. The acid anions, sulfate and nitrate, represent important acid inputs from sulfuric and nitric acids. The base cation, ammonium, represents important base inputs of ammonia. Other potentially important influences on precipitation pH can come from inputs of soil dust and from inputs of weak organic acids (e.g., formic acid, acetic acid, and oxalic acid). For typical pH values observed during RoMANS, gas-phase organic acids like formic acid and acetic acid are quite soluble and mostly dissociate in solution to release hydrogen ions.

Average pH values at sites in RMNP are very tightly grouped, varying between 5.35 and 5.46. The lowest average pH, 5.21, was observed at Gore Pass. Average pH values ranging from 6.43

to 7.11 were observed at the sites on the eastern plains. The average pH at Lyons, 5.71, was intermediate between the plains and RMNP sites, consistent with its location at the boundaries between plains and mountains. The average pH at Dinosaur National Monument was also above 6.

Average pH values decreased somewhat in summer. The average pH at Lyons, for example, decreased from 5.71 in spring to 5.16 in summer. Likewise, the average pH at the core site decreased from a spring value of 5.43 to 4.52. Most sites in RMNP exhibited average pH values, ranging from approximately 4.4 to 4.6, similar to the core site observation. The average pH at Beaver Meadows during summer (4.24), however, was somewhat lower. A higher average pH at Hidden Valley (5.07) appears to be the result of a strong influence from dust and/or plant debris, as the average concentrations of Ca^{2+} and K^{+} in these samples (not shown) were also high.

Not surprisingly, the dominant species in the spring and summer RoMANS precipitation samples are generally nitrate, sulfate, and ammonium. We begin with a review of these observations with a presentation of results from the RoMANS core site and then turn to presentation of precipitation observations from other RoMANS measurement locations inside and outside RMNP.

3.4.1. Precipitation Observations at the RoMANS Core Site

Precipitation was sampled at the RoMANS core site, using both event and subevent sampling approaches. Figures 3.10a and 3.10b depict a time line of major species measured in daily precipitation samples at this location during the spring (Figure 3.10a) and summer (Figure 3.10b) field campaigns. Included in the plots are the daily precipitation amounts and the concentrations of sulfate, nitrate, ammonium, and organic nitrogen (ON or DON) in the daily samples. All concentrations are presented as micrograms of nitrogen (or sulfur) per liter. Considerable variability is observed between events, with concentrations during summer typically exceeding those during spring. Amounts of nitrogen associated with ammonium, nitrate, and organic forms are often similar. No strong pattern is clearly evident between precipitation solute concentrations and the amount of precipitation associated with each event, although a general tendency is observed that many of the higher solute precipitation events are associated with smaller precipitation totals, especially in summer.

The RoMANS core site precipitation observations are presented as deposition fluxes in Figures 3.11a and 3.11b for the spring and summer campaigns, respectively. A deposition flux represents the input of material per unit area per unit time. These are derived for a given species as the product of the measured precipitation solute concentration of that species and the precipitation volume, divided by the cross-sectional area of the collector and collection period (here taken as 1 day). Implicit in the deposition flux calculations is an assumption that the precipitation collector samples a representative amount of precipitation.

Once again we see in Figure 3.11 important wet deposition inputs of sulfur and all three nitrogen forms (nitrate, ammonium, and ON) at the RoMANS core site. Particularly noticeable are the differences between the spring and summer periods. By far, the highest core site deposition fluxes during spring occur during precipitation events shown in Figure 3.11a as April 23 and 24. These two samples actually come from a single snow event that began late on April 23 and

continued until early on April 25. The sample labeled April 23 actually ran through approximately noon on April 24; the April 24 sample was collected from 12:15 pm on the 24th until 1:30 pm on the 25th. This single period of precipitation contributed the vast majority of the total spring wet deposition fluxes of sulfate, nitrate, ammonium, and ON. The high deposition fluxes are the result of the large precipitation amount associated with this event, combined with reasonably high average precipitation solute concentrations.

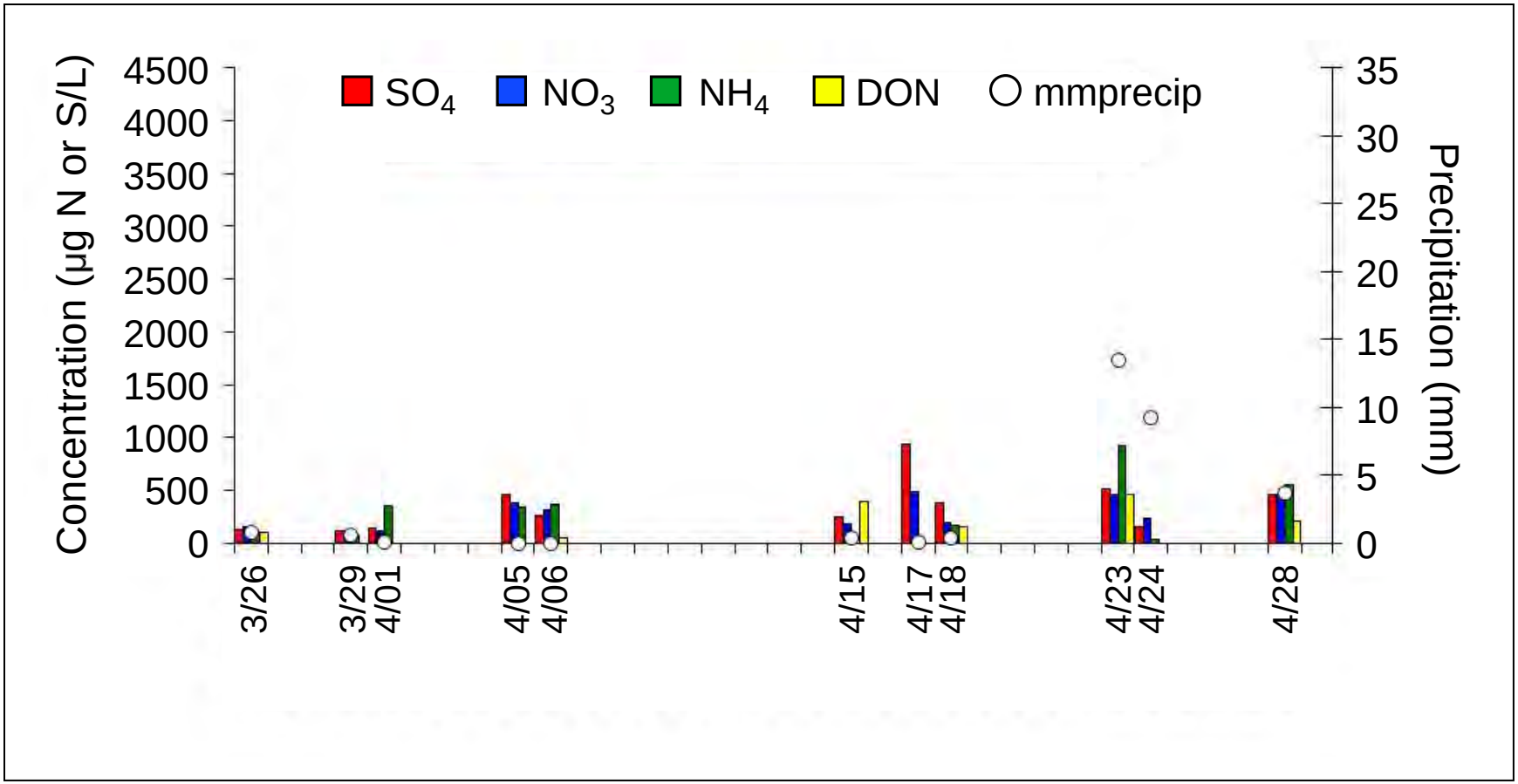
Concentration (µg N or S/L)
4500
4000
3500
3000
2500
2000
1500
1000
500
0
SO4
NO3
NH4
DON
mmprecip
35
30
25
20
15
10
5
0
Precipitation (mm)
3/26
3/29
4/01
4/05
4/06
4/15
4/17
4/18
4/23
4/24
4/28

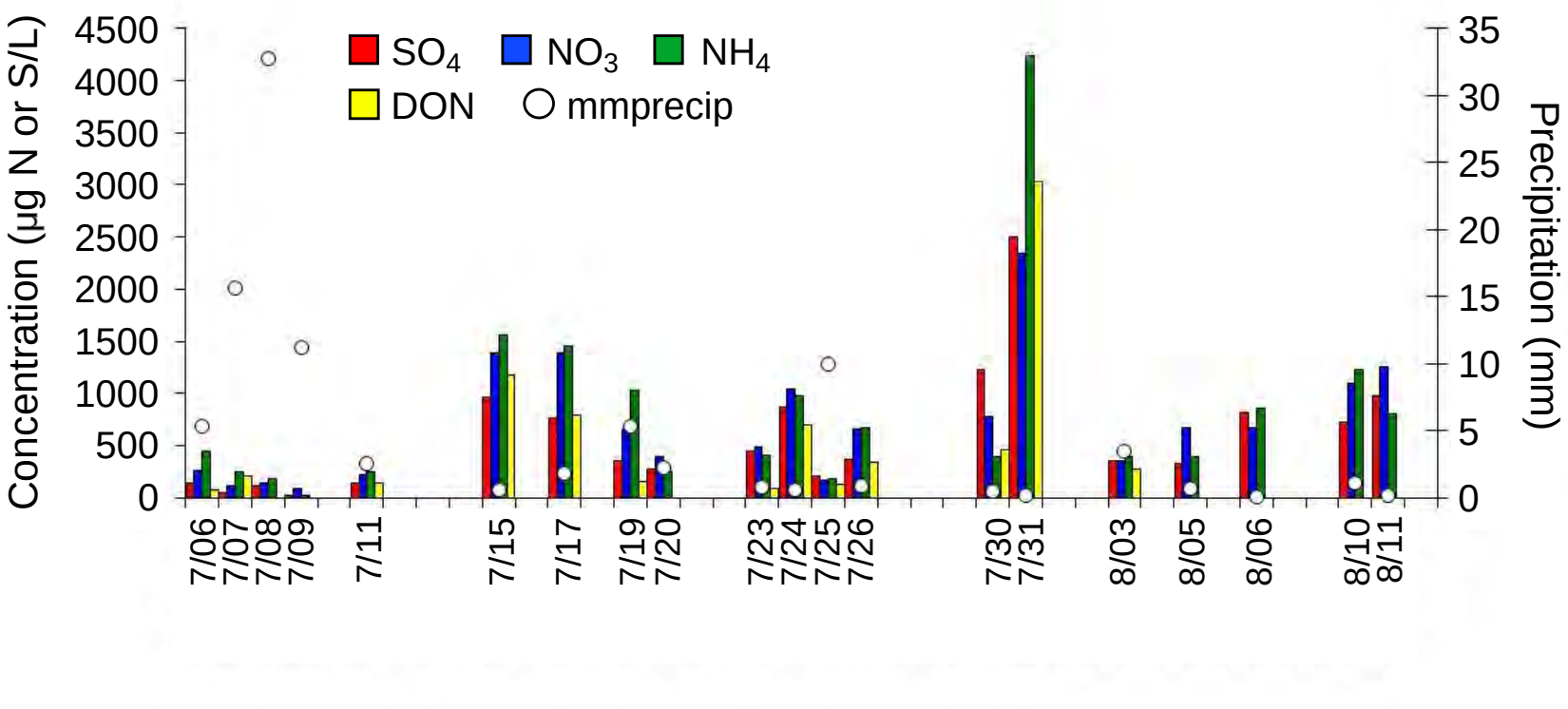

Figure 3.10. Time line of major species concentration (µg/L) measured in precipitation collected at the RoMANS core site during the (a) spring and (b) summer field campaigns.

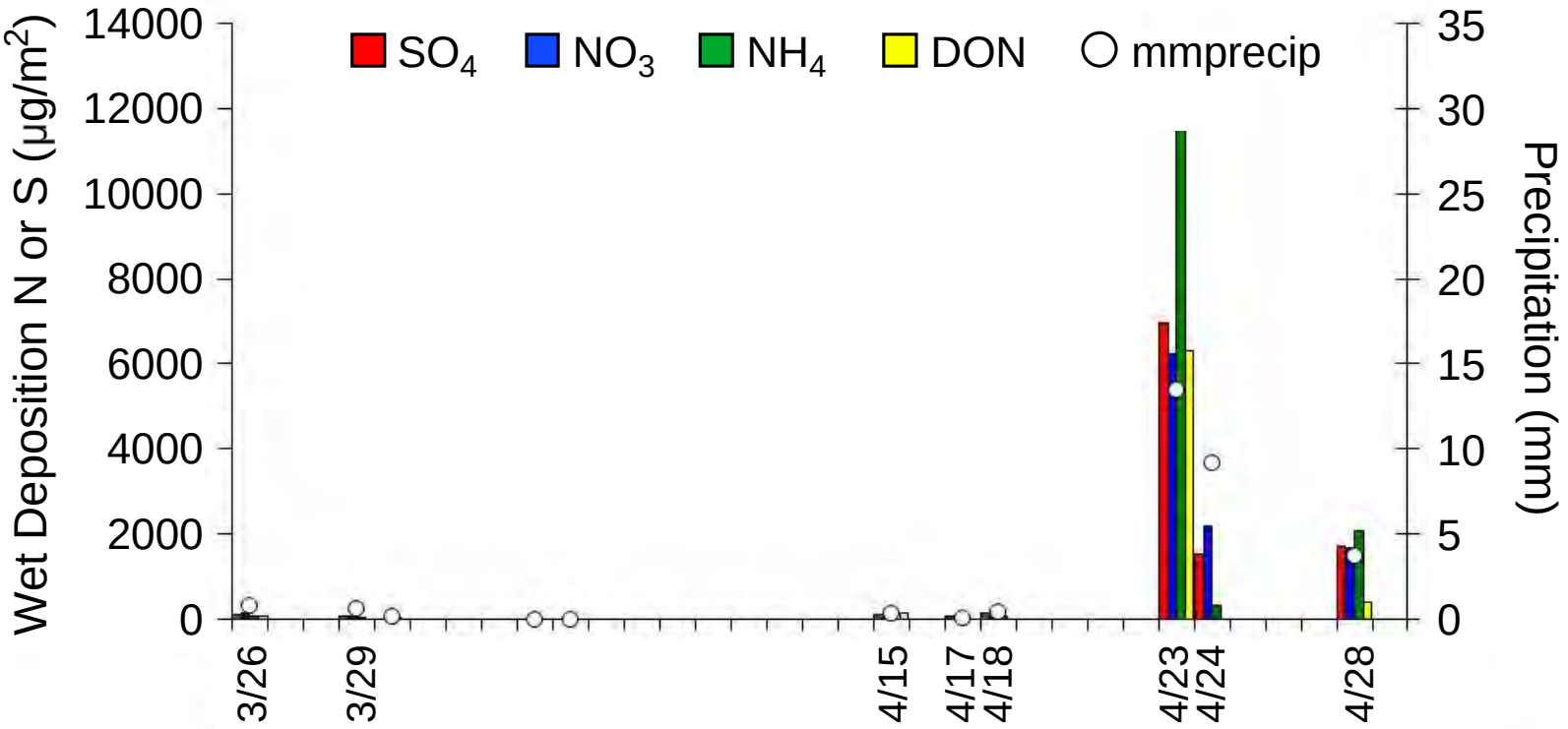
Wet Deposition N or S (µg/m2)
14000
12000
10000
8000
6000
4000
2000
0
SO4
NO3
NH4
DON
mmprecip
35
30
25
20
15
10
5
0
Precipitation (mm)
3/26
3/29
4/15
4/17
4/18
4/23
4/24
4/28

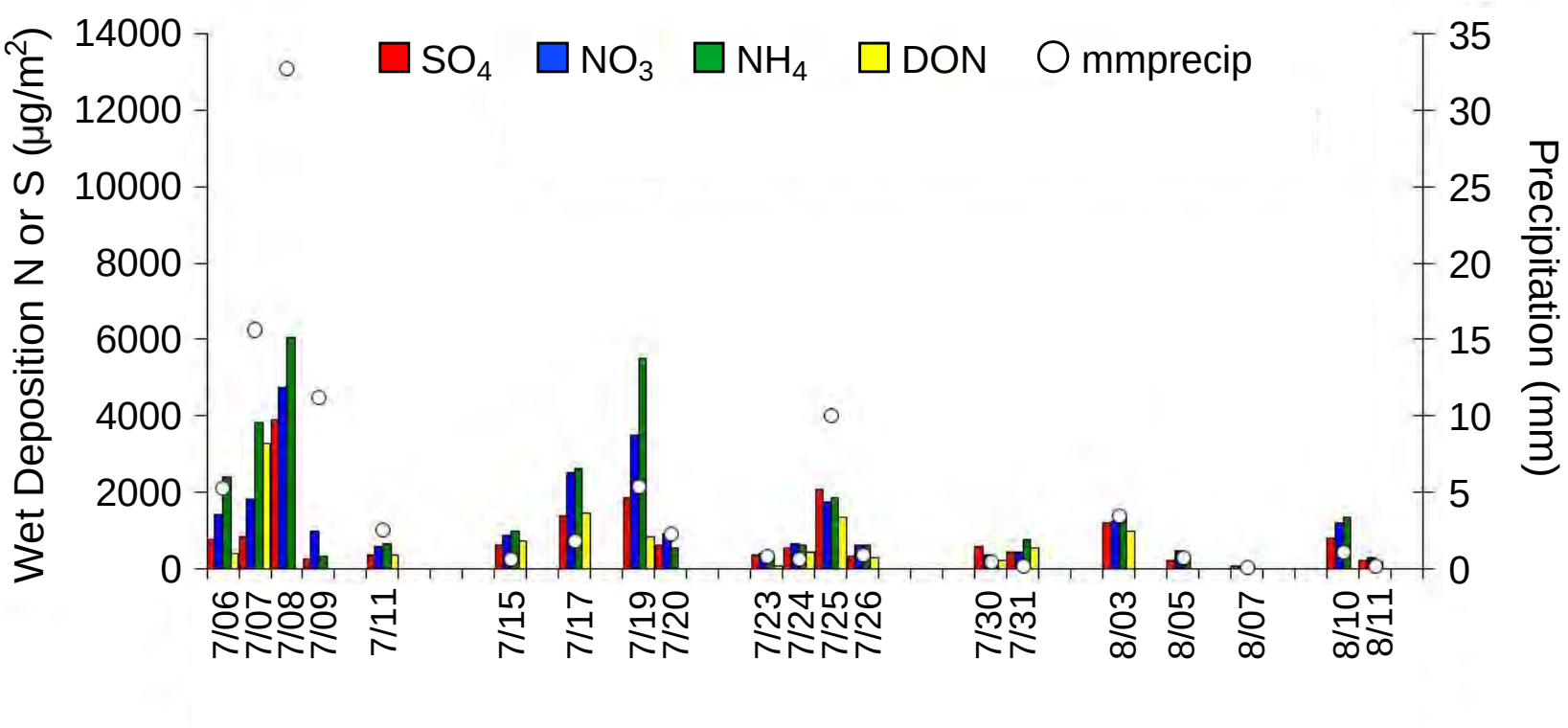

Figure 3.11. Time line of daily wet deposition fluxes (µg/m^2) of major nitrogen and sulfur species at the RoMANS core site during the (a) spring and (b) summer field campaigns.

The time evolution of precipitation solute concentrations during this important spring wet deposition event at the core site is depicted in Figure 3.12. The highest concentrations are observed at the start of the event, followed by a steep decline over the first 4 hours of snowfall. As precipitation intensity picks up around midnight, the solute concentrations remain low. Interestingly, the highest initial concentrations of nitrogen species during this event are seen for ammonium, followed by ON.

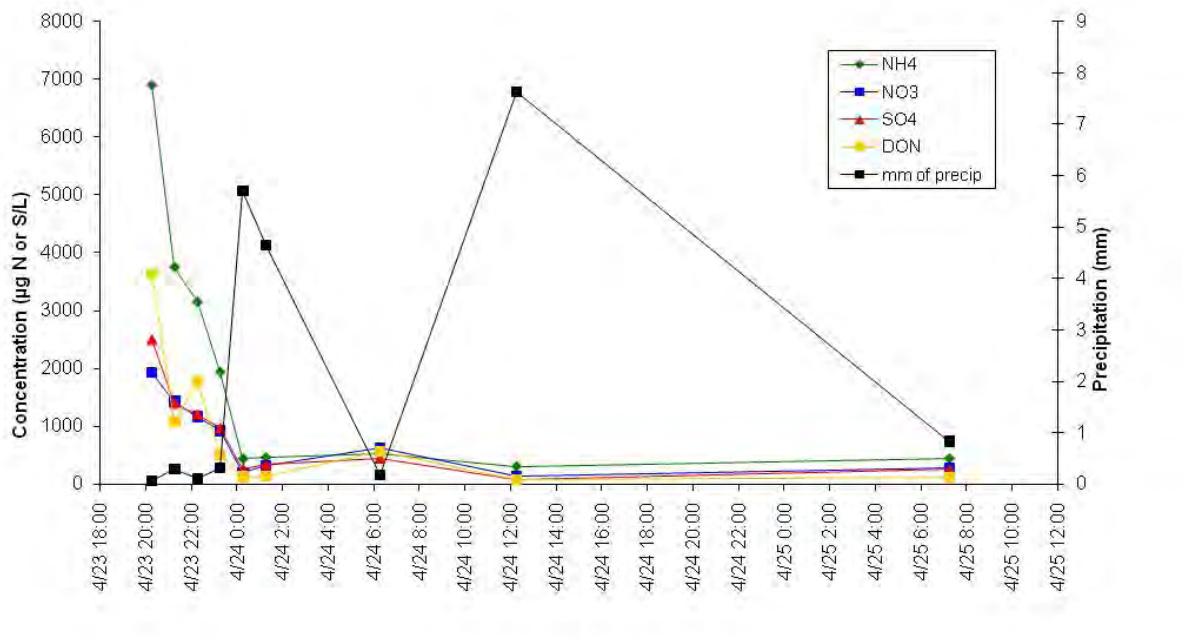

Figure 3.12. Time evolution of precipitation solute concentrations (µg/L) at the RoMANS core site during the period April 23 through April 25, 2006.

A cumulative plot of deposited nitrogen and sulfur for this snow event is shown in Figure 3.13. Here, one sees a steady climb in deposited nitrogen and sulfur for the first several hours of the event, followed by a more gradual increase later on. During this particular episode, ammonium is the main species contributing to total nitrogen deposition, followed by nitrate and ON. Note that the cumulative deposition fluxes of individual species during this event differ somewhat between the subevent and daily precipitation samples, with the daily sample fluxes exceeding those from the subevent sampler. The greater deposition in the event sampler is at least partly due to greater precipitation collection by this sampler (almost 24 mm precipitation), compared to the subevent sampler (approximately 20 mm). Subevent precipitation concentration and deposition flux time lines for other spring precipitation episodes studied at the RoMANS core site are shown in Appendix 1.

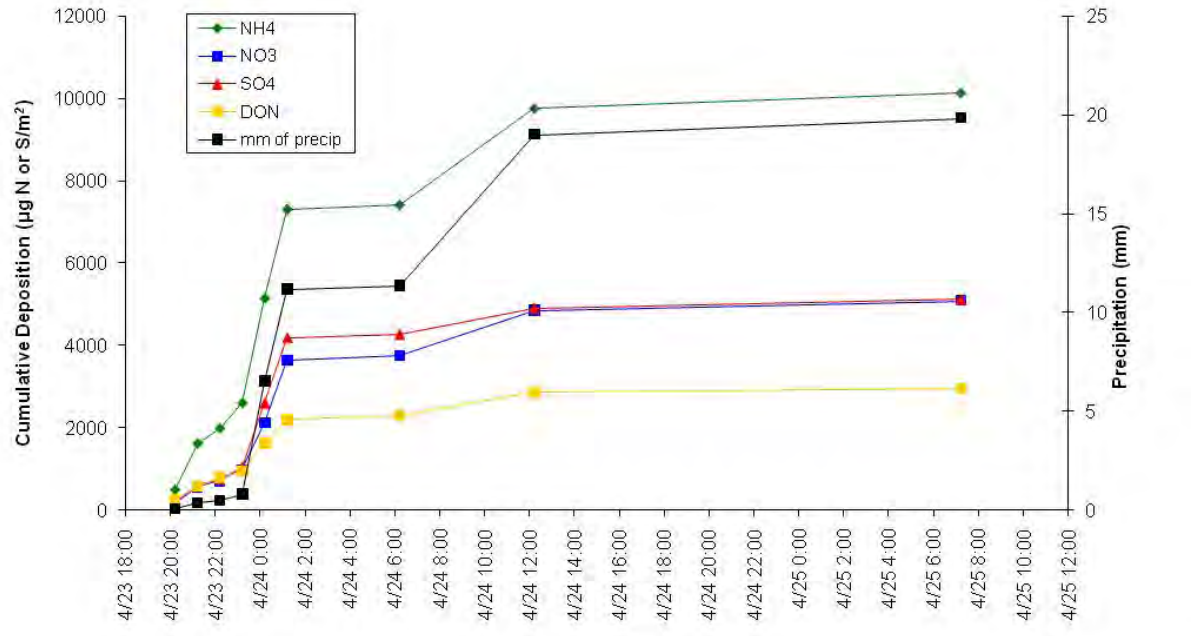

Figure 3.13. Time evolution of cumulative precipitation (mm) and wet deposition (µg/m^2) of major solute species at the RoMANS core site during the period April 23 through April 25, 2006.

Comparing Fig. 3.11a and 3.11b, one also notices that the total wet deposition of major species is more evenly spread across numerous precipitation episodes during the summer campaign than was observed during spring. The bulk of the summer campaign wet deposition was observed during July, with significantly smaller deposition fluxes measured in August. The more abundant summer deposition fluxes result in general from a combination of greater precipitation amounts and higher average precipitation solute concentrations. None of the summer episodes, however, individually contribute as much to wet deposition as the late April snowfall discussed above.

Figures 3.14 and 3.15 illustrate time series of major solute concentrations and deposition amounts for a rain episode at the RoMANS core site during the summer campaign. This particular rainfall is associated with convective activity on the afternoon and evening of July 7. This event is chosen here for illustration because it exhibits interesting temporal patterns in precipitation solute concentrations and because it is one of the important contributors to summer wet deposition.

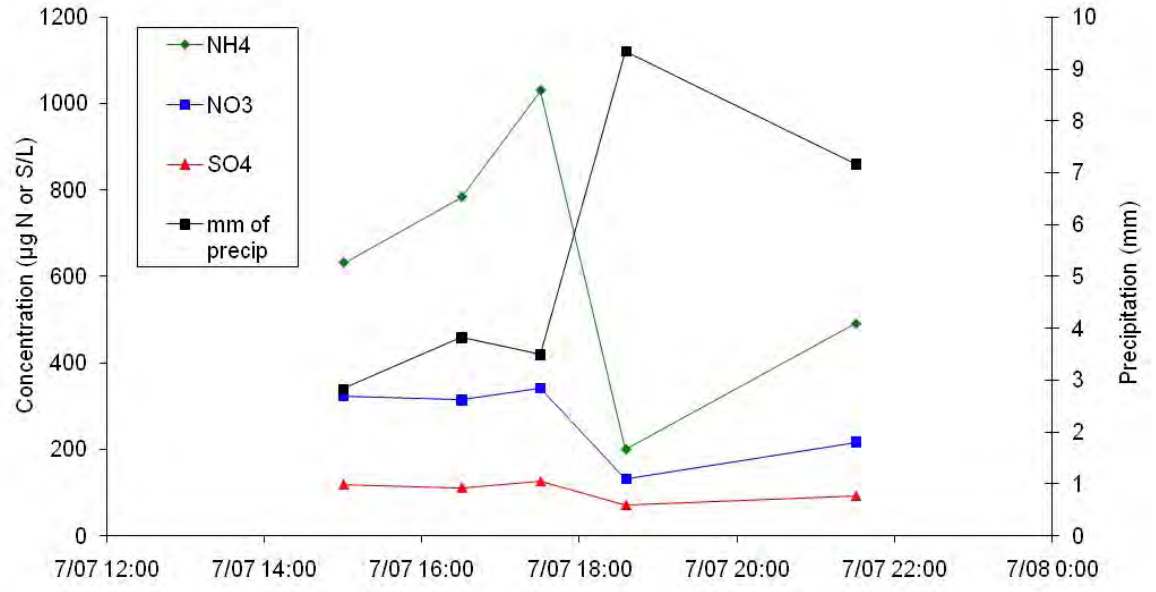

Figure 3.14. Time evolution of precipitation solute concentrations (µg/L) and precipitation amounts (mm) during rainfall at the RoMANS core site during the period July 7 through July 8, 2006.

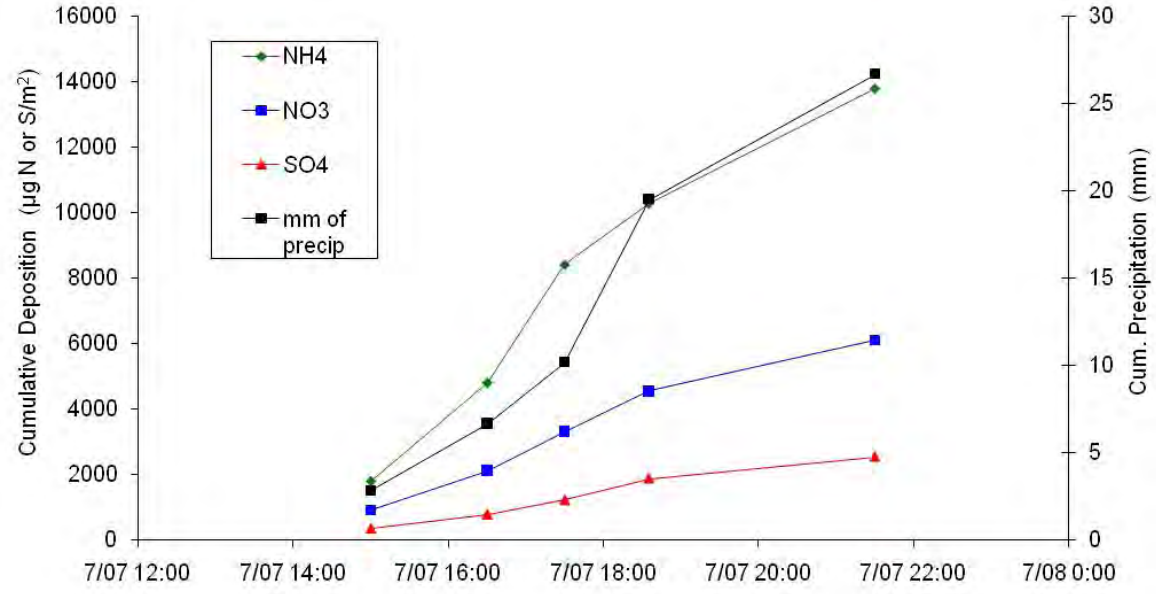

Figure 3.15. Time evolution of cumulative precipitation (mm) and wet deposition (µg/m^2) of major solute species during rainfall at the RoMANS core site during the period July 7 through July 8, 2006.

In contrast to the April 23–25 episode described above, precipitation solute concentrations during the July 7–8 event do not show a rapid decline with time (see Figure 3.14). In fact, even with substantial precipitation rates at the start of the episode, concentrations of ammonium climb significantly while nitrate and sulfate concentrations hold rather steady. When heavier precipitation begins in the evening, concentrations do decline. Like the April event described

earlier, nitrogen from ammonium is a more important contributor to nitrogen deposition in this episode than nitrogen from nitrate.

The cumulative deposition time lines for this event included in Figure 3.15 reveal a steady climb in the deposition of nitrate, ammonium, and sulfate. Wet deposition of nitrogen from ammonium is more than double that of wet nitrogen deposition in the form of nitrate during this event. ON was not measured in subevent samples during this precipitation episode. A comparison of precipitation amount and wet deposition solute fluxes for this event between the subevent sampler and the automated precipitation collector reveals a significant discrepancy. In contrast to the April 23–26 event, both precipitation amount and solute deposition are substantially higher in this case for the subevent sampler. Approximately 27 mm (just over 1 in) of rainfall was measured by the subevent sampler during the period ending at approximately 8:30 am on July 8. This contrasts with approximately 16 mm of rainfall measured over the same period with the wet-only automated precipitation sampler. A check of an independent rain gauge at the site, included in the meteorological measurement station, reveals precipitation for this period of approximately 23 mm, consistent with the value measured using the subevent sampler. The low bias in precipitation collected for this event by the automated precipitation collector suggests a malfunction in instrument operation or some bias in precipitation collection efficiency.

As a check on the accuracy of measurements from the automated event precipitation collector and the manually operated subevent sampling system across the RoMANS study, a comparison of precipitation amounts and deposition fluxes between these samplers was made. As illustrated in Figure 3.16, deposited amounts of nitrate, sulfate, and ammonium generally show reasonable agreement between the two sampling approaches. Figure 3.17 reveals a similar tendency for sampled precipitation amounts. A tendency of the subevent sampler to sometimes underestimate deposition fluxes is expected, since it is manually deployed and relies on site operators watching for the onset of precipitation to deploy it. Clearly, though, the strong negative bias in precipitation amount and solute deposition recorded by the automated collector July 7–8 is an outlier. Time lines of subevent precipitation chemistry and deposition for other summer episodes measured at the core site are included in Appendix 1. A comparison was also made between deposition fluxes measured by the open bucket and wet-only autosampler at the core site. These measurements were highly correlated, with correlation coefficients for measured fluxes of ammonium, nitrate, sulfate, and water all above 0.98. There was, however, a modest bias between the two samplers, with regression slopes of 0.93, 0.87, 0.82, and 0.75 for water, nitrate, sulfate, and ammonium, respectively.

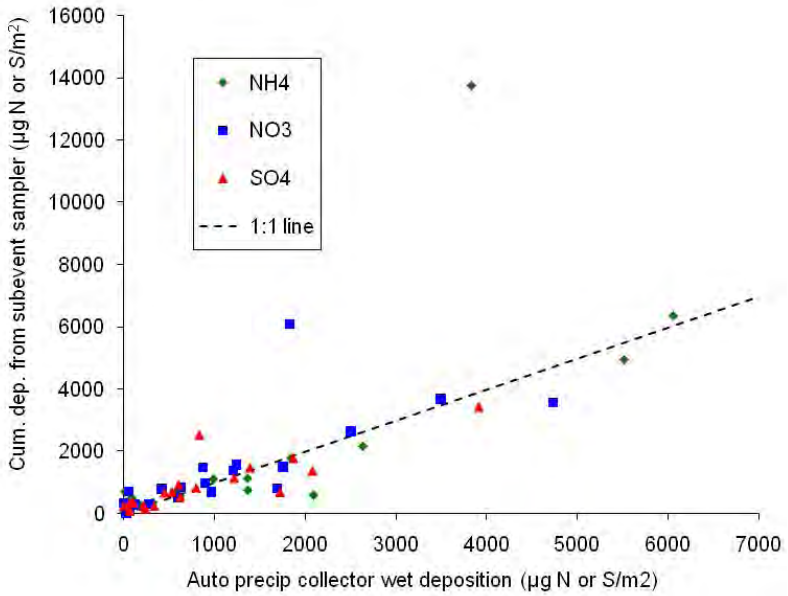

Figure 3.16. Comparison of deposited amounts (µg/m^2) of ammonium, nitrate, and sulfate measured using the subevent (y-axis) and automated event precipitation collectors (x-axis) at the RoMANS core site. A 1:1 line is shown for comparison. The three high outlier points correspond to the July 7 precipitation episode described above.

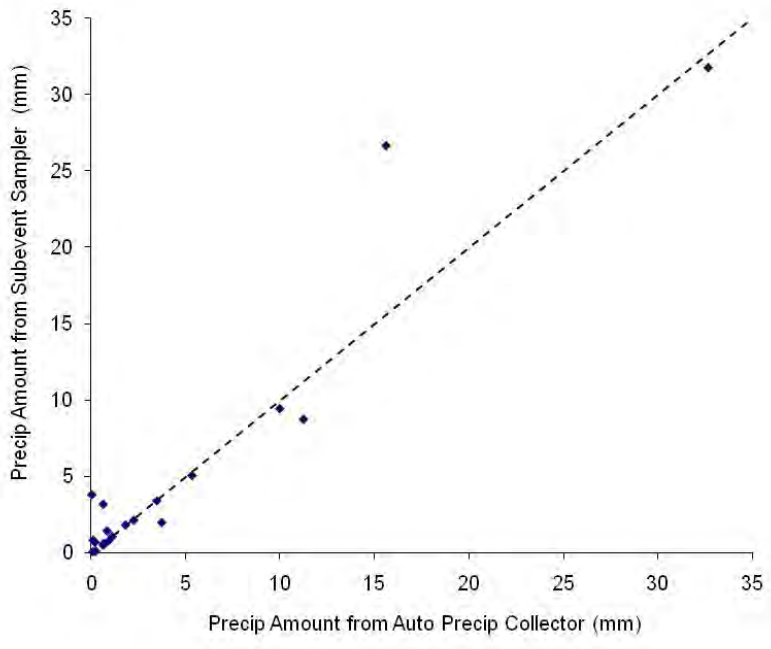

Figure 3.17. Comparison of precipitation amounts (mm) measured using the subevent (y-axis) and automated event precipitation collectors (x-axis) at the RoMANS core site. A 1:1 line is shown for comparison. The outlier point in the upper middle part of the figure corresponds to the July 7 episode discussed above.

3.4.2. Precipitation Observations at RoMANS Secondary and Satellite Sites

Precipitation amounts and solute concentrations measured during the spring and summer RoMANS campaigns were used to calculate total wet deposition fluxes of major inorganic nitrogen and sulfur species at each of the RoMANS satellite sites where precipitation was sampled. Figure 3.18 depicts the total measured precipitation and wet deposition amounts of nitrate, ammonium, and sulfate for the spring campaign. Figure 3.19 depicts the same information for the summer campaign. In both figures the sites are plotted from west to east.

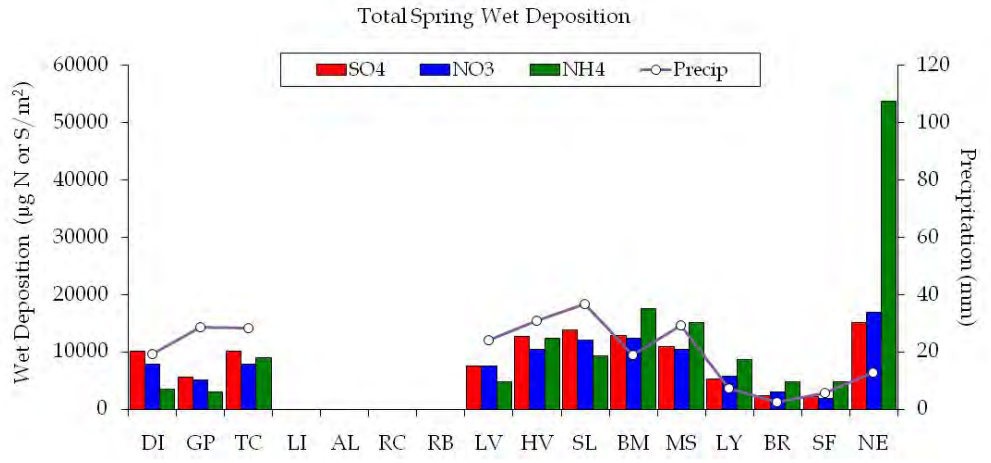

Figure 3.18. Total precipitation (mm) and wet deposition (µg/m^2) of nitrate, ammonium, and sulfate measured in the RoMANS sampling network during the spring campaign. Sites are arranged from west to east. Sites at Lake Irene (LI), the Alpine Visitor Center (AL), Rock Cut (RC), and Rainbow Curve (RB) were not included in the spring RoMANS network due to inaccessibility.

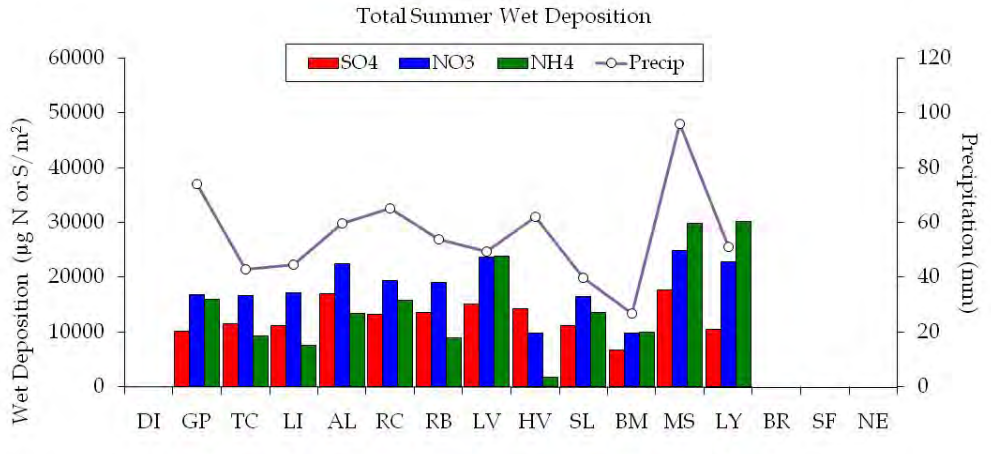

Figure 3.19. Total precipitation (mm) and wet deposition (µg/m^2) of nitrate, ammonium, and sulfate measured in the RoMANS sampling network during the summer campaign. Sites are arranged from west to east. Sites at Dinosaur (DI), Brush (BR), Springfield (SF), and Grant, Nebraska (NE), were not included in the summer RoMANS network due to budget and personnel constraints.

The spring data in Figure 3.18 reveal the typical tendency for higher-elevation sites to receive more precipitation. Measured precipitation at sites on the eastern slope of RMNP ranged from 19 mm at Beaver Meadows to almost 37 mm at Sprague Lake. Timber Creek, near RMNP's western boundary, was in this range as well, with 28 mm of precipitation measured. Moving east of RMNP, spring precipitation dropped off sharply, with sampled amounts ranging between 7 and 13 mm at sites on the eastern plains. Higher precipitation amounts were collected at western sites, with 19 mm at Dinosaur and 29 mm at Gore Pass.

Substantial differences were also observed in wet-deposited nitrogen and sulfur across the network during spring. While wet-deposited ammonium was by far the highest at Grant (NE), the second and third highest amounts of deposited ammonium were measured at Beaver Meadows (BM) and at the RoMANS core site (MS). Interestingly, deposited amounts of ammonium at Loch Vale were less than measured at the other RMNP sites. This was also the case for nitrate and sulfate, although the differences were somewhat smaller for these species. Spring nitrate and sulfate wet deposition were also highest at Grant (NE), followed closely by several sites in RMNP, including Beaver Meadows, Sprague Lake, Hidden Valley, and the core site. Timber Creek had slightly lower amounts of nitrate and sulfate deposition. However, deposited amounts of nitrate, sulfate, and ammonium at Timber Creek significantly exceeded amounts at Gore Pass, despite higher total precipitation at Gore Pass.

Summer observations show some different patterns than observed in spring. First, amounts of precipitation and solute deposition fluxes observed in summer were generally much higher than measured in spring. Greater variability was also observed between sites in RMNP. For example, 96 mm of precipitation was sampled at the core site (MS) while only 27 mm was sampled at Beaver Meadows (BM). Such a large difference in precipitation for two locations so close together (the core site is approximately 10 km SSE of Beaver Meadows) illustrates the strongly localized nature of summer convective precipitation events in this region. Other RMNP study sites had precipitation amounts between these two extremes, as did the Lyons and Gore Pass sites. The highest amounts of ammonium nitrogen deposited during the summer campaign were at the core site (MS) and at Lyons (LY), each receiving approximately 30 mg of ammonium nitrogen per square meter. The highest amounts of wet-deposited nitrate were observed at the core site (24.9 mg NO_3-N/m^2), Loch Vale (23.7 mg NO_3-N/m^2), Lyons (22.8 mg NO_3-N/m^2), and Alpine (22.4 mg NO_3-N/m^2). Sulfate deposition shows only modest changes across the entire summer monitoring network, with all sites measuring between 6.7 and 17.6 mg S/m^2.

Moving from the western RoMANS sites toward the east, one also sees a shift in the relative summer contributions of nitrogen from nitrate and ammonium. For sites near or to the west of the Continental Divide, nitrate contributes as much or more nitrogen to measured wet deposition than ammonium does. Inputs of nitrogen from ammonium and nitrate are nearly identical during summer at Loch Vale and at Beaver Meadows. Sprague Lake shows slightly more nitrate than ammonium contributions. At the RoMANS core site (MS) and at Lyons, however, ammonium nitrogen inputs exceed those from nitrate. A similar trend was observed during spring as well, with nitrate dominating nitrogen deposition at the westernmost sites (Dinosaur and Gore Pass) and a transition to ammonium dominance at sites on the eastern plains. RMNP sites make up part of this transition as well, with many exhibiting similar nitrate and ammonium inputs but with ammonium becoming more important at the easternmost core site and Beaver Meadows site. Note that in summer there is relatively little ammonium deposition at the RMNP Hidden

Valley site. As discussed earlier, samples at this site appear to be influenced by plant debris. It is likely that ammonium was lost by exchange to the canopy at this location as it was not possible to position the bucket in an area free of canopy influence.

In order to examine spatial and seasonal trends in total inorganic nitrogen wet deposition, combined nitrate and ammonium nitrogen deposition has been plotted by site for the spring and summer RoMANS measurement campaigns in Figure 3.20. Sites are included that were operational during both the spring and summer campaigns, although Hidden Valley was excluded from this group, due to the suspected canopy/precipitation interaction issues at this site. This figure clearly illustrates the increased deposition fluxes measured during summer, relative to spring, at all sites except Beaver Meadows (BM). The reduction in nitrogen input at this site is associated with the reduced amount of precipitation collected at this location during summer. Among the RMNP and secondary sampling sites compared here, the highest inorganic nitrogen wet deposition inputs were measured in summer at the core site (MS) and Lyons (LY), followed closely by Loch Vale (LV). The largest relative increase between spring and summer was observed at Gore Pass (GP). Referring back to Figures 3.18 and 3.19, it is clear that the increase at Gore Pass is the result of large increases in wet deposition of both nitrate and ammonium.

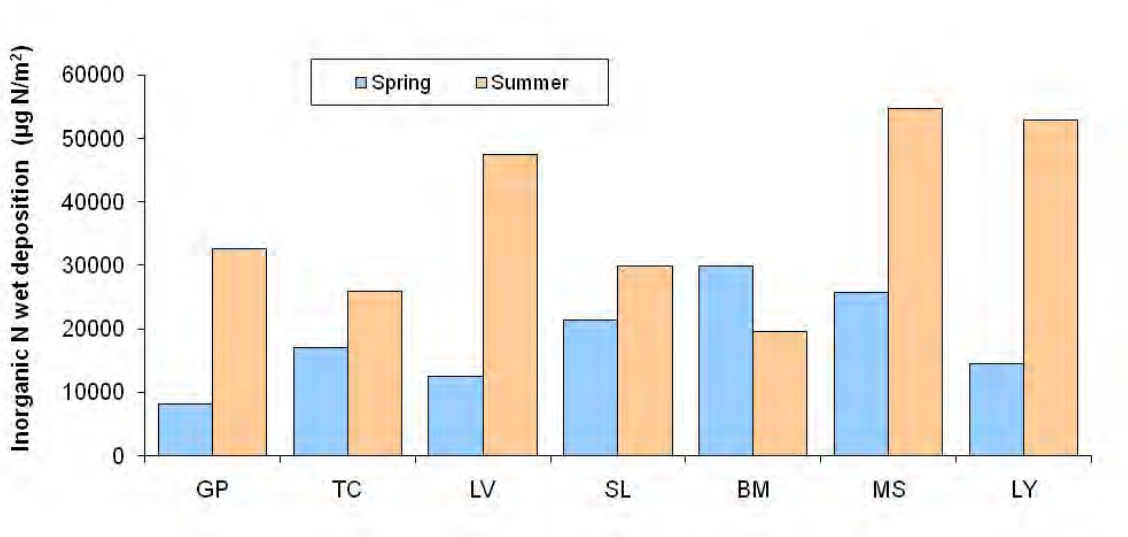

Figure 3.20. Total inorganic nitrogen wet deposition (µg/m^2) measured in the spring and summer RoMANS sampling networks.

Figure 3.21 depicts the spring and summer sulfate wet deposition inputs at the same sites included in Figure 3.20. Although most sites again experienced an increase in sulfate deposition in summer, that increase was much more modest than observed for inorganic nitrogen. In addition, both Beaver Meadows (BM) and Sprague Lake (SL) exhibited a decrease in sulfate wet deposition from spring to summer.

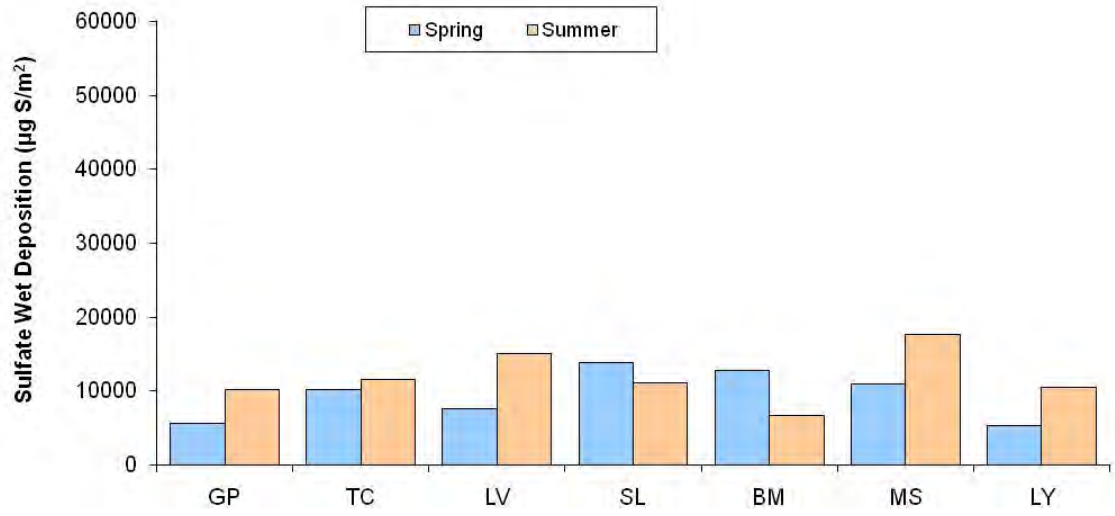

Figure 3.21. Sulfate wet deposition ($\mu g/m^2$) measured in the spring and summer RoMANS sampling networks.

Figures 3.22 and 3.23 depict time lines of wet deposition of nitrate, ammonium, ON, and sulfate at Lyons and at Gore Pass, respectively, during the spring and summer field campaigns. Some similarity is seen in the days with precipitation events at these sites compared to the core site, especially at Lyons, which is located several miles southeast of the core site near the base of the foothills. For example, the large late April snowfall and a period of active convective precipitation activity in the July 7–9 period strongly affected deposition at both Lyons and at the core site. While the late April snow event made the largest contribution to spring campaign wet deposition at Lyons, both the amount of precipitation and the amounts of deposited pollutants were considerably lower than at the higher altitude core measurement site.

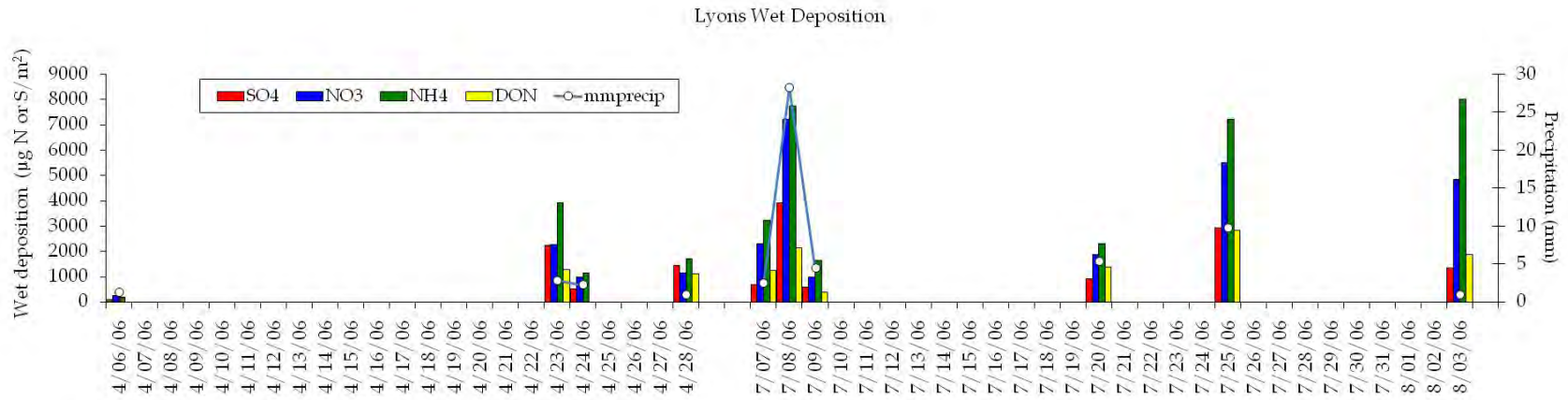

Figure 3.22. Time line of precipitation amount (mm) and major solute wet deposition (µg/m^2) at the RoMANS secondary site in Lyons.

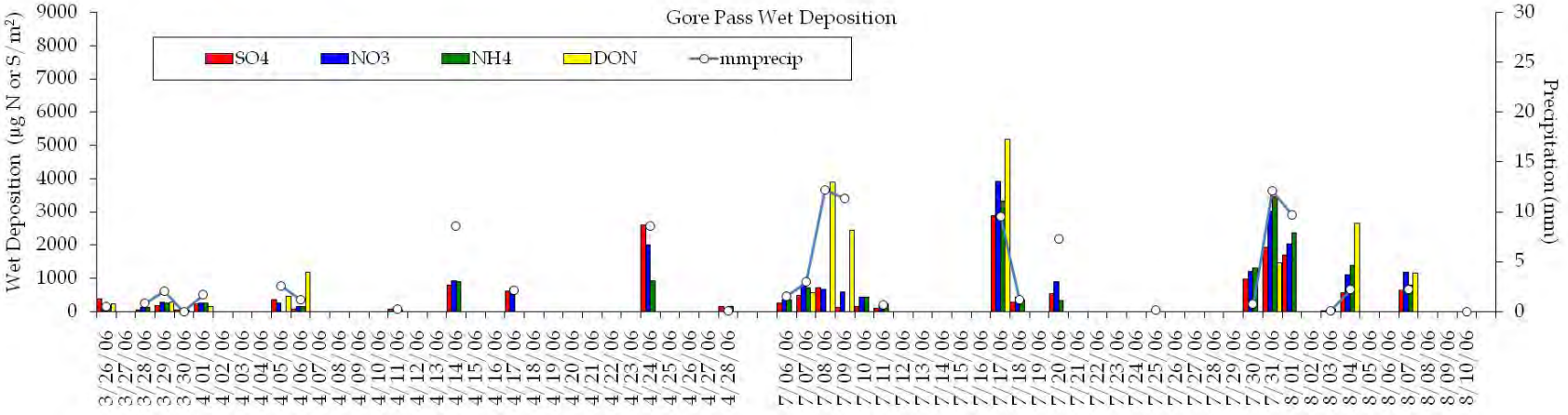

Figure 3.23. Time line of precipitation amount (mm) and major solute wet deposition (µg/m^2) at the RoMANS secondary site at Gore Pass.

Observations of organic nitrogen made in Lyons and Gore Pass deposition samples are illustrated in the wet deposition time lines of Figures 3.22 and 3.23. As at the RMNP core site, we observe significant contributions of ON to total nitrogen wet deposition in most events at both locations. Gore Pass had several precipitation events when measured ON even exceeded the inputs from inorganic ammonium and nitrate.

3.5. INTEGRATED 24-HR MEASUREMENTS OF $PM_{2.5}$ AND TRACE GAS CONCENTRATIONS USING URG SAMPLERS

Denuder/filter-pack samplers were operated at RoMANS core and secondary sites and at many RoMANS satellite sites to measure daily concentrations of $PM_{2.5}$ composition and concentrations of key trace gases. Measurements included inorganic anions and cations and measurements of gas-phase sulfur dioxide, nitric acid, and ammonia. Samples were typically collected over 24-hr periods, from 8:00 am to 8:00 am. Forty-eight-hr collection periods were used in some cases when site access was limited. Details of the sample collection and analysis procedures are provided in Chapter 2.

Table 3.6 lists mean concentrations of key gas and particle species measured using the URG samplers for each site during the spring and summer RoMANS campaigns. Entries are flagged where less than 15 measurements were available for a particular species. During spring the highest concentrations of gaseous ammonia and $PM_{2.5}$ ammonium were measured at Brush (BR) and Grant (NE), respectively. The average gaseous ammonia concentration at Brush increased from 4.9 $\mu g/m^3$ in spring to 8.1 $\mu g/m^3$ in summer. Gaseous nitric acid concentrations were highest during both spring and summer at Lyons (LY), averaging 0.60 $\mu g/m^3$ in spring and 1.6 $\mu g/m^3$ in summer. $PM_{2.5}$ nitrate concentrations were on average highest at Lyons (0.62 $\mu g/m^3$) in spring and at Brush (0.37 $\mu g/m^3$) in summer. The highest average gaseous sulfur dioxide concentrations were observed at Brush in both spring (0.79 $\mu g/m^3$) and summer (0.64 $\mu g/m^3$). $PM_{2.5}$ sulfate concentration averages were highest in spring at Grant (0.95 $\mu g/m^3$) and in summer at Lyons (1.0 $\mu g/m^3$).

Table 3.6. Mean concentrations (and standard deviations, s) of key $PM_{2.5}$ and trace gas species measured across the RoMANS sampling network during the spring and summer 2006 field campaigns. All samples were collected with URG denuder/filter-pack samplers.

	$PM_{2.5}$ cations (µg/m^3)				$PM_{2.5}$ anions (µg/m^3)				gases (µg/m^3)					
	Ca^{++}		NH_4^+		NO_3^-		SO_4^{--}		HNO_3		SO_2		NH_3	
	mean	s	mean	s	mean	s	mean	s	mean	s	mean	s	mean	s
Spring														
DI	0.022	0.012 †	0.281	0.157	0.225	0.144	0.418	0.300	0.343	0.157	0.175	0.113	1.869	0.808
GP	0.014	0.015 †	0.055	0.036	0.192	0.099	0.504	0.258	0.254	0.121	0.133	0.089	0.120	0.069
TC	0.018	0.016 †	0.306	0.237	0.113	0.048	0.375	0.177	0.104	0.052	0.061	0.039	0.057	0.023
MS	0.053	0.026	0.271	0.146	0.320	0.353	0.484	0.262	0.261	0.139	0.184	0.180	0.174	0.063
BM	0.046	0.041	0.233	0.269	0.360	0.457	0.583	0.369	0.289	0.148	0.204	0.154	0.140	0.163
LY	0.073	0.041	0.416	0.427	0.616	0.647	0.634	0.423	0.599	0.340	0.535	0.425	1.086	0.862
BR	0.180	0.074	0.591	0.722	0.543	0.341	0.707	0.347	0.317	0.171	0.794	0.739	4.941	3.014
SF	0.005	n/a †	0.376	0.089	0.266	0.239	0.752	0.293	0.289	0.108	0.233	0.212	0.782	0.399
NE	0.151	0.066	0.656	0.375	0.566	0.340	0.946	0.451	0.447	0.369	0.379	0.262	3.287	1.691
Summer														
GP	0.141	0.025	0.237	0.077	0.092	0.032	0.490	0.172	0.473	0.200	0.102	0.095	0.313	0.096
TC	0.036	0.027 †	0.213	0.093	0.081	0.055	0.689	0.252	0.181	0.065	0.072	0.048	0.207	0.065
AL	0.074	n/a †	0.321	0.093 †	0.197	0.165 †	0.512	0.108 †	0.554	0.123 †	0.421	0.153 †	0.442	0.244 †
MS	0.140	0.039	0.306	0.150	0.146	0.132	0.619	0.186	0.562	0.271	0.152	0.125	0.397	0.273
BM	0.107	0.033	0.318	0.158	0.126	0.095	0.610	0.212	0.602	0.283	0.174	0.133	0.500	0.303
LY	0.143	0.039	0.384	0.208	0.272	0.272	0.999	0.407	1.608	1.033	0.346	0.274	2.341	1.221
BR	0.072	0.053	0.576	0.230	0.374	0.218	0.833	0.252	0.809	0.333	0.644	0.648	8.147	3.518

ROMANS URG data, seasonal averages and standard deviations, values in µg/m ^{3}
All data n = 34 to 37 data points, except <15 where indicated (†)

Figures 3.24 and 3.25 depict the average concentrations of key particle- and gas-phase species measured across the RoMANS network during the spring and summer field campaigns, respectively. In the figures, a bar diagram of the campaign average concentrations of $PM_{2.5}$ nitrate, ammonium, and sulfate and of gas-phase sulfur dioxide, nitric acid, and ammonia is included at the location of each RoMANS network site. The bar diagrams show species mass concentrations in $\mu g/m^3$. Each figure also contains a series of pie diagrams showing the average concentrations of sulfur, reduced nitrogen, and oxidized nitrogen species measured at each monitoring location, with the total size of the pie representing the sum of all of these species concentrations. The sulfur slice of the pie includes gas-phase sulfur dioxide plus $PM_{2.5}$ sulfate. The oxidized nitrogen pie slice includes nitrogen species in the +V oxidation state: the sum of $PM_{2.5}$ nitrate and gas-phase nitric acid. The reduced nitrogen pie slice includes nitrogen species in the –III oxidation state: $PM_{2.5}$ ammonium plus gaseous ammonia. Concentrations represented in the pie diagrams are in units of $\mu mole/m^3$.

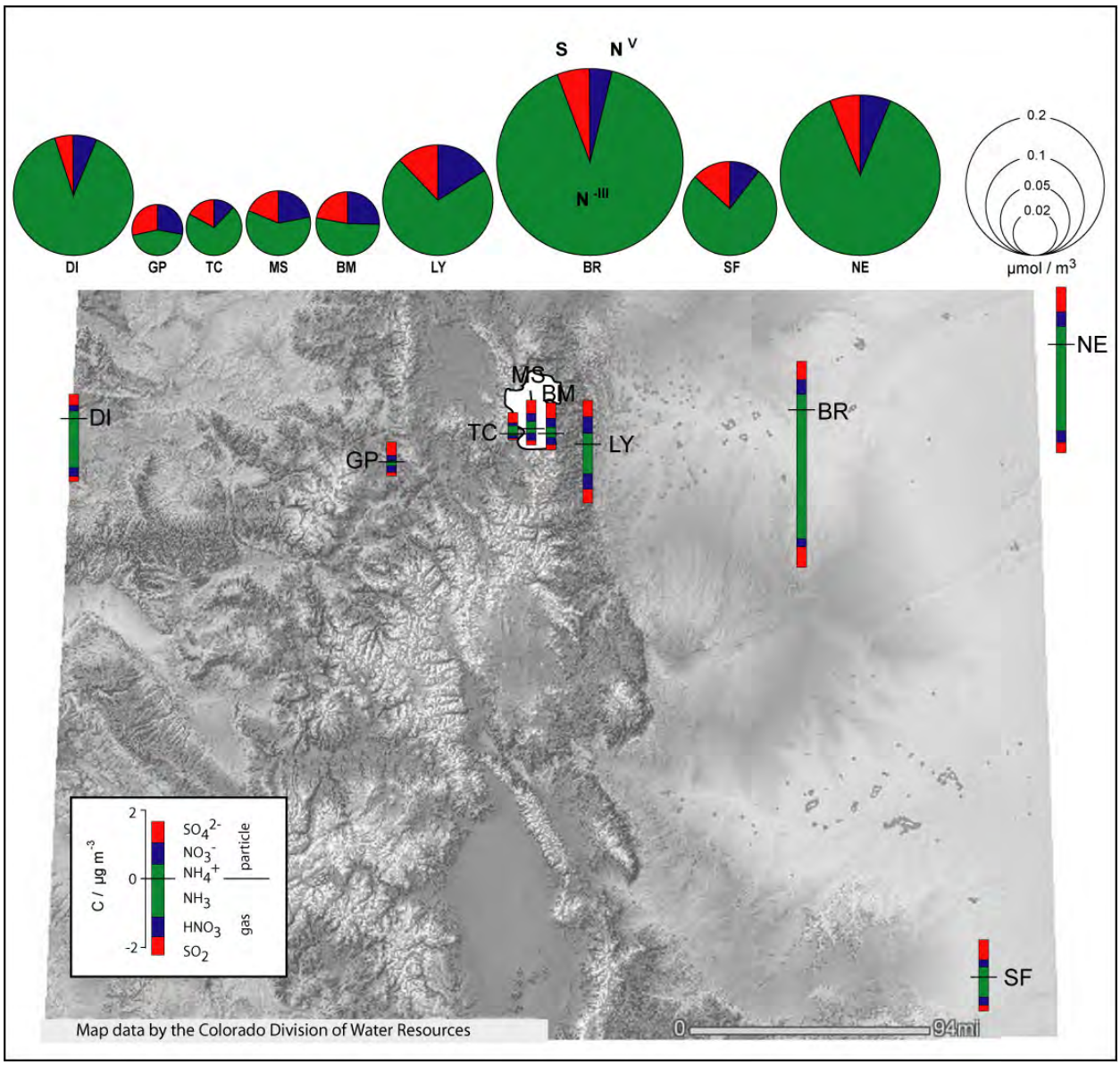

Figure 3.24. Average concentrations of key particle- and gas-phase species measured across the RoMANS network during the spring field campaign shown as bar diagrams positioned at the location of each RoMANS network site. Pie diagrams show the average concentrations of sulfur (S), reduced nitrogen (N^{-III}), and oxidized nitrogen (N^{V}) species measured at each site. The size of the pies is proportional to the sum of these average concentrations at each location.

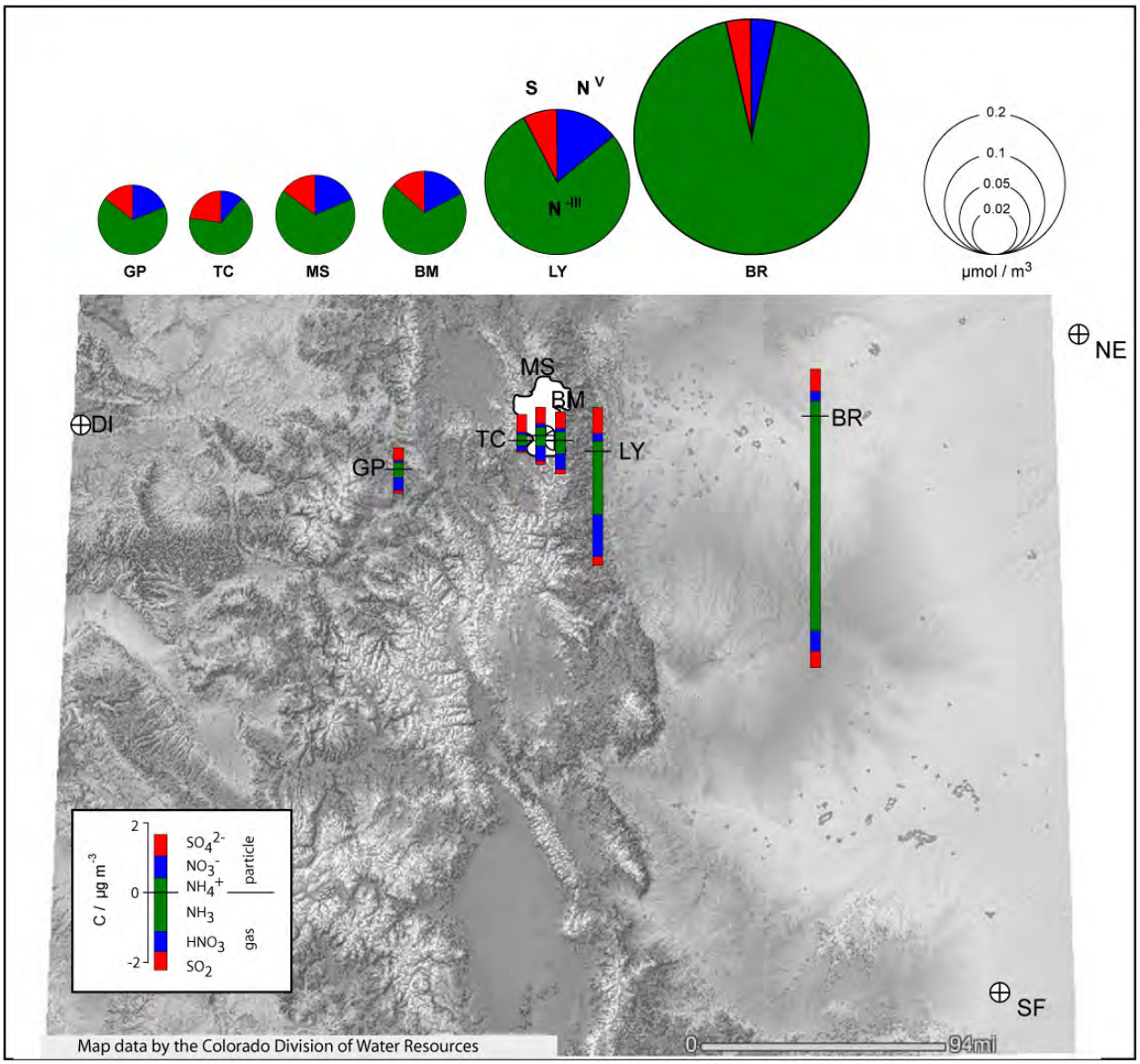

Figure 3.25. Average concentrations of key particle- and gas-phase species measured across the RoMANS network during the summer field campaign shown as bar diagrams positioned at the location of each RoMANS network site. Pie diagrams show the average concentrations of sulfur (S), reduced nitrogen (N^{-III}), and oxidized nitrogen (N^{V}) species measured at each site. The size of the pies is proportional to the sum of these average concentrations at each location.

The observations summarized in Figure 3.24 show a strong gradient in the spring concentrations of many species and in gas/particle partitioning of reduced and oxidized nitrogen species across the RoMANS network. The highest total concentrations measured in the network were at the Brush site (BR) in northeastern Colorado, followed by the site across the Colorado-Nebraska border in Grant (NE). The next highest average total species concentrations were measured at Dinosaur (DI) and at Lyons (LY), followed by the Springfield site (SP) in southeastern Colorado. Total measured species concentrations were substantially lower, on average, at the mountain sites on the eastern slope of RMNP (BM and MS). The lowest concentrations measured in the network were at Gore Pass and at Timber Creek, both west of the Continental Divide. The high total measured species levels measured at sites on the eastern plains and at Dinosaur are strongly dominated by high concentrations of reduced nitrogen. At Grant, Brush, Dinosaur, and Springfield, three-fourths or more of the species budget was composed of reduced nitrogen, with gas-phase ammonia the most important component. The relative importance of reduced nitrogen decreased somewhat further at the Lyons site and then strongly dropped off moving west to the eastern slope RMNP core and Beaver Meadows sites. On the western slope, reduced nitrogen composed less than half the species budget at Gore Pass, with a higher contribution at Timber Creek. It is also worth noting that the dominant contribution of gaseous ammonia to the reduced nitrogen budget seen at lower elevation sites on the eastern plains and at Dinosaur was not observed at the higher elevation RoMANS sites where $PM_{2.5}$ ammonium tends to be more important, on average. While sulfur and oxidized nitrogen species concentrations also varied across the network, the changes were not as dramatic as seen for reduced nitrogen. Average concentrations of $PM_{2.5}$ sulfate showed a modest increase, moving across the network from west to east. Sulfur dioxide concentrations were on average highest at the Lyons and Brush sites. Average $PM_{2.5}$ nitrate concentrations were highest in the northeastern part of the RoMANS network. Gas-phase nitric acid concentrations were highest at Lyons, consistent with its proximity to Front Range NO_x emissions sources.

The average RoMANS network summer concentrations depicted in Figure 3.25 show some important differences compared to spring observations. First, concentrations tended overall to be significantly higher in summer than in spring. Reduced nitrogen species composed more than half of the total measured species budget at all sites in the RoMANS summer network, but contributions remained proportionally largest at the Brush and Lyons sites. Warmer summer temperatures were also accompanied by a shift in nitrogen species phase partitioning toward the gas phase. This is particularly noticeable at the mountain sites where gaseous ammonia was comparable to particulate ammonium concentrations and gaseous nitric acid far surpassed $PM_{2.5}$ nitrate concentrations. This shift is consistent with thermodynamic expectations that predict a shift in ammonium nitrate equilibrium to favor gas-phase ammonia and nitric acid in warmer environments.

The patterns shown in Figures 3.24 and 3.25 represent an average picture of particle- and gas-phase concentrations across the RoMANS network during spring and summer. Further discussions of daily spatial patterns are presented in section 4.4.

3.6. COMPARISON OF 24-HR TO SEMICONTINUOUS MEASUREMENTS AT THE CORE SITE

Compliance under the Regional Haze Rule is based on protocols for reconstructing aerosol mass concentrations and light extinction coefficients (b_{ext}). Reconstruction equations are used to estimate $PM_{2.5}$ mass concentrations (for particles with aerodynamic diameters < 2.5 μm) as well as light extinction coefficients. Dry $PM_{2.5}$ fine mass is computed with Equation 3.1, based on assumed components:

Equation 3.1. $PM_{2.5} = (NH_4)_2SO_4 + NH_4NO_3 + POM + LAC + Soil + SS$

In this form, sulfate is assumed to be fully neutralized ammonium sulfate ($(NH_4)_2SO_4$), nitrate is assumed to be in the form of ammonium nitrate (NH_4NO_3), and organic carbon is included as particulate organic material (POM), computed by multiplying organic carbon (OC) concentrations by a molecular-weight-per-carbon-weight ratio ($POM = R_{oc} * OC$). Light-absorbing carbon is referred to as LAC. We use the term LAC because it is more representative of the optical properties of absorbing carbon than elemental (EC) or black carbon (BC), although these terms are often used interchangeably in the literature. Fine soil concentrations include the contributions from the following assumed forms of elemental species (Equation 3.2) (Malm et al., 1994). Mass concentrations are given in units of $\mu g/m^3$.

Equation 3.2. $Soil = 2.2Al + 2.49Si + 1.94Ti + 1.63Ca + 2.42Fe$

SS refers to sea salt and is estimated as $SS = 1.8*Cl^-$.

The organic carbon multiplier (R_{oc}) used to estimate POM takes into account contributions from other elements associated with the organic matter, such as N, O, and H. As Turpin and Lim (2001) review, the often-used value of 1.4 dates back to samples collected in Pasadena, California, in the early 1970s and 1980s (Grosjean and Friedlander, 1975; White and Roberts, 1977; Van Vaeck and Van Cauwenberghe, 1978; Countess et al., 1980; Japar et al., 1984). More recently, Turpin and Lim (2001) have reviewed several estimates of R_{oc} in terms of the types of compounds known to compose POM, and that review will not be repeated here. However, to summarize their findings, they recommend a factor of 1.6 ± 0.2 for urban organic aerosols, a factor of 2.1 ± 0.2 for nonurban organic aerosols, and values ranging from 2.2 to 2.6 for samples with impacts from biomass burning. Russell (2003) used Fourier Transform Infrared (FTIR) spectroscopy to estimate POM from the number of carbon bonds present and the molecular mass of each functional group associated with the carbon bonds. Over 90% of R_{oc} from estimates from samples in northeastern Asia and the Caribbean were between 1.2 and 1.6, with mean values below 1.4.

Values of R_{oc} as those reported by Turpin and Lim (2001) and Russell (2003) are derived using techniques that depend on the functional groups and molecular compounds of organic carbon aerosols. El-Zanan et al. (2005) used solvent extractions from archived IMPROVE filters at five sites to directly measure POM mass and carbon content and derive an average R_{oc} of 1.92 (range of 1.58–2.58). They also used a mass balance approach to estimate the R_{oc} ratio, using the IMPROVE data that resulted in an average value of 2.07 across the IMPROVE network.

Other types of methods result in similar findings. Reconstruction of fine mass and light scattering coefficients allow estimates of R_{oc} to be derived, as was done in a 2-month study in Yosemite National Park by Malm et al. (2005), where POM dominated the fine mass. They found that an R_{oc} factor of approximately 1.8 allowed for closure in fine mass and light scattering coefficients for periods that encompassed both pristine conditions as well as the impacts of biomass burning and regional haze. Poirot and Husar (2004) found better agreement between measured and reconstructed fine mass by applying an R_{oc} factor of 1.8 during a biomass burning event in the New England and mid-Atlantic state regions. Based on recent work by Malm and Hand (2007) and consistent with the above described analysis, we use an R_{oc} multiplier of 1.8.

3.6.1. Closure between the Sum of Measured Fine and Coarse Mass Species and Gravimetric Mass Concentrations.

Tables 3.7a and 3.7b are statistical summaries of 24-hr-average $PM_{2.5}$ gravimetric mass, ammonium sulfate and nitrate, organic and elemental carbon, soil, and sea salt at the core site as measured using the Interagency Monitoring of Protected Visual Environments (IMPROVE) sampling system during the spring and summer field campaigns. Tables 3.8a and 3.8b show the same summaries for the PM_{10} - $PM_{2.5}$ measurements. The fourth column in each table is the fraction of each variable compared to reconstructed mass. Note, negative coarse mass concentrations can occur at low concentrations due to uncertainties in the PM_{10} and $PM_{2.5}$ measurements.

Table 3.7a. Statistical summary of aerosol species derived from the IMPROVE $PM_{2.5}$ monitoring system for the spring campaign. The number of data points is 37. Units are in $\mu g/m^3$.

Variable	Mean	Std dev	Fraction	Minimum	Maximum
$PM_{2.5}$	2.51	1.45	0.87	0.27	6.15
$PM_{2.5recon}$	2.90	1.45		0.72	6.09
$(NH_4)_2SO_4$	0.66	0.36	0.23	0.16	1.76
NH_4NO_3	0.35	0.44	0.12	0.01	1.65
POM	0.88	0.36	0.30	0.31	1.69
LAC	0.09	0.07	0.03	0.02	0.30
Soil	0.91	0.73	0.31	0.08	3.69
Seasalt	0.01	0.01	0.00	0.00	0.03

Table 3.7b. Statistical summary of aerosol species derived from the IMPROVE $PM_{2.5}$ monitoring system for the summer campaign. The number of data points is 35. Units are in $\mu g/m^3$.

Variable	Mean	Std dev	Fraction	Minimum	Maximum
$PM_{2.5}$	5.57	2.18	1.02	1.15	12.46
$PM_{2.5recon}$	5.47	2.11		1.37	12.39
$(NH_4)_2SO_4$	0.90	0.26	0.16	0.21	1.67
NH_4NO_3	0.16	0.15	0.03	0.04	0.53
POM	3.20	1.62	0.58	0.94	9.10
LAC	0.24	0.10	0.04	0.06	0.54
Soil	0.97	0.53	0.18	0.04	1.84
Seasalt	0.00	0.00	0.00	0.00	0.01

Table 3.8a. Statistical summary of aerosol species derived from the IMPROVE PM_{10} - $PM_{2.5}$ monitoring system for the spring campaign. The number of data points is 37. Units are in $\mu g/m^3$.

Variable	Mean	Std dev	Fraction	Minimum	Maximum
PM_{10} - $PM_{2.5}$	2.45	1.62	0.80	-0.10	7.58
PM_{10} - $PM_{2.5recon}$	3.06	2.16		-0.21	10.19
$(NH_4)_2SO_4$	0.07	0.04	0.02	0.00	0.18
NH_4NO_3	0.15	0.10	0.05	0.00	0.45
POM	0.43	0.36	0.14	-0.07	1.44
LAC	0.03	0.06	0.01	-0.08	0.14
Soil	2.37	1.86	0.77	-0.19	9.02
Seasalt	0.02	0.02	0.01	0.00	0.10

Table 3.8b. Statistical summary of aerosol species derived from the IMPROVE PM_{10} - $PM_{2.5}$ monitoring system for the summer campaign. The number of data points is 35. Units are in $\mu g/m^3$.

Variable	Mean	Std dev	Fraction	Minimum	Maximum
PM_{10} - $PM_{2.5}$	4.14	2.46	0.84	-0.55	9.03
PM_{10} - $PM_{2.5recon}$	4.94	2.45		0.59	9.46
$(NH_4)_2SO_4$	0.03	0.04	0.01	-0.05	0.12
NH_4NO_3	0.16	0.11	0.03	0.05	0.48
POM	1.30	0.45	0.26	0.17	2.03
LAC	0.06	0.06	0.01	-0.03	0.23
Soil	3.36	2.15	0.68	-0.28	7.41
Seasalt	0.02	0.04	0.00	0.00	0.19

Figure 3.26 shows scatter plots of reconstructed $PM_{2.5}$ versus gravimetric mass for both spring and summer datasets. For an ordinary least square (OLS) regression between reconstructed and measured fine mass with the intercept set to 0, the R^2 values for the spring and summer scatter plots are 0.93 and 0.98, respectively, with slopes of 1.11 ± 0.02 and 0.95 ± 0.01. Both the regression and the average ratio of gravimetric to measured $PM_{2.5}$ mass show that reconstructed mass is about 10–15% high in the spring and 5% low in the summer. In spite of the many assumptions of the chemical forms of each species, the agreement between the two variables is quite good. Comparison of reconstructed and gravimetric mass for PM_{10} - $PM_{2.5}$ shows that the agreement is less robust. During the spring and summer campaigns reconstructed mass was respectively 25% and 19% greater than gravimetric PM_{10} - $PM_{2.5}$ mass. An OLS regression between gravimetric mass as the dependent variable and the various species as independent variables suggests that both PM_{10} - $PM_{2.5soil}$ and POM concentrations are being overestimated.

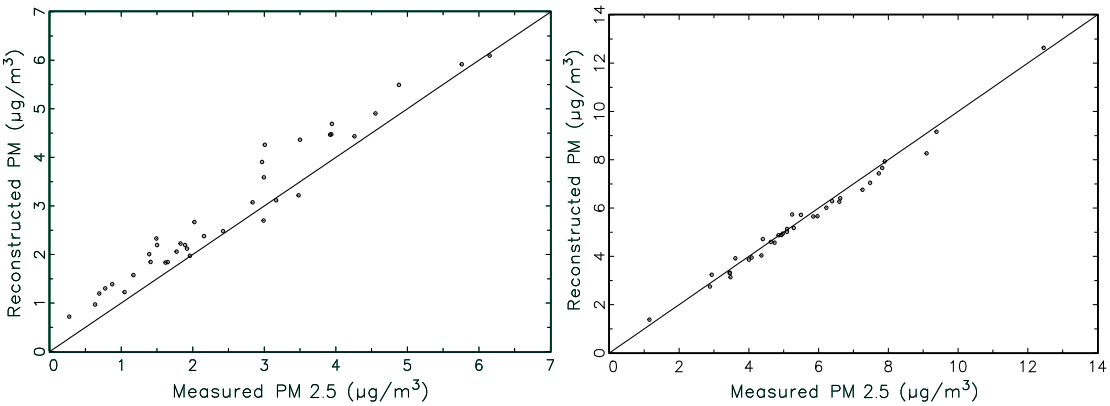

Figure 3.26. Reconstructed (y-axis) versus gravimetric mass (x-axis) (µg/m^3) for the spring (left) and summer (right) time periods.

Referring to Tables 3.7a–b and 3.8a–b, one can see that both $PM_{2.5}$ and PM_{10} - $PM_{2.5}$ were about a factor of 2 higher in the summer than spring. In the $PM_{2.5}$ mode the difference in mass concentrations was primarily due to POM concentrations being about 3½ times greater during the summer than spring. Conversely, $PM_{2.5}$ nitrate concentrations were about 2 times greater in the spring than summer; however, they made up a smaller percentage of reconstructed mass at 12% and 3%, respectively, for the summer and spring months. During the summer campaign organic mass made up 60% of the $PM_{2.5}$, with ammonium sulfate and soil mass concentrations each contributing about 15%. During the spring season, sulfates, POM, and soil concentrations made up about equal fractions of $PM_{2.5}$ at about 30%. The PM_{10} - $PM_{2.5}$ fraction was dominated by soil at about 75% for both seasons, and organic aerosols were the second largest contributor at 24% and 14% for the summer and spring seasons, respectively.

3.6.2. Comparison of Semicontinuous to 24-hr-average Measurements of Aerosols and Gases

As discussed in Chapter 2, a suite of continuous gas monitors was operated at the RoMANS core site during the spring and summer campaigns. Measured species included TN_x, NO_x, NO, NO_2, NH_3, O_3, CO, and SO_2. In addition, the particle-into-liquid sampler (PILS) was operated continuously during the two campaigns to obtain the concentrations of major ions (NH_4^+, Na^+, K^+, Ca^{2+}, Mg^{2+}, Cl^-, NO_3^-, and SO_4^{2-}) with a time resolution of 15 min. However, all 15-min data were averaged to 1 hr for the analysis presented here. The performance of the PILS system is evaluated by comparing its measurements of various species to those collected using 24-hr bulk sampling techniques.

As an example, Figure 3.27 shows time lines of nitrate and sulfate mass concentrations as collected by the semicontinuous PILS and URG 24-hr-average measurements for the spring time period. The most striking feature of Figure 3.27 is the extreme, short-time-scale variability of mass concentrations. Typically, any 24-hr bulk measured concentration is made up of short-term episodes that are 12 hrs or less in duration. The 24-hr-average maximum nitrate concentration for the data shown in Figure 3.27 is 1.48 µg/m^3, while the maximum 1-hr concentration is 4.95 µg/m^3, a factor of 3.3 higher. The standard deviation of the 1-hr dataset is 0.5, while for the 24-hr-average dataset it is 0.32, a factor of 1.7 times lower. Plots of other ions and gases are similar to Figure 3.27 for both the spring and summer months.

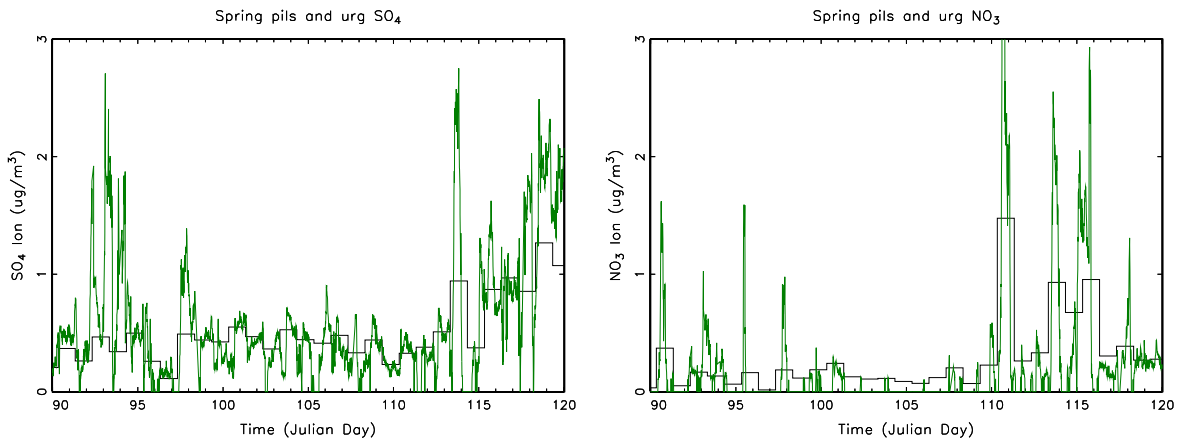

Figure 3.27. Graphs of spring time series showing (left) sulfate (right) and nitrate ion mass concentrations (µg/m^3) for the semicontinuous PILS (green) and 24-hr-average URG measurement systems.

The implication of the high temporal variability in aerosol concentrations on visibility is very significant. Because visibility impairment is an instantaneous phenomenon, the highly variable aerosol concentrations resulted in visibility that was changing from a fairly high to a fairly low level of impairment within time scales of less than an hour. This issue will be further addressed in the section on atmospheric extinction estimates.

Tables 3.9 and 3.10 present statistical summaries of ion and gas concentrations measured using the IMPROVE, URG, and PILS measurement systems as well as continuous gas analyzers for both the spring and summer time periods. Summaries are reported for only those 31 time periods when all sampling systems had valid data. Figures 3.28–3.30 are scatter plots of sulfate, ammonium, and nitrate ion concentrations, respectively, with the URG measurements presented on the x-axis and IMPROVE and PILS data averaged to 24 hrs on the y-axis. Figure 3.31 presents a comparison of potassium (K) measured using the IMPROVE sampler with K from PILS. Figures 3.32 and 3.33 are scatter plots of NH_3 and SO_2 measured using denuder systems and continuous gas analyzers whose data has been averaged to 24 hrs. Table 3.11 presents the results of OLS regression analysis without an intercept for the scatter plots shown in Figures 3.28–3.33.

Table 3.9. Statistical summary of ion and gas measurements made by the IMPROVE (I), URG (U), PILS (P) and continuous gas (C) measurement systems for the spring time period. Units are in µg/m^3 unless otherwise noted.

Variable	Mean	Std Dev	Variance	Minimum	Maximum	Valid
NH_4 (I)	0.19	0.13	0.02	0.04	0.52	31
NH_4 (U)	0.24	0.16	0.03	0.05	0.64	31
NH_4 (P)	0.23	0.11	0.01	0.04	0.56	31
SO_4 (I)	0.49	0.28	0.08	0.11	1.28	31
SO_4 (U)	0.51	0.27	0.07	0.11	1.27	31
SO_4 (P)	0.57	0.40	0.16	0.12	1.81	31
NO_3 (I)	0.23	0.29	0.08	0.01	1.28	31
NO_3 (U)	0.28	0.32	0.10	0.01	1.48	31

Variable	Mean	Std Dev	Variance	Minimum	Maximum	Valid
NO_3 (P)	0.22	0.34	0.11	0.00	1.53	31
K (I) (ng/m^3)	10.11	6.75	45.50	0.00	21.54	31
K (P) (ng/m^3)	231.92	245.64	60338.75	0.00	803.21	31
NH_3 (C)	0.58	0.24	0.06	0.22	1.40	31
NH_3 (U)	0.17	0.11	0.01	0.05	0.61	31
SO_2 (C)	0.21	0.23	0.05	-0.04	1.16	31
SO_2 (U)	0.16	0.15	0.02	0.02	0.65	31
O_3 (ppb)	73.39	9.77	95.44	51.65	88.59	31
HNO_3	0.24	0.15	0.02	0.06	0.70	31

Table 3.10. Statistical summary of ion and gas measurements made by the IMPROVE (I), URG (U), PILS (P) and continuous gas (C) measurement systems for the summer time period. Units are in $\mu g/m^3$ unless otherwise noted.

Variable	Mean	Std Dev	Variance	Minimum	Maximum	Valid
NH_4 (I)	0.23	0.08	0.01	0.11	0.44	31
NH_4 (U)	0.35	0.14	0.02	0.15	0.76	31
NH_4 (P)	0.23	0.11	0.01	0.04	0.56	31
SO_4 (I)	0.68	0.17	0.03	0.27	1.21	31
SO_4 (U)	0.65	0.17	0.03	0.28	1.20	31
SO_4 (P)	0.84	0.20	0.04	0.39	1.47	31
NO_3 (I)	0.13	0.12	0.02	0.03	0.41	31
NO_3 (U)	0.15	0.14	0.02	0.03	0.52	31
NO_3 (P)	0.19	0.15	0.02	0.04	0.57	31
K (I) (ng/m^3)	32.87	32.59	1062.26	0.00	124.58	31
K (P) (ng/m^3)	53.17	39.13	1531.09	0.57	157.28	31
NH_3 (C)	1.04	0.28	0.08	0.64	2.06	31
NH_3 (U)	0.44	0.27	0.07	0.10	1.59	31
SO_2 (C)	0.41	0.20	0.04	0.11	1.01	31
SO_2 (U)	0.17	0.13	0.02	0.02	0.51	31
O_3 (ppb)	68.98	11.15	124.33	49.28	92.76	31
HNO_3	0.60	0.26	0.07	0.29	1.46	31

Table 3.11. Results of an OLS regressions analysis for the data shown in Figures 3.34–3.39. The regression in all cases was carried out without an intercept. "IMP" refers to IMPROVE data, "PIL" refers to PILS data, and "Cont" refers to continuous gas measurement data.

	Variable	Coefficient	Std Error ($\mu g/m^3$)	t-value	Prob>|t|	R^2
Spring	IMP SO_4	0.99	0.01	92.97	0.00	0.99
	PIL SO_4	1.17	0.07	17.84	0.00	0.73
Summer	IMP SO_4	1.03	0.02	67.46	0.00	0.89
	PIL SO_4	1.27	0.02	72.73	0.00	0.89
Spring	IMP NH_4	0.79	0.02	37.76	0.00	0.93
	PIL NH_4	1.08	0.07	14.99	0.00	0.77

	Variable	Coefficient	Std Error ($\mu g/m^3$)	t-value	Prob>|t|	R^2
Summer	IMP NH_4	0.61	0.03	19.29	0.00	0.31
	PIL NH_4	0.64	0.03	18.78	0.00	0.53
Spring	IMP NO_3	0.86	0.01	73.98	0.00	0.99
	PIL NO_3	0.92	0.04	24.17	0.00	0.93
Summer	IMP NO_3	0.83	0.05	17.37	0.00	0.80
	PIL NO_3	1.13	0.04	27.33	0.00	0.90
Spring	PIL K	19.20	3.64	5.27	0.00	0.00
Summer	PIL K	1.39	0.06	24.2	0.06	0.86
Spring	Cont NH_3	2.86	0.19	15.23	0.00	0.27
Summer	Cont NH_3	1.98	0.13	15.39	0.00	0.75
Spring	Cont SO_2	0.62	0.23	2.73	0.01	0.48
Summer	Cont SO_2	2.04	0.14	14.52	0.00	0.33

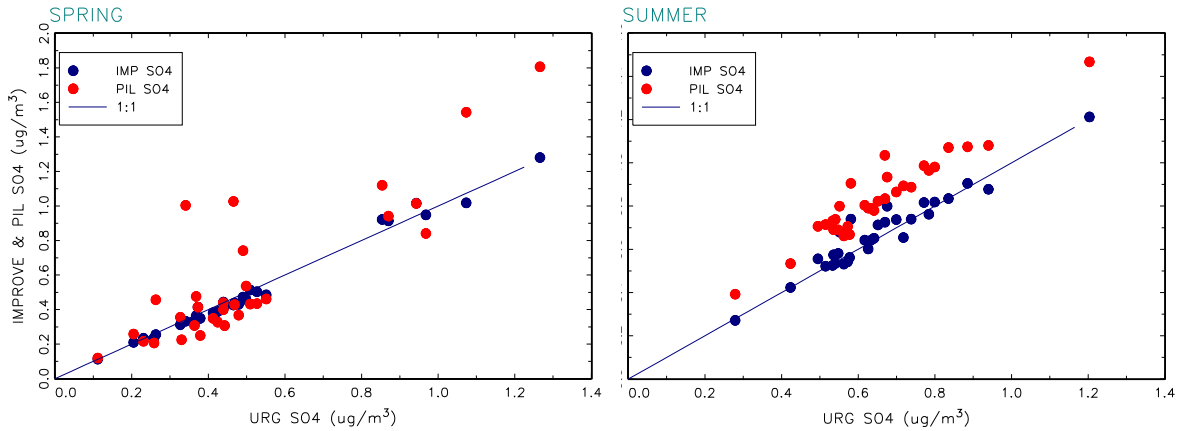

Figure 3.28. $PM_{2.5}$ sulfate concentration ($\mu g/m^3$) comparisons from IMPROVE and PILS (24-hr average) on the y-axis and URG on the x-axis for spring (left) and summer (right). The 1:1 line is shown for reference.

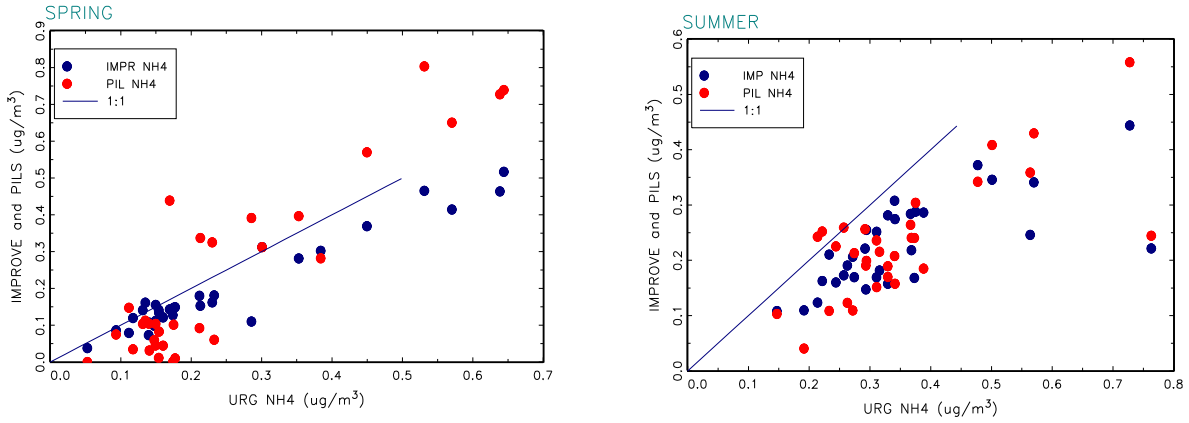

Figure 3.29. $PM_{2.5}$ ammonium concentration (µg/m^3) comparisons from IMPROVE and PILS (24-hr average) on the y-axis and URG on the x-axis for spring (left) and summer (right). The 1:1 line is shown for reference.

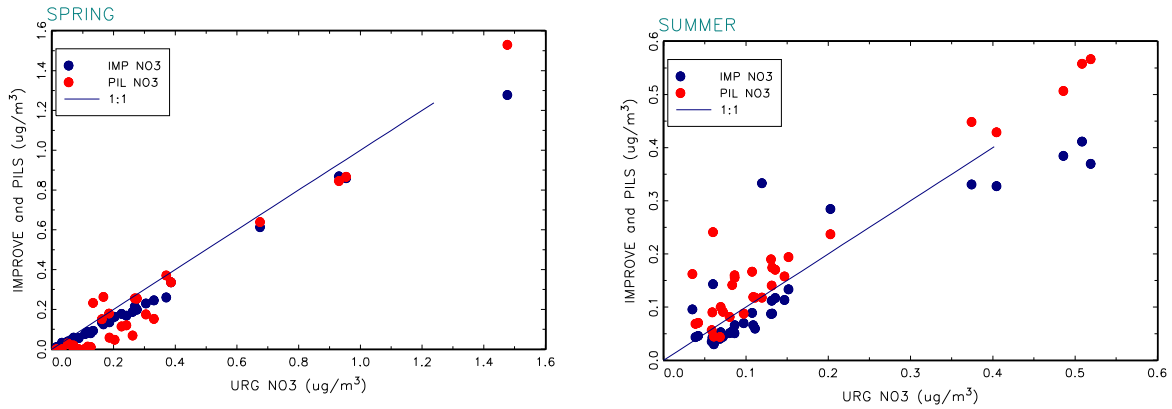

Figure 3.30. $PM_{2.5}$ nitrate concentration (µg/m^3) comparisons from IMPROVE and PILS (24-hr average) on the y-axis and URG on the x-axis for spring (left) and summer (right). The 1:1 line is shown for reference.

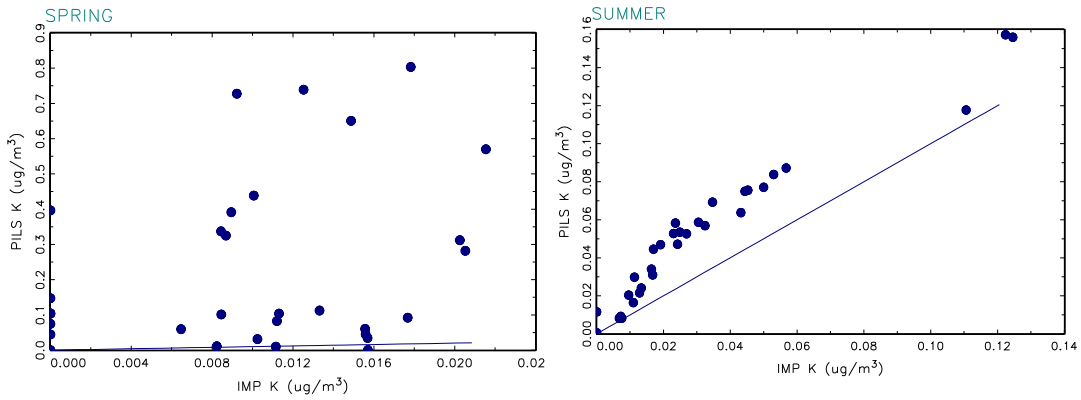

Figure 3.31. $PM_{2.5}$ potassium concentration (µg/m^3) comparisons from PILS (24-hr average) on the y-axis and IMPROVE on the x-axis for spring (left) and summer (right). The 1:1 line is shown for reference.

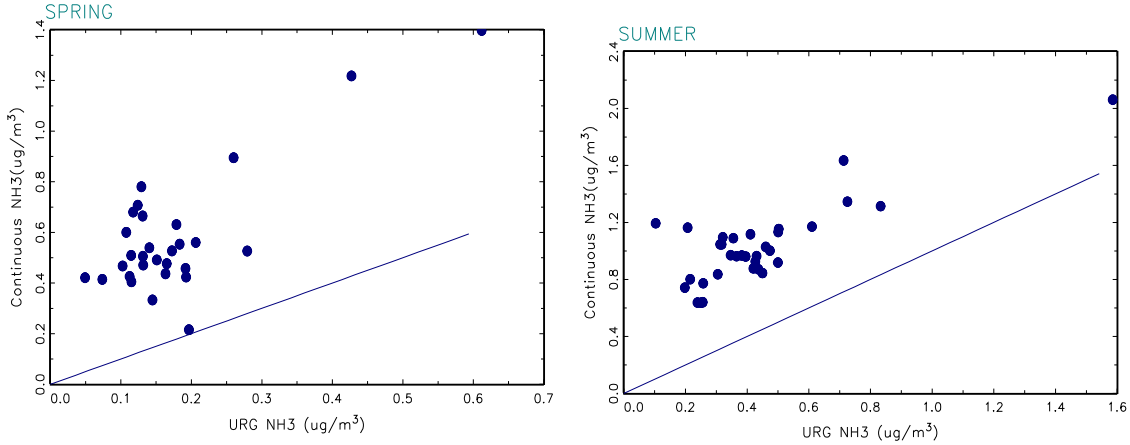

Figure 3.32. Ammonia concentration (µg/m^3) comparisons from continuous gas measurements (24-hr average) on the y-axis and URG on the x-axis for spring (left) and summer (right). The 1:1 line is shown for reference.

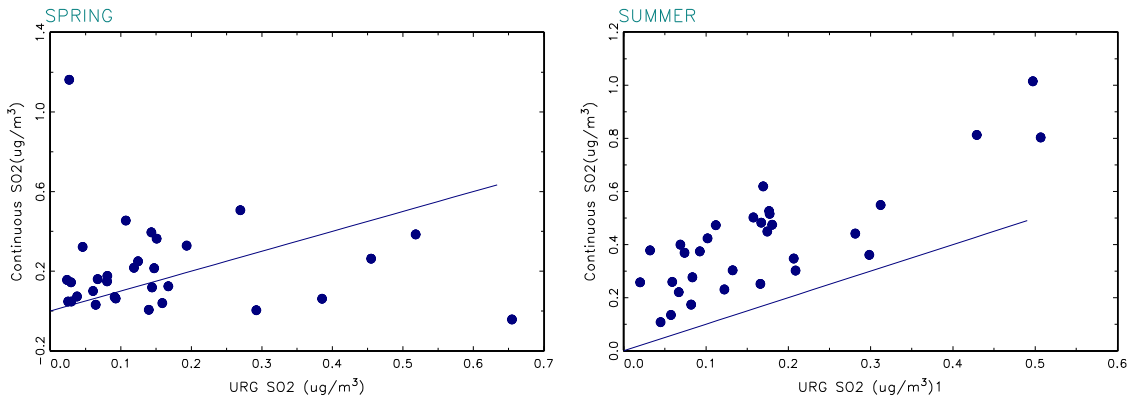

Figure 3.33. Sulfur dioxide concentration (µg/m^3) comparisons from continuous gas measurements (24-hr average) on the y-axis and URG on the x-axis for spring (left) and summer (right). The 1:1 line is shown for reference.

Referring to Figures 3.28 and Tables 3.10 and 3.11, one can see that all three sulfate measurements agreed reasonably well during the spring season. PILS and URG average values were nearly the same while IMPROVE sulfate was about 10% lower. The R^2 is 0.73 and 0.99 for the PILS/URG and IMPROVE/URG datasets, respectively. During the summer the URG and IMPROVE datasets agreed well; however, there appears to be a multiplicative and additive bias between the URG and PILS measurements.

During the spring season the URG and PILS ammonium measurements were about the same on the average, with IMPROVE ammonium measurements being about 20% lower. The R^2 between URG and PILS measurements is high (R^2 = 0.93) while for URG and IMPROVE it is 0.77. During the summer time period the average ammonium concentration as measured by the URG system was 34% higher than either the PILS or IMPROVE average concentration, and the corresponding R^2s are lower at 0.31 and 0.53, respectively. In general, it is expected that the IMPROVE measurements of ammonium should be biased low because of volatilization of ammonium to ammonia, while the URG system captures the volatilized ammonium on a backup denuder system.

On average during the spring season, the average PILS nitrate ion concentration was 20% less than the URG average concentration but similar to the IMPROVE average concentration, while during the summer the PILS average concentration was about 25% and 40% greater than the URG and IMPROVE concentrations, respectively. For the most part the correlation coefficients, as reflected by the R^2 values, are high between all measurements.

During the spring, K measurements made using the PILS system were a factor of 23 greater than for IMPROVE. During the summer, K measurements agreed better on average (with a difference of about 50%). These measurements for PILS are near the MDL and should be used with some caution.

The PILS data were adjusted both additively and multiplicatively, using the URG data as a reference, to yield the best "perceived" match between the two measurements. The adjustments

for each variable are summarized in Table 3.12. Adjustments were not made for those variables not listed in the table.

Table 3.12. Additive and multiplicative bias adjustments made to the PILS dataset. PILS data are referred to by "PIL" and the continuous gas data are referred to by "Cont".

	Variable	Additive bias	Multiplicative bias
Spring	PIL SO_4	0.0	1.0
Summer	PIL SO_4	-0.1	0.9
Spring	PIL NH_4	0.1	0.8
Summer	PIL NH_4	0.1	1.0
Spring	Cont NH_3	-0.2	1.0
Summer	Cont NH_3	-0.4	1.0

Based on these adjustments, a charge balance was performed and the results are shown in Figure 3.34. The R^2 values for spring and summer are 0.92 and 0.81, respectively, with slopes of 1.00 ± 0.001 and 1.02 ± 0.007 indicating good agreement.

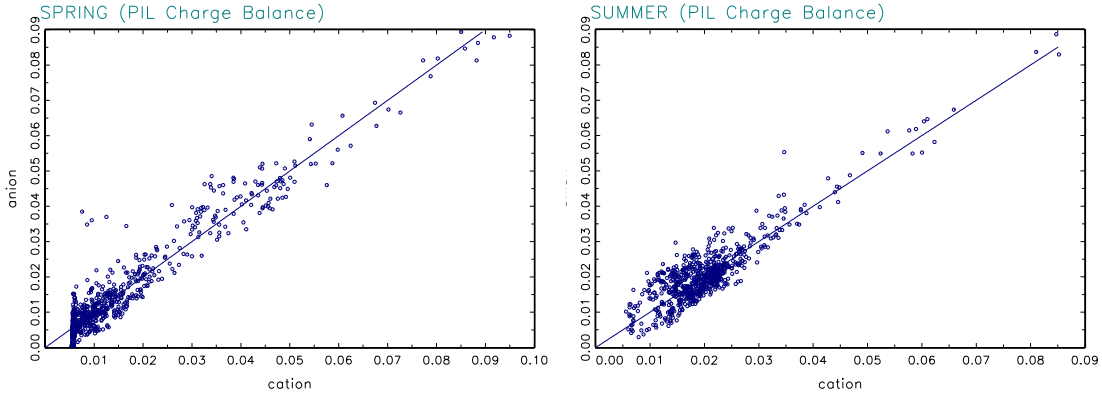

Figure 3.34. Charge balance calculation for the spring and summer time periods. Cations are on the x-axis and anions are on the y-axis.

Also summarized in Tables 3.9 and 3.10 are the comparisons of continuous and 24-hr denuder SO_2 and NH_3 measurements. The average springtime difference between the continuous and denuder ammonia measurements is a factor of 3.4, while for the summer the factor is 2.4. In both cases the difference appears to be primarily additive. It is assumed that the URG is a more accurate measurement of ammonia on the average, and therefore the continuous data were corrected downward by subtracting a 0.2 and 0.4 $\mu g/m^3$ offset for the spring and summer datasets and then normalized to the URG measurements. No corrections were made to the SO_2 datasets.

3.7. PARTICLE SIZE DISTRIBUTION MEASUREMENTS AT THE ROMANS CORE SITE

A description of the particle size distribution measurements and the alignment method applied to those data was described in Section 2.2.9. In this section we present the results of the size distribution measurements.

Table 3.13 lists the mean and 1 standard deviation for total aerosol number and volume concentrations as well as accumulation and coarse mode concentrations and mode statistics. Time lines of aerosol number and volume distribution parameters are shown in Figures 3.35 and 3.36. Measured aerosol number concentrations in RMNP during RoMANS were lower than reported values for remote continental aerosol number concentrations (Bashurova et al., 1992; Koutsenogii et al., 1993; Seinfeld & Pandis, 2006). The summer time period, however, had significantly higher number concentrations than the spring. Figures 3.35a and 3.36a show the total integrated number and volume concentrations, respectively, for both study periods. The mean and 1-standard-deviation aerosol number concentration in the spring was 876 ± 772 cm^{-3}, while in the summer it was 2075 ± 935 cm^{-3}, and total integrated volume concentrations were 2.17 ± 2.56 μm^3 cm^{-3} in the spring and 6.53 ± 3.92 μm^3 cm^{-3} in the summer. The large standard deviations show the high variability in aerosol concentrations, especially in the spring. Although these standard deviations are large, aerosol concentrations (both number and volume) are significantly different between spring and summer at the 95% confidence level, using a two-tailed t-test.

Table 3.13. Mean and standard deviations for number and volume aerosol concentrations and mode statistics measured during the RoMANS spring and summer campaigns.

		Total Conc. [cm^{-3}]	**Accumulation**			**Coarse**		
			Conc. [cm^{-3}]	**D_g [µm]**	**σ_g [µm]**	**Conc. [cm^{-3}]**	**D_g [µm]**	**σ_g [µm]**
Spring	**Number**	876 ± 772	875 ± 771	0.078 ± 0.013	1.69 ± 0.095	0.64 ± 0.55	1.08 ± 0.077	1.46 ± 0.11
	Volume [μm^3]	2.56 ± 2.17	0.91 ± 0.83	0.2 ± 0.026	1.75 ± 0.12	1.64 ± 1.59	3.35 ± 1.27	2.01 ± 0.19
Summer	**Number**	2075 ± 935	2074 ± 934	0.092 ± 0.015	1.76 ± 0.075	0.46 ± 0.34	1.17 ± 0.11	1.58 ± 0.084
	Volume [μm^3]	6.53 ± 3.92	3.70 ± 2.10	0.21 ± 0.026	1.61 ± 0.072	2.83 ± 2.40	4.65 ± 0.89	1.94 ± 0.11

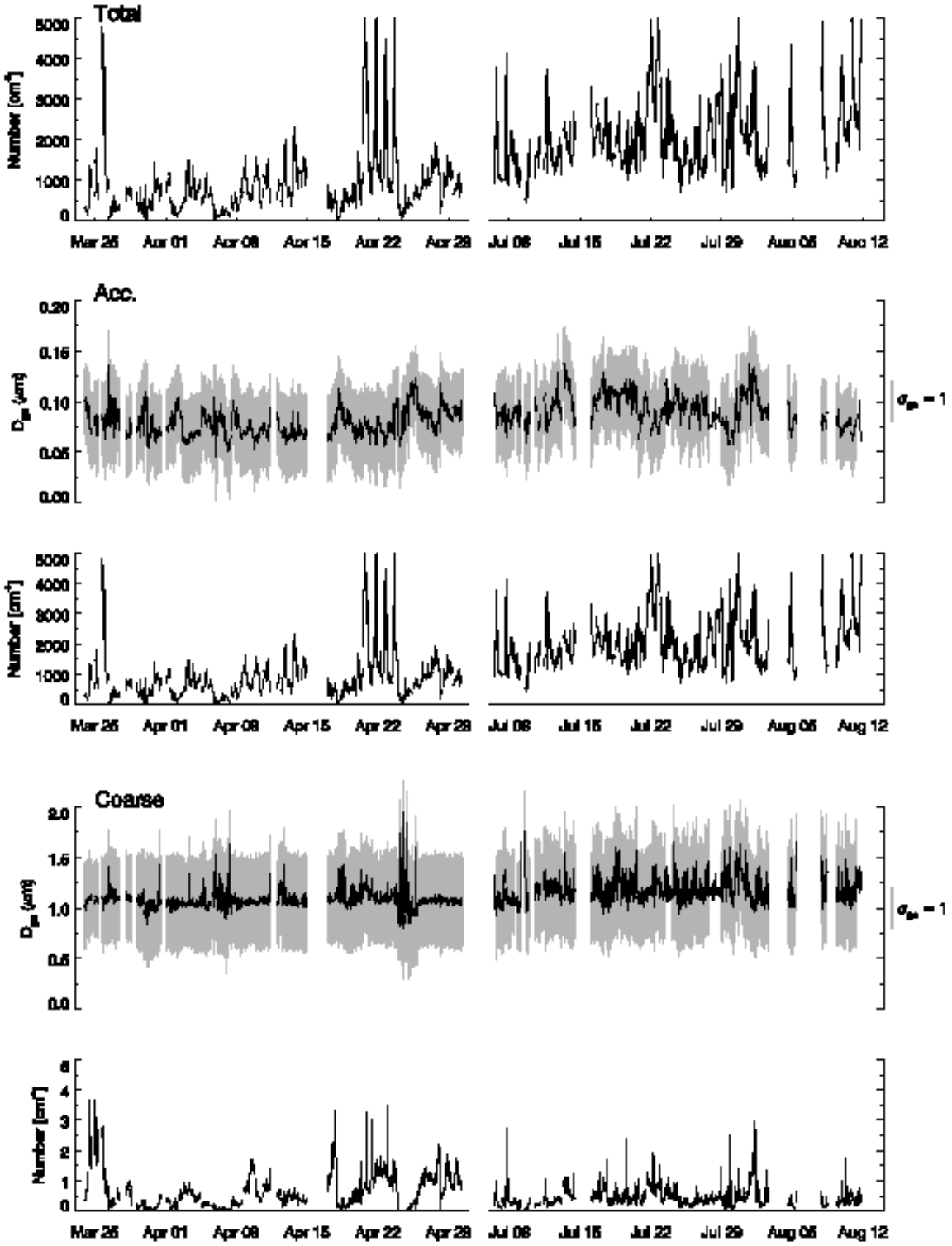

Figure 3.35. (top panel) Integrated total, (middle panel) accumulation mode, and (bottom panel) coarse mode aerosol number concentrations [cm^{-3}]. Top time series in the middle and bottom panels show mode geometric mean diameter (μm, black line) and geometric standard deviation (right axis, gray shading).

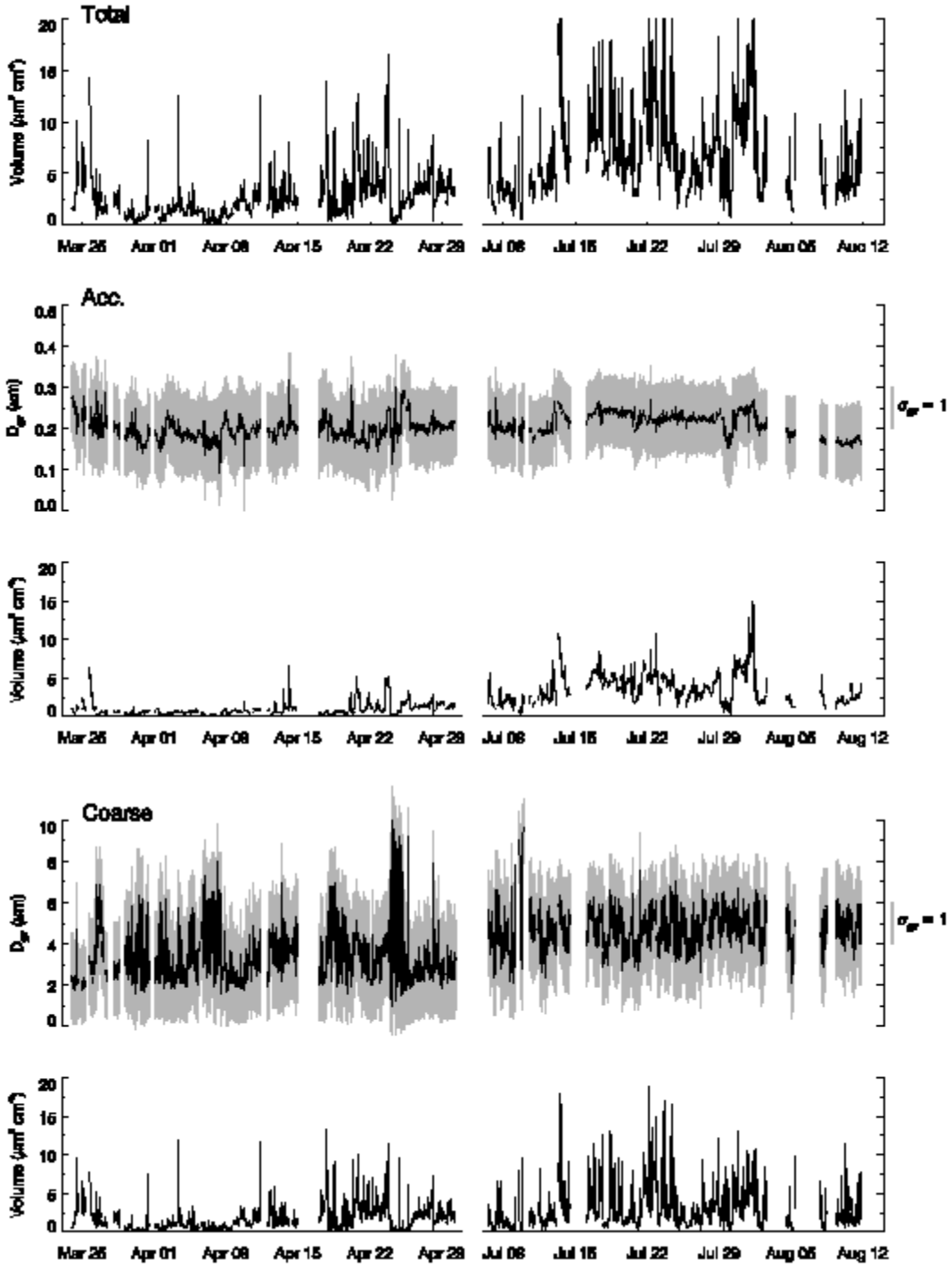

Figure 3.36. (top panel) Integrated total, (middle panel) accumulation mode and (bottom panel) coarse mode aerosol volume concentrations [$\mu m^3\ cm^{-3}$]. Top time series in the middle and bottom panels show mode geometric mean diameter (μm, black line) and geometric standard deviation (right axis, gray shading).

Aerosol distributions were split into accumulation and coarse modes, based on the minimum values between the modes. This minimum value was found by an automated routine that

searched for the minimum between 0.4 μm and 1.0 μm. The lower limit of the accumulation mode was fixed at 0.04 μm and the upper limit of the coarse mode was fixed at 20 μm. The minimum between the two modes occurred at an average value of 0.63 μm in the spring and 0.74 μm in the summer. In the spring, the coarse mode dominated the volume distribution, accounting for 60% of the total aerosol volume. In the summer, however, the accumulation mode made up 60% of the aerosol volume. Figure 3.37 shows a time line of the accumulation mode volume fraction for each period.

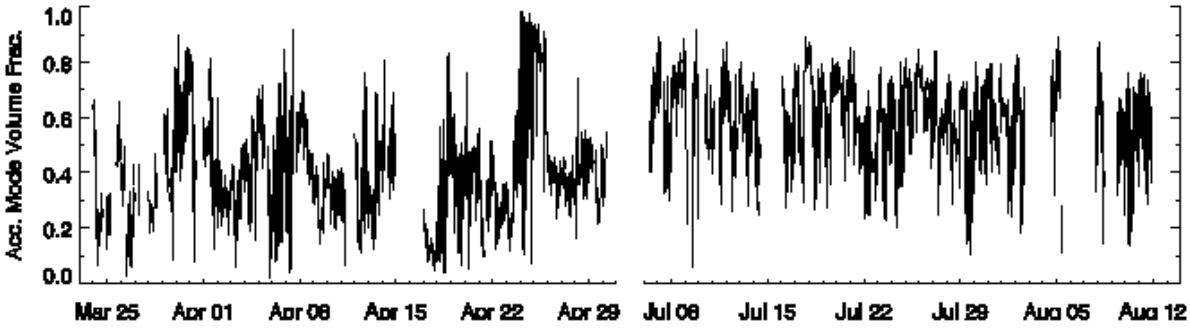

Figure 3.37. Accumulation mode volume fraction time series for the spring and summer RoMANS campaigns.

Geometric mean diameters (D_g) and standard deviations (σ_g) were calculated for each number and volume distribution (Figures 3.35 and 3.36 middle and bottom panels). The accumulation mode, volume mean diameter (D_{gv}) remained fairly constant throughout both study periods with an average value of 0.2 ± 0.026 μm in the spring and 0.21 ± 0.026 μm in the summer. For the coarse mode, however, D_{gv} increased significantly in the summer when its average value was 4.65 ± 0.89 μm as opposed to the spring value of 3.35 ± 1.27 μm. In the spring, the average σ_{gv} for the accumulation and coarse modes were 1.75 ± 0.12 μm and 2.01 ± 0.19 μm, respectively. In the summer, both modes of the volume distribution were narrower with σ_{gv} of 1.61 ± 0.072 for the accumulation mode and 1.94 ± 0.11 for the coarse mode.

In addition to having lower aerosol concentrations, the spring also exhibited greater variability. The standard deviation variation of the number concentration about the mean was 88% during the spring, while during the summer the variation was only 42%. The percent variations about the mean for the volume concentration, coarse mode D_{gv}, and σ_{gv} for both modes, were also larger in the spring than in the summer.

3.7.1. Comparison of Average Fine and Coarse Particle Density Derived from Size Distribution Data to Those Estimated from 24-hr-average Species Mass Concentration Measurements

The volume size distribution data were used to estimate POM on a semicontinuous basis by differencing the fine mass estimates derived from the size distributions and the inorganic mass species obtained from the PILS monitoring system. Carrying out this calculation requires assumptions of fine and coarse mass chemical composition and the associated densities of each species. Typical densities and indices of refraction used for ammonium sulfate and nitrate, organic and elemental carbon, and soil are summarized in Table 3.14.

Table 3.14. Summary of the indices of refraction and densities used for modeling particle scattering and absorption from DMA number size distributions (based on values reported in Hand and Kreidenweis, 2002).

Species	Density (g cm^{-3})	Index of Refraction
$(NH_4)_2SO_4$	1.76	1.53
Organic Carbon	1.4	1.55
Light Absorbing Carbon	2.0	1.8-0.5
NH_4NO_3	2.26	1.59
Soil	2.3	2

In Tables 3.7a and 3.7b it is evident that $PM_{2.5}$ was predominantly inorganic salts, POM, and soil dust and that the PM_{10} - $PM_{2.5}$ fraction (see Tables 3.8a and3.8b) was overwhelmingly soil dust with about a 10–20% contribution of organic material. This distribution of aerosol species is typical between $PM_{2.5}$ and PM_{10} - $PM_{2.5}$, and a number of measurements have shown that concentrations of soil-dust-related elements are small to near 0 in the $PM_{2.5}$ fraction. Here, a differentiation is made between entrained soil dust and soil-related elements emitted during the burning of carbonaceous material, whether it is coal- or forest/agriculture-related material. As such, it is usually assumed that the soil dust in the 0.0–2.5 µm size range is the fine "tail" of the coarse mode. Therefore it is assumed that the $PM_{2.5}$ fraction was primarily made up of ammonium sulfate and nitrate and POM. An average $PM_{2.5}$ fraction density can be derived by estimating the slope of a scatter plot of particle volume and measured gravimetric $PM_{2.5}$ mass.

Table 3.15 presents a statistical summary of volume-weighted densities for the $PM_{2.5}$ - $PM_{2.5soil}$ and PM_{10} - $PM_{2.5}$ + $PM_{2.5soil}$, derived from the individual species densities given in Table 3.14. If the assumption of volume conservation is approximately true and the individual species densities are correct, the volume-weighted densities should be comparable to the average densities derived from slope estimates of scatter plots of gravimetric mass versus volume as derived from the number size distribution measurements. An example scatter plot of 24-hr PM_{10} versus 24-hr-average volume derived from the number distribution measurements is shown in Figure 3.38 for the spring dataset. The slope of the line, 2.09 ± 0.07 g/cm^3, is interpreted as the average density of fine plus coarse particles over the measurement time period. The slope was determined using an OLS regression with the intercept set equal to 0.

Table 3.15. Statistical summary of volume-weighted densities (ρ) for $PM_{2.5}$ - $PM_{2.5soil}$, PM_{10} - $PM_{2.5}$ + $PM_{2.5soil}$, and PM_{10} for the spring and summer time periods. Units are g/cm^3.

Variable	Mean	Std dev	Minimum	Maximum	Valid
$\rho_{PM2.5 - PM2.5soil}$					
$\rho_{PM10 - PM2.5 + PM2.5soil}$	1.63	0.07	1.50	1.82	37
ρ_{PM10}	2.15	0.18	1.77	2.80	37
Summer	1.91	0.10	1.68	2.10	37
$\rho_{PM2.5 - PM2.5soil}$					
$\rho_{PM10 - PM2.5 + PM2.5soil}$	1.51	0.03	1.47	1.57	35
ρ_{PM10}	1.99	0.11	1.77	2.19	35
$\rho_{PM2.5 - PM2.5soil}$	1.75	0.11	1.58	1.98	35

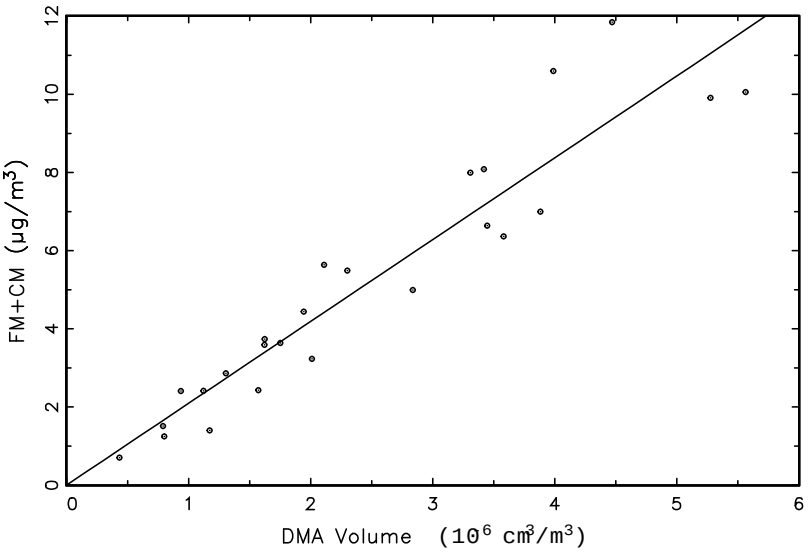

Figure 3.38. An example scatter plot of PM_{10} mass concentrations (µg/m^3) (y-axis) versus total particle volume concentration as derived from the particle number size distributions.

Table 3.16 is a summary of the regressions carried out for total volume and volumes corresponding to the fine ($D_p \approx 0.1–0.8$ µm) and coarse ($D_p \approx 0.8–15.0$ µm) modes of volume size distribution data. The fine mass was estimated using $PM_{2.5}$ - $PM_{2.5soil}$, and coarse fraction gravimetric mass was set equal to PM_{10} - $PM_{2.5}$ + $PM_{2.5soil}$. Undoubtedly, some coarse fraction POM contributes to $PM_{2.5}$ organics, and $PM_{2.5}$ soil-related elements may not all be associated with the tail of the coarse mode. Not correcting for the coarse POM in the fine mode will serve to somewhat inflate the fine mode density and underestimate the coarse mode density. Furthermore, the gravimetric mass contains some water in that the filters are weighed at about 40% ± 5% relative humidity (RH) and hygroscopic species retain some water at these humidities.

Table 3.16. Results of an OLS regression with the intercept set equal to 0 for the dependent variable shown, with the independent variable being the corresponding volume derived from the number size distribution measurements. Units are in g/cm^3.

Variable	Estimate	Std Error	t-value	>|t|
Spring				
$PM_{2.5}$ - $PM_{2.5soil}$	1.60	0.09	18.50	0.00
PM_{10} - $PM_{2.5}$ + $PM_{2.5soil}$	2.21	0.09	25.39	0.00
PM_{10}	2.09	0.07	28.82	0.00
Summer				
$PM_{2.5}$ - $PM_{2.5soil}$	1.46	0.06	24.70	0.00
PM_{10} - $PM_{2.5}$ + $PM_{2.5soil}$	1.87	0.17	10.74	0.00
PM_{10}	1.65	0.11	15.47	0.00

The relative error between the two calculations for PM_{10} volumes and mass concentrations were 6% and 9% for the spring and summer months, respectively, with the volume-weighted density being smaller in the spring but larger in the summer. Interestingly, the relative errors for the individual fine and coarse modes were less at about 1–6%. The assumed species densities appear to be quite reasonable. Notice that because the fine mode on a relative basis had more POM than

the coarse mode, its average density was lower than the coarse fraction, and vice versa for the coarse mode, which was dominated by soil dust with its higher density.

3.8. ESTIMATING SEMICONTINUOUS PARTICULATE ORGANIC MASS FROM NUMBER SIZE DISTRIBUTIONS.

The fine and coarse mass associated with the number size distributions can be estimated in a variety of ways. One could assume the average density arrived at using the regression technique described above, use the average, volume-weighted density derived using the bulk 24-hr-average mass concentration data, or use each 24-hr time increment, volume-weighted density derived from the 24-hr-average data to estimate mass associated with the size distribution data in 24-hr increments. It is the latter approach that is used here.

Once the mass concentrations are estimated for the fine and coarse mode, the fine total carbon mass concentrations (TCM = POM + LAC) can be estimated by differencing the mass concentrations derived from the number size distribution (NSD) measurements and the sum of ammonium sulfate and nitrate from the PILS measurements. This approach assumes that the fine mode contains only sulfates, nitrates, and carbonaceous material. A plot of these three species is shown for the spring season in Figure 3.39. As stated before, the PILS measurements have been normalized to the 24-hr-average data collected with the IMPROVE system, so if all the assumptions were correct, the average TCM estimated in this fashion should compare to the TCM measured using the IMPROVE sampling system. The average of the TCM derived in this manner is 0.51 $\mu g/m^3$, while the average from the IMPROVE dataset is 0.97 $\mu g/m^3$ (POM + LAC). The IMPROVE TCM value is about 1.9 times greater than that derived from the size distribution data. This difference could be because the IMPROVE $PM_{2.5}$ measurement of TCM contains some coarse-mode TCM, or the R_{oc} multiplier for OC may be too high, or both. The agreement between IMPROVE reconstructed and measured fine mass is somewhat improved when using an R_{oc} factor of 1.2, and the difference between the two TCM measurements drops to about 25%.

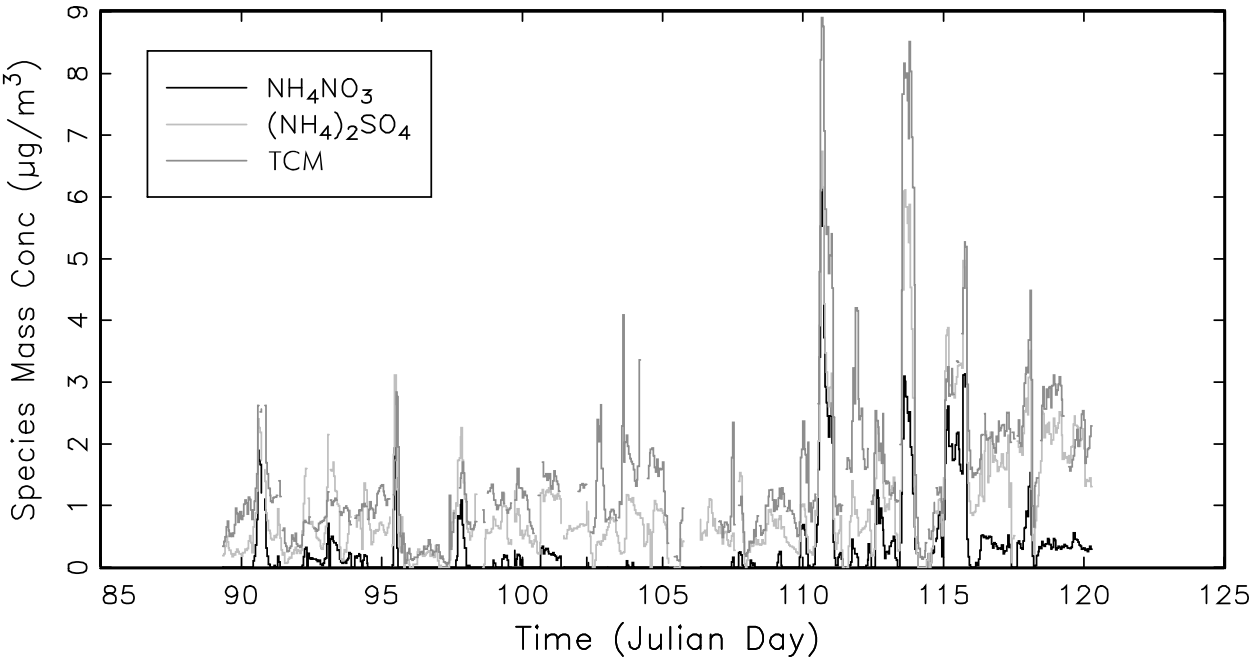

Figure 3.39. Time series of ammonium sulfate and nitrate measured using the PILS system and TCM derived from the particle size distribution data. Units are in µg/m^3.

Referring to Figure 3.39, note that there is one episode on JD = 111 when ammonium nitrate was over 6 µg/m^3 and other species concentrations were quite low. The episode on JD = 113 had about equal amounts of ammonium sulfate and nitrate at about 3 µg/m^3. Both ammonium sulfate and nitrate were elevated on JD = 115, with nitrates decreasing on JD = 116 and sulfate staying at about 3 µg/m^3 through the end of the study period. POM concentrations were on the average lower than either sulfates or nitrates, with no notable episodes over the course of the measurement period.

The data for the summer campaign show quite different characteristics. First, it should be noted that while the POM for the spring dataset made up only 30% of $PM_{2.5}$ mass, during the summer that fraction was near 60%. The average TCM for the IMPROVE dataset was 3.44 µg/m^3, while for the NSD dataset it was 5.0 µg/m^3, a difference of about 30%. During the spring time period the IMPROVE TCM value was greater than derived from the NSD data. A scatter plot of NSD TCM versus IMPROVE TCM shows a high correlation coefficient of $R^2 = 0.97$ and a slope of 1.27 ± 0.02, showing that while the correlation coefficient is high, TCM estimated from NSD is high by about 30%. Interestingly, when $PM_{2.5soil}$ is added back into the 2.5 µm fraction (IMPROVE $PM_{2.5TCM}$ + $PM_{2.5soil}$), the agreement between IMPROVE and what was assumed to be NSD TCM is much improved. The correlation coefficient is still high at 0.93, but the slope now is 1.04 ± 0.03, showing that within the uncertainty the measurements are the same. Perhaps for this time period the soil elements found in the $PM_{2.5}$ mode are indeed in the fine mode and not the fine tail of the coarse mode. The POM during this time period was associated with major wildfire activity in the western United States. It has been reported by Allen and Miguel (1995) that there is a significant amount of soil-related elements during some types of fire activity. As with the inorganic variables, the excursions of TCM concentrations within a 24-hr interval were quite dramatic compared to the variability of 24-hr averages. During the summer campaign the maximum TCM, 24-hr-average concentration was 11.5 µg/m^3, while for the NSD dataset it was

20.7 µg/m^3. The corresponding numbers for the spring dataset were 2.0 µg/m^3 and 3.7 µg/m^3, about a factor of 2 in both cases.

For a portion of the summer campaign, a Sunset carbon analyzer was used to measure OC and LAC on a semicontinuous basis. It is of interest to compare these measurements to the TCM estimates derived from the NSD measurements. Figure 3.40 shows a scatter plot and temporal plot of Sunset-measured TC and TCM derived from the NSD measurements. The correlation coefficient is high with an $R^2 = 0.81$ and the slope was 1.7 ± 0.02.

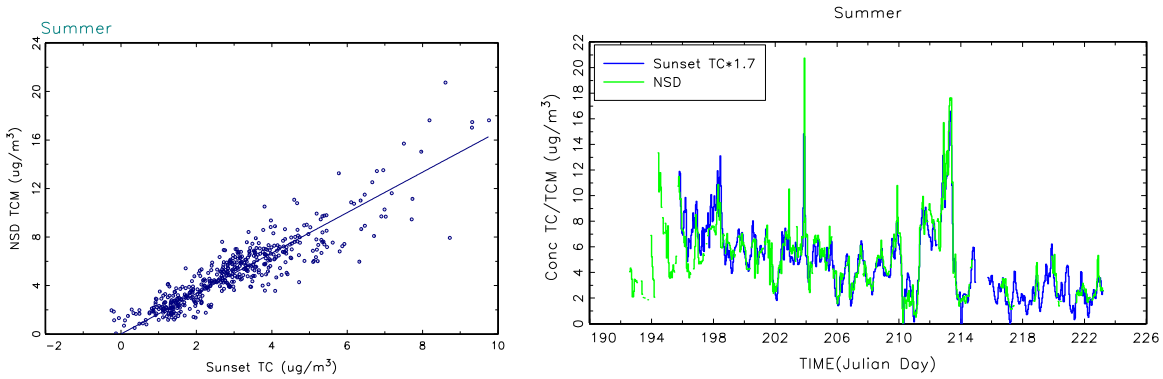

Figure 3.40. (left) Scatter plot of total carbon (TC = POM + LAC) as measured by the Sunset carbon analyzer (x-axis) and total carbon mass (TCM) derived from total number size distributions (y-axis). (right) Time series of Sunset total carbon (blue) and total carbon derived from size distributions (green). Units of µg/m^3.

Chapter 4. Discussion of RoMANS Field Observations

4.1. OVERALL DEPOSITION BUDGET AT THE ROMANS CORE SITE

Wet deposition fluxes observed during RoMANS were discussed in the previous chapter. Here we present an analysis of the total deposition budget for nitrogen and sulfur species, including both dry and wet deposition pathways. This analysis makes use of meteorological measurements made at the RoMANS core site by the CASTNet program, in order to calculate dry deposition velocities, which can be multiplied by observed aerosol and trace gas concentrations to determine dry deposition fluxes. We begin by examining dry deposition flux budgets and then combine wet and dry deposition fluxes to obtain total deposition fluxes for spring and summer.

4.1.1. Dry Deposition Fluxes

Dry deposition is the removal of atmospheric species, both gases and particles, to the surface of the Earth without precipitation. Deposition to all types of surfaces is possible, with the rate of deposition dependent upon the turbulent transport of material to a point near the surface, transport via diffusion (gases), or sedimentation (particles) through a laminar surface sublayer, and the surface reactivity of the species (including, where applicable, stomatal resistance). These parameters are typically described in terms of an electrical resistance analogy to calculate a deposition velocity, which is inversely proportional to the sum of the transport resistances for gases and also includes addition of the gravitational settling velocity for particles. Dry deposition flux, the amount of material transferred per unit area and per unit time, is calculated as the product of a species deposition velocity (V_d) and concentration (C).

Species concentrations were measured during RoMANS, while deposition velocities were calculated by CASTNet for sulfur dioxide, nitric acid, and fine particles. The lack of NH_3(g) measurements in the CASTNet network means that CASTNet does not calculate deposition velocities for NH_3. Since V_d is site specific and the core site is the only RoMANS site collocated with a CASTNet site, it is the only site where dry deposition fluxes were calculated.

Deposition velocities for nitric acid, sulfur dioxide, and fine particles were calculated by CASTNet using the NOAA Multilayer Deposition Velocity Model (MLM) described by Meyers et al. (1998). The model separates the vegetative canopy into 20 layers. Once site survey data are provided to the model, dry deposition velocities can be calculated utilizing observed meteorological parameters. Each CASTNet site is surveyed for input information, including type and quantity of vegetation with an estimation of leaf area index (LAI). Finklestein et al. (2000) and Meyers et al. (1998) compared deposition velocities modeled to observations in order to determine if the MLM calculates a representative deposition velocity. Meyers et al. (1998) found that average deposition velocities showed good agreement with little average bias, but for specific periods the model under- or overpredicted deposition velocity. Finkelstein et al. (2000) found similar results but found that the model generally underpredicts higher values of both O_3 and SO_2 deposition velocities during the day and at night; seasonal and diurnal cycles are reproduced quite well, but the times and magnitudes of the average daily peaks are missed. Both of these studies focused on O_3 and SO_2, since HNO_3 observations were only available during the daytime. Meyers et al. (1998) observed that for HNO_3 the model biases the deposition velocity low, but the ranges of predicted and observed values are similar.

Since the focus of the RoMANS project includes determining total nitrogen deposition in the park, it is important that dry deposition of ammonia, not currently measured by CASTNet, is taken into account. The deposition velocity for ammonia is not modeled in the MLM because of the bidirectional nature of NH_3 exchange with the environment. Ammonia exchange has been shown to be a result of interaction between physical, chemical, and biological processes (Wyers and Erisman, 1998). In some environments ammonia has been found to be both emitted and deposited depending on atmospheric conditions, concentrations, and the time of day (Langford and Fehsenfeld, 1992; Wyers and Erisman, 1998; Pryor et al., 2001). Flux evaluation in a forest generally shows deposition, unlike agricultural croplands where emissions are observed (Sutton et al., 1994). The net canopy compensation point, the air concentration below which NH_3 is emitted and above which it is deposited, has been suggested to be near or below 1 $\mu g/m^3$ for a coniferous forest (Langford and Fehsenfeld, 1992; Duyzer et al., 1994). In seminatural (not fertilized) and forest ecosystems, the compensation point is frequently negligible, but exceptions have been observed in very dry conditions (RH < 60%) and when an area is subject to large NH_3 concentrations. While NH_3 dry deposition is likely concentration dependent as well as dependent on other factors, there is currently not a model available to represent the net flux of NH_3 as ammonia exchange.

In order to estimate an appropriate ammonia deposition velocity for the RoMANS core site, we examined results from previously published studies that measured deposition velocities of ammonia to see if there was a relationship between the deposition velocities of nitric acid and ammonia or to determine if there was an appropriate fixed value to use. In addition, we compared the CASTNet-calculated, HNO_3 deposition velocities to measured literature values.

Table 4.1 summarizes nitric acid and ammonia deposition velocities measured in a number of studies. Given the strong dependence of deposition velocities on surface characteristics and local meteorology, it is not surprising that large differences are seen in time and space. At one Rocky Mountain site, for example, over the course of a single study (Sievering et al., 2001) a wide range, 0.8–20 $cm \cdot s^{-1}$, of nitric acid deposition velocities were measured. A consensus deposition velocity value, especially for NH_3, is difficult to find. There is evidence from previous observations, however, to suggest that the deposition velocity of ammonia is typically similar to that of nitric acid. $V_d(NH_3)$ certainly appears to be at least half and could be equal to $V_d(HNO_3)$. A conservative estimate that agrees well with Namiesnik et al. (2003) and Nemitz et al. (2004) is $V_d(NH_3) = 0.7\ V_d(HNO_3)$. This relationship was used to estimate ammonia dry deposition velocities during RoMANS, based on MLM-modeled nitric acid deposition velocities.

CASTNet nitric acid deposition velocities during the RoMANS spring campaign period ranged from 0.86 to 3.18 $cm \cdot s^{-1}$, with an average deposition velocity of 2.01 $cm \cdot s^{-1}$. During the summer campaign period, HNO_3 deposition velocities ranged from 1.11 to 2.31 $cm \cdot s^{-1}$, with an average of 1.71 $cm \cdot s^{-1}$. These deposition velocities for nitric acid were slightly lower than literature values for similar environments (conifer mixed forest). The highest deposition velocity occurred in the spring, while reported values for this type of environment are generally above 4 $cm \cdot s^{-1}$. There may be factors unique to the core site study area that caused the deposition velocity to be slightly lower, or it could be a function of the CASTNet modeling approach.

Table 4.1. Measured deposition velocities of nitric acid and ammonia from a number of studies. Shaded rows refer to studies where both species were measured.

				HNO_3 (cm/s)		NH_3 (cm/s)	
Source Year		**Environment**	**Location Ra**	**nge**	**Avg**	**Range**	**Avg**
Andersen and Hovmand	1995	Forest	Denmark		1		2
Zimmerman et al.	2006	Forest	Germany		6.48		3.33
Pryor and Klemm	2004	Forest - conifer	Germany		7.5		
Duyzer et al.	1994	Forest - conifer (Douglas fir)	The Netherlands			2-3.0	
Wyers et al.	1992	Forest - conifer (Douglas fir)	The Netherlands				3.2
Sievering et al.	2001	Forest - conifer (mixed)	Niwot Ridge, CO	0.8- >20	7.6		
Sievering et al.	1994	Forest - conifer (mixed)	Southern Germany		5.5		
Neirynacket et al.	2007	Forest - conifer (mixed)	Belgium		4.35		3.0+4.6
Janson and Granat 1	999	Forest – conifer (Scots pine)	Northern Sweden	3-11.0			
Andersen and Hovmand	1993	Forest - conifer (spruce)	Denmark				4.5
Andersen et al.	1999	Forest - conifer (spruce)	Denmark				4
Pryor et al.	2002	Forest - deciduous	Midwestern USA		3		
Meyers et al.	1989	Forest - deciduous (fully leafed)	Southeastern USA	2.2-6	4		
Yamulki et al.	1996	Arable	Unspecified			0.2-2.6	
Muller et al.	1993	Grassland/ agriculture	UK/Germany	0.4-8.0			
Nemitz et al.	2004	Heathland	The Netherlands		0.424		0.311
Duyzer et al.	1994	Heathland	The Netherlands				1.4
Erisman et al.	1994	Heathland	Unspecified				0.8
Goulding et al.	1998	Winter wheat	Unspecified	3.5-13.5			
Duyzer et al.	1992	Unspecified	Unspecified				3.6
Ivens et al.	1988	Unspecified	Unspecified				3.8
Zimmerling et al. 2	001	Unspecified	Unspecified				3.8
Harrison and Allen	1991	Unspecified	Unspecified		2.2		2.2

Variations in deposition velocity, especially when they covary with species concentrations, directly impact dry deposition flux calculations and are important to examine. Average deposition velocities for particles, HNO_3, NH_3, and SO_2 were calculated as a function of time of day for the spring and summer RoMANS field campaign periods. The deposition velocities

typically exhibited a regular diurnal variation, with the maximum at midday and the minimum at night (Figure 4.1). SO_2 did not fit this pattern in the spring when a larger V_d occured during the night. The range of deposition velocities was different for each species, with HNO_3 and NH_3 having the largest range of V_d. This is the case for both the spring and the summer, but the range of average deposition velocities in the spring was larger compared to the summer, while the average diurnal variability for nitric acid and ammonia deposition velocities was greater during summer.

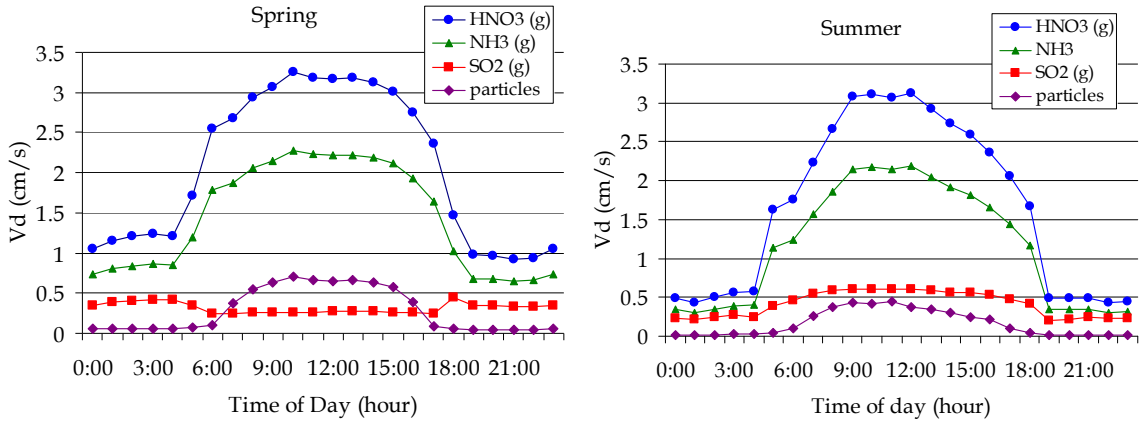

Figure 4.1. Average diurnal variation of deposition velocities(cm/s) for HNO_3, NH_3, SO_2, and particles for the spring (left) and summer (right) campaigns.

In addition to the diurnal variations, there were also daily variations in both spring (Figure 4.2) and summer (Figure 4.3). These daily changes reflect variability in daily meteorological conditions at the site. The daily maxima and minima during the spring were more extreme, compared to the average, than in the summer. This is likely a function of the large changes in temperature and boundary layer stability that occurred during the spring in Colorado.

To determine how much the daily deposition velocity changes over the course of a season and from season to season, frequency distributions of deposition velocities for SO_2, HNO_3, and particles were examined. Figure 4.4 shows the distributions of sulfur dioxide daily deposition velocities for the RoMANS spring and summer campaigns. Deposition velocities in the spring are bimodally distributed, with values 0.225–0.25 cm/s and 0.40–0.425 cm/s occurring most frequently. In summer the deposition velocities also have a bimodal distribution, but the range of deposition velocities is greater. Nitric acid deposition velocities are plotted in Figure 4.5. In spring the distribution of nitric acid deposition velocities is bimodal, while in the summer there is a high frequency of deposition velocities in the 1.75–2.0 cm/s range. Unlike for SO_2, the spring has a wider distribution of deposition velocities than the summer for HNO_3 and for particles (Figure 4.6). In the case of particle deposition velocities, we see that the spring deposition velocities are shifted somewhat higher than in summer. Since $V_d(NH_3)$ was calculated simply as 0.7 times $V_d(NHO_3)$, the distribution is not shown.

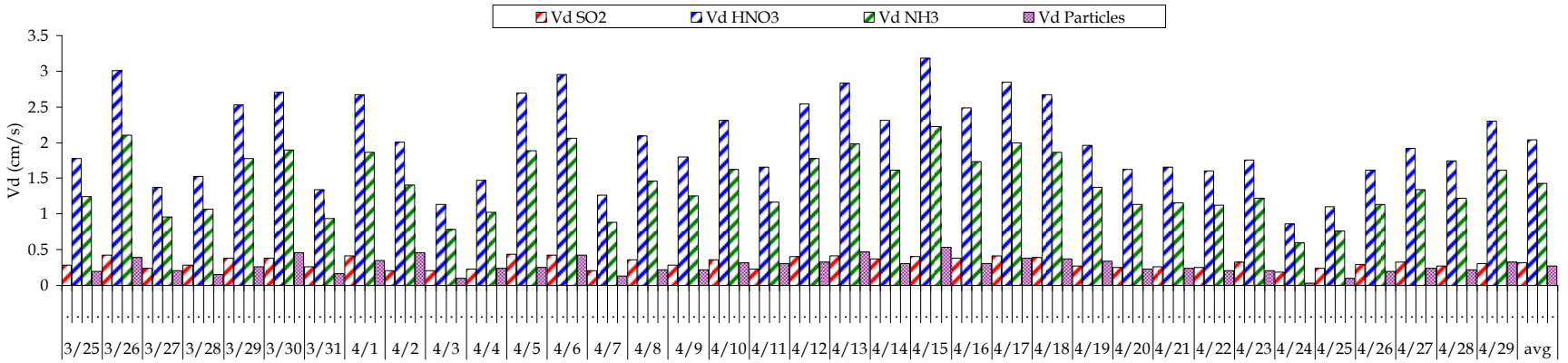

Figure 4.2. Spring deposition velocities (cm/s) for SO_2, HNO_3, NH_3 and particles.

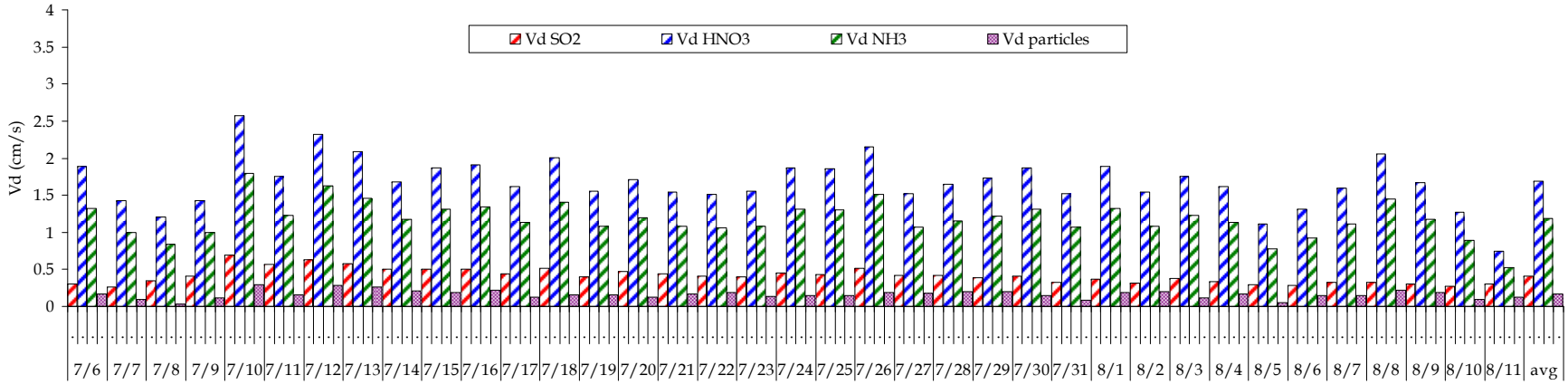

Figure 4.3. Summer deposition velocities (cm/s) for SO_2, HNO_3, NH_3 and particles.

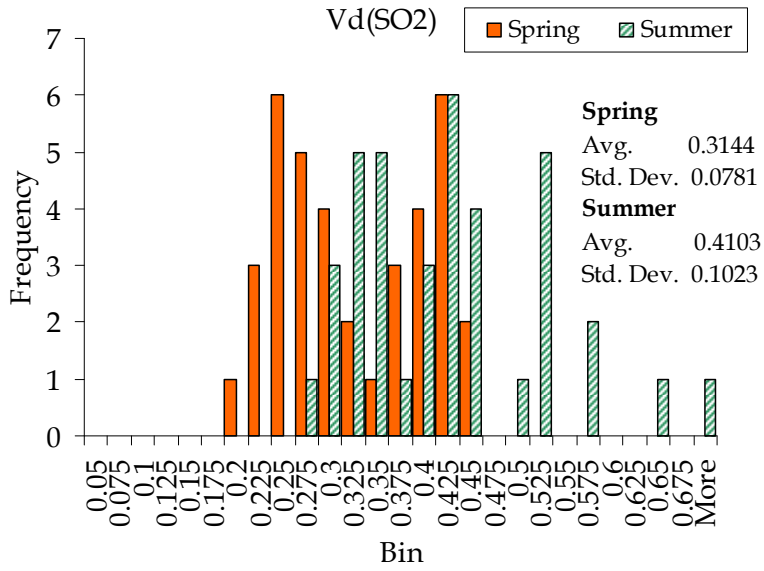

Figure 4.4. Frequency distributions of daily averaged deposition velocities for SO_2 for the spring and summer RoMANS study periods. X-axis bin values are the upper range for each bin.

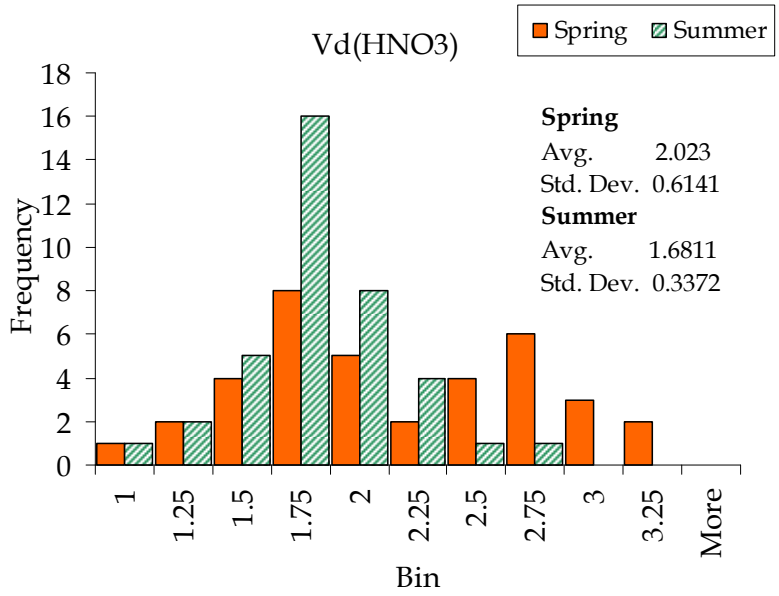

Figure 4.5. Frequency distributions of daily averaged deposition velocities for HNO_3 for the spring and summer RoMANS study periods. X-axis bin values are the upper range for each bin.

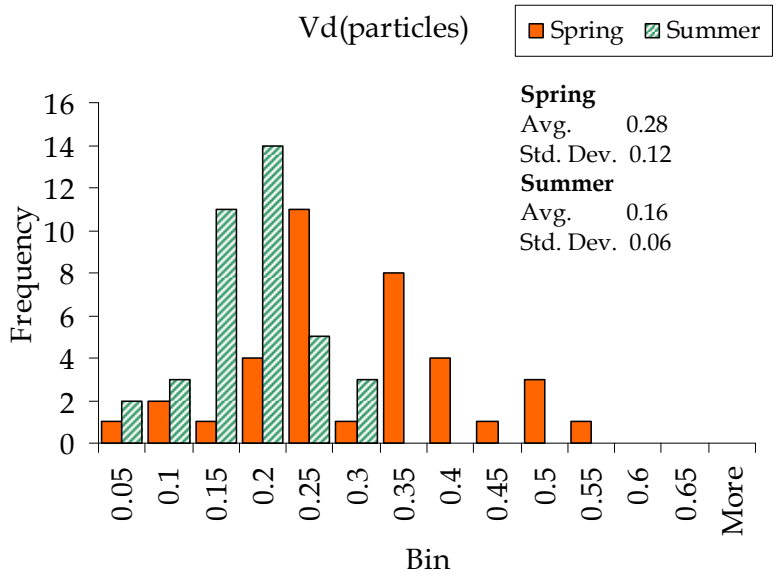

Figure 4.6. Frequency distributions of daily averaged particle deposition velocities for the spring and summer RoMANS study periods. X-axis bin values are the upper range for each bin.

Daily dry deposition fluxes were determined for the RoMANS spring and summer campaigns, using $PM_{2.5}$ and trace gas concentrations measured with the URG sampler and deposition velocities derived as described above. As shown in Figures 4.7 and 4.8, considerable variability in deposition fluxes is observed from day to day, reflecting changes in pollutant concentrations and meteorology at the RoMANS core site.

Gas species, with their higher deposition velocities, were typically bigger contributors to dry deposition fluxes than particulate species. The importance of particle deposition of nitrogen was somewhat more significant in spring, when gas-particle-phase partitioning often favored particle-phase nitrogen components. On most RoMANS study days, the dry deposition of ammonium plus ammonia contributed more to nitrogen fluxes than deposition of nitric acid plus nitrate. Since the deposition velocity of nitric acid is always greater than ammonia while the deposition velocities of particulate nitrate and ammonium are the same, the greater fluxes of reduced nitrogen reflect higher concentrations of these species. Nitrate plus nitric acid dry deposition exceeded ammonia plus ammonium dry deposition for only 4 days in the spring campaign and for only 3 days during the summer.

Table 4.2 summarizes the total deposition of individual species for spring and summer at the core site. During both seasons gas deposition fluxes exceeded those of their particle-phase counterparts. In both spring and summer, the relative contributions to nitrogen dry deposition were $NH_{3(g)} > HNO_{3(g)} > NH_4^+{}_{(p)} > NO_3^-{}_{(p)}$. Deposition fluxes for all three gas species increased from spring to summer, with ammonia and nitric acid fluxes more than doubling. Particle deposition fluxes, by contrast, decreased from spring to summer.

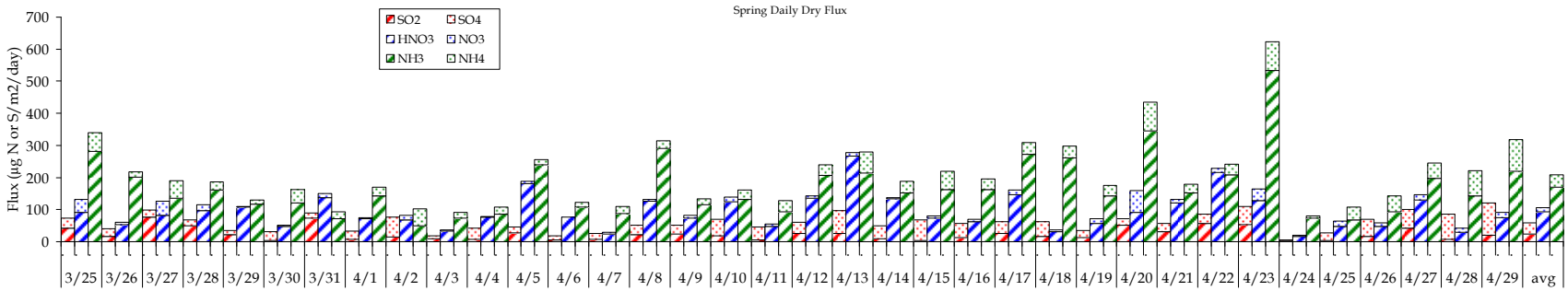

Figure 4.7. Spring dry daily deposition (µg/m^2/day) of reduced and oxidized nitrogen and of sulfur at the RoMANS core site. Particle fluxes are shown in the dotted bars and gas fluxes are shown in the hatched bars. Red: SO_4^{2-}/SO_2, blue: NO_3^-/HNO_3, and green: NH_4^+/NH_3.

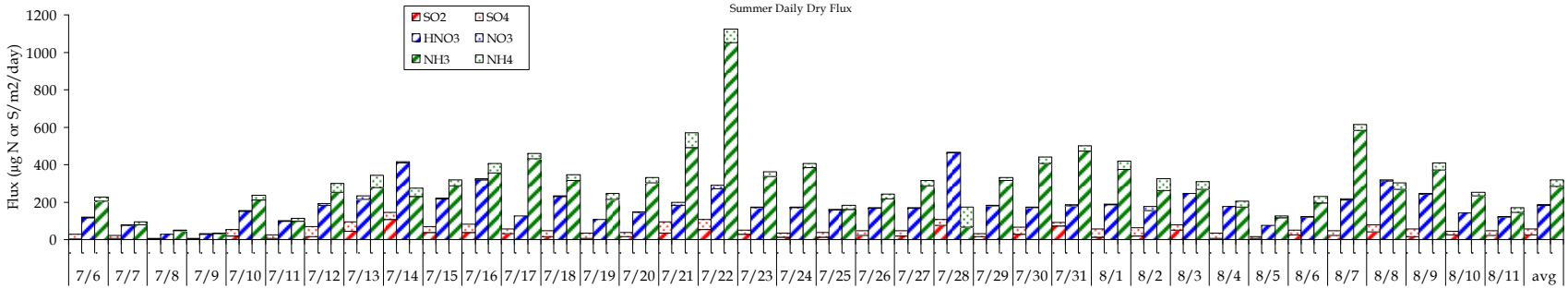

Figure 4.8. Summer dry daily deposition (µg/m^2/day) of reduced and oxidized nitrogen and of sulfur at the RoMANS core site. Particle fluxes are shown in the dotted bars and gas fluxes are shown in the hatched bars. Red: SO_4^{2-}/SO_2, blue: NO_3^-/HNO_3, and green: NH_4^+/NH_3.

Note scale change from Figure 4.7

Table 4.2. Dry deposition totals by species for spring and summer campaigns at the RoMANS core site. Units are μg N/m^2 or μg S/m^2.

Species	Spring Deposition	Summer Deposition
NO_3^- (p)	478.36	181.45
HNO_3 (g) 3	325.22	6704.37
NH_4^+ (p)	1401.07	1261.44
NH_3 (g) 6	109.74	14723.54
SO_4^{2-} (p)	1294.32	1086.03
SO_2 (g) 84	0.83	979.98

The observed seasonal changes in dry deposition fluxes are driven largely by concentration changes for the gas-phase species and by both concentration changes and deposition velocities for particles. Higher gas concentrations in the summer increase the deposition fluxes of these species, while reduced summertime particle deposition velocities and particle concentrations of nitrogen species decrease deposition of particles. Figures 4.9–4.14 show time lines of daily species concentrations, species deposition velocities, and deposition fluxes for gaseous nitric acid, ammonia, and sulfur dioxide, and for particulate ammonium, nitrate, and sulfate. Examination of these plots allows one to see the relative importance of changing concentrations versus changing deposition velocities on day-to-day variability in calculated dry deposition. For example, spikes in dry deposition of gaseous ammonia observed on April 23, July 22, and August 7 were due primarily to increasing ammonia concentrations rather than to increases in the daily average ammonia deposition velocity. Similar patterns are seen for other species as well. Dry deposition of nitric acid, sulfur dioxide, and particulate ammonium, for example, all showed a substantial increase on July 28. In each case the deposition spike was associated with a concentration increase and not with an increase in the species deposition velocity. Deposition on this date, July 28, also showed another interesting feature. While concentrations and deposition of gaseous nitric acid and particulate ammonium all increased on this day, both the concentration and deposition of gaseous ammonia decreased. This was one of the few days where dry deposition of oxidized nitrogen significantly exceeded dry deposition of reduced nitrogen.

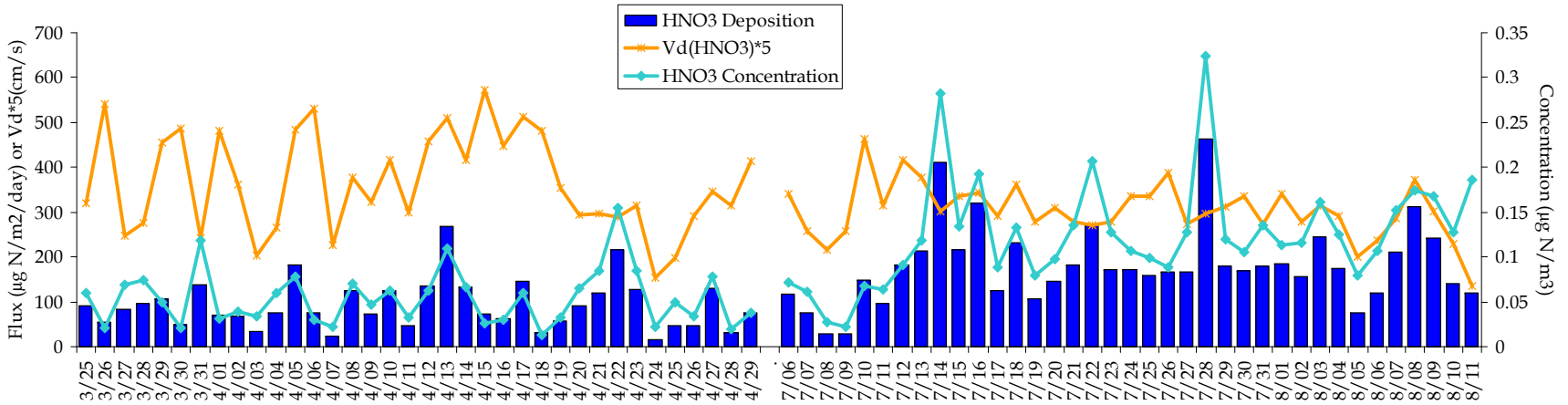

Figure 4.9. Time lines of daily deposition flux (µg/m^2/day, blue bar), deposition velocity (cm/s, orange), and concentration (µg/m^3, light blue line) for nitric acid. The deposition velocity was multiplied by a factor of 5 so all three parameters could be shown on the same plot.

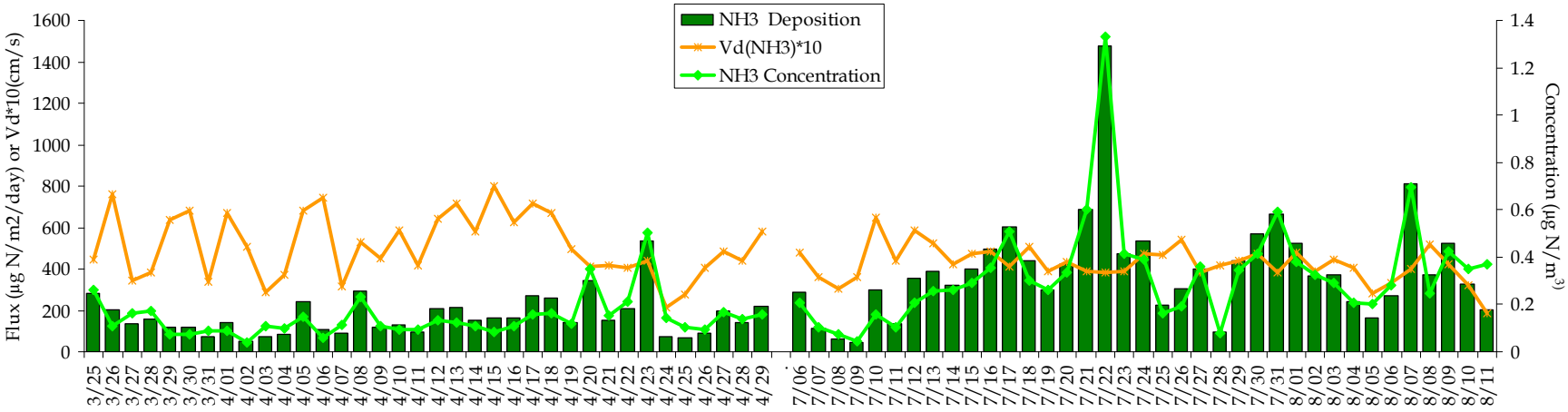

Figure 4.10. Time lines of daily deposition flux (µg/m^2/day, green bar), deposition velocity (cm/s, orange), and concentration (µg/m^3, light green line) for ammonia. The deposition velocity was multiplied by a factor of 10 so all three parameters could be shown on the same plot.

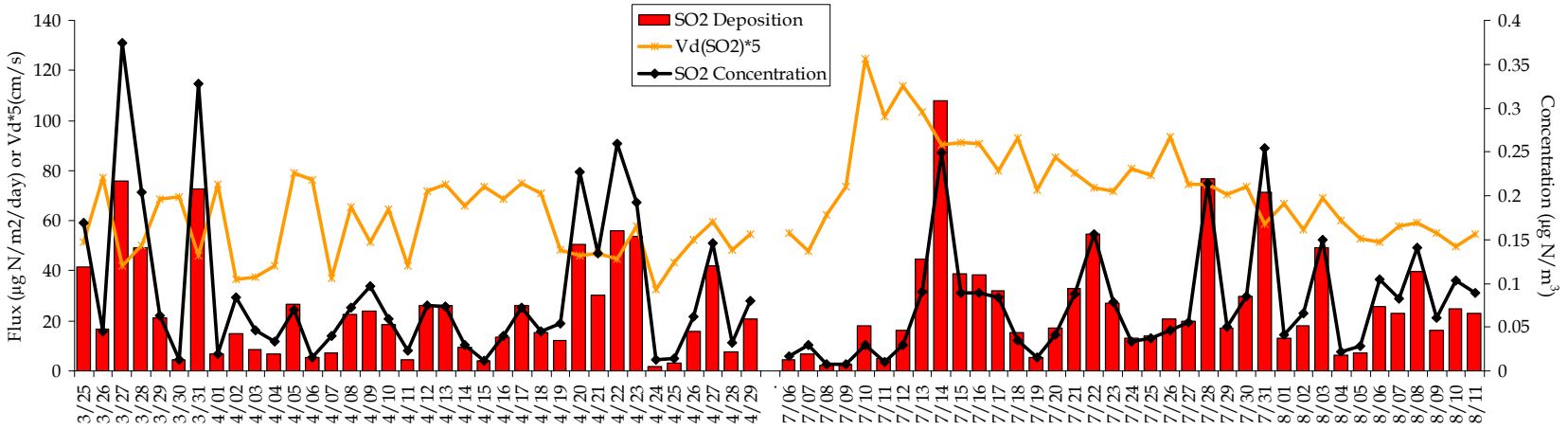

Figure 4.11. Time lines of daily deposition flux (µg/m^2/day, red bar), deposition velocity (cm/s, orange), and concentration (µg/m^3, black line) for sulfur dioxide. The deposition velocity was multiplied by a factor of 5 so all three parameters could be shown on the same plot.

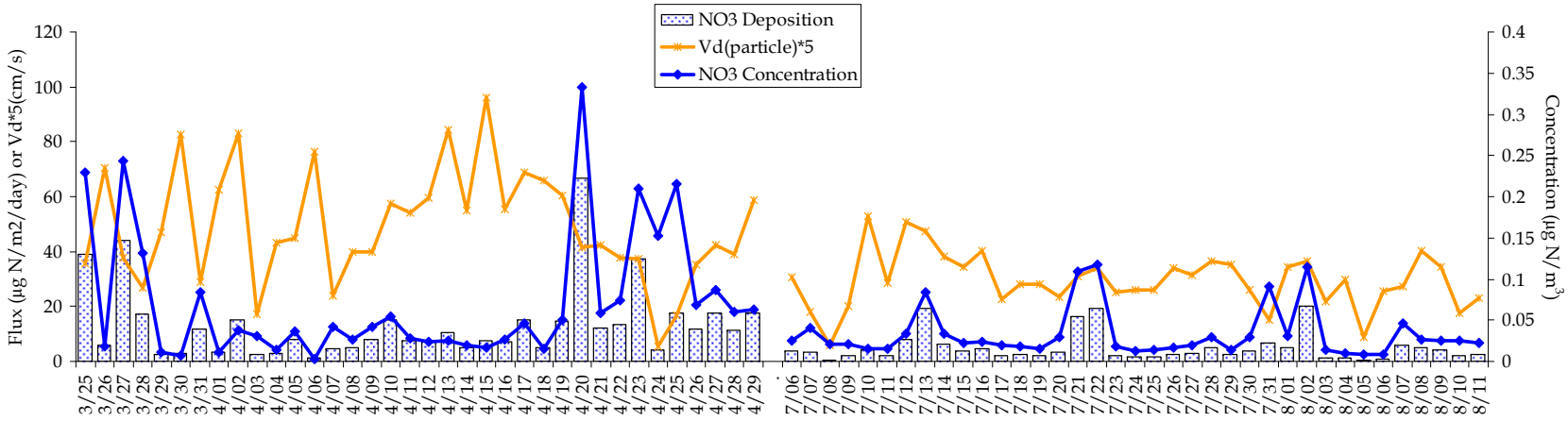

Figure 4.12. Time lines of daily deposition flux (µg/m^2/day, bar), deposition velocity (cm/s, orange), and concentration (µg/m^3, blue line) for fine particle nitrate. The deposition velocity was multiplied by a factor of 5 so all three parameters could be shown on the same plot.

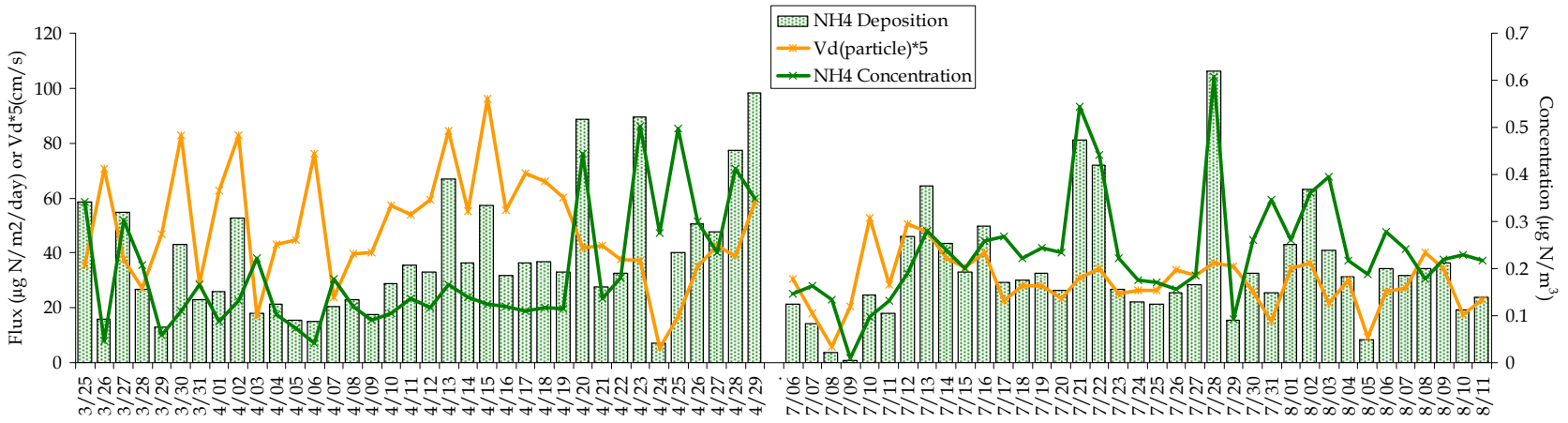

Figure 4.13. Time lines of deposition flux (µg/m^2/day, bar), deposition velocity (cm/s, orange), and concentration (µg/m^3, green line) for fine particle ammonium. The deposition velocity was multiplied by a factor of 5 so all three parameters could be shown on the same plot.

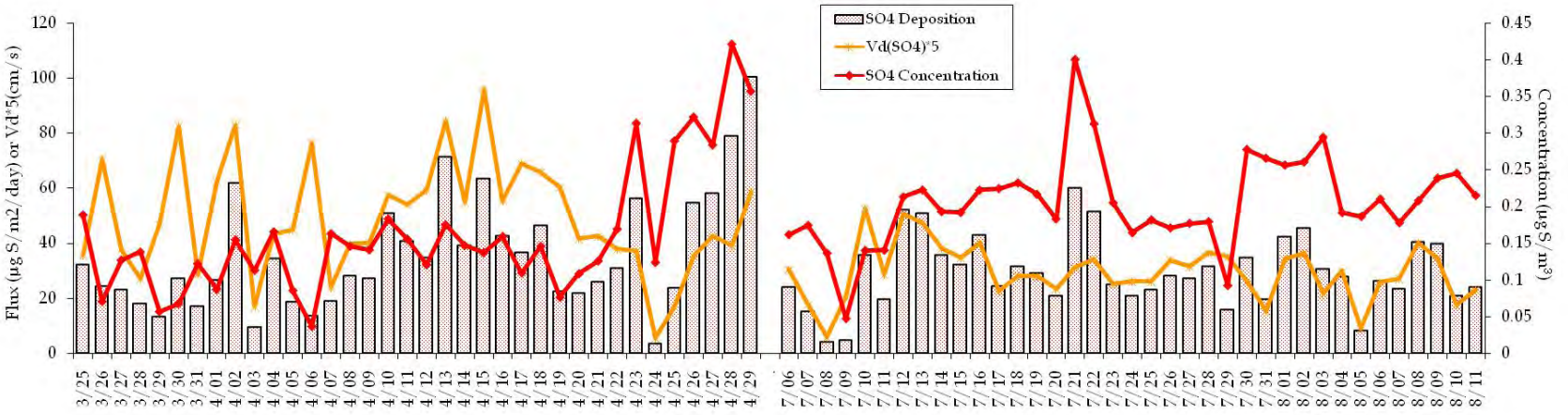

Figure 4.14. Time lines of deposition flux (µg/m^2/day, bar), deposition velocity (cm/s, orange), and concentration (µg/m^3, green line) for fine particle sulfate. The deposition velocity was multiplied by a factor of 5 so all three parameters could be shown on the same plot.

4.1.2. The Importance of Averaging Time in Determining Dry Deposition Fluxes

Dry deposition fluxes are determined as the product of a species deposition velocity and the corresponding species concentration. The CASTNet program currently measures meteorological parameters at high time resolution (time scale of minutes), permitting the computation of diurnally varying deposition velocities. Concentrations of nitrogen and sulfur species, however, are measured only as weekly averages. Consequently, deposition fluxes of nitrogen and sulfur species are determined as the product of weekly average deposition velocities and weekly average concentrations. It is unlikely in the near future for nitrogen and sulfur species concentrations to be routinely measured at time scales shorter than daily.

Because deposition fluxes are the product of two time-varying quantities, there is no guarantee that deposition fluxes determined using high time resolution measurements can be accurately reproduced when using observations averaged over much longer time intervals. Dry deposition fluxes calculated using observations made at different time scales may differ substantially if there is a temporal correlation between a species concentration and its deposition velocity. Positive (negative) correlations between deposition velocity and concentration produce higher (lower) deposition fluxes if calculated at high time resolution, compared to calculations made using longer-time-averaged values. If deposition velocities and concentrations vary in time but independently of each other, deposition fluxes will be unaffected by the choice of averaging time scales.

The RoMANS dataset provides a unique opportunity to examine the importance of making high time resolution measurements of species concentrations and deposition velocities for accurate determination of deposition fluxes. To determine the importance of averaging time, both daily averages and hourly averages of V_d and concentrations of ammonia were utilized. Daily ammonia fluxes were determined in two ways. In the first method, hourly deposition fluxes were determined from hourly average concentrations and deposition velocities. These hourly fluxes were then averaged over 24 hrs to determine the average deposition flux for the day. In the second method, daily average concentrations and deposition velocities were first determined and then multiplied to obtain a daily deposition flux. Mathematically, these two approaches can be expressed as a comparison of $F'_{24} = \langle V_d \cdot C \rangle_{24}$ and $F_{24} = \langle V_d \rangle_{24} \cdot \langle C \rangle_{24}$, where V_d and C are hourly data. F'_{24} is considered the better estimate of the daily average ammonia deposition flux. The difference between F_{24} and F'_{24} represents the bias in daily flux, resulting from degrading the measurement time resolution from hourly to daily.

Figure 4.15 compares the deposition fluxes calculated by the two methods (hourly versus daily measurements) for the spring and summer measurement campaigns. Agreement between the flux values obtained using the two methods is overall quite good. This is especially true during spring when the two methods yield daily fluxes that are essentially equivalent, showing only a very small positive bias for the case with daily average input values. The overall bias during summer is also quite small, although small positive or negative biases appear on individual days.

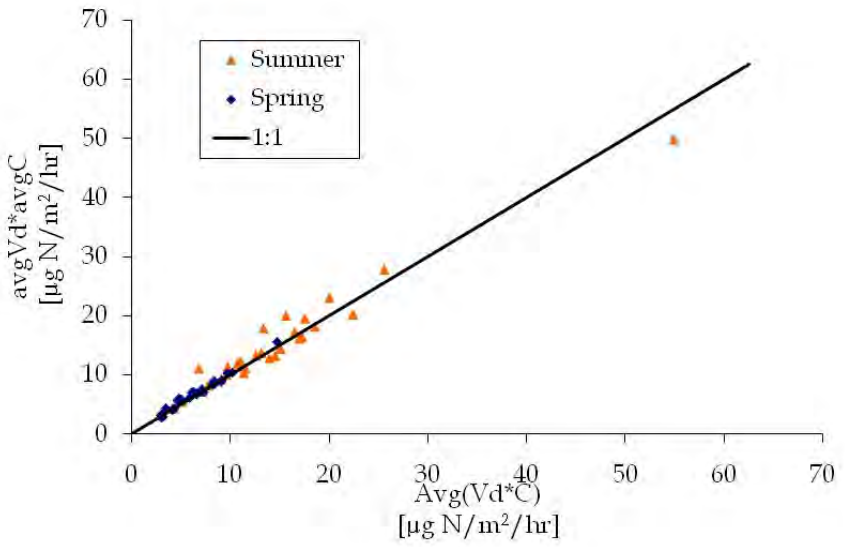

Figure 4.15. Comparison of ammonia daily average dry deposition fluxes determined using hourly (x-axis) and daily (y-axis) average concentrations and deposition velocities. Units are $\mu g/m^2/hr$.

The slight increase in bias from spring to summer can be understood by examining the diurnal profiles of ammonia deposition velocity and ammonia concentration depicted in Figure 4.16. During spring, the average ammonia concentrations observed at the RoMANS core site do not vary much with time of day. Consequently, there is little difference between a daily deposition flux determined using hourly concentration values or its daily averaged counterpart. In summer, a more pronounced diurnal variability is observed in ammonia concentrations, with a concentration minimum in the early morning and a concentration maximum in the early evening. The peak in ammonia concentration, however, is typically delayed somewhat from the peak in the ammonia deposition velocity that occurs from midmorning to early afternoon, preventing the creation of a significant negative bias from arising when daily average concentration and deposition velocity are used to determine the ammonia flux.

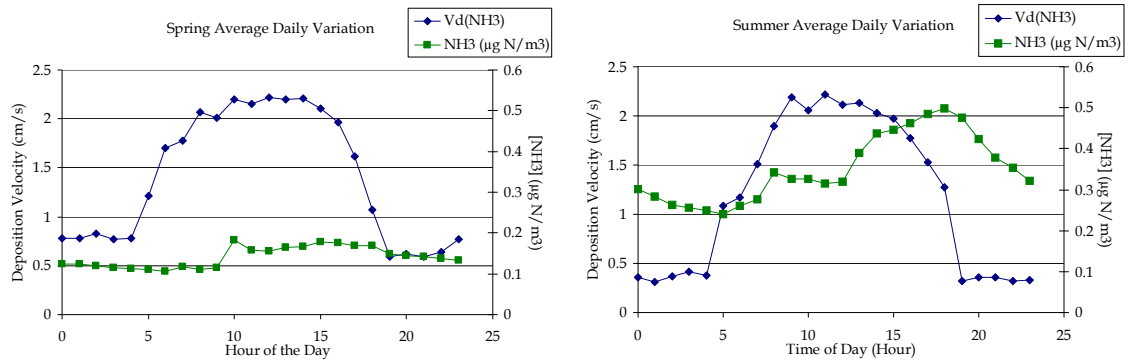

Figure 4.16. Average diurnal variation of RoMANS core site NH_3 concentrations ($\mu g/m^3$, green, right axis) and deposition velocities (cm/s, blue, left axis) for the spring (left panel) and summer (right panel) campaigns.

To determine the influence of averaging over a larger time scale, monthly and weekly averages were also compared. In Table 4.3 the influence of multiple averaging time scales on total dry deposition is presented. The daily total deposition was calculated by summing the products of daily averaged deposition velocities and concentrations (column labeled "daily"). Weekly averages were taken from Tuesday to Tuesday during each study period of the RoMANS campaign, resulting in averages for 4 weeks (for both the spring and summer study) for concentrations and deposition velocities. These weekly averages were used to calculate a weekly average deposition flux. The weekly average depositions were then added together to get a monthly deposition based on weekly averages (column labeled "weekly"). In addition, monthly averages of concentration and deposition velocity were taken over the same 4-week period to get a monthly deposition bases on monthly average (column labeled "monthly").

Table 4.3. Influence of averaging time scale on total deposition. Column titles correspond to the time scale over which averages of deposition velocity and concentration were taken.

		Daily Weekly		Monthly	Daily to Weekly	Daily to Monthly
		µg N (or S)/m^2	µg N (or S)/m^2	µg N (or S)/m^2 %	difference	
NO_3^-(p)	Spring	330.8	364.1 47	8.6 -9	.6%	-36.5%
	Summer	151.6	144.2 13	0.6 5.	0%	14.9%
HNO_3(g)	Spring	2816.0	2778.9	2666.6	1.3%	5.5%
	Summer	5393.5	5538.4	5097.0	-2.7%	5.7%
SO_4^{2-}(p)	Spring	922.1 93	1.4	1069.6	-1.0%	-14.8%
	Summer	859.1	874.6 81	7.3 -1	.8%	5.0%
SO_2 (g)	Spring	621.1	608.4	705.2	2.1%	-12.7%
	Summer	837.0	871.5	757.4	-4.0%	10.0%
NH_4^+(p)	Spring	997.7	1053.2 12	60.4 -5	.4%	-23.3%
	Summer	1064.8 10	62.7	942.3	0.2%	12.2%
NH_3(g)	Spring	4839.2	4628.2	4931.8	4.5%	-1.9%
	Summer	12356.9	10464.0	9355.5	16.6%	27.6%

The extent of agreement between the deposition fluxes calculated from daily, weekly, and monthly averages varies between each species, but they often do not compare as well as for the hourly and daily average ammonia flux comparison presented above. There is not a consistent pattern of increasing or decreasing deposition with averages over larger time scales. Even trends for the same species do not stay the same from spring to summer. For example, the daily-to-monthly bias for ammonia flux in spring is approximately -2% but grows to almost 28% in the summer measurement period. Differences between daily average and weekly average deposition are smaller for all species than between fluxes determined from daily average and monthly average concentrations and deposition velocities. The largest flux bias was observed for fine particle nitrate (-36.5%) during the spring study period. The smallest difference in predicted monthly flux was 0.2% for fine particle ammonium during the summer. Most differences were less than 20% for all time scale comparisons, suggesting that the value of making highly time-resolved measurements of parameters needed to calculate deposition velocities at time scales of a day or less is limited if a determination of flux budgets is the only objective.

4.1.3. Combined Wet and Dry Deposition Fluxes

The total amount of dry deposition flux was significantly smaller than wet deposition flux for all species measured during both the spring (Figure 4.17) and summer (Figure 4.18) at the core site. Wet deposition fluxes of nitrate, ammonium, ON, and sulfate all increased from spring to summer. Ammonium increased by 101.9%, nitrate by 135.6%, ON by 48.9%, and sulfate by 61.6%. Dry deposition fluxes of nitric acid, ammonia, and sulfur dioxide also increased in summer by 101.6%, 141.0%, and 16.5%, respectively. By contrast, dry deposition fluxes of particulate nitrate, ammonium, and sulfate decreased by 62.1%, 10.0%, and 16.1%, respectively.

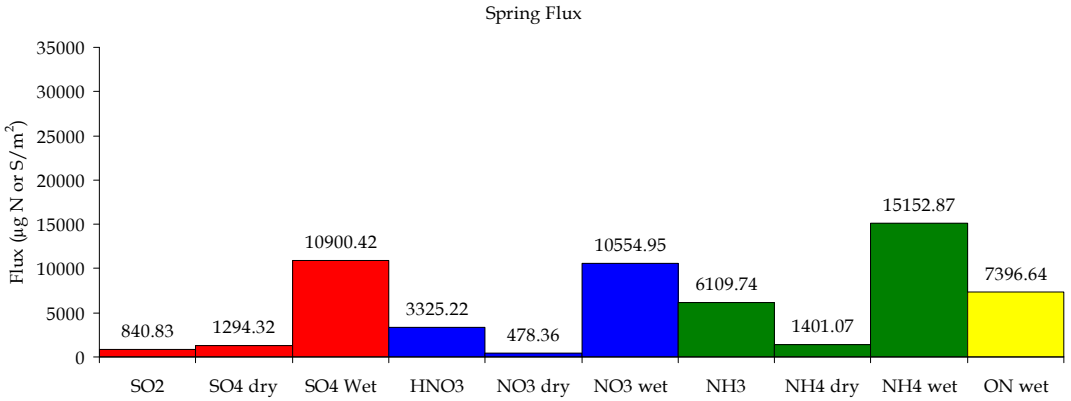

Figure 4.17. RoMANS core site spring deposition fluxes (µg/m^2) broken down for each species by dry gaseous, dry particle, and wet.

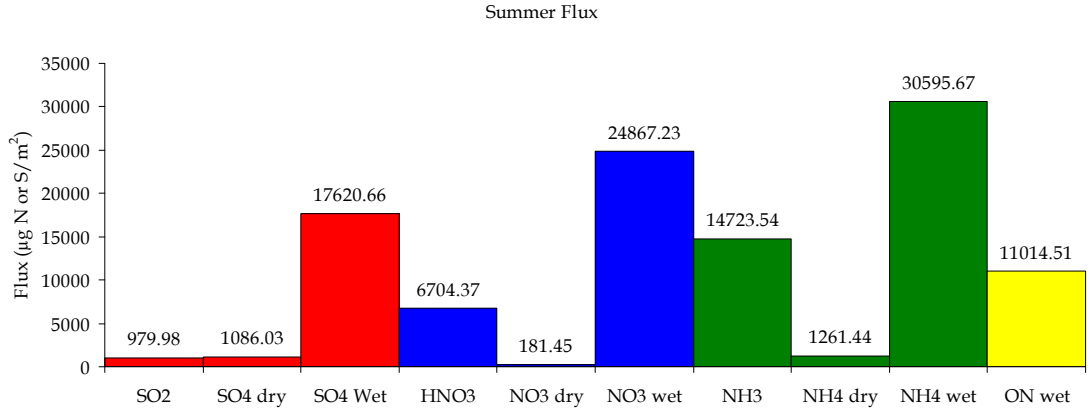

Figure 4.18. RoMANS core site summer deposition fluxes (µg/m^2) broken down for each species by dry gaseous, dry particle, and wet.

In the spring a total of 44419 µg/m^2 of nitrogen was deposited by measured dry and wet deposition pathways at the RoMANS core site, along with 13036 µg/m^2 of sulfur (see Figure 4.19). In the summer campaign, nitrogen deposition more than doubled to 89348 µg/m^2 while sulfur deposition increased by approximately 50% to 19687 µg/m^2.

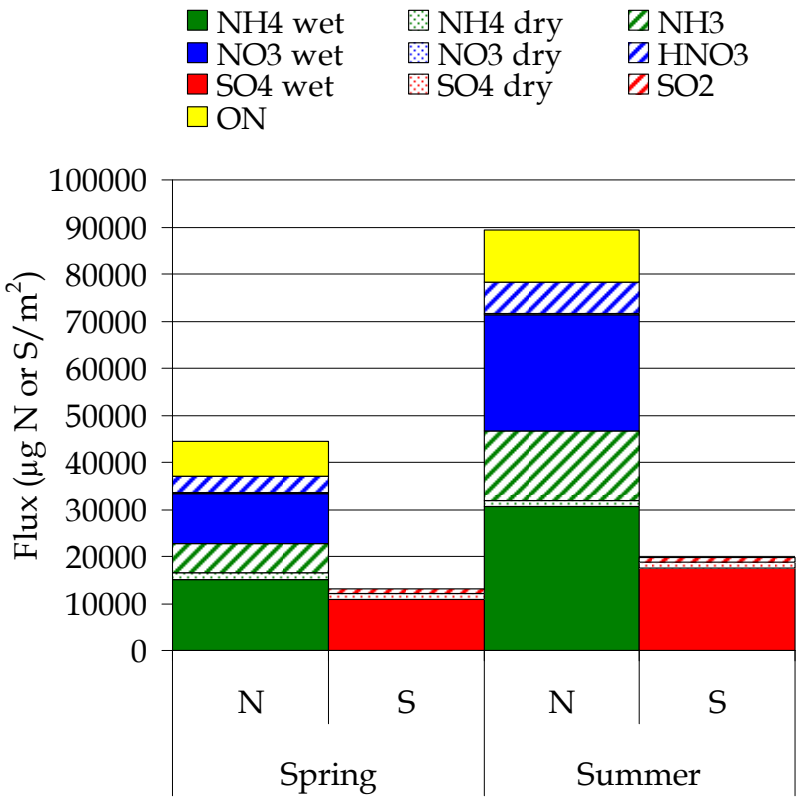

Figure 4.19. Total measured nitrogen and sulfur deposition ($\mu g/m^2$) for the RoMANS core site showing the amount of deposition due to each species and process.

Wet deposition is the major process by which nitrogen is deposited in RMNP during both spring and summer. In the spring, only 25.5% of measured nitrogen deposition occurred by dry processes (Figure 4.20): 13.8% from NH_3, 7.5% from HNO_3, 3.2% from NH_4^+(p), and 1% from NO_3^-(p). NH_4^+ wet deposition alone exceeded all the dry processes combined with 34.1% of deposited nitrogen, followed by wet NO_3^- deposition with 23.8% and wet organic nitrogen (ON) deposition with 16.7%. Despite the large increase in nitrogen deposition from spring to summer, the relative inputs of various nitrogen pathways and species were rather similar (see Figure 4.21). Wet deposition of ammonium again represents the largest nitrogen input (34.2%), followed by wet deposition of nitrate (27.8%), dry deposition of gaseous ammonia (16.5%), wet deposition of ON (12.3%), and dry deposition of gaseous nitric acid (7.5%). The dry deposition inputs of fine particle ammonium (1.4%) and nitrate (0.2%) are even less important contributors than during spring.

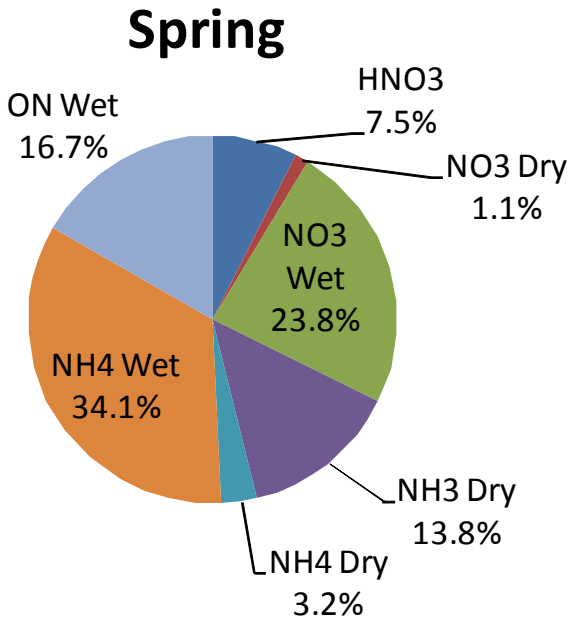

Figure 4.20. Relative contributions of individual nitrogen deposition pathways to total measured nitrogen deposition at the RoMANS core site during the spring campaign. The area of the pie is proportional to the total nitrogen deposition during each field campaign.

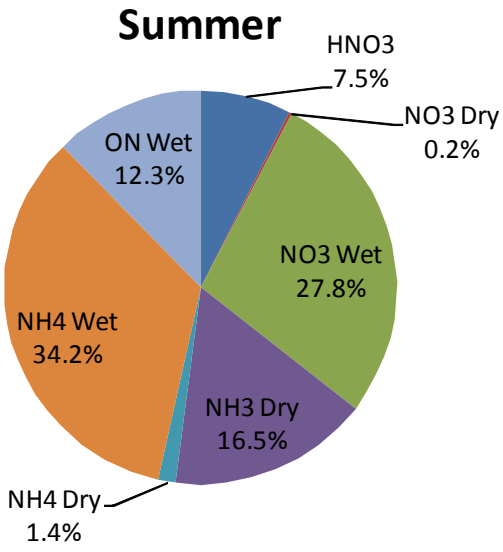

Figure 4.21. Relative contributions of individual nitrogen deposition pathways to total measured nitrogen deposition at the RoMANS core site during the summer campaign. The area of the pie is proportional to the total nitrogen deposition during each field campaign.

Neither wet deposition of ON nor dry deposition of ammonia are quantified in routine monitoring networks such as NADP/NTN or CASTNet. Addition of these measurements during RoMANS clearly demonstrates the importance of both pathways to total nitrogen inputs in RMNP. Figure 4.22 shows nitrogen deposition inputs by the various pathways, arranged from the largest contributors on the left to the smallest contributors on the right. ON wet deposition and ammonia dry deposition constitute the third and fourth most important nitrogen deposition

pathways in spring. In summer the order of these two inputs is reversed. In both seasons, these two pathways are exceeded in importance only by wet deposition of ammonium and nitrate. They are significantly more important than dry deposition inputs of nitric acid and fine particle nitrate and ammonium, both of which are measured in RMNP by CASTNet.

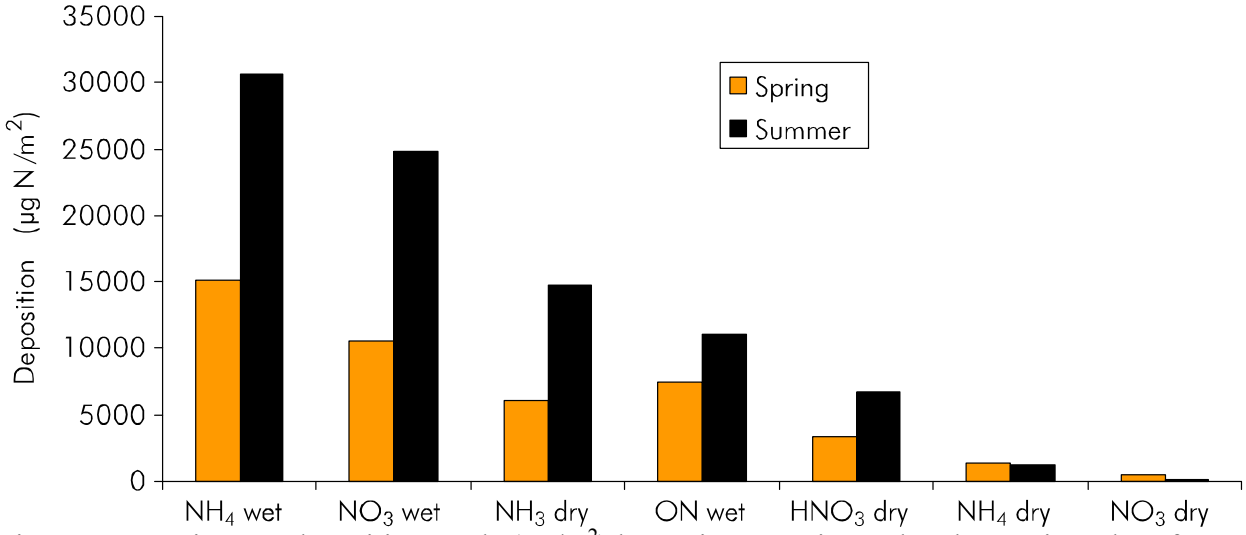

Figure 4.22. Nitrogen deposition totals (µg/m^2) by various species and pathways in order of contribution to total nitrogen deposition at the RoMANS core site.

Together, wet deposition of ON and dry deposition of gaseous ammonia compose approximately 30% of the total RoMANS nitrogen deposition budget. In order to better quantify total nitrogen inputs into RMNP and determine which source types and regions are the biggest contributors to the problem, these two deposition pathways need to be measured more routinely. That will require routine measurements of gaseous ammonia concentrations and of ON in precipitation. There is also a need to examine dry deposition inputs of ON, a pathway not examined in the RoMANS study.

It is instructive to compare total nitrogen deposition inputs from the RoMANS spring and summer campaigns with the recently established critical load for nitrogen wet deposition in RMNP of 1.5 kg/N/ha/ yr. Although the two RoMANS field campaigns covered only a little over 2 months, the total wet nitrogen deposition, excluding ON, measured in these campaigns was 0.81 kg/N/ha/ yr, already more than half the annual critical load. A full annual cycle of deposition measurements is clearly needed to better constrain annual nitrogen inputs to RMNP ecosystems.

4.2. ORGANIC NITROGEN

As outlined above, wet deposition of ON comprised substantial fractions of both wet and total nitrogen deposition in RMNP. While measurements made during RoMANS quantified the amount of ON deposited in precipitation, they did not provide any information about dry deposition of ON species nor did they provide much insight into the types of sources responsible for the ON measured.

Atmospheric ON can include contributions from biological sources (Jones and Cookson, 1983; Littmann, 1997), oxidation products of combustion emissions (Roberts, 1990), and reduced forms of nitrogen primarily from agricultural sources (Schade and Crutzen, 1995). Other studies have focused on some subsets of ON compounds: aliphatic amines (Gronberg et al., 1992), amino compounds (Gorzelska et al., 1992), urea and free amino acids (Mace et al., 2003), and free and combined amino nitrogen (Zhang and Anastasio, 2001).

During RoMANS, total ON was measured in precipitation samples to determine its importance to the total nitrogen deposition budget. ON deposition varied by event just as the other nitrogen species deposition fluxes did. In general, ON concentrations did not appear to reach the same levels as nitrate or ammonium. In only a few instances during the summer, at the core site and Gore Pass, did the concentrations of ON exceed concentrations of nitrate or ammonium.

Deposition fluxes of ON were compared with deposition fluxes of NH_4^+ and NO_3^- in Figure 4.23. In each case a best-fit least squares regression line was fit to the data. Reasonably strong correlations were seen in both comparisons. The comparison of ON and ammonium fluxes yielded a linear relationship with a squared correlation coefficient of 0.77. The slope of the line was 0.37, suggesting that ON fluxes are typically a bit over one-third of ammonium fluxes. Comparing the flux values measured at the three sites revealed that smaller fluxes of both ON and ammonium were typically observed at Gore Pass than at the two sites on the eastern slope of the Continental Divide. The best-fit line to the ON-nitrate relationship had a slope of 0.52, indicating that ON deposition fluxes were typically about half of nitrate fluxes. The R^2 value of 0.64 for this dataset suggested a slightly weaker relationship between ON and nitrate fluxes than was observed for ON and ammonium.

The stronger relationship with ammonium might suggest common source types or regions for these species; however, one should be careful not to overinterpret the observed correlations. Concentrations and deposition fluxes of many precipitation solutes tended to strongly covary in many cases because they all tended to be influenced by precipitation physics. For example, concentrations of all solutes commonly decreased over time in extended precipitation events. At the same time, greater amounts of precipitation tended to produce higher deposition fluxes of all solutes. To illustrate the tendency for many species' deposition fluxes to be correlated, a correlation matrix is included (Table 4.4) for the summer study at the RoMANS core site. Solute pairs with Pearson's R values above $\pm$ 0.8 include Na^+ and K^+, NH_4^+ and Ca^{2+}, Na^+ and Cl^-, NO_3^- and Ca^{2+}, NO_3^- and NH_4^+, NO_3^- and SO_4^{2-}, and SO_4^{2-} and NH_4^+. Major species deposition fluxes also tended to be strongly related with precipitation amount, as evidenced by high correlations of precipitation amount with nitrate (R = 0.81), sulfate (R = 0.86), and ammonium (R = 0.77). Note, too, that in this more limited dataset, the correlations of ON fluxes with inorganic nitrogen fluxes were lower than in the full RoMANS dataset discussed above. Pearson's R values in this smaller dataset are only 0.41 for the relationship between ON and ammonium and 0.27 for ON and nitrate.

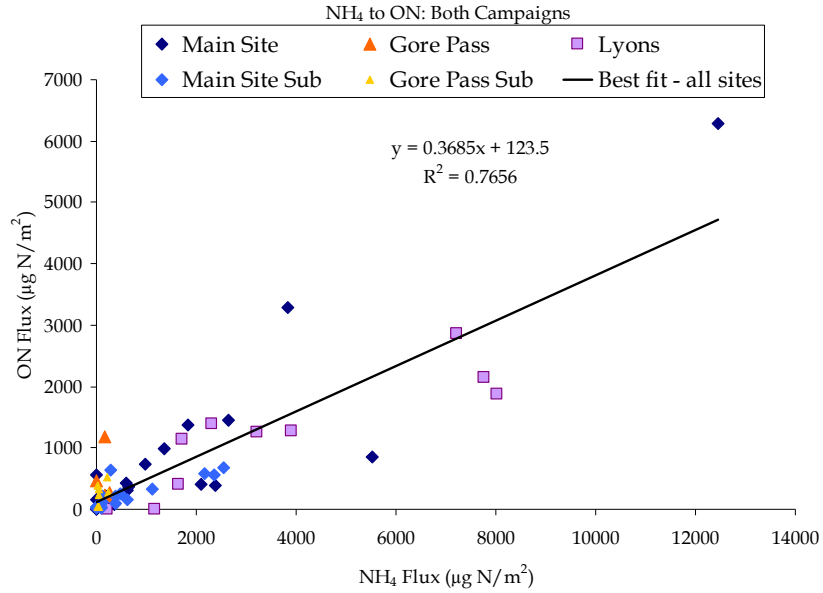

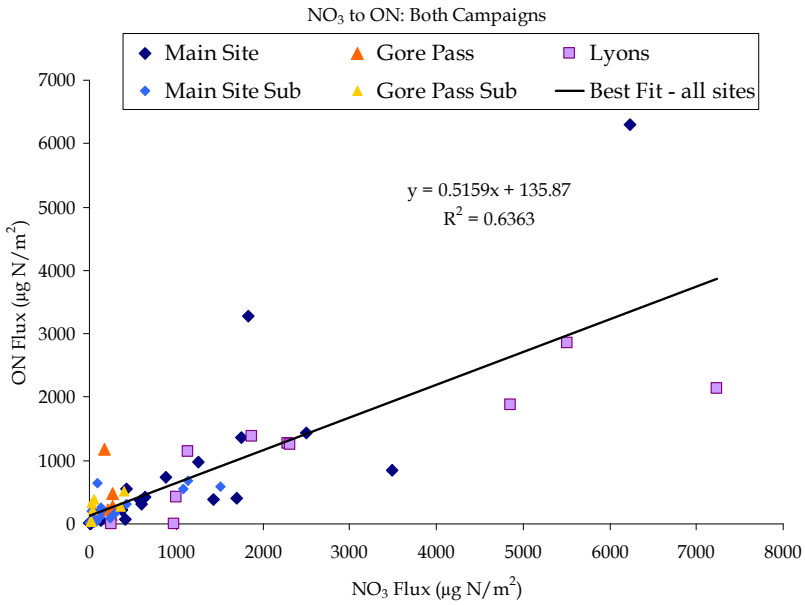

Figure 4.23. Relationship between organic and inorganic nitrogen wet deposition fluxes (µg/m^2) during the RoMANS study. Data are included from the three locations where ON was measured: the core site, Lyons, and Gore Pass.

Table 4.4. Correlation table for precipitation solute fluxes during the summer campaign measured at the core site for samples collected with the automated precipitation sampler. Pearson's R values of at least + 0.8 are highlighted in yellow.

	Ca^{2+}	K^+	Mg^{2+}	Na^+	NH_4^+	Cl^-	NO_2^-	NO_3^-	SO_4^{2-}	ON	$[H^+]$	Precip.
Ca^{2+}	1.000	0.612	0.446	0.784	0.842	0.687	-0.087	0.801	0.607	0.604	0.073	0.562
K^+		1.000	-0.169	0.862	0.694	0.631	-0.015	0.565	0.460	0.682	-0.211	0.661
Mg^{2+}			1.000	0.074	0.313	0.372	0.087	0.312	0.332	0.279	0.251	0.094

	Ca^{2+}	K^+	Mg	$^{2+}$	Na	$^+$	NH	$_4^+$	Cl	$^-$	NO	$_2^-$	NO	$_3^-$	SO	$_4^{2-}$	ON	$[H^+]$	Precip.
Na^+					1.000		0.668		0.851		-0.224		0	.558	0.406		0 .702	-0.237	0 .620
NH_4^+							1.000		0.489		-0.053		0.957		0.837		0. 410	0.038	0.772
Cl^-									1.000		-0.203		0.398		0.336		0.790	-0.181	0.438
NO_2^-											1.000		-0.033		0.059		0.140	0.104	-0.026
NO_3^-													1.000		0.922		0. 273	0.115	0.808
SO_4^{2+}															1.000		0.175	0.064	0.858
ON																	1.000	-0.056	0.290
$[H^+]$																		1.000	-0.230
Precip.																			1.000

ON fluxes did not appear to be strongly related to the amount of precipitation received, as illustrated in Figure 4.24. In the spring, the maximum ON flux occurred with the maximum amount of precipitation at the core site and Lyons but not at Gore Pass. In summer, Lyons was the only site where the maximum event ON flux occurred with maximum precipitation amount. Even within a given season, the relationship between ON deposition and precipitation amount was not as strong as observed for some other major species. In Table 4.4, for example, Pearson's R values for correlations between the RoMANS core site, summer campaign, species wet deposition flux, and precipitation amount fell between 0.77 and 0.86 for nitrate, sulfate, and ammonium, but the correlation for ON yielded a value of only 0.29.

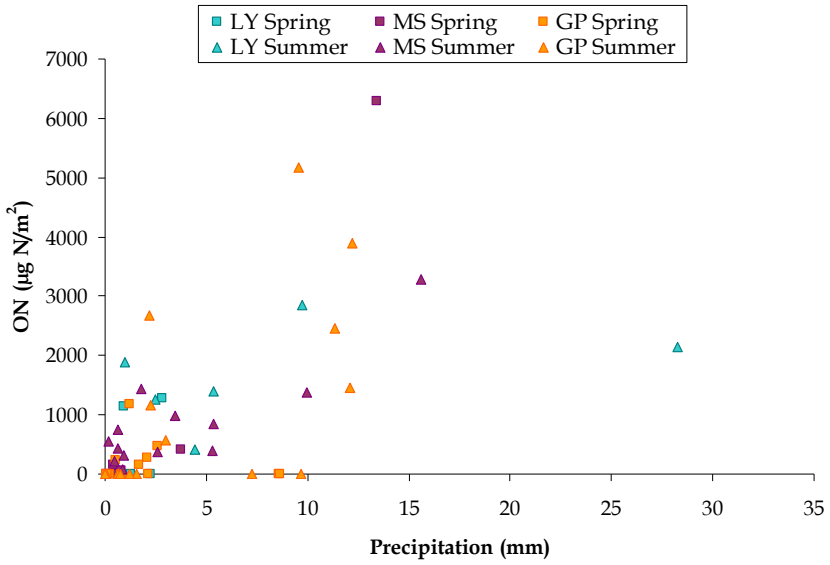

Figure 4.24. Organic nitrogen flux ($\mu g/m^2$) versus precipitation amount (mm) by site and campaign.

The relative wet deposition inputs of ON and inorganic nitrogen species are compared by site and season in Figure 4.25. The total amount of ON deposited varied by site and season, while the fraction of nitrogen as ON for the entire campaign did not vary significantly between Lyons and the core site or the spring and summer at those sites. At Lyons, nitrate, ammonium, and ON

composed 33%, 50%, and 17% of the wet-deposited nitrogen in spring. Similar fractional contributions were observed in summer. At the RoMANS core site, nitrate, ammonium, and ON contributed 32%, 46%, and 22%, respectively, of total spring nitrogen deposition. In the summer there was a slight shift between the ON and nitrate contribution: ON decreased to 17% and nitrate increased to 37% of total nitrogen deposited in the summer. In the spring at Gore Pass, nitrate, ammonium, and ON composed 49%, 29%, and 22% of nitrogen wet deposition. In summer at Gore Pass, the ON contribution increased to 35% and nitrate contribution decreased to 34% of total wet nitrogen deposited at the site.

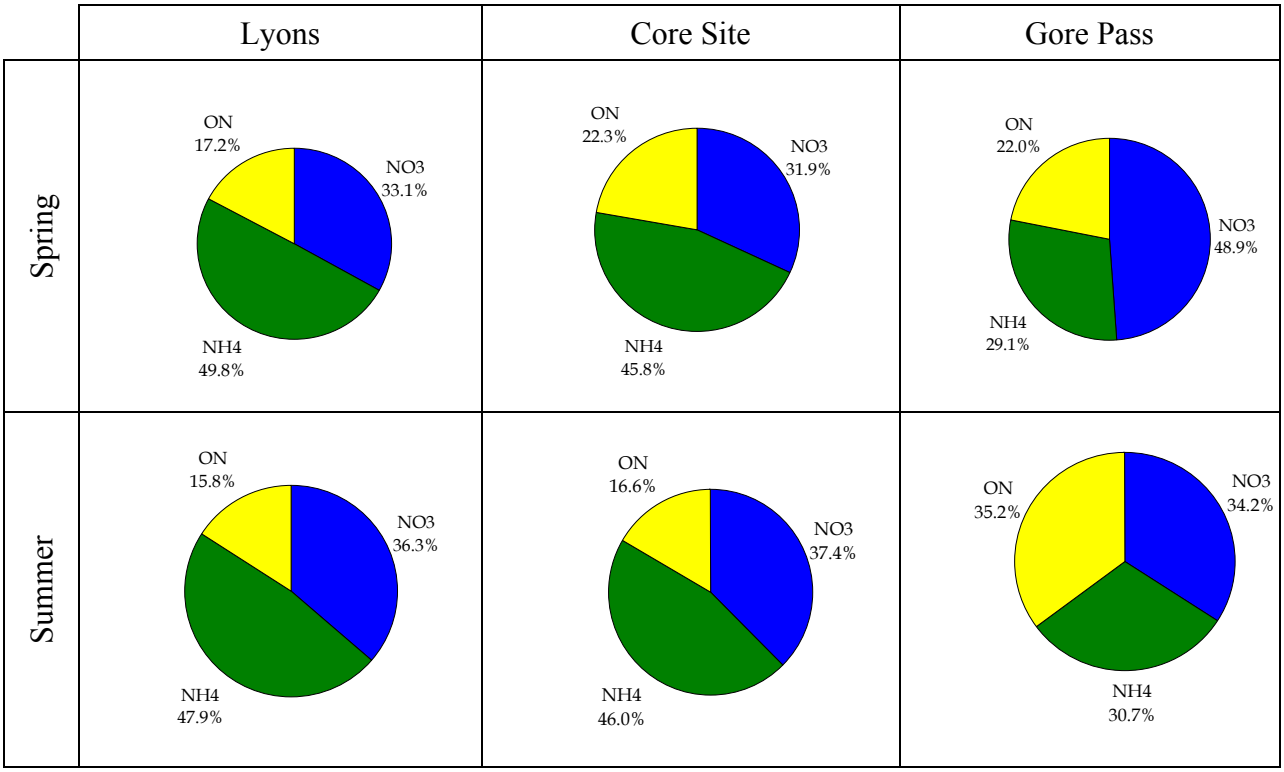

Figure 4.25. Contribution of each nitrogen species measured to total nitrogen deposition at Lyons, the core site, and Gore Pass for both the spring and summer RoMANS sampling periods.

Deposited-nitrogen budget results from RoMANS (16–35% ON) are fairly comparable to results from other studies that examined the contribution of ON to total nitrogen in precipitation. The amount of ON relative to total nitrogen has been found to vary with location. In southern Quebec it was found that ON was 38% of total nitrogen deposited (Dillon et al., 1991), in the Colorado Front Range 16% was organic (Williams et al., 2001), and in drier areas such as central and western Colorado 25% of nitrogen deposited was thought to be organic (Sickman et al., 2001).

While quantifying wet deposition fluxes of ON is important for understanding the total nitrogen input budget, little information can be gathered pertaining to sources and ecosystem availability from a bulk total ON measurement. Further work toward speciation of ON compounds would help to determine the sources and likely impacts of ON on the ecosystems of concern in RMNP. In addition, the method used for quantifying ON in RoMANS precipitation samples (measurement of inorganic nitrogen species concentrations before and after UV photooxidation)

is labor intensive and slow. Use of online, combustion-based total nitrogen measurement methodology, currently in testing at CSU, has the potential to greatly improve the ease of sample measurements, opening the way for more routine analysis of ON in wet deposition samples.

4.3. SPATIAL GRADIENTS IN THE ROMANS NETWORK AND POLLUTION EPISODES AT THE ROMANS CORE SITE

The spatial concentration patterns shown earlier in Figures 3.24 and 3.25 represent an average picture of particle- and gas-phase concentrations across the RoMANS network during spring and summer, respectively. These average data show strong gradients in nitrogen species concentrations across the RoMANS sampling network. For example, average concentrations of ammonia increase strongly from the mountain sites moving eastward, with the highest average value at the Brush site in northeastern Colorado. Elevated ammonia concentrations were also observed in spring at the westernmost site in the network, Dinosaur, although concentrations there were much lower than at Brush or at the Grant, Nebraska, site. Here we examine whether the spatial gradients observed in the spring and summer campaign average datasets are typical of gradients on individual days and look specifically at gradients on days where elevated concentrations and/or deposition fluxes are observed in RMNP.

Figure 4.26 depicts a time series of the daily spring concentration observations for reduced and oxidized nitrogen species. For each day a series of bars is plotted. Each bar represents the sum of either gaseous ammonia plus $PM_{2.5}$ ammonium (reduced nitrogen) (top panel) or gaseous nitric acid plus $PM_{2.5}$ nitrate (oxidized nitrogen) (bottom panel). A series of eight bars is plotted for each data point, with the bars arranged from left to right representing sites extending across the northern part of the RoMANS spring network from west to east. Dinosaur (DI) is on the left, followed by Gore Pass (GP), Timber Creek (TC), Beaver Meadows (BM), the core site (MS), Lyons (LY), Brush (BR), and Grant, Nebraska (NE). Springfield, located in southeastern Colorado, is not included in the figure. The data depict large, day-to-day variability in observed concentrations of both reduced and oxidized nitrogen. The overall spatial pattern depicted in reduced nitrogen species is similar, however, for most individual days to the average pattern depicted in Figure 3.24: concentrations were usually highest at the eastern and western network sites, with the absolute maximum almost always at Brush in northeastern Colorado. For oxidized nitrogen the pattern is a bit different. On most days the highest oxidized nitrogen concentrations were usually observed at Lyons, Brush, and Grant. On selected days, the Beaver Meadows and core site oxidized nitrogen concentrations were among the highest in the network. There is typically a smaller gradient in oxidized nitrogen concentrations to the west of RMNP than is observed for reduced nitrogen.

Figure 4.27 depicts daily spatial patterns in reduced (upper panel) and oxidized (lower panel) nitrogen for the summer RoMANS study. Fewer bars are included in the daily plots as a result of the elimination of the Dinosaur, Springfield, and Grant sites from the summer monitoring network. Within this smaller network, reduced nitrogen concentrations remained consistently highest at Brush on the eastern plains, usually followed by Lyons, at the base of the foothills. Oxidized nitrogen was typically highest at Lyons. Moving into the mountains, both oxidized and reduced nitrogen concentrations were often, but not always, higher at the sites east of the Continental Divide (Beaver Meadows and core site) than at sites west of the divide (Timber Creek and Gore Pass).

Figure 4.28 depicts daily concentrations of $PM_{2.5}$ sulfate and of gaseous sulfur dioxide measured across the RoMANS network during the spring and summer campaigns. Mass concentrations of sulfur dioxide tended to be low (below approximately 0.5 $\mu g/m^3$) at most sites on most days during both spring and summer. This is not the case for Brush, where concentrations periodically reached a few micrograms per cubic meter during both seasons. Occasional excursions to 1 $\mu g/m^3$ or more were also seen at Lyons in both seasons. Less extreme variability is observed in network measurements of sulfate. Sulfate concentrations across the network ranged from close to 0 up to approximately 2.5 $\mu g/m^3$. Similar variability is seen in the summer period. During much of the spring campaign the highest sulfate concentrations tended to occur at Grant, Nebraska. This pattern is not observed during the last several days of the spring campaign when concentrations across the network all approached approximately 1 $\mu g/m^3$. During summer, the Lyons site frequently measured the highest sulfate concentration, although there were also many days when there was relatively little variability in sulfate across the network.

Figure 4.29 provides a closer look at east-west gradients in reduced nitrogen concentrations in and near RMNP during the spring campaign. Here, total reduced nitrogen concentrations at Gore Pass, the "background" RoMANS site west of RMNP, are compared with those measured at Beaver Meadows and the core study site on the park's eastern slope. On most days, concentrations at Beaver Meadows and the core site were modestly higher than those measured at Gore Pass. There were several high-concentration-episode days observed at the eastern slope sites, however. The spring samples on April 20 and 23, for example, showed substantially increased levels of reduced nitrogen at Beaver Meadows and at the core site. No significant increase is observed on these dates at Gore Pass, suggesting that the reduced nitrogen source impacting the eastern slope RMNP sites did not simultaneously exert much influence on concentrations west of the park. A similar pattern is observed on several days during the summer study as well. For example, reduced nitrogen concentrations were substantially elevated on July 21, 22, 31, and August 7 at the core site and at Beaver Meadows, relative to concentrations on the same days at Gore Pass. It is important to note that the concentrations of reduced nitrogen at Beaver Meadows and at the RoMANS core site often exhibited similar high concentration episodes. When the concentration was high at one site it generally also was high at the other. This pattern is suggestive of simultaneous influence from a regional ammonia source.

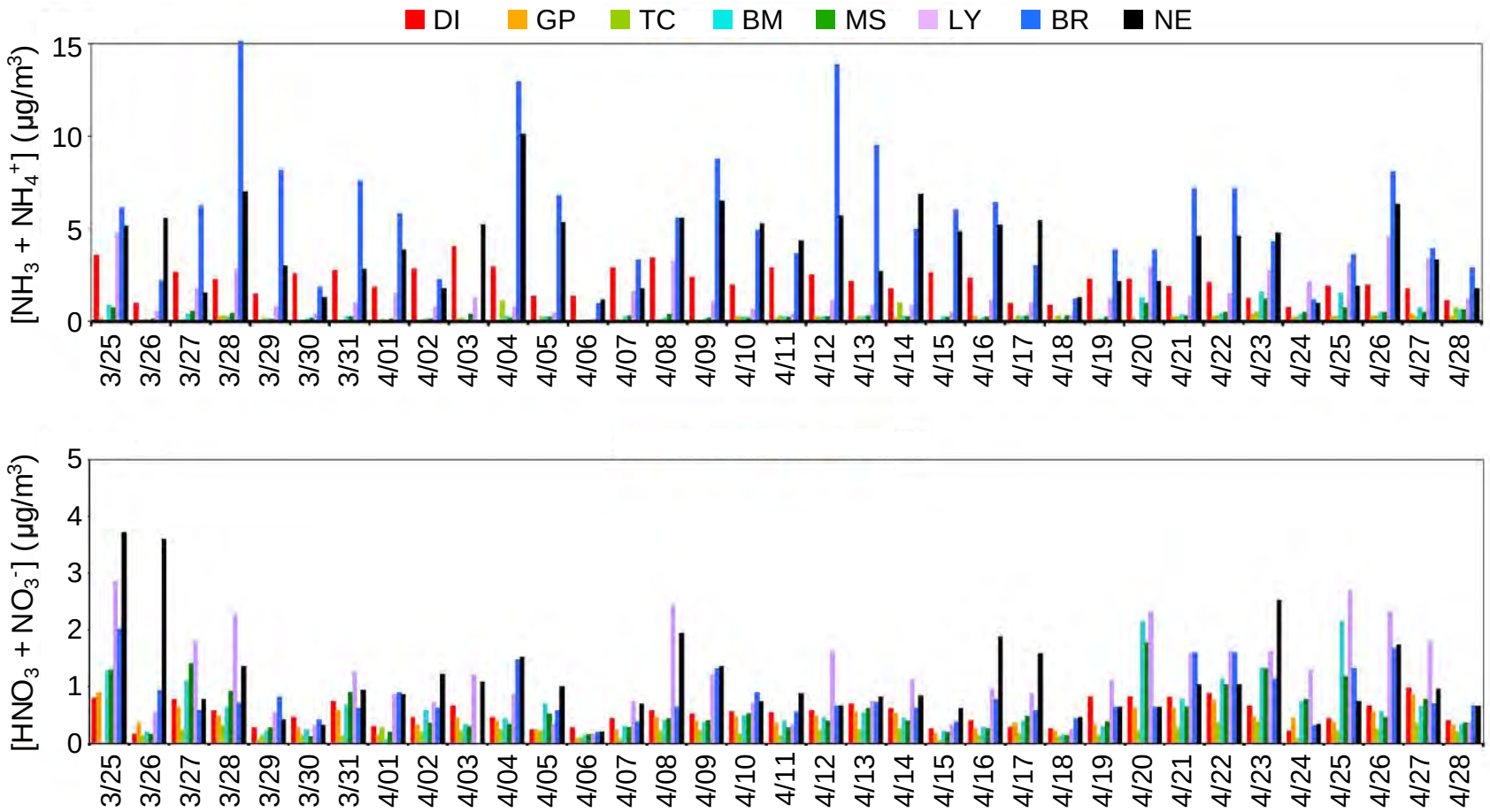

Figure 4.26. Daily concentrations (µg/m^3) of reduced (top panel) and oxidized (bottom panel) nitrogen measured at selected RoMANS network sites during the spring campaign. Sites are arranged from west to east, starting with a red bar for Dinosaur and ending with a black bar for Grant, Nebraska. Plotted reduced nitrogen bars represent the sum of gaseous ammonia and $PM_{2.5}$ ammonium. Plotted oxidized nitrogen bars represent the sum of gaseous nitric acid and $PM_{2.5}$ nitrate.

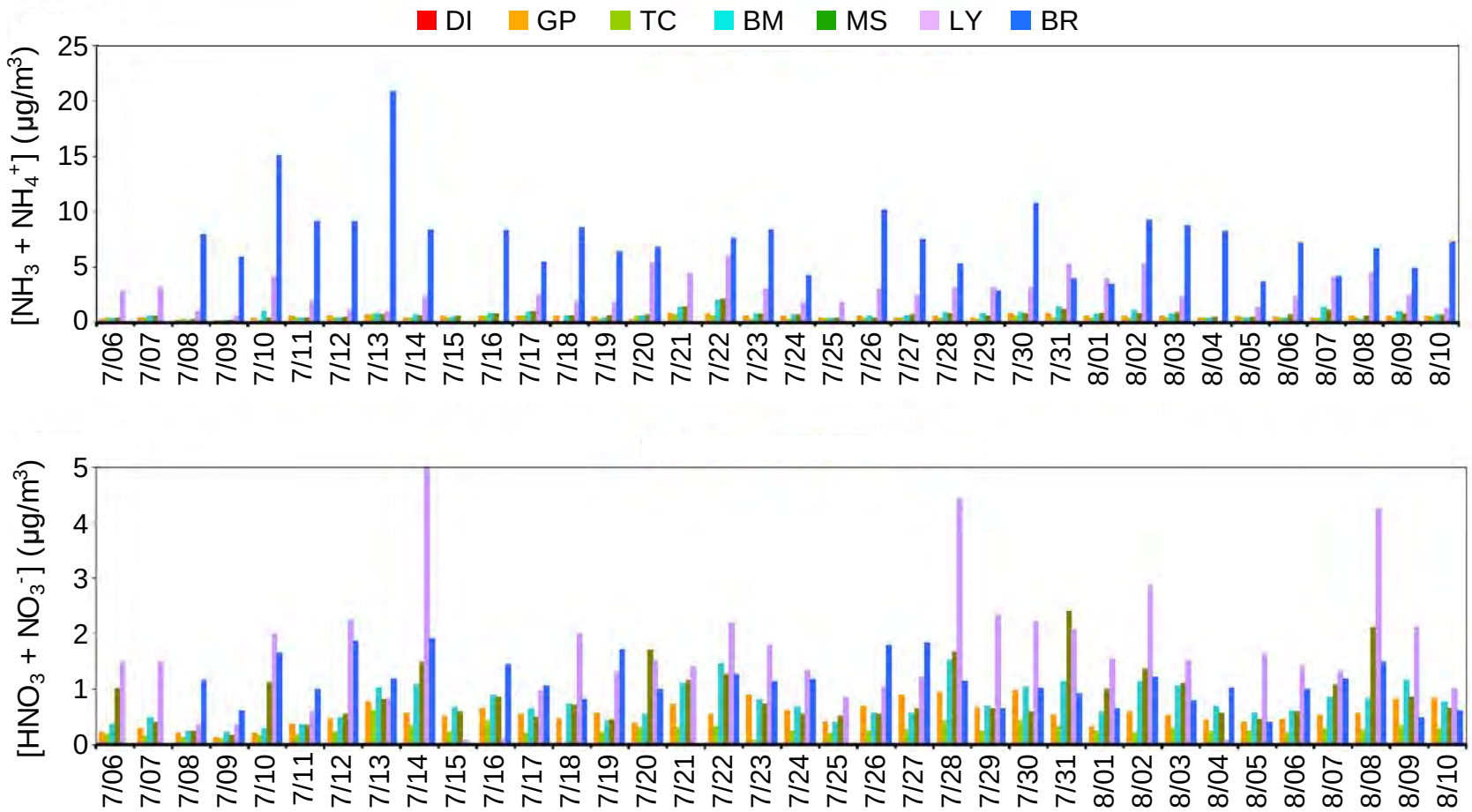

Figure 4.27. Daily concentrations (µg/m^3) of reduced (top panel) and oxidized (bottom panel) nitrogen measured at selected RoMANS network sites during the summer campaign. Sites are arranged from west to east, starting with an orange bar for Gore Pass and ending with a blue bar for Brush. Plotted reduced nitrogen bars represent the sum of gaseous ammonia and $PM_{2.5}$ ammonium. Plotted oxidized nitrogen bars represent the sum of gaseous nitric acid and $PM_{2.5}$ nitrate.

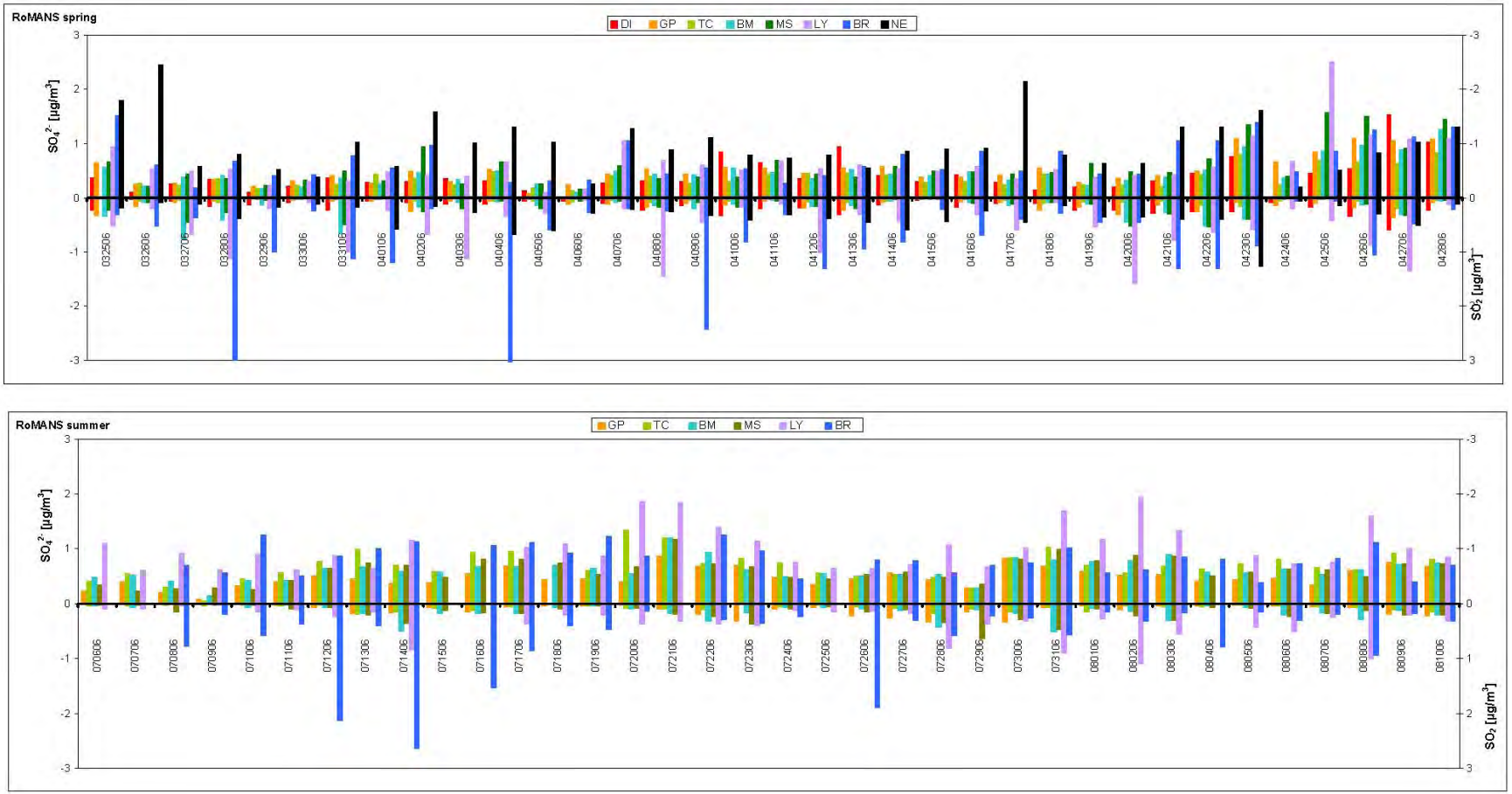

Figure 4.28. Daily concentrations (µg/m^3) of sulfate and sulfur dioxide measured at selected RoMANS network sites during the spring (top panel) and summer (bottom panel) campaigns. Sites are arranged from west to east. $PM_{2.5}$ sulfate concentrations are represented by bars extending upward from the center of each plot; sulfur dioxide concentrations are represented by bars extending downward (right axis).

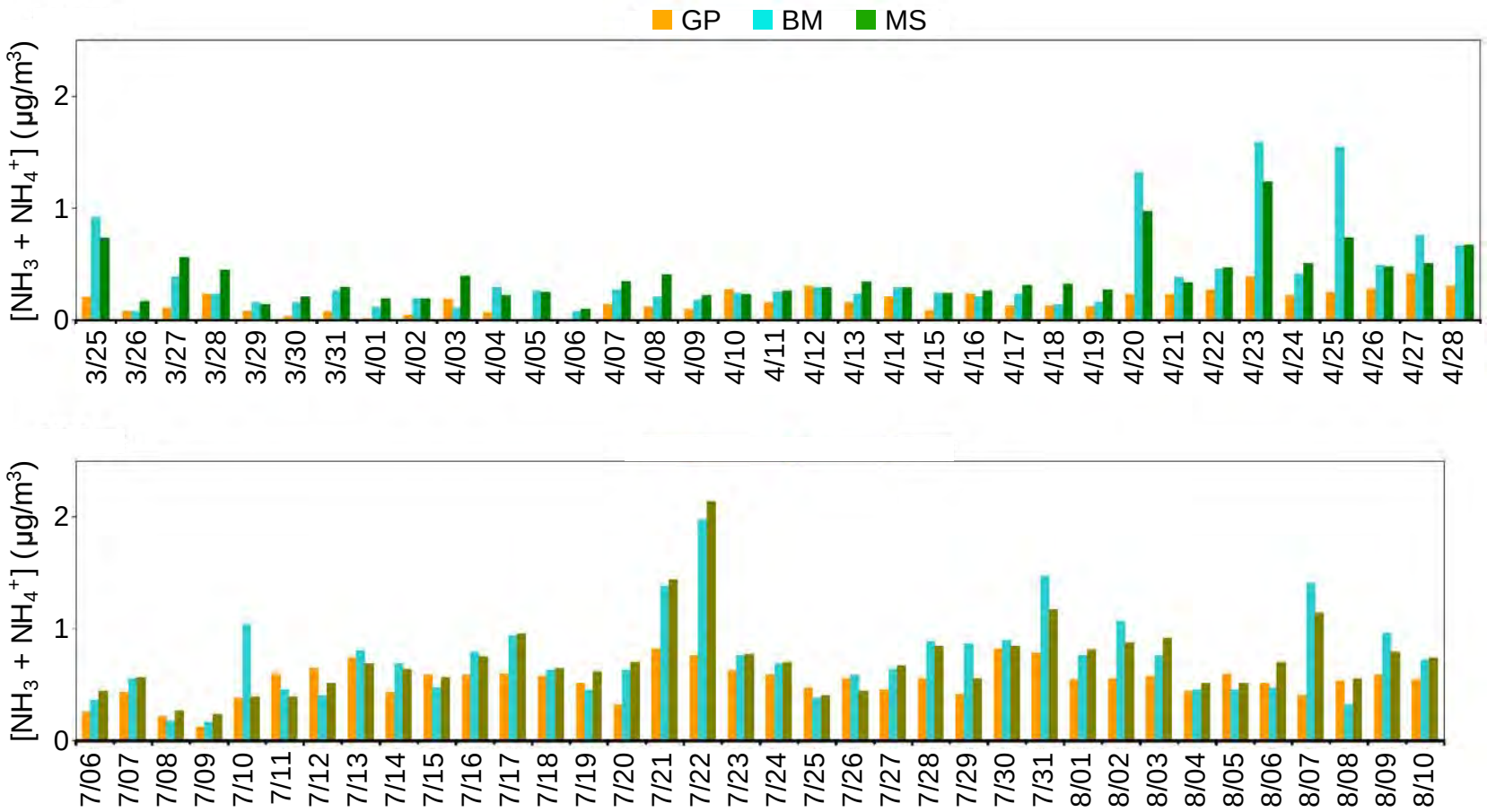

Figure 4.29. Daily concentrations (µg/m^3) of reduced nitrogen measured at Gore Pass, on the western slope, and at Beaver Meadows and the RoMANS core site, on the eastern slope, during the RoMANS spring and summer campaigns.

The Gore Pass monitoring site was selected for inclusion in the RoMANS network to provide information about the background concentration of material found in air west of RMNP. If we assume concentrations, for example of reduced nitrogen, measured at Gore Pass are representative of a regional background, we can subtract these values from concentrations measured at other sites (e.g., in RMNP) to determine the "excess" amount of material present above background. This was done in Figure 4.30 for reduced nitrogen concentrations at the RoMANS core site. The top panel shows spring reduced nitrogen "excess" amounts; the bottom panel displays the same data for summer. This analysis once again emphasizes the high reduced nitrogen concentration episode days at the core site. The largest "excess" reduced nitrogen amounts were seen on April 20, April 23, July 21, July 22, and August 7; on all of these days the reduced nitrogen excess was 1 $\mu g/m^3$ or higher. The excess reduced nitrogen exceeded 2 $\mu g/m^3$ on July 22.

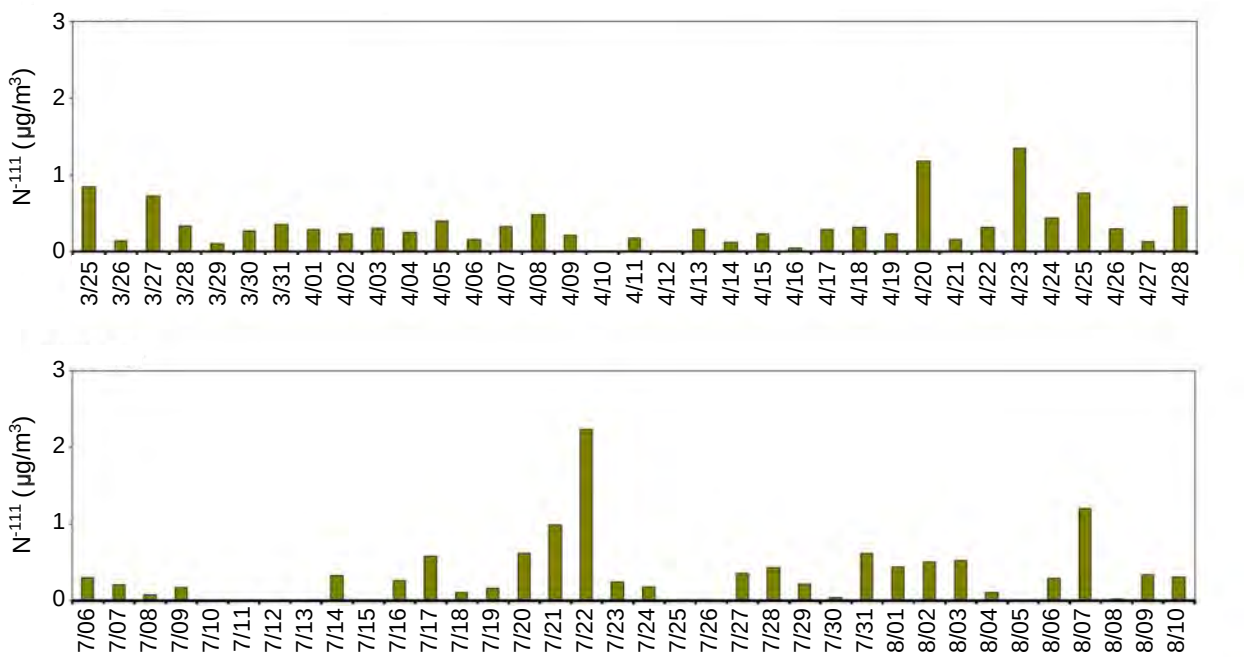

Figure 4.30. Daily concentrations ($\mu g/m^3$) of excess reduced nitrogen measured at the RoMANS core site during the spring and summer campaigns. Excess reduced nitrogen is calculated as the reduced nitrogen amount measured at the core site minus the reduced nitrogen amount measured on the same date at the RoMANS regional background site at Gore Pass.

By focusing on these reduced nitrogen episode days, we can examine spatial gradients in nitrogen species concentrations during periods when fixed nitrogen transport into the park and associated nitrogen deposition are high. We begin by looking at July 22, 2006, the date with the highest excess reduced nitrogen concentration. Figure 4.31 depicts the spatial pattern of nitrogen and sulfur species concentrations measured on this date. On this date we see a clear difference between the concentrations of oxidized and reduced nitrogen at sites on the east side of the Continental Divide (Beaver Meadows, the core site, Lyons, and Brush) and those on the west side (Gore Pass and Timber Creek). In particular, concentrations of gaseous nitric acid and gaseous ammonia are much higher at the sites east of the divide. The highest nitric acid concentration on this date was observed at Lyons while the highest ammonia concentration was

measured at Brush. The atmosphere east of RMNP on this date represents a potential reservoir for transport of both oxidized and reduced nitrogen into the park.

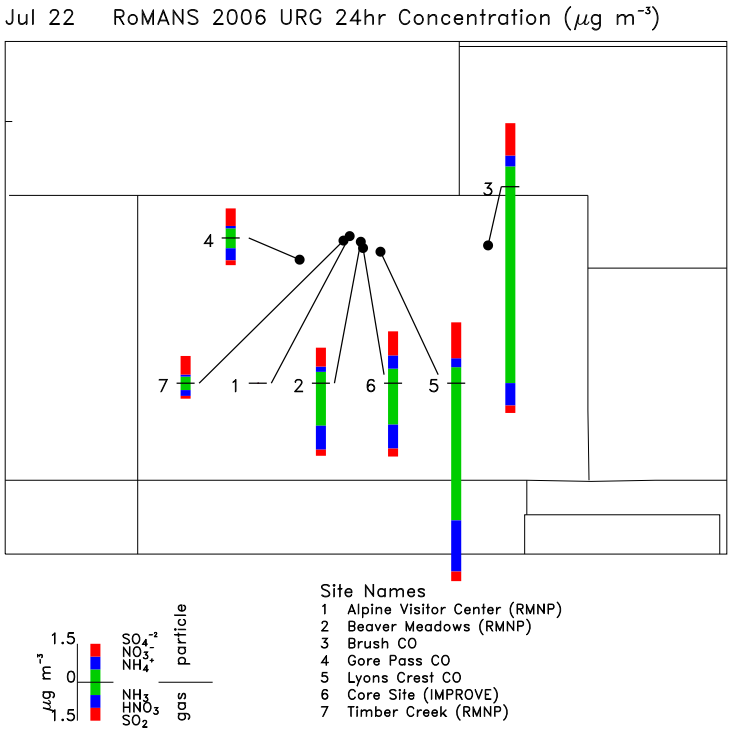

Figure 4.31. Concentrations (μg/m^3) of oxidized and reduced fixed nitrogen species and of sulfur species measured in the RoMANS network on July 22, 2006. $PM_{2.5}$ concentrations of nitrate, sulfate, and ammonium extend upward from the center of each bar plot; gas-phase concentrations of ammonia, nitric acid, and sulfur dioxide extend downward. Data are not available on this date for the Alpine Visitor Center site.

Figure 4.32 depicts the spatial gradient in nitrogen and sulfur species concentrations measured on the prior day, July 21, also a day with significant excess reduced nitrogen at the RoMANS core site. The overall patterns on this date are similar to those observed on the 22nd, with higher nitrogen species concentrations at locations east of the Continental Divide and a substantial reservoir of both oxidized and reduced nitrogen east of the park. The absence of Brush data on this date limits our view of the extent of the reduced nitrogen reservoir in northeastern Colorado.

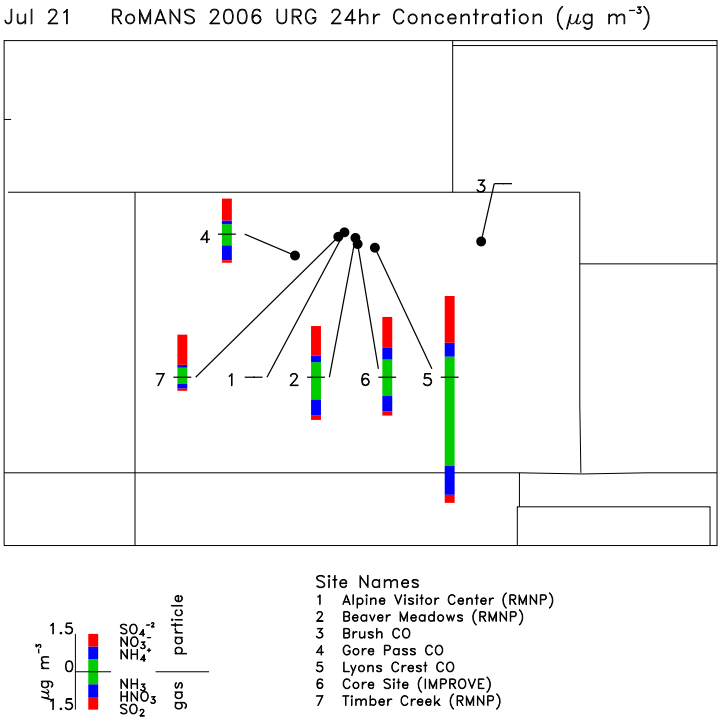

Figure 4.32. Concentrations (μg/m^3) of oxidized and reduced fixed nitrogen species and of sulfur species measured in the RoMANS network on July 21, 2006. $PM_{2.5}$ concentrations of nitrate, sulfate, and ammonium extend upward from the center of each bar plot; gas-phase concentrations of ammonia, nitric acid, and sulfur dioxide extend downward. Data are not available on this date for the Alpine Visitor Center or Brush sites.

Spatial patterns in nitrogen and sulfur species concentrations are depicted in Figure 4.33 for the sample period beginning on August 7, 2006. Elevated concentrations of ammonia and nitric acid are again seen at sites on the eastern slope of the park, with even higher concentrations at Lyons and Brush. The availability of measurements at the Alpine Visitor Center on this date reveals that higher concentrations of ammonia, in particular, reach up to the Continental Divide. Note, however, that ammonia concentrations decreased substantially moving west from the divide to the sites at Timber Creek (near the western boundary of RMNP) and Gore Pass.

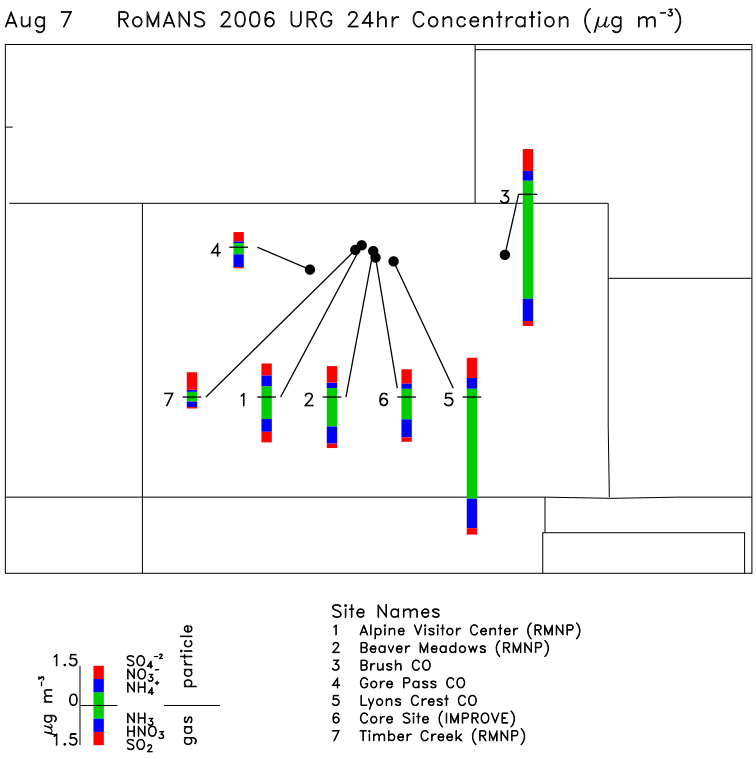

Figure 4.33. Concentrations (μg/m^3) of oxidized and reduced fixed nitrogen species and of sulfur species measured in the RoMANS network on August 7, 2006. $PM_{2.5}$ concentrations of nitrate, sulfate, and ammonium extend upward from the center of each bar plot; gas-phase concentrations of ammonia, nitric acid, and sulfur dioxide extend downward.

The highest spring levels of excess reduced nitrogen at the RoMANS core site were observed on April 20 and on April 23. Figures 4.34 and 4.35 depict the spatial variability in nitrogen and sulfur species concentrations measured across the RoMANS network on these two dates. The observations on April 20 include data from sites in and near RMNP and show the same sort of pattern observed in the summer episode days: greater amounts of both reduced and oxidized nitrogen east of the Continental Divide. These spring data, in contrast to the summer observations, however, show enhancement at the mountain sites, primarily in fine particle ammonium and nitrate concentrations rather than in concentrations of their gas-phase counterparts. This is consistent with the thermodynamic tendency for formation of particulate ammonium nitrate when temperatures are lower. Observations at the Brush and Grant, Nebraska, sites on this date were part of a 48-hr sample collected beginning on April 19, so are not included in the comparison in Figure 4.34. A more complete view of spatial gradients is available for the other spring episode day, April 23 (See Figure 4.35). As with other episode days, reduced and oxidized nitrogen species concentrations on the east side of the Continental Divide (at the core site and Beaver Meadows) are higher than on the west side (Timber Creek and Gore Pass). Higher reduced and oxidized nitrogen concentrations are also seen at the northeastern network sites, including Lyons, Brush, and Grant, Nebraska.

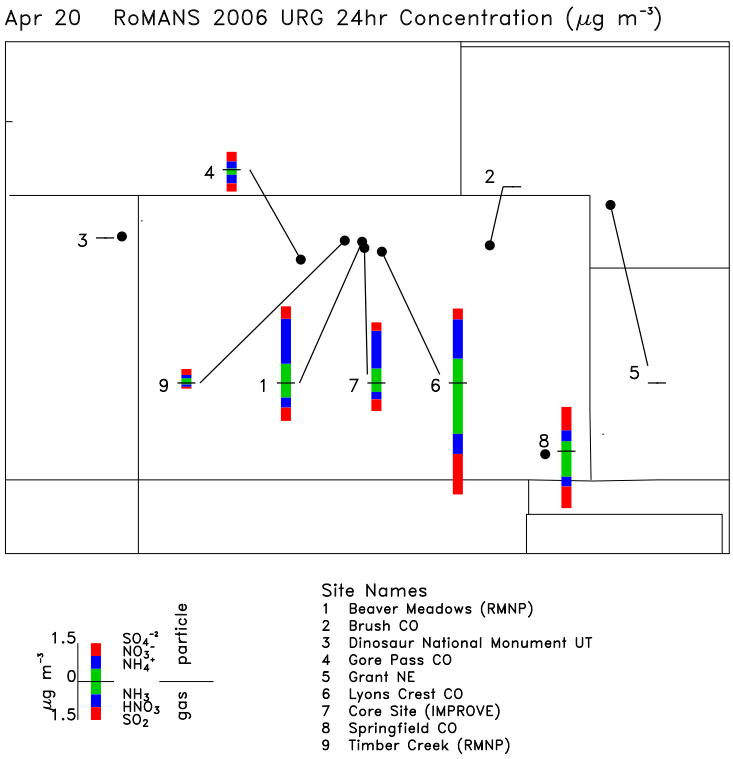

Figure 4.34. Concentrations (μg/m^3) of oxidized and reduced fixed nitrogen species and of sulfur species measured in the RoMANS network on April 20, 2006. $PM_{2.5}$ concentrations of nitrate, sulfate, and ammonium extend upward from the center of each bar plot; gas-phase concentrations of ammonia, nitric acid, and sulfur dioxide extend downward. Twenty-four-hr data are unavailable on this date for the Dinosaur, Brush, and Nebraska sites, which collected 48-hr samples beginning on April 19.

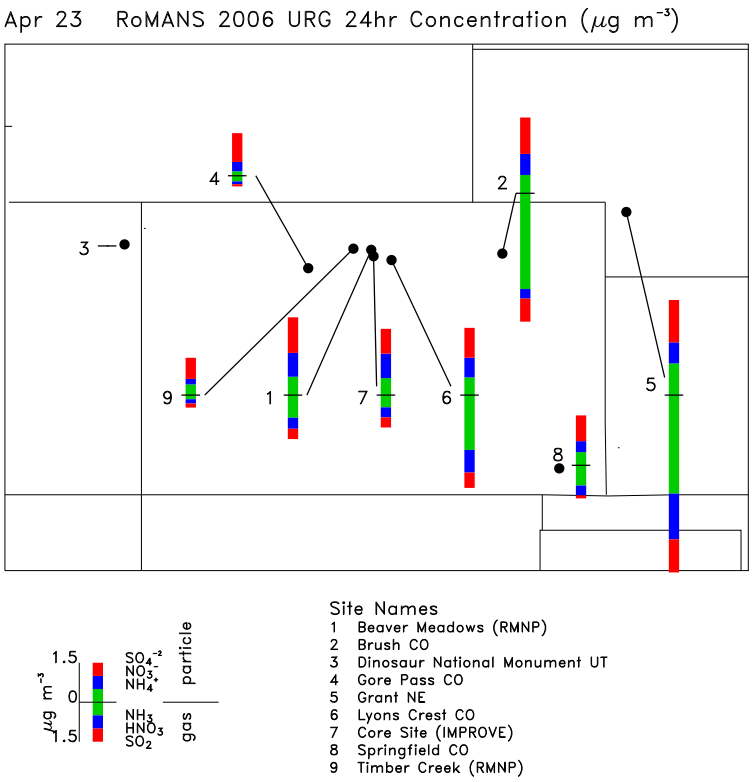

Figure 4.35. Concentrations (μg/m^3) of oxidized and reduced fixed nitrogen species and of sulfur species measured in the RoMANS network on April 23, 2006. $PM_{2.5}$ concentrations of nitrate, sulfate, and ammonium extend upward from the center of each bar plot; gas-phase concentrations of ammonia, nitric acid, and sulfur dioxide extend downward. Twenty-four-hr data are unavailable on this date for the Dinosaur site.

On each of the pollution episode days examined above, we see strong spatial gradients in nitrogen species concentrations, with higher concentrations of both oxidized and reduced nitrogen east of the Continental Divide. Further, we see a gradient in nitrogen concentrations moving from sites in the park toward eastern Colorado. Concentrations measured at Springfield in southeastern Colorado (spring campaign only) are generally lower than those in northeastern Colorado. Oxidized nitrogen concentrations often peak at the Lyons site, while reduced nitrogen concentrations typically peak further east. These pollution episode patterns are broadly consistent with the overall spatial gradients in nitrogen species concentrations discussed in Chapter 3.

One consequence of the observed gradients is that nitrogen species concentrations are likely to increase in RMNP if transport is from the east, where concentrations tend to be higher. During periods of transport from the west, with its lower concentrations, we expect nitrogen species concentrations in the park to typically remain low.

We can examine the link between transport and eastern slope RMNP pollutant concentrations by examining the continuous particle measurements made using the PILS-IC system at the

RoMANS core site. As an example, a time line of PILS-IC concentrations of $PM_{2.5}$ nitrate, sulfate, and ammonium is shown in Figure 4.36. In this time line, which runs from April 20 through April 26, we see the two core site pollution episodes discussed above, on April 20 and April 23. We also see a period of elevated concentrations on April 25. Elevated concentrations of ammonium and nitrate are seen at the core site on April 20. On April 20 and 25 concentrations of nitrate, sulfate, and ammonium are all elevated. Other periods during this time line show very low concentrations, especially for ammonium and nitrate, illustrating how clean conditions at the park can be between pollution episodes.

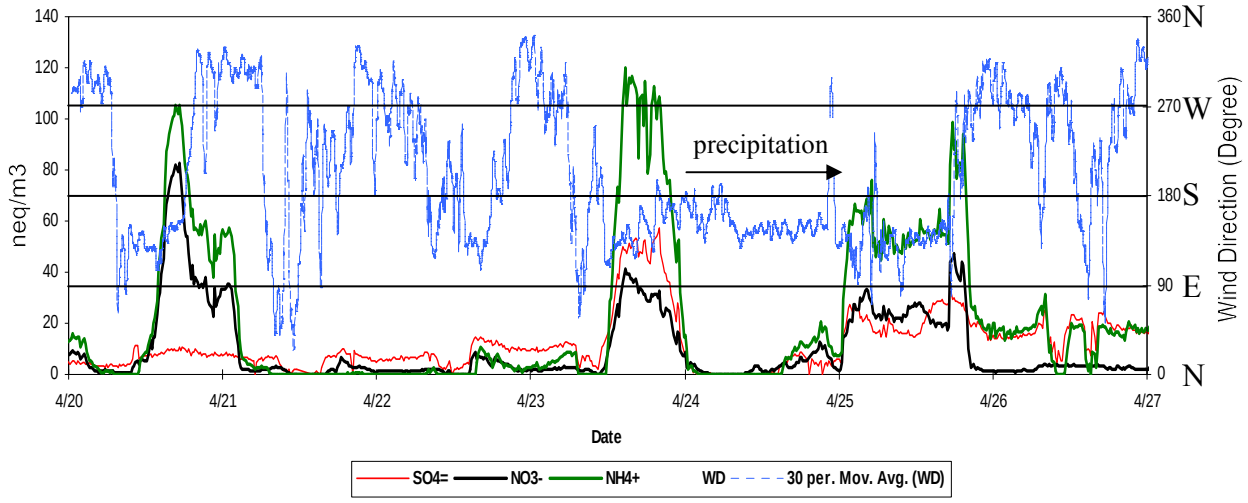

Figure 4.36. Semicontinuous (15-min time resolution) $PM_{2.5}$ major ion concentration (neq/m^3) and local 10-m wind direction (degree) time lines measured at the core site during late April 2006.

Figure 4.36 also includes a time line of the local wind direction measured on the CASTNet tower at the RoMANS core site. As discussed in Chapter 1, winds at this site from the west or northwest reflect downslope transport; winds from the east or southeast represent upslope transport as channeled by the local topography. The rise in $PM_{2.5}$ concentrations observed on both April 20 and April 23 was preceded by a change in wind direction to an upslope flow situation with air coming from the southeast. Note also that there is some lag between the change to upslope flow and the subsequent rapid increase in concentrations. This time lag is consistent with time required to transport material from the pollutant reservoir that resides at lower elevations east of the park. Note, too, that when concentrations increased in the park they did so very rapidly, with a concentration increase of greater than a factor of 10 in a period over a time scale on the order of 1 hr. This rapid increase is a sign of a transport-driven concentration change and reflects the arrival at the site of a different, much more polluted air mass. Changes in concentration due to local emission processes are unlikely to be so dramatic.

On April 20 we see a return to downslope (northwesterly) flow in the evening, accompanied by a rapid drop in ammonium nitrate concentrations. Concentrations at the core site remain somewhat elevated until early on the morning of April 21, when they drop off to very low levels, following a period of sustained downslope transport.

The relationship between $PM_{2.5}$ concentrations and wind direction was a bit different during the April 23–25 period. As mentioned above, the initial concentration rise on April 23 followed a shift in wind direction to upslope transport. The observed increases in the amounts of $PM_{2.5}$ ammonium, nitrate, and sulfate measured at the core site on April 23 are an indication that pollutants to the east of the park (see Figure 4.35) were transported up into the park in conjunction with the change in transport. In contrast to the April 20 episode, we see significant increases in concentrations of sulfate as well as of ammonium and nitrate. A review of Figures 4.34 and 4.35 shows that sulfate concentrations east of the park were significantly higher on April 23 than on April 20, consistent with the difference in the PILS observations on these two dates.

In contrast to April 20, when downslope transport resumed during the evening hours, transport patterns in the episode beginning April 23 continued to produce upslope (southeasterly) flow through the evening of April 25. The sustained upslope flow during this period not only brought increased pollution into the park from the east but was also responsible for the formation of widespread precipitation. As air is forced westward, up against the mountains, it is forced to rise. As the air rises, it cools and becomes supersaturated with water vapor. This excess water vapor initially leads to cloud formation followed by the onset of heavy precipitation. Despite sustained upslope flow overnight on April 23 and through the entire day of April 24, $PM_{2.5}$ major ion concentrations were observed to drop off around midnight on the 23rd. This dramatic decrease in concentrations is associated with the development of heavy precipitation associated with this upslope snowstorm. Heavy precipitation at the core site was observed approximately from midnight on April 23 to midnight on April 24. This time period is indicated by an arrow on Figure 4.36. Active scavenging of fine particles by the precipitating clouds reduced airborne concentrations of $PM_{2.5}$ nitrate, sulfate, and ammonium to very low levels, despite continued airflow from more polluted regions east of the park. As precipitation diminished near midnight on the 24th, $PM_{2.5}$ major ion concentrations bounced back up; they dropped substantially later that day as the winds returned to a more westerly pattern.

The period from April 23 to April 25 illustrates many of the key features observed during RoMANS to be important contributors to the deposition of large amounts of nitrogen and sulfur to park ecosystems. First, transport from the east brought polluted air up into the park. Second, this transport from the east was also responsible during this period for the formation of heavy precipitation, due to topographically forced lifting of the westward moving air. As discussed earlier, wet deposition is a much more effective mechanism than dry deposition for the input of material to the surface. The result, in this case, was the single most important deposition event observed during the entire RoMANS campaign.

Transport from the east is also an important contributor to periods of significant dry deposition of oxidized and reduced nitrogen in RMNP. The greatest daily dry deposition flux of nitrogen observed in the RoMANS study was on July 22. Transport from the east on this day raised reduced nitrogen species concentrations in the park to several $\mu g/m^3$, producing a dry deposition flux in excess of 1 mgN/m^2*day. In the spring, the highest nitrogen dry deposition fluxes were observed on April 23 and on April 20. The high fluxes on April 23 reflect deposition of the high concentrations of particle and gas-phase nitrogen species observed at the core site before the onset of precipitation. As we saw above, these high concentrations were tied to upslope transport from the east. Transport from the east on April 20, as described above, also produced

high nitrogen species concentrations in the park. An absence of precipitation on that day resulted in high dry deposition fluxes (reduced N ~ 0.5 mgN/m^2*day) but no wet deposition.

The spatial gradients observed across the RoMANS network and the relation between upslope/downslope transport and species concentrations at the RoMANS core site suggest an important link between pollutant emissions east of the park and nitrogen deposition inside RMNP. A more sophisticated analysis is required to relate emissions from different source types and from specific source regions to observed deposition. A variety of such analyses will be presented later in this report.

4.4. USING HIGH TIME RESOLUTION AEROSOL AND NUMBER SIZE DISTRIBUTION MEASUREMENTS TO ESTIMATE ATMOSPHERIC EXTINCTION

The semicontinuous measured and derived speciated aerosol concentrations, along with normalized NSDs, can be used to estimate particle mass scattering/absorption efficiencies and atmospheric scattering and absorption coefficients. The fine and coarse modes as defined by the NSD measurements were treated as externally mixed from each other but uniformly mixed within each mode. Furthermore, based on the above analysis, for the spring time period the $PM_{2.5}$ soil was assumed to be the fine tail of coarse fraction soil, while during the summer $PM_{2.5}$ soil was assumed to reside in the fine mode (< 0.8 μm). Volume-weighted indices of refraction and densities were calculated based on the values of these variables listed in Table 3.14. Semicontinuous organic and light-absorbing-carbon concentrations for the spring were estimated using the average ratio of POM and LAC to TCM derived from the IMPROVE dataset. As described in section 3.8, the POM/TCM ratio for spring was 0.91 while LAC/TCM was 0.09. For the summer dataset the average IMPROVE fractions of $PM_{2.5}$ soil, POM, and LAC to the total of these three variables were used to apportion NSD TCM to these three species. The fractions were 0.73, 0.22, and 0.05 for POM, soil, and LAC, respectively.

An estimation of ammonium sulfate and nitrate particle growth (D/Do) was calculated using the AIM (Aerosol Inorganics Model, Clegg et al., 1998) "no solids" model (which assumes equilibrium below the crystallization point) over a range of 10–98% relative humidity. The growth of the internally mixed soil-carbon-sulfate/nitrate aerosol was then estimated using Zdanovskii-Stokes-Robinson (ZSR, Saxena and Peterson, 1981) assumptions and aerosol densities presented in 3.14. ZSR assumptions imply that the amount of water a hygroscopic component brings into a mixture at some RH is equal to the amount of water it would have in a binary solution in equilibrium at the same RH. If it is assumed that in the internally mixed aerosol size distribution the chemical species are mixed in fixed proportions to each other across all sizes and the index of refraction is not a function of composition or size, the specific mass scattering efficiency can be prorated to the chemical constituents as if they were externally mixed, based on their relative densities using

Equation 4.1. $$e_{ik} = e_{mix} M_k / (m_{ik} + \rho_{ik} \sum_{j \neq i} (m_{jk} / \rho_{jk}))$$

where

k = a specific sampling period

e_i and e_{mix} = mass scattering efficiencies of species i and the mixed aerosol, respectively

M = total mass

m_i and ρ_i = the mass and density of species i

the sum is over all species j not equal to i

In Tables 4.5 and 4.6, "eff" with subscripts of "s" or "a" refers to hydrated mass scattering or absorption efficiencies, respectively, while b_{sp} and b_{abs} refer to the scattering and absorption coefficients, respectively. B_{sp} is measured scattering, and b_{ext} is estimated total extinction (fine plus coarse particle scattering plus absorption). Eff_{s_fine} is the mixed particle mass scattering efficiency, while subscripts of SO_4, NO_3, POM, LAC, and soil refer to the mass scattering efficiencies associated with ammonium sulfate, ammonium nitrate, particulate organic matter, light-absorbing carbon, and soil mass concentrations, respectively. BF+BC/2 is just b_{sp_fine}+ ½ of coarse particle scattering, which should correspond to measured scattering, assuming that the nephelometer on the average underestimated coarse particle scattering by a factor of 2.

Table 4.5. Statistical summary of measured scattering and derived mass scattering and absorption coefficients (Mm^{-1}) for various species and estimated scattering and absorption efficiencies (m^2/g) associated with these species for the spring time period. Estimates correspond to a wavelength of 550 nm.

Variable	Mean	Std Dev	Minimum	Maximum	Valid
effs_fine 2.	61	0.49	1.01	5.29	565
effs_so4 2.	62	0.51	1.15	4.72	565
effs_no3 2.	43	0.50	0.94	5.39	565
effs_POM	2.73	0.45	0.98	5.66	565
effs_LAC 2.	12	0.35	0.76	4.40	565
effs_coarse 0.	60	0.17	0.20	1.00	603
effa_fine 0.	21	0.16	0.00	0.69	565
effa_coarse 0.	00	0.00	0.00	0.00	603
bsp_so4 3.	43	4.26	0.10	34.43	565
bsp_no3 1.	29	3.45	0.00	25.61	565
bsp_POM 1.	26	1.48	0.00	10.47	565
bsp_LAC 0.	10	0.11	0.00	0.81	565
bsp_fine 6.	22	8.32	0.28	74.92	565
bsp_coarse 1.	84	1.50	0.02	8.40	603
babs_fine 0.	37	0.54	0.00	9.23	565
babs_coarse 0.	00	0.00	0.00	0.01	603
BF+BC/2 7.	32	8.73	0.39	75.66	545
bsp	9.12	10.33	-1.00 8	3.00 5	87
bext 8.	67	9.39	0.53	85.63	545

Table 4.6. Statistical summary of measured scattering and derived mass scattering and absorption coefficients (Mm^{-1}) for various species and estimated scattering and absorption efficiencies (m^2/g) associated with these species for the summer time period. Estimates correspond to a wavelength of 550 nm.

Variable	Mean	Std Dev	Minimum	Maximum	Valid
effs_fine 3.	17	0.53	1.81	4.11	533
effs_so4 3.	36	0.60	1.91	4.74	460
effs_no3 3.	42	0.61	1.96	4.78	460
effs_POM	3.40	0.57	1.85	4.47	460
effs_soil 2.	07	0.35	1.12	2.72	460
effs_LAC 2.	50	0.42	1.43	3.23	533
effs_coarse 0.	43	0.10	0.26	0.95	437
effa_fine 0.	31	0.06	0.06	0.41	533
effa_coarse 0.	10	0.07	0.00	0.28	437
bsp_so4 5.	23	3.04	0.88	20.59	460
bsp_no3 1.	40	2.57	0.10	29.41	460
bsp_POM 14	.33	8.51	0.93	52.96	460
bsp_soil 2.	01	1.19	0.13	7.41	460
bsp_LAC 0.	49	0.32	0.00	2.05	533
bsp_fine 23	.25	14.71	0.80	117.11	533
bsp_coarse 2.	24	1.52	0.08	10.73	570
babs_fine 2.	26	1.33	0.02	8.56	533
babs_coarse 0.	44	0.48	0.00	2.51	742
BF+BC/2 24	.39	15.22	0.84	121.18	533
bsp 20	.66	14.29	0.00	135.00	570
bext 28	.36	17.33	0.91	135.16	533

Figures 4.37a and 4.37b are scatter plots of measured versus reconstructed fine particle plus ½ coarse particle scattering for the spring and summer datasets, respectively. In both cases the coefficient of determination (R^2) is high at 0.80 and 0.91 for the spring and summer plots, respectively; however, during the spring, measured scattering is higher than reconstructed scattering by about 20%, while during the summer it is lower by about 18%. During the spring the agreement is quite good except for a few data points where the nephelometer-measured scattering was at times a factor of 2 higher than reconstructed scattering. The disagreement was greatest under the highest RH conditions, suggesting that the RH inside the nephelometer may have been greater than at the RH sensor. During the summer the agreement between measured and reconstructed scattering is quite good at lower scattering levels (< 20 Mm^{-1}). At intermediate scattering levels ($20 < b_{sp\_fine} < 50$ Mm^{-1}), reconstructed scattering is systematically biased high by about 15–20%.

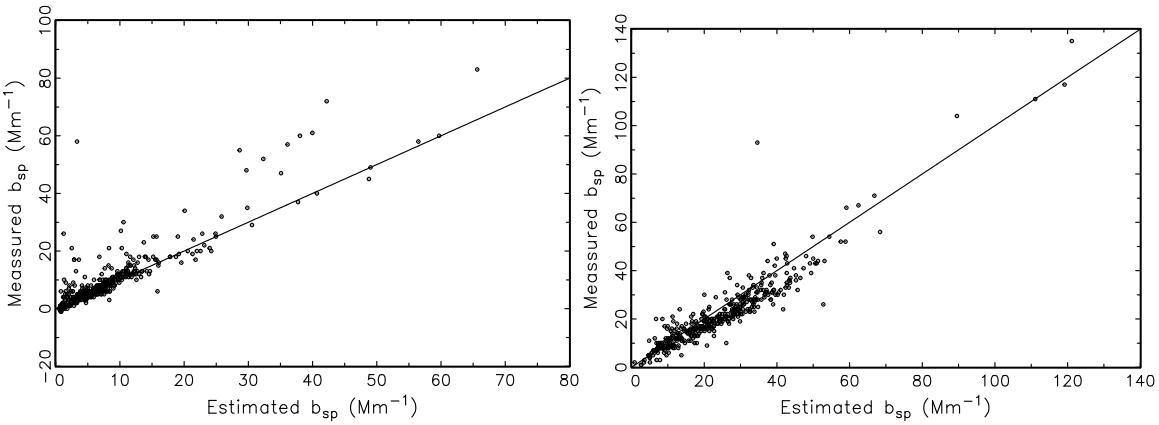

Figure 4.37. Scatter plots of reconstructed (x-axis) versus measured fine + ½ coarse particle scattering (y-axis) (Mm^{-1}) for the (a) spring and (b) summer measurement periods**.**

The mass scattering efficiencies for the spring dataset are generally lower than for summer by about 20%, primarily because size distributions are, on the average, more narrow and have mass mean diameters more conducive to efficiently scatter light. The relative humidities for the two sampling periods were about the same, with averages of 42% and 51% for spring and summer, respectively, and the highest humidities being about 95%. The average efficiency for the coarse mode was 0.43 m^2/g during the spring and 0.60 m^2/g during the summer.

The approximate particle extinction budgets for spring and summer are summarized in Figures 4.38a and 4.38b. During the spring, ammonium sulfate is the largest contributor to extinction at about 40%, with ammonium nitrate and POM contributing about 15% to overall extinction. Coarse mass scattering contributes another 22%, and particle absorption (sum of fine and coarse absorption) contributes another 5%.

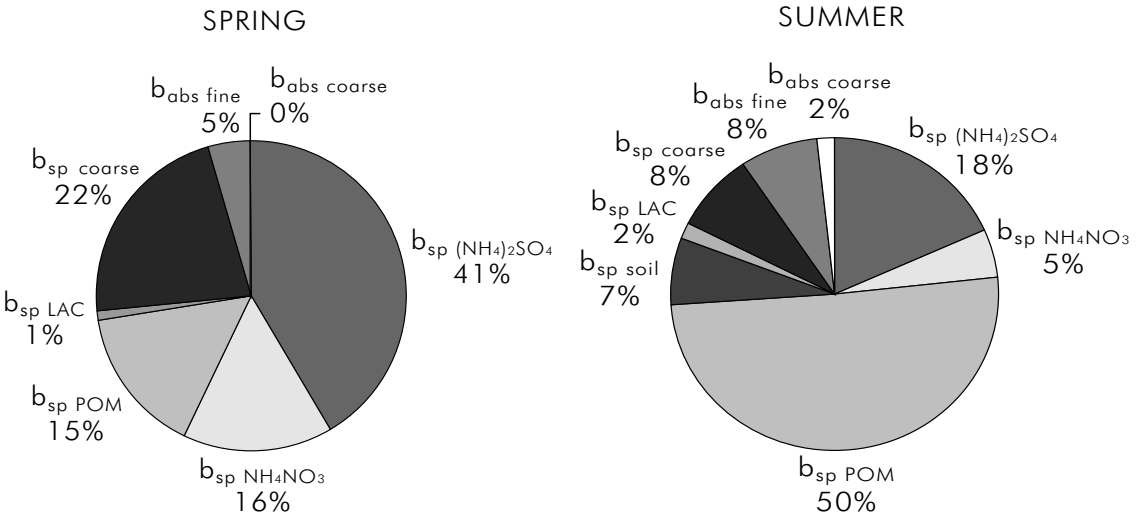

Figure 4.38. Approximate extinction budgets for the (a) spring and (b) summer time periods.

During the summer the average extinction budget is quite different. POM contributed 50% to aerosol extinction while ammonium sulfate contributed another 18%. Coarse particle scattering contributed only 8% and total absorption contributed 10% to total extinction.

The average contribution of each species can be quite misleading in that averages can be made of up of extreme events. Figure 4.39 is a stacked temporal plot for the summer time period of the scattering contribution of each species as well as the nephelometer-measured atmospheric scattering coefficient. The variables include scattering coefficients due to fine ammonium sulfate and nitrate, POM, soil, and coarse mass. Notice, as discussed previously, the large excursions in extinction that can take place in time periods as short as hours. On the average, ammonium nitrate only contributes about 5% of the extinction; however, on August 1 (JD = 213) the ammonium nitrate scattering coefficient is near 20 Mm^{-1}, which is more than 13% of total extinction. On a relative basis, the scattering coefficients due to nitrate are also high on July 13, 21, and 22 (JD = 194, 202, and 203). Most hours, however, ammonium nitrate concentrations are very low and near the detection limit of the PILS monitoring system. The extreme event on about 6:00 am on August 1 (JD = 213) corresponds to a nephelometer-measured aerosol scattering coefficient of 135 Mm^{-1}. If Rayleigh scattering and absorption are added to the measured scattering, the corresponding visual range is approximately 25 km. The corresponding lowest visual range during the spring season was approximately 40 km.

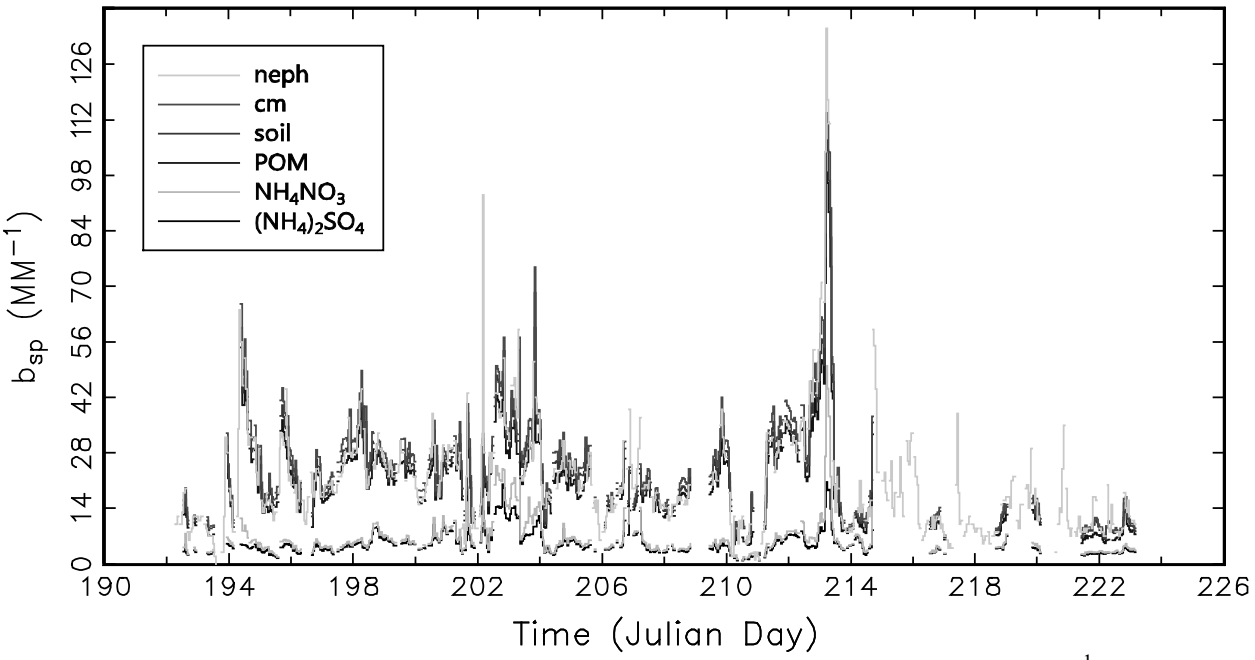

Figure 4.39. Temporal plot of measured and estimated atmospheric scattering (Mm^{-1}) of major aerosol species.